Zelluläre und biomolekulare medizinische Diagnostik mit Hilfe der Raman-Spektroskopie und statistischer Datenanalyse

DISSERTATION

zur Erlangung des akademischen Grades
doctor rerum naturalium (Dr. rer. nat.)

seit 1558

vorgelegt dem Rat der Chemisch-Geowissenschaftlichen Fakultät
der Friedrich-Schiller-Universität Jena

von Diplom-Ingenieurin Michaela Harz
geboren am 06.10.1979 in Apolda

Gutachter:

1. .....

2. .....

3. .....

Tag der öffentlichen Verteidigung: .....

Inhaltsverzeichnis

Kapitel 1

Zusammenfassung

1.1 Motivation und Stand der Forschung

Das Auftreten von Krankheiten verhindern, diese schnell zu diagnostizieren und gezielt und nebenwirkungsfrei zu behandeln, ist das Ziel in der biomedizinischen Diagnostik und Therapie. In den letzten Jahren haben sich verschiedene Verfahren der optischen Spektroskopie zur Erforschung der Struktur und Dynamik der an biologischen Systemen und Prozessen beteiligten Moleküle bewährt und bieten darüberhinaus neue Ansätze in der Medizin, Biotechnologie, Pharmazie als auch in den Lebenswissenschaften und in der Umwelttechnik. Diese optischen Methoden beruhen auf der Wechselwirkung von Licht mit toter und selbst lebender Materie, da im Gegensatz zu anderen spektroskopischen Analysemethoden die Verfahren der optischen Spektroskopie nicht-invasiv und somit berührungslos sein können. Es können sowohl extrem kleine Proben, als auch sehr kleine Stoffmengen untersucht werden. [1]

Schwingungs-spektroskopische Methoden, wie die Infrarot (IR)-Absorptions- und Raman-Spektroskopie sind in den letzten Jahren als vielversprechende und zuverlässige Analysemethode bei der Beantwortung von biologischen und medizinischen Fragestellungen etabliert worden [2–11]. Hierbei werden umfassende chemische Informationen zur Charakterisierung oder auch Identifizierung von (zell-)biologischen Systemen auf molekularer Ebene gewonnen [12–15]. Speziell die Schwingungs-Raman-Spektroskopie zeichnet sich durch eine hohe Spezifität aus und bietet die Möglichkeit, zerstörungsfrei biologisches Material zu untersuchen. Da die Raman-Spektroskopie eine markierungsfreie Methode ist und sich dahingehend auch durch eine minimale Probenpräparation auszeichnet, birgt diese ein

großes Potential in der klinischen Diagnose, Lebensmittelüberwachung bzw. pharmazeutischen Produktionskontrolle [9, 16–25]. Der Hauptvorteil für biologische Anwendungen der Schwingungs-Raman-Spektroskopie verglichen zur IR-Spektroskopie liegt darin, dass bei der Raman-Spektroskopie auch wässrige Proben vermessen werden können, weil das Raman-Spektrum von Wasser in der Regel eine geringe Raman-Intensität aufweist. Im Gegensatz dazu werden die IR-Spektren durch starke Wasserabsorptionsbanden überlagert [8]. Die Schwingungs-Raman-Spektroskopie ist somit eine besonders geeignete Methode zur *In-vitro*-Analyse von zellulären Zielstrukturen und Biomolekülen in ihrer physiologischen Umgebung [22, 26–31].

Die Kombination des Raman-Spektrometers mit einem optischen Mikroskop und der Verwendung eines Objektivs mit einer hohen numerischen Apertur sowie Vergrößerung ermöglicht es, eine hohe räumliche Auflösung im Mikrometerbereich zu erhalten. Diese sogenannte Mikro-Raman-Spektroskopie erlaubt die Untersuchung von selbst kleinsten Objekten, wie einzelne Bakterienzellen oder Strukturen innerhalb einer Zelle mit einer Größe von etwa 1 μm. Hierbei wird eine beugungsbegrenzte laterale Auflösung im Bereich der Laserwellenlänge erreicht, und das Streuvolumen der Probe bzw. des umgebenden Materials kann durch zusätzliche konfokale Blenden eingeschränkt werden. Die Mikro-Raman-Spektroskopie hat weiterhin das Potential mittels zellulärer *Imaging*- und *Mapping*-Experimente zu ortsaufgelösten *In-vivo*-Studien an zellbiologischen Organismen, wie beispielsweise Mikroorganismen, um dadurch Einblicke in lebende Zellen auf Einzelzellniveau liefern zu können [32–35].

Diese Methoden erzeugen hoch-spezifische multidimensionale Daten, die es notwendig machen, die komplexe Datenmenge mittels multivariater statistischer Datenanalysen [36–39] auszuwerten. Zur Klassifizierung können unüberwachte chemometrische Verfahren wie die hierarchische Clusteranalyse (HCA) [37] und Hauptkomponentenanalyse (engl.: *Principal Component Analysis*: PCA) [40,41] sowie überwachte Klassifizierungsmethoden wie die *K-Nearest Neighbours* (KNN), *Soft Independent Modelling of Class Analogies* (SIMCA), Artifizielle Neuronale Netzwerke (ANN) [42] und Support-Vektor-Maschinen (SVM) [43, 44] zum Einsatz kommen, um signifikante und charakteristische Informationen aus dem multidimensionalen Spektren-Datensatz zu extrahieren. Hierbei besteht die Aufgabe, geringste Unterschiede in den Raman-Spektren zu visualisieren, damit die aus einer Überlagerung von verschiedenen biomolekularen Raman-Signalen (wie von DNA/RNA, Proteinen, Lipiden, Kohlenhydraten) bestehenden Spektren interpretiert werden können. Der Vorteil

überwachter gegenüber unüberwachter Klassifizierungsmethoden liegt darin, dass mathematische Modelle erzeugt werden können, die im Anschluss eine Identifizierung von unbekannten Proben, wie mikrobiellen Kontaminationen, ermöglichen. Die Raman-Spektren beinhalten zahlreiche Banden, zu denen über die Lage, Intensität und Breite der Raman-Peaks molekulare Schwingungsnormalmoden von funktionellen Gruppen, zellulären Komponenten oder Substrukturen zugeordnet werden können. Diese Raman-Banden repräsentieren daher sensitive und spezifische Informationen, um wichtige Aussagen über die dreidimensionale Molekülstruktur, intermolekulare Wechselwirkung und Dynamik und somit chemische Zusammensetzung der untersuchten komplexen Systeme treffen zu können. Demzufolge ist die Mikro-Raman-Spektroskopie in Kombination mit chemometrischen Klassifizierungsmethoden ein sehr geeigneter Ansatz für eine schnelle und zuverlässige, nicht-zerstörende Charakterisierung, Differenzierung und Online-Identifizierung beispielsweise von einzelnen Bakterienzellen [45–51].

Im Gegensatz zu prokaryotischen Zellen wie Bakterien sind eukaryotische Zellen wie Hefen komplexe biologische Strukturen mit einer großen Anzahl von in einer Zellmembran eingeschlossenen Biomolekülen [52, 53]. Die Fokussierung auf bestimmte Komponenten bzw. Regionen innerhalb der Zelle und der dahin gehenden Identifizierung ist für das Verständnis von zellulären Prozessen ein wichtiger Faktor. In dieser Beziehung ist die konfokale Mikro-Raman-Spektroskopie ein vielversprechendes Werkzeug bei der Identifizierung von Hefe-, Blut-, Gewebe- oder Krebszellen bzw. bei der Detektion von darin enthaltenen subzellulären Molekülen wie DNA/RNA, Lipid- und Proteinstrukturen über deren Molekülschwingungsmoden [13, 33, 54–59]. Des Weiteren können Körperflüssigkeiten wie beispielsweise Urin-, Blutplasma- oder Serumproben analysiert werden, um deren qualitative und quantitative Zusammensetzung aus diversen Biomoleküle zu bestimmen [26,29,30,60].

Der Raman-Prozess ist häufig von einer geringen Streueffizienz charakterisiert. Weiterhin sind die Raman-Spektren bei Anregung im sichtbaren oder nahen infraroten Spektralbereich oft vom Fluoreszenzeffekt überlagert [32, 54, 61]. Zu dessen Überwindung bedient man sich häufig verschiedener Verstärkungsmethoden, wie der Resonanz-Raman-Spektroskopie [62] oder Oberflächen-verstärkten Raman-Streuung (engl.: *Surface Enhanced Raman Scattering*: SERS). Bei der Resonanz-Raman-Spektroskopie liegt die Anregungswellenlänge im Bereich der elektronischen Absorptionsbanden gewisser Moleküle. Dies führt zu einer Intensitätserhöhung des Streuprozesses bis zu einem Faktor von 10^6 für die an diesen elektronischen Übergang gekoppelte Schwingungen [2, 63, 64]. Durch eine geeignete Wahl der Laseranregungswellenlänge ist es möglich, Moleküle bzw. Molekülteile mittels Schwingungen, die an die resonant elektronischen Übergänge gekoppelt sind,

selektiv anzuregen [13, 65]. Wenn für die Raman-Anregung eine Wellenlänge knapp unterhalb von 260 nm verwendet wird, werden fast ausschließlich die Schwingungsmoden der Purin- und Pyrimidinbasen der Nukleinsäuren [66–68] sowie die Moden der aromatischen Aminosäuren [65, 68–70] verstärkt, während bei einer Anregungswellenlänge um 200 nm lediglich Rückgratschwingungen der Proteine selektiv erhöht werden [71]. Folglich können mit der sogenannten UV-Resonanz-Raman-(UVRR)-Spektroskopie durch die selektive und sensitive Anregung im Wellenlängenbereich von 200 nm bis 260 nm, Schwingungen von bestimmten Biomolekülen wie DNA/RNA-Nukleinsäurebasen bzw. aromatische Aminosäuren in Proteinen in einer komplexen (zell-)biologischen Umgebung, wie beispielsweise lebenden Bakterienzellen, selbst in geringsten Konzentrationen spezifisch detektiert werden [72–77]. Ein weiterer Vorteil der UVRR-Spektroskopie liegt darin, da die meisten Biomoleküle und taxonomischen Marker im Spektralbereich unter 260 nm absorbieren [74, 78] und Fluoreszenzemissionsbanden im sichtbaren Spektralbereich liegen, dass mit einer Anregung im tief-ultravioletten Spektralbereich (<260 nm) fluoreszenzfreie Raman-Spektren detektiert werden können [72, 79]. Umfassende UV-Resonanz-Raman-Studien wurden hierbei an verschiedenen biologischen Systemen durchgeführt, um beispielsweise aromatische Aminosäuren in Proteinen, Peptidsekundärstrukturen, DNA-Strukturen sowie deren Bindungen und intermolekulare Wechselwirkungen zu analysieren [67, 68, 80–84]. Demzufolge können charakteristische Resonanz-Raman-Banden dieser UV-absorbierenden Chromophore oder Chromophorsegmente nicht nur zu deren Identifizierung, sondern auch innerhalb von lebenden Zellen als Markersubstanzen zur Differenzierung von Zellen bzw. Zellstrukturen erfolgreich eingesetzt werden.

Im Rahmen dieser Arbeit wird die hohe Leistungsfähigkeit der Raman-Spektroskopie, die eine Analyse von biologischen Molekülen, selbst innerhalb komplexer Systeme ermöglicht, ausgenutzt. Diese Methode erlaubt nach spezifischen Biomarkern in einer umgebenden Matrix zu suchen bzw. darin zu identifizieren. Auf dieser Grundlage können eventuell Rückschlüsse über den Gesundheitszustand von Patienten gewonnen werden bzw. Krankheiten detektiert werden. Um die vielfältigen Raman-spektroskopischen Anwendungsmöglichkeiten zu illustrieren, befasst sich ein Kapitel dieser Arbeit mit der pharmazeutischen Produktionskontrolle von Kontaminationen in Reinraumumgebung. Mikrobielle Verunreinigungen können mit den gängigen mikrobiologischen Identifizierungsmethoden meist erst nach mehreren Tagen eindeutig zugeordnet werden. Innerhalb des Biophotonik-Projektes OMIB (Online-Monitoring und Identifizierung von Bioaerosolen)

liegt, zur Überwindung dieser Beschränkung einer zeitnahen Klassifizierung, der Schwerpunkt in der akkuraten und schnellen Identifizierung von Mikroorganismen in der Reinraumproduktionsüberwachung. Das Ziel hierbei ist es in Kooperation mit dem Institut für Informatik der Universität Freiburg, dem Fraunhofer Institut für Produktionstechnik und Automatisierung, der rap.ID particle systems GmbH, der Kayser-Threde GmbH, der Schering AG sowie dem Institut für Photonische Technologien (IPHT) Jena, neue Fortschritte in der Diagnose durch Raman-spektroskopische Methoden zu ermöglichen. Eventuell auftretende Gesundheitsprobleme, als auch Produktionsausfallzeiten in der pharmazeutischen Produktion im Reinraum könnten durch eine zeitigere, zuverlässige Detektion minimiert werden [43]. Biologische Moleküle wie Nukleinsäuren, Proteine, Lipide und Kohlenhydrate erzeugen spezifische *fingerprint*-Raman-Signale. Anhand dieses hohen spektralen Informationsgehalts bezüglich der charakteristischen biochemischen Zusammensetzung werden Aussagen über den Aufbau, die Wechselwirkung und Funktion von Biomolekülen innerhalb der untersuchten Zellen erlangt. Beispielsweise ist es möglich, die Wirkung von Antibiotika auf das Bakterienwachstum von ausgewählten Bakterienarten *S. epidermidis, B. pumilus* und *E. coli* zu verfolgen [85]. Die Mikro-Raman-Spektroskopie kann in Kombination mit multivariaten Klassifikationsmethoden zur Unterscheidung von Bakterienzellen auf Artebene und selbst auf Stammebene dienen. Die Differenzierung kann auf einen großen Datensatz angewendet werden, denen verschiedenste Bakterienarten angehören, die im Reinraum der pharmazeutischen Produktion auftreten können. Ein Teil dieser Arbeit beinhaltet somit neben der Mikroorganismendetektion, durch die Verwendung der Raman-Anregungswellenlänge im sichtbaren Spektralbereich, eine phänotypische Differenzierung anhand der gesamten biochemischen Zusammensetzung von Bakterien- und Hefezellen. Hierbei werden in einem ersten Schritt zur generellen Funktionalitätserprobung der Methode mikrobielle Kolonieschichten studiert, gefolgt von der Einzelzellanalyse von Bakterien und Hefen. [MH3, MH6]

Die Differenzierung von Mikroorganismen mittels Mikro-Raman-Spektroskopie kann durch große intra-Stamm-spezifische Variationen der untersuchten Zelle erschwert werden, die aus einem schwankenden Kulturalter und Umgebungstemperatur sowie dem Nährstoffangebot resultieren. Der Ursprung bzw. die Wachstumsbedingungen (u. a. Temperatur, Nährstoffangebot, Alter, pH-Wert und Sauerstoffgehalt der Umgebung) einer fremden, zu analysierenden Bakterienzelle sind unbekannt. Infolgedessen führen unterschiedliche Kultivierungsbedingungen zu einer Variabilität in der biochemischen Zusammensetzung der Zelle, was im Raman-Spektrum wiedergegeben wird und sich somit auf die Identifizierung

der Zelle auswirken kann. Um reale Bedingungen simulieren zu können, die für die Identifizierung von unbekannten Mikroorganismen von entscheidender Bedeutung sind, wurde anhand der Modellorganismus-Bakterien der Gattung Staphylococcus der Effekt von verschiedenen Wachstumsbedingungen auf die Klassifizierungsfähigkeit erforscht. Bei der Analyse von Bakterienschichten und einzelnen Bakterienzellen der Gattung Staphylococcus anhand ihres Raman-Spektrums kann das große Potential der Raman-Spektroskopie in Kombination mit verschiedenen statistischen Klassifizierungsverfahren gezeigt werden. Es offenbaren sich die Grenzen der Anwendbarkeit der unüberwachten Mustererkennungsmethode, der hierarchischen Clusteranalyse auf einen heterogenen komplexen Datensatz, der vielfältige Kultivierungsparameter beinhaltet. Vielmehr kann eine Klassifizierung dieses heterogenen Bakteriendatensatzes erstmalig mit Hilfe einer überwachten Mustererkennungsmethode, der Support-Vektor-Maschine, gezeigt werden. [MH2]

Die Identifizierung von Mikroorganismen in Reinraumumgebung umfasst neben der Unterscheidung von einzelnen Bakterienzellen (Prokaryoten) zusätzlich eine Differenzierung von einzelnen Hefezellen (Eukaryoten). Prokaryoten besitzen im Unterschied zu Eukaryoten keinen von einer Membran umschlossenen Zellkern, in dem die Erbinformation lokalisiert ist. Die genomische DNA und eine eventuell vorhandene extrachromosomale Plasmid DNA befindet sich in ringförmiger Form innerhalb der Zelle. Demgegenüber besitzen Eukaryoten neben einen Zellkern weitere, vom Zytoplasma durch eine Zellmembran abgegrenzte Reaktionsunterräume, sogenannte Organellen, wie beispielsweise endoplasmatisches Retikulum, Vesikel und Mitochondrien [52, 53]. Aufgrund dieser ausgeprägten Kompartimentierung und somit Heterogenität innerhalb der Zelle sowie der Zellgröße von etwa 10 μm im Durchmesser im Vergleich zur räumlichen Auflösung des Mikro-Raman-Spektrometers von etwa 1 μm kann man Hefezellen nicht wie Bakterien durch ein einzelnes Raman-Spektrum charakterisieren. Durch die spektroskopische Zellkartierung in lateraler und axialer Richtung mit Hilfe von Raman-Scans über die gesamte Zelle kann die räumliche Verteilung von verschiedenen Makromolekülen wie DNA/RNA, Proteinen bzw. Lipiden innerhalb einer einzelnen Hefezelle visualisiert werden [MH4]. Mit Hilfe chemometrischer Datenanalyse, der hierarchischen Clusteranalyse, ist es trotz subzellulärer Heterogenität dennoch möglich, eine Differenzierung anhand von Mittelwert-Raman-Spektren auf Stamm- und Artebene vorzunehmen. In weiterführenden Experimenten kann auf einen größeren Datensatz von Mittelwert-Raman-Spektren eine Hefezell-Identifizierung auf Stamm- und Artebene unter Verwendung einer Support-Vektor-Maschine, vorgenommen werden. [MH4, MH5]

Zusätzlich zur phänotypischen Differenzierung von Mikroorganismen erfolgt eine genotypische Unterscheidung basierend auf der UV-Resonanz-Raman-Spektroskopie. Diese Methode liefert eine Reihe von signifikanten Signalen, die vorrangig von Proteinuntereinheiten, Nukleinsäuren und einigen anderen, im UV-Bereich stark absorbierenden Biomolekülen dominiert werden. Trotz der Förderlichkeit der UV-Resonanz-Raman-Spektroskopie in Bezug auf eingeschränkte Hintergrundfluoreszenz und der Verstärkung von Raman-Banden chromophorer Makromolekülsegmente gegenüber normaler Raman-Spektroskopie, kann der photochemische Verbrennungseffekt aufgrund der hohen Energiedichte von UV-Licht Probleme bezüglich Probenpräparation hervorrufen. Demzufolge können bei der Untersuchung von biologischen Proben bisher keine einzelnen Bakterien- bzw. Hefezellen, wie bei der Mikro-Raman-Spektroskopie mit einer Anregung im Sichtbaren, sondern nur Kolonieschichten von etwa 10^4 bis 10^5 Zellen [86] analysiert werden. Mittels der Support-Vektor-Maschine wird eine exzellente Unterscheidung der bei einer Anregungswellenlänge von 244 nm detektierten UVRR-Spektren von Bakterien auf Art- und Stammebene erreicht. [MH1]

Ein weiteres Kapitel beschäftigt sich mit einem neuen methodologischen Ansatz zur Analyse der Gehirn-Rückenmarks-Flüssigkeit (Liquor Cerebrospinalis, engl.: *Cerebrospinal Fluid*: CSF), die bei der Diagnose von akuten und chronischen Krankheiten des Zentral-Nervensystems herangezogen werden kann. Im Rahmen dieser Arbeit liegt der Schwerpunkt speziell auf der Identifizierung von zellulären Bestandteilen, wie Bakterien- und Körperzellen (z. B. Granulozyten, Lymphozyten oder Monozyten), die bei der bakteriellen Meningitis in der Gehirn-Rückenmarks-Flüssigkeit vorhanden sind. Die spezifische Identifizierung, die Quantifizierung und/oder Anreicherung lebender Einzelzellen sind Grundprobleme labormedizinischer Methodik, bei der im Allgemeinen automatisierte Hämatologiesysteme oder aber Durchflusszytometer zum Einsatz kommen. Bei der Liquordiagnostik ist nicht nur die Identifizierung des Erregers wesentlich, sondern auch die Beurteilung der Leukozytenzahl und -arten, der im allgemein zellarmen CSF ist bedeutend. Gegenwärtig eingesetzte mikrobiologische Methoden zum Erregernachweis sind auf eine zeitaufwändige Kultivierung angewiesen. Weiterhin stellt die Sensitivität des Erregernachweises durch mikroskopische Beurteilung aufgrund der Spezies- bzw. Konzentrationsabhängigkeit ein grundlegendes Problem in der labormedizinischen Liquordiagnostik dar. Dementsprechend wird im Rahmen des DFG-Projektes PO 563/7-1 'Raman-spektroskopische Differenzierung und Identifizierung körpereigener Zellen und Mikroorganismen im Liquor für die medizinische Diagnostik' in Kooperation mit Prof. Dr. Thomas Deufel und Dr. Dr. Michael

Kiehntopf aus dem Institut für Klinische Chemie und Laboratoriumsdiagnostik am Universitätsklinikum Jena eine neuartige und zuverlässige Methodenentwicklung eruiert. Dieses Verfahren konzentriert sich auf eine rasche und zuverlässige Raman-spektroskopische Analyse und eine möglichst zeitnah zur Probennahme erfolgende Identifizierung von isolierten einzelnen Bakterien- und Blutzellen aus der Gehirn-Rückenmarks-Flüssigkeit. Damit schwingungs-spektroskopische Methoden zur Differenzierung von Blutzellen, die im CSF während der bakteriellen Meningitis enthalten sind, eingesetzt werden können, liegt zunächst das Interesse eines Teilbereichs dieser Arbeit darin, die räumliche Verteilung und chemische Zusammensetzung verschiedener subzellulärer Bestandteile in Blutzellen zu lokalisieren und aufzuklären. Zur Erhöhung des Informationsgehaltes bezüglich der Analyse von Zellen bzw. sub-mikroskopischen Strukturen wird erstmals die Raman-Spektroskopie mit Hilfe der Fluoreszenzmarkierung gekoppelt. In diesem Sinne wird ein neuer Ansatz zur Blutzellanalyse von Einzelzellen der Gehirn-Rückenmarks-Flüssigkeit aufgegriffen, der die simultane Anwendung der einzigartigen Kapazitäten der Fluoreszenzmarkierung in Kombination mit der Raman-Spektroskopie an derselben Probe vereint. Die Zielstellung liegt in der schnellen Bestimmung von bestimmten Zellparametern wie z. B. dem Aktivierungsgrad von einzelnen Blutzellen. Diese neuartige Technologie ermöglicht eine zeitnahe und zuverlässige Zellidentifizierung zwischen Untertypen weißer Blutzellen mittels Fluoreszenzfärbung, während die Raman-Spektroskopie zusätzlich noch molekülspezifische *fingerprint*-Informationen mit einer räumlichen Auflösung bis zum Beugungslimit enthält. [MH7]

Zunächst werden aus Vollblut isolierte Blutzellen als Modellsystem analysiert, um methodologische Parameter bezüglich der Auswahl an fluoreszenzmarkierten Antikörpern zu optimieren. Die Ergebnisse demonstrieren, dass der ausgewählte Fluoreszenzfarbstoff das Raman-Spektrum einer gefärbten Zelle verglichen zu einer ungefärbten Blutzelle nicht störend beeinflusst oder überlagert. Weiterhin erfolgt eine Charakterisierung von Blutzellen, die aus der nativen Umgebung - der Gehirn-Rückenmarks-Flüssigkeit - isoliert worden sind, um zu prüfen, inwieweit die CSF-Matrix die Anwendbarkeit der Raman-Spektroskopie beeinflusst. Durch die gekoppelte Anwendung der Raman-Spektroskopie mit statistischer multivariater Datenanalyse kann zwischen Zellsubstrukturen innerhalb weißer Blutzellen unterschieden werden. Da sich zusätzlich die verschiedenen Subtypen von Blutzellen in der Menge und Art von bestimmten Zellbestandteilen unterscheiden, gibt es zukünftig die Möglichkeit, dass eine Differenzierung diverser Blutzelltypen vorgenommen werden kann. Dafür muss in der Datenbank eine Blutzelle mit einer Vielzahl von verschiedenen, in der sub-mikroskopischen Auflösung vorkommenden Raman-Spektren

hinterlegt sein. Das Potential der Raman-Spektroskopie der akkuraten und schnellen Identifizierung von einzelnen, im CSF vorkommenden Blutzellen, liefert somit für die Implementierung in der klinischen Diagnostik einen vielversprechenden Ansatz. [MH7]

Der große Vorteil der Raman-Spektroskopie, geringe molekulare Unterschiede zu detektieren, wird nicht nur als zerstörungsfreie *In-vivo*-Analysemethode zur Untersuchung der Morphologie und biochemischen Zusammensetzung an einzelnen Geweben, Zellen und deren sub-zellulären Strukturen angewendet, um daraus Abnormalitäten ableiten zu können. Dieses Potential ist außerdem hilfreich, um zwischen gesunden und kranken Gewebestrukturen zu unterscheiden, Krankheiten zu detektieren und Krankheitsverläufe zu überwachen bzw. um Wirkprinzipien von Medikamenten auf molekularer Ebene verfolgen zu können [4]. Zahlreiche Anwendungen betreffen vielmehr die Untersuchung von Körperflüssigkeiten für die klinische Diagnose mit einer Raman-Anregung im nahen infraroten Spektralbereich. Bei der Serum-, Blutplasma oder Urinanalyse ist es möglich, Konzentrationen vieler medizinisch wichtiger Analyten wie Glukose, Cholesterin oder Triglyceriden auf einem klinisch relevanten Niveau zu bestimmen [26, 29, 30, 60, 87]. Da verschiedene Krankheiten die Protein-Zusammensetzung des Blutplasmas verändern, bietet die relative Quantifizierung von Plasmabestandteilen die Möglichkeit, Informationen für neue diagnostische und prognostische Faktoren zu erhalten. Das Ziel der Untersuchungen dieses Kapitels stellt erstmalig einen innovativen Ansatz zur medizinischen Diagnose von Blutplasmaproben von Gesunden und Patienten einer entzündungs-assoziierten Gerinnungsstörung, in diesem Fall der thrombotischen Mikroangiopathie (TMA), mittels UVRR-Spektroskopie dar. Die Analyse von Plasmaproteinen, speziell die genaue Bestimmung von deren Konzentration oder Aktivität bzw. im Allgemeinen die molekulare Zusammensetzung der Probe, ist von entscheidender Bedeutung für die Diagnose von mit einer Entzündungsreaktion einhergehenden Gerinnungsstörung, sowie der Möglichkeit der Unterscheidung zu infektiösen Krankheiten wie Sepsis. Im Falle der thrombotischen Mikroangiopathie findet man bei erkrankten Personen von Willebrand Faktor (VWF)-Multimere einer veränderten Biofunktionalität vor; diese besitzen ein erhöhtes Molekulargewicht. Die konventionelle Blutplasmaanalyse beruht auf elektrophoretischen Methoden, die bis zu mehreren Tagen dauern können und somit für therapeutisches Monitoring ungeeignet sind. [MH8, MH9]

Um einen Fortschritt für eine schnellere Methode zur Blutplasmaanalyse zu erlangen, wird zur Gewährleistung einer zeitnahen Diagnose von Entzündungen, Gerinnungsstörungen oder Infektionen bzw. zum therapeutischen Monitoring dieser Erkrankungen ein neues

Verfahren unter Verwendung der Raman-Spektroskopie in Kombination mit chemometrischen Datenanalysemethoden vorgestellt. In dieser Studie werden in Kooperation mit Dr. Ralf Claus von der Klinik für Anästhesiologie und Intensivtherapie der Friedrich-Schiller-Universität Jena kryopräzipitierte Blutplasmaproben von gesunden Spendern und Patienten mit thrombotischer Mikroangiopathie mit Hilfe der UV-Resonanz-Raman-Spektroskopie charakterisiert und identifiziert. Gegenwärtige Studien zur Blutplasmaanalyse bedienen sich der FTIR-Spektroskopie oder Raman-Spektroskopie mit einer Anregung im nahen infraroten Spektralbereich [26,29,87,88]. Durch die Raman-Anregung im tiefen UV-Wellenlängenbereich bei 244 nm werden die Raman-Signale der in den Blutplasma-Kryopräzipitaten angereicherten spezifischen Proteine - der von Willebrand Faktor-Multimere - sensitiv und selektiv in ihrer biologischen Umgebung verstärkt. Mit Hilfe von verschiedenen chemometrischen Klassifizierungsmethoden, wie der hierarchischen Clusteranalyse und der Hauptkomponentenanlyse, kann erstmals eine effektive und zuverlässige Differenzierung der UVRR-Spektren von Blutplasmaproben gesunder Spender und Patienten gezeigt werden. Diese Studie präsentiert die Leistungsfähigkeit der UV-Resonanz-Raman-Spektroskopie als eine innovative Methode zur Blutplasmaanalyse und darin enthaltenen proteinogenen Bestandteilen ohne aufwändige Probenpräparation. Durch die Vermessung von in Kryropräzipitaten enthaltenen proteinogenen Bestandteilen können anhand der Raman-Spektren deren Zusammensetzung charakterisiert werden und Präparationsfehler aufgedeckt werden. Zukünftige Untersuchungen streben einen UV-Resonanz-Ramanspektroskopischen Datenbankaufbau an, die Referenzdaten enthält. Dies umfasst einerseits Daten von gesunden Spendern, andererseits von auf einer Entzündung beruhenden Patientendaten, die verschiedene Krankheitsstadien aufweisen. Ziel hierbei ist es, unbekannte Proben sofort nach Probennahme anhand dieser Referenzdatenbank als gesund oder krank mit Feststellung des Schweregrades der Entzündungsreaktion zu identifizieren. Des Weiteren gibt es die Möglichkeit, die Datenbank mit Referenzdaten von infektiösen Krankheiten, wie Sepsis, zu erweitern, bei der Mikroorganismen beiteiligt sind. Da beide Krankheitsbilder ähnliche Symptome zeigen und eine Sepsis oft zu spät erkannt wird, wäre eine zuverlässige und rechtzeitige Abgrenzung einer Entzündung von einer Sepsis für die klinische Diagnostik erstrebenswert. [MH8, MH9]

Eine weitere Ausnutzung der hohen Selektivität und Sensitivität für DNA/RNA- und Protein-Schwingungen mittels UV-Resonanz-Raman-Spektroskopie liegt in der minimalinvasiven Identifizierung des Vogelgeschlechts anhand der unterschiedlichen DNA-Menge.

Die Bestimmung des Vogelgeschlechts ist bei Vogelzüchtern bei der Einrichtung von Brutpaaren oder Schwärmen für eine erfolgreiche Vogelvermehrung bzw. Züchtung ein entscheidender Faktor. Für die Geflügelindustrie ist die Feststellung des Vogelgeschlechts aus ökonomischen Gründen aufgrund unterschiedlicher Fütterungsgewohnheiten wichtig. Im Gegensatz zu Säugetieren besitzen Vögel keine äußerlich sichtbaren Geschlechtsorgane. Im Allgemeinen kann aber häufig eine Unterscheidung des Geschlechts anhand sekundärer verhaltenstypischer oder morphologischer Parameter wie beispielsweise der Körpergröße, Stirnhöcker oder des Gefieders vorgenommen werden. Beispielsweise besitzt der Erpel ein farbenprächtiges Federkleid, während das Weibchen nur ein unscheinbares Gefieder aufweist. Bei bestimmten Vogelarten wie Großpapageien, bei jungen Vögeln oder auch im embryonalen Stadium ist die Geschlechtsunterscheidung anhand äußerer phänotypischer Merkmale hingegen nicht so einfach. Hierbei kommen oft molekulargenetische oder endoskopische Verfahren bzw. Blutanalysen zum Einsatz [89–92]. Allerdings birgt die Blutentnahme bzw. Narkose immer eine Gefahr für das Tier. Dieses Gesundheitsrisiko sollte bei teuren Großpapageienarten vermieden werden. Eine günstigere und stressfreie Methode zur Geschlechtsidentifzierung stellt die UV-Resonanz-Raman-Spektroskopie dar, die nicht-invasiv arbeitet. [MH10]

Im Rahmen dieses Forschungsprojektes in Kooperation mit Dr. Thomas Bartels von der Klinik für Vögel und Reptilien der Universität Leipzig wird im folgenden Kapitel der Arbeit untersucht, inwieweit die UV-Resonanz-Raman-Spektroskopie eine geeignete Methode für die neuartige Geschlechtsbestimmung von Vögeln am Beispiel der Vogelart Haushuhn (*Gallus gallus domesticus*) darstellt. Hierbei erfolgt die Raman-spektroskopische Analyse des Federpulpamaterials aus einer im Wachstum befindlichen Feder. Die erstmals an Vogelfedern durchgeführten UVRR-spektroskopischen Untersuchungen haben eine 95%ige Bestimmung des Geschlechts anhand des Raman-Spektrums mit Hilfe von statistischen Klassifikationsmethoden, wie unüberwachter Klassifizierungsmethoden, der hierarchischen Clusteranalyse und der Hauptkomponentenanalyse sowie eines überwachten Klassifizierungsalgorithmus', der Support-Vektor-Maschine, gezeigt. Weiterhin wird zur Charakterisierung der Zusammensetzung der Federpulpaextrakte der Einfluss der durch die Raman-Anregung mit UV-Strahlung selektiv verstärkten Federbestandteile, wie Proteine und DNA, untersucht. Mit Hilfe einer Hauptkomponentenanalyse können außerdem 13 verschiedene, für eine Geschlechtsbestimmung entscheidende, spektrale Bereiche zwischen 1660 und 1336 cm^{-1} festgestellt werden. Durch Kombination der UVRR-Spektroskopie mit einer Hauptkomponentenanalyse wird das Potential der neuen Methode deutlich. Es zeigt sich neben der erfolgreichen Geschlechtsunterscheidung am Beispiel des Haushuhns, dass nur 3 Hauptkomponenten, die bereits 83% der Datensatzvariation

beschreiben, für eine zuverlässige Differenzierung zwischen männlichem und weiblichem Federpulpamaterial ausreichend sind.
Im Zuge des Projektes soll zukünftig die Referenzdatenbank auch bezüglich weiterer Vogelarten erweitert werden, so dass durch einen Vergleich der Raman-Spektren auf der Basis dieser Datenbank eine Geschlechtsbestimmung von unbekannten Federpulpaproben vorgenommen werden kann. Zusätzlich ist eine Optimierung bezüglich Probenpräparation und Vermessung angedacht, damit daraus eine erhöhte Genauigkeit der Geschlechtsbestimmung in dem Bereich der kommerziellen Akzeptanz von 98.5% resultieren kann. Ein weiterer Ansatz wäre eine Ausweitung der Methode auf die Legehennenzucht, so dass sich durch eine Geschlechtsbestimmung am Ei das routinemäßige Töten männlicher Küken vermeiden ließe. [MH10]

1.2 Eigene Forschungsergebnisse

1.2.1 Chemotaxonomische Klassifizierung von Mikroorganismen mittels Raman-Spektroskopie und statistischer Datenanalyse

Mikroorganismen sind allgegenwärtig - auf unserer Haut, in unserem Darm, im Boden und Wasser, in Lebensmitteln und in der Raumluft. In verschiedenen industriellen Bereichen, wie der Nahrungsmittelproduktion, der pharmazeutischen und chemischen Industrie, werden Bakterien und Hefen für die Herstellung von Joghurt, Käse, Alkohol, Antibiotika, Hormonen, Zitronensäure etc. genutzt. Allerdings sind Mikroorganismen auch für den Nahrungsmittelverderb verantwortlich z. B. in Fleischprodukten. In Operationssälen oder in Reinräumen kann schon die Anwesenheit einzelner Mikroben fatal sein. Mikrobielle Kontaminationen am Fließband im Reinraum der pharmazeutischen Produktion bzw. in Arzneimittelprodukten können aufgrund des Produktionsausfalls zu hohen Kosten führen [93].

Treten beispielsweise im Krankenhaus gefährliche Keime auf, müssen diese schnellstmöglich und eindeutig identifiziert werden. Hierbei ist es sehr wichtig, Krankheitserreger zuverlässig zu detektieren, um eine zeitnahe Diagnose zu realisieren, einen schnellen Therapiebeginn zu initiieren und um schließlich die Ausbildung von Antibiotikaresistenzen gegen die verabreichten Arzneimittel zu verhindern [94, 95]. Bei den gängigen mikrobiologischen Identifizierungstechniken ist eine Kultivierung auf verschiedenen Nährböden nötig. Die mikrobiologische Diagnose beginnt mit einer Isolation und Anreicherung der Bakterien, gefolgt von einer Gram-Färbung zur Unterscheidung zwischen Gram-positiven und Gram-negativen Bakterien, sowie einer ersten Differenzierung nach morphologischen Gesichtspunkten wie Form, Größe und physiologischen Tests. Mit diesen Tests sind Identifizierungsergebnisse anhand verschiedener Stoffwechselreaktionen und -produkte erst nach mehreren Tagen verfügbar [45, 95–97]. Die Verabreichung von Breitbandantibiotika als ersten Therapieschritt ist in diesem Sinne nicht zufrieden stellend, da die Rate von Antibiotika-resistenten Bakterienstämmen zunimmt [94]. Für eine effektive und erfolgreiche Behandlung ist eine zeitnahe und sichere Differenzierung der Krankheitserreger unabdingbar. Außerdem sind alternative Methoden zur Identifizierung von individuellen bakteriellen Kontaminationen auf Einzelzellebene wünschenswert. In diesem Zusammenhang wurden viele neue Methoden zur Mikroorganismenidentifizierung entwickelt, wie beispielsweise die Massenspektroskopie [45, 98], Polymerase-Ketten-Reaktion (engl.:

Polymerase Chain Reaction: PCR) [99–102], Durchflusszytometrie (engl.: *Fluorescence Activated Cell Sorting*: FACS) [102–105], Fluoreszenz-Spektroskopie [102, 105, 106] oder immunologische Verfahren [102, 104, 107]. Jedoch erfordern diese Tests ebenfalls Reinkulturen und sind nicht für alle Arten verfügbar [51, 107].

Schwingungs-spektroskopische Methoden, wie die FT-IR (Fourier-Transform Infrarot)- und Raman-Spektroskopie bieten hierfür als vielversprechende nicht-invasive Techniken die Möglichkeit, innerhalb einer sehr kurzen Zeit komplexe und genaue Informationen über die gesamte biochemische Zusammensetzung eukaryotischer und prokaryotischer Zellen zu erhalten. Die aus diesen Verfahren resultierenden Spektren können daher als spektraler 'Fingerabdruck' des jeweiligen Organismus' angesehen werden [108].
Ein Spezialfall der Raman-Streuung stellt die Resonanz-Raman-Streuung dar. Hier führt das einfallende Photon zu einem elektronisch angeregten Zustand des Moleküls. Ein solcher Vorgang ist zu beobachten, wenn die eingesetzte Anregungswellenlänge einer Absorptionsbande des Moleküls entspricht. Durch Lasereinstrahlung im UV-Wellenlängenbereich kommt es zur selektiven Raman-Streuung des Lichtes an chromophoren Segmenten bzw. Makromolekülen, wie beispielsweise aromatischen Aminosäuren (Tryptophan, Tyrosin, Phenylalanin und Histidin) in Proteinen und DNA/RNA-Bausteinen, während die restlichen Moleküle keinen wesentlichen Beitrag zum Raman-Spektrum liefern. Somit lassen sich wichtige Signale von Makromolekülen bzw. bestimmten Chromophorsegmenten innerhalb komplexer Systeme selektiv verstärken, wodurch eine sensitive und selektive genotypische Mikroorganismen-Identifizierung durchgeführt werden kann. Weiterhin wird durch die Resonanzverstärkung die Streuintensität um etwa 10^6 erhöht. Aufgrund dieser Überlegungen sind zahlreiche Untersuchungen zur Klassifizierung von Bakterienschichten bei einer Laseranregungswellenlängen im Bereich von 250 nm durchgeführt worden [70, 73, 74, 77, 78]. Die dafür genutzte Wellenlänge liegt im Bereich der starken elektronischen Absorptionsbanden der untersuchten Moleküle. Diese UV-Anregungswellenlängen führen neben der Resonanzverstärkung, auch zu einer erheblichen intrinsischen Verstärkung des Streuprozesses, womit das Signal-Rausch-Verhältnis verbessert wird.
Bei der Raman-Anregung im sichtbaren Wellenlängenbereich erhält man biomolekulare Informationen von Wasser, DNA/RNA, Proteinen, Kohlenhydraten und Lipiden der zu analysierenden Zelle. Die bei einer Anregung im sichtbaren Spektralbereich erhaltenen Mikro-Raman-Spektren liefern hochspezifische biochemische Informationen als Ergebnis aus der Überlagerung der gesamten zellulären Bestandteile. Infolgedessen erreicht

man eine phänotypische Identifizierung [43]. Aufgrund der Schnelligkeit und Empfindlichkeit schwingungs-spektroskopischer Methoden zur Charakterisierung und Differenzierung biologischer Systeme gewinnen diese in den letzten Jahren immer mehr an Bedeutung. Speziell in der mikrobiologischen Klassifizierung haben die FT-IR-Spektroskopie [109–114] und die Raman-Spektroskopie große Erfolge verbucht [13, 95, 108, 115–117]. Gegenwärtig können Raman-Spektren erfolgreich eingesetzt werden, um zwischen verschiedenen mikrobiellen Arten und Stämmen in Zellschichten und Mikrokolonien zu differenzieren [12, 25, 49, 118]. Jedoch sind für die Untersuchung an Schichten und Mikrokolonien Kultivierungsschritte von mindestens 6 Stunden erforderlich [95, 96]. Daher besteht ein großes Interesse an der Analyse von einzelnen Zellen direkt nach der Abscheidung der Partikel, wie dies beispielsweise im Reinraum oder in der Umgebung der Lebensmittelverarbeitung durchgeführt wird. Mit Hilfe der Mikro-Raman-Spektroskopie mit einer Anregungswellenlänge im sichtbaren Spektralbereich ist es aufgrund der hohen räumlichen Auflösung von etwa 1 μm möglich, einzelne Bakterienzellen zu analysieren [50, 119] und mit Hilfe statistischer Mustererkennungsalgorithmen zu klassifizieren [47]. Damit entfallen zeitaufwändige Kultivierungsschritte, die unter anderem bei konventionellen mikrobiologischen Identifizierungsmethoden zur Zellanreicherung und Identifizierung nötig sind.

Im Rahmen des Biophotonik-Projektes OMIB (Online-Monitoring und Identifizierung von Bioaerosolen) werden in Kooperation mit dem Institut für Informatik der Universität Freiburg, dem Fraunhofer Institut für Produktionstechnik und Automatisierung, der rap.ID particle systems GmbH, der Kayser-Threde GmbH, der Schering AG sowie dem Institut für Photonische Technologien (IPHT) Jena bei der Reinraumproduktionsüberwachung neue Maßstäbe in der schnellen Erregeridentifizierung bei Diagnose und Therapie mittels Raman-spektroskopischer Methoden gesetzt. Das Ziel besteht dabei in der Minimierung von möglichen Gesundheitsrisiken als auch Produktionsausfallzeiten [43]. Von dem im Reinraum auf einem geeigneten Träger abgeschiedenen Bakterien sind die Wachstumsbedingungen und das Alter völlig unbekannt. Unterschiedliche Kultivierungsbedingungen führen zu einer Variabilität der biochemischen Zusammensetzung der Zellen, die im Raman-Spektrum wiedergegeben werden. Für eine erfolgreiche Klassifizierung ist es also entscheidend zu wissen, ob die Variationen aufgrund des Metabolismus während der verschiedenen Wachstumsphasen gering oder sogar vernachlässigbar, verglichen mit den beobachtbaren Unterschieden zwischen den verschiedenen Stämmen, sind. Demzufolge ist es von äußerster Bedeutung, eine große Vielfalt von verschiedenen Kultivierungsparametern auf die Identifizierungsfähigkeit zu untersuchen. Dieser Sachverhalt wird in diesem Teil der Arbeit aufgegriffen, der die Identifizierung von Bakterienschichten und einzelnen

Bakterienzellen anhand ihres Raman-Spektrums beinhaltet. Es wird die Leistungsfähigkeit der Kopplung der Raman-Spektroskopie mit verschiedenen statistischen Klassifizierungsmethoden, wie der hierarchischen Clusteranalyse, gezeigt und erstmalig das Potential der Support-Vektor-Maschine auf einen heterogenen komplexen Datensatz studiert. Gegenstand dieser Untersuchungen sind Bakterienausstriche. Dabei erfolgt vorher die Kultivierung von verschiedenen Bakterienstämmen auf Agarplatten. Hierzu werden Bakterien mit einer Impföse auf einem Quarzträger ausgestrichen und deren Raman-Spektren aufgenommen. Bei der Kultivierung auf Agarplatten findet man eine Mischung von Zellen vor, die verschiedenen physiologischen Stadien angehören, bei denen die Wachstumsphasen nicht definiert sind. Im Gegensatz dazu liegt bei der Kultivierung der Bakterien in Flüssigkulturen vorrangig eine homogene physiologische Kultur vor.

Genotypische Klassifizierung von Bakterienschichten mittels UV-Resonanz-Raman-Spektroskopie

Zunächst werden Bakterienschichten mit Hilfe der UV-Resonanz-Raman-Spektroskopie studiert. Die Lasereinstrahlung im UV-Wellenlängenbereich liegt im Bereich der starken elektronischen Absorptionsbanden von Makromolekülen bzw. bestimmten Chromophorsegmenten, wie beispielsweise aromatischen Aminosäuren (Tryptophan, Tyrosin, Phenylalanin und Histidin) in Proteinen und DNA/RNA-Bausteinen. Bei dieser Anregungswellenlänge werden diese Signale innerhalb komplexer Systeme selektiv verstärkt, während die restlichen Moleküle keinen wesentlichen Beitrag zum Raman-Spektrum liefern. Somit kann eine sensitive und selektive genotypische Mikroorganismen-Identifizierung durchgeführt werden.
Diese UV-Anregungswellenlängen führen neben der Resonanzverstärkung und erheblichen intrinsischen Verstärkung des Streuprozesses bei Verwendung einer Wellenlänge im Bereich um 250 nm zu einer Fluoreszenzanregung. Ein Raman-Spektrum über einen Bereich von 4000 cm^{-1} erstreckt sich bei dieser Anregungswellenlänge über einen Bereich von etwa 30 nm oberhalb der Raman-Anregungswellenlänge. Die Raman-Signale werden nicht von Fluoreszenzemissionsbanden überlagert, da diese im sichtbaren Wellenlängenbereich liegen. Durch die separierten Raman- und Fluoreszenzsignale können gut aufgelöste, fluoreszenzfreie Raman-Spektren von Bakterienschichten erzielt werden [73]. Die UV-Resonanz-Raman-Spektroskopie kann zur Bestimmung der relativen Anteile der Nukleinsäurezusammensetzung von beispielsweise *E. coli* bei wohl definierten Wachstumsphasen verwendet werden [70]. In Kombination mit der hierarchischen Clusteranalyse und Hauptkomponentenanalyse ist die UVRR-Spektroskopie gegenwärtig zur Klassifizierung

von verschiedenen Bakterienarten angewendet worden [72, 79]. Hierbei kann das Klassifizierungspotential allerdings nur für eine limitierte Anzahl von Arten gezeigt werden.

Im Rahmen des Biophotonik-Projektes OMIB (Online-Monitoring und Identifizierung von Bioaerosolen) wird in dieser Studie die UV-Resonanz-Raman-Spektroskopie mit einer Anregungswellenlänge von 244 nm angewendet. Diese Anregungswellenlänge wird von einem frequenzverdoppelten Argon-Ionen-Laser (Innova 300, FReD) erzeugt, der bei Fokussierung auf die Probe eine Laserleistung von etwa 1-2 mW besitzt. In Verbindung mit einer Support-Vektor-Maschine erfolgt die genaue Differenzierung von Bakterienschichten auf Art- und Stammebene. Dabei sind 34 verschiedene in Reinraum-Umgebung vorhandene Bakterienstämme untersucht worden, die 9 verschiedenen Arten anghören. Die UV-Laserstrahlung besitzt eine relativ hohe Energiedichte. Daher können biologische Proben sehr leicht photochemisch bzw. photothermisch zerstört werden. Infolgedessen ist bisher keine Analyse von einzelnen Bakterienzellen, sondern nur von Bakterienschichten von etwa 10^4 bis 10^5 Zellen [86] möglich [120, 121]. Zur Minimierung der photochemischen Degradation wird die Probe unter dem Laserstrahl bewegt.
Die UVRR-Spektren von 34 Stämmen (Abb. 3 in [MH1]) können mit Hilfe der Support-Vektor-Maschine (SVM) klassifiziert werden. Tab. 2 in [MH1] zeigt die Klassifizierungsergebnisse mittels SVM. Die geringste mittlere Erkennungsrate ist auf Stammebene für *E. coli* mit 96.4% ermittelt worden. Alle anderen Stämme zeigen höhere mittlere Erkennungsraten, sowohl auf Stamm- als auch auf Artebene. Insgesamt kann für die Untersuchung von Bakterienschichten eine mittlere Erkennungsrate von 98.7% auf Stammebene bzw. 99.9% auf Artebene erreicht werden. [MH1]

Die Einstrahlung von UV-Laserlicht bei der Anwendung der UVRR-Spektroskopie führt zu einer photochemischen Zerstörung der untersuchten biologischen Proben. Damit ist gegenwärtig eine geplante Einzelzellanalyse von im Reinraum vorhandenen Mikroorganismen nicht realisierbar. Im Folgenden wird zur Vermeidung der Verbrennung der Probe die Raman-Anregungswellenlänge gewechselt. Gegenstand der folgenden Kapitel ist die Analyse von Bakterienzellen mit einer Raman-Anregungswellenlänge im sichtbaren Spektralbereich.

Phänotypische Klassifizierung von Bakterienschichten mittels Mikro-Raman-Spektroskopie

In diesem Kapitel erfolgt zur generellen Überprüfung der Funktionalität dieser Methode zur Einzelzellanalyse die Untersuchungen mit einer Anregung im sichtbaren Spektralbereich. Im Rahmen dieser Untersuchungen findet die Mikro-Raman-Spektroskopie (HR LabRam invers system, Jobin Yvon, Horiba, Bensheim, Deutschland) Anwendung. Als Raman-Anregungswellenlänge dient die 532 nm Laserlinie eines frequenzverdoppelten Nd:YAG, der bei Fokussierung auf die Probe eine Laserleistung von etwa 2,4 mW besitzt. Zunächst werden Analysen zur Charakterisierung und Differenzierung von Bakterienschichten auf einen ausgewählten Datensatz von Bakterien der Gattung Staphylococcus durchgeführt. Die Klassifizierung der verschiedenen Bakterienstämme anhand ihres Raman-Spektrums erfolgt durch verschiedene chemometrische Methoden, wie der hierarchischen Clusteranalyse. Erstmalig wird das Klassifizierungspotential der Support-Vektor-Maschine auf einen heterogenen und komplexen Datensatz studiert. Bei der Analyse von Bakterienschichten resultiert das Raman-Spektrum aus dem gemittelten Signal über verschiedene physiologische Stadien der Bakterien (Abb. 2 in [MH2]).
Insgesamt können für die Untersuchung von Bakterienschichten der Gattung Staphylococcus mit Hilfe der hierarchischen Clusteranalyse 97.0% der Bakterien auf Stammebene bzw. 97.7% auf Artebene Raman-spektroskopisch richtig zugeordnet werden (Abb. 3 in [MH2]). Mittels Support-Vektor-Maschine kann eine mittlere Erkennungsrate von 94.9% auf Stammebene bzw. 97.0% auf Artebene erreicht werden (Tab. 3 in [MH2]).

In weiterführenden Experimenten wird für die Anwendung dieser schnellen, nicht zerstörenden und zuverlässigen Identifizierungsmethode von Mikroorganismen als Einzelpartikel der Datensatz erweitert. Hierfür erfolgt die Einrichtung einer größeren Raman-spektroskopischen Datenbank mit mehreren Bakterienstämmen bezüglich der in der Reinraumproduktionskontrolle vorhandenen möglichen Kontaminationsquellen. Auf diese Referenzdaten kann dann bei der Identifizierung von unbekannten mikrobiellen Keimen zurückgegriffen werden.
Mittels Raman-Spektroskopie und Support-Vektor-Maschine wird bei der Analyse des gesamten Datensatzes von 339 Raman-Spektren von Bakterienschichten (Abb. 2 in [MH3]), die 20 verschiedenen Stämmen und 9 Arten angehören, eine mittlere Erkennungsrate von 98.0% (332/339 Raman-Spektren) auf Stammebene bzw. 98.9% (335/339 Raman-Spektren) auf Artebene (Tab. 1 in [MH3]) erreicht.

Phänotypische Klassifizierung von einzelnen Bakterienzellen mittels Mikro-Raman-Spektroskopie

Für die Untersuchung von Bakterienschichten benötigt man eine Kultivierung von mindestens 6 Stunden, um genug biologisches Material und somit auch Spektren mit einem guten Signal-Rausch-Verhältnis zu erhalten. Um jedoch eine Beschleunigung im Klassifizierungsprozess zu realisieren, ist die Identifizierung diverser Spezies und Stämme an Einzelzellen vorzuziehen. Die Untersuchung von einzelnen Bakterienzellen zeigt, dass aufgrund der fehlenden Kompartimentierung innerhalb der Zelle eine räumliche Homogenität besteht. Das heißt, man erhält vergleichbare Raman-Spektren, unabhängig davon, an welcher Messposition innerhalb der Zelle die Messung erfolgt (Abb. 3 in [MH3]). Somit ist es möglich, einzelne Bakterienzellen anhand eines Spektrums zu charakterisieren und zu identifizieren.

Im Folgenden werden einzelne Bakterienzellen zunächst der Gattung Staphylococcus Raman-spektroskopisch analysiert, wodurch auf den bisher zur Differenzierung von Bakterienschichten notwendigen Kultivierungsschritt verzichtet werden kann. Ein Mikroskopbild eines Ausstrichs einzelner Bakterienzellen auf Quarz ist in Abb. 1 in [MH2] dargestellt, während Abb. 4 in [MH2] repräsentative Mikro-Raman-Spektren von einzelnen Bakterienzellen zeigt.
Die Umgebungsbedingungen und Wachstumsparameter einer im Reinraum aufgefundenen Kontaminationsquelle sind unbekannt und können deren Klassifizierung auf Art- und Stammebene erschweren. Infolgedessen müssen wachstumsabhängige intra-Stamm spezifische Variationen der zu untersuchenden Bakterienzelle bei deren Identifizierung mit in Betracht gezogen werden. Unterschiedliche Kultivierungsbedingungen führen zu einer veränderten biochemischen Zusammensetzung der Zelle und folglich zu einen charakteristischen Raman-Spektrum (Abb. 6 in [MH2]). Anhand der Zell-spezifischen Raman-Spektren wird der Einfluss verschiedener Kultivierungsbedingungen (Nährstoffangebot, Temperatur und Kulturalter) auf die chemotaxonomische Klassifizierungsfähigkeit von einzelnen Bakterienzellen analysiert. Allerdings kann mit Hilfe der hierarchischen Clusteranalyse keine Klassifizierung dieses komplexen Datensatzes vorgenommen werden, so dass eine Trennung der Bakterienstämme bzw. Arten in separaten Gruppen möglich gewesen wäre. Vielmehr kann das großartige Potential der SVM als eine überwachte statistische Methode gezeigt werden, die eine Unterscheidung dieses heterogenen Datensatzes einzelner verschieden kultivierter Bakterienzellen zu 94.1% (1248/1280 Raman-Spektren) auf Stamm- und zu 97.6% (1266/1280 Raman-Spektren) auf Artebene Tab. 4 in [MH2] erlaubt. Die aus verschiedenen Kultivierungsbedingungen resultierenden Variationen im

Raman-Spektrum der einzelnen Bakterienzellen stören folglich nicht die chemotaxonomische Klassifizierungsfähigkeit der Bakterien der Gattung Staphylococcus. [MH2]

Durch die signifikante Unterscheidung von Arten und Stämmen, sogar für einzelne Bakterien bei verschiedenen Wachstumsphasen und Wachstumsbedingungen anhand eines ausgewählten Datensatzes der Gattung Staphylococcus ist im vorangegangenen Abschnitt gezeigt worden, dass sich die Raman-Spektroskopie mit Einbeziehung des statistischen Mustererkennungsalgorithmus' der Support-Vektor-Maschine als empfindliche und aussagekräftige Technik zur Einzelzellanalyse erweist.
Um im Folgenden im Reinraum auftretende mikrobielle Keime identifizieren zu können, wird für diese schnelle und zuverlässige Raman-spektroskopische Identifizierungsmethode der Datensatz an Einzelzellspektren erweitert. In Abb. 8 in [MH3] sind repräsentative Raman-Spektren einzelner Bakterienzellen von 9 Bakterienstämmen dargestellt. Zur Erhöhung der möglichen Variabilitäten werden erneut wachstums-charakteristische Raman-Spektren einzelner Bakterien mit in die Datenbank aufgenommen. Weiterhin erfolgt die Untersuchung von *Bacillus* Stämmen, die zur Sporenbildung befähigt sind. Dazu werden Raman-Spektren von vegetativen Zellen (Abb. 6 A in [MH3]) und Endosporen mit in die Datenbank integriert (Abb. 4 und 5 in [MH3]). Zusätzlich zu bisher betrachteten chromophorlosen Bakterienstämmen, können im Reinraum häufig gelb pigmentierte Bakterienarten von *M. luteus* auftreten. Deren Raman-Spektren weisen typische Carotinoidbanden von Sarcinaxanthin auf (Abb. 6 B in [MH3]), deren Intensität durch Laserbestrahlung mit der 532 nm Laserlinie aufgrund von Bleichungseffekten abnimmt (Abb. 7 in [MH3]). Daraus resultiert eine erhöhte Variation der Raman-Spektren, was zu einer erschwerten Identifizierung von unbekannten Mikroorganismen führt. Insgesamt kann mit Hilfe der Support-Vektor-Maschine von 2257 Raman-Spektren einzelner Zellen, die 20 verschiedenen Stämmen und 9 Arten angehören, eine mittlere Erkennungsrate von 89.2% (2136/2257 Raman-Spektren) auf Stammebene bzw. 93.6% (2180/2257 Raman-Spektren) auf Artebene (Tab. 2 in [MH3]) erzielt werden, was mit herkömmlich eingesetzten mikrobiologischen Verfahren vergleichbar ist. [MH3]

Phänotypische Klassifizierung von einzelnen Hefezellen mittels Mikro-Raman-Spektroskopie

Dieses neuartige Verfahren zur Detektion und Identifizierung von Mikroorganismen in Reinraumumgebung umfasst neben der Unterscheidung von prokaryotischen Bakterienzellen zusätzlich eine Differenzierung von eukaryotische Hefezellen. Prokaryoten besitzen

im Unterschied zu Eukaryoten keinen Zellkern; die Erbinformation findet man als genomische DNA und falls vorhanden als Plasmid DNA, in beiden Fällen in ringförmiger Form innerhalb der Zelle vor. Das Zytoplasma der Eukaryoten ist wie bei Prokayoten von einer Zellmembran umgeben. Jedoch sind bei Eukaryoten in dieses Zytoplasma eine Fülle von Membransystemen eingeschlossen, die unter anderem als endoplasmatisches Retikulum, Vesikel und Mitochondrien eigene, vom Zytoplasma abgegrenzte Reaktionsunterräume, sogenannte Organellen, darstellen [52, 53]. Durch diese Kompartimentierung weisen eukaryotische Zellen eine ausgeprägte räumliche Heterogenität auf. Aufgrund der Zellgröße von ca. 10 μm im Durchmesser im Vergleich zum effektiven Messvolumen des Mikro-Raman-Spektrometers von etwa 1 μm ist es demzufolge unzureichend, diese Zellen im Gegensatz zu prokaryotischen Zellen (Zellgröße von ca. 1 μm) mit Einzelspektren zu charakterisieren bzw. zu klassifizieren. Zur Analyse von einzelnen Hefezellen sind Raman-*Mapping*-Experimente in Kombination mit chemometrischer Auswertung unumgänglich, um in lateraler und auch axialer Richtung das gesamte Zellvolumen spektroskopisch zu erfassen bzw. um auf bestimmte Zellbereiche oder Komponenten, wie DNA, Proteine oder Lipidbestandteile zu fokussieren. In diesem Zusammenhang erfolgt eine Charakterisierung von Reinraum-relevanten Hefezellen auf Einzelzellebene anhand von Raman-*Mapping*-Experimenten. Bildtafel 1 (A) in [MH4] zeigt repräsentative Raman-Spektren, die bei der Kartierung von zwei in Bildtafel 1 (B) in [MH4] dargestellten Hefezellen an den indizierten Messpositionen aufgenommen worden. Die in Bildtafel 1 (C)-(F) in [MH4] angezeigten Falschfarbenbilder resultieren aus der Integration der Raman-Intensität bestimmter Markerbanden und liefern demzufolge Rückschlüsse über die räumliche Verteilung dieser Substanzen. Mittels hierarchischer Clusteranalyse kann eine Klassifizierung von einzelnen Hefezellen dreier Hefearten auf Stammebene vorgenommen werden. Dabei werden 60 Mittelwert-Raman-Spektren der Hefezellen verwendet, die aus der Mittelwertbildung von 10 statistisch ausgewählten Raman-Spektren (Abb. 1 (A) in [MH4] innerhalb einer Zelle resultieren. Im berechneten Dendrogramm (Abb. 1 (B) in [MH4]) zeigen die zwei *S. cerevisiae* Stämme eine größere Homogenität innerhalb der Cluster, sowie eine größere Ähnlichkeit zueinander als zur Trockenhefe. [MH4]

In weiteren Experimenten erfolgt die Anwendung der Mikro-Raman-Spektroskopie in Kombination mit der Support-Vektor-Maschine auf einen größeren Datensatz von 8 verschiedenen Hefestämmen. Um hierbei die variierenden Informationen der gesamten Hefezelle aufgrund deren Heterogenitätsstruktur einzubeziehen, werden Linienscans entlang der Hauptachse der Zelle durchgeführt (Abb. 1 in [MH5]). In Abb. 2 in [MH5] sind Mittelwert-Raman-Spektren von 10 bis 18 Einzelzellspektren dargestellt, die für die Differenzierung auf Art- und Stammebene mittels Support-Vektor-Maschine herangezogen

werden. Von 92 Mittelwert-Raman-Spektren wird eine mittlere Erkennungsrate von 86.2% auf Stammebene bzw. 94.8% auf Artebene (Tab. 1 in [MH5]) erreicht, was im Bereich der Genauigkeit gegenwärtig eingesetzter mikrobiologischer Methoden liegt. [MH5]

Gesamtkonzept zur Identifizierung von Mikroorganismen in Reinraumumgebung der pharmazeutischen Produktion

Zur Gewährleistung einer Online-Überwachung, inklusive Detektion und Identifizierung von so genannten Bioaerosolen in der pharmazeutischen Produktion unter Reinraumbedingungen, ist eine Vorselektion der zu klassifizierenden biologischen Partikel notwendig, um die Analysezeit zu minimieren. Abb. 1 (C) in [MH6] veranschaulicht schematisch das sogenannte OMIB-Prinzip zum Online-Monitoring und der Identifizierung von Bioaerosolen. Nach Abscheidung der biologischen (biotischen) und abiotischen Partikel (wie Staub, Gummiabrieb, etc.) aus der Luft, erfolgt die Aufnahme eines Weißlicht-Mikroskopbildes. Dieses gibt eine Aussage über die Größe, Struktur und Verteilung der vorhandenen Kontaminationen, wobei lediglich Partikel biologischen Ursprungs identifiziert werden müssen. In einem weiteren Schritt erfolgt eine Vorselektion der relevanten, zu differenzierenden mikrobiellen Infektionskeime. Dies geschieht anhand unterschiedlicher Autofluoreszenzeigenschaften zwischen biotischen und abiotischen Partikeln (Abb. 2 und 3 in [MH6]). Mittels Fluoreszenz-Monitoring kann zwischen biotischen und abiotischen Partikeln unterschieden werden. Schließlich kann im Anschluss daran mit Hilfe der Raman-Spektroskopie in Kombination mit statistischen Datenauswerteverfahren eine chemotaxonomische Identifizierung, ohne Zeitverzögerung innerhalb weniger Stunden, ermöglicht werden. Repräsentative Mikro-Raman-Spektren von einzelnen Bakterienzellen sind in Abb. 4 in [MH6] dargestellt. Für eine zuverlässige Datenanalyse ist die Verwendung von lernfähigen chemometrischen Methoden, wie die Support-Vektor-Maschine, notwendig. Neben der Klassifizierung von Bakterien anhand einzelner Raman-Spektren, werden zusätzlich verschiedene Hefestämme, die häufig zu Kontaminationen im Reinraum führen, untersucht. Aufgrund der Heterogenität von Hefen werden keine Einzelzellspektren, sondern Mittelwert-Raman-Spektren diverser Hefestämme mit in den Datensatz integriert.
Von 3235 Raman-Spektren einzelner Bakterien- und Hefezellen, die 28 verschiedenen Stämmen und 10 Arten angehören, können 2951 Spektren auf Stammebene korrekt zugeordnet werden, was einer mittleren Erkennungsrate von 85.6% entspricht. Auf Artebene können 3164 korrekt zugeordnet werden (mittlere Erkennungsrate von 95.4%) (Tab. 1 in [MH6]). Diese Resultate sind denen gängiger eingesetzter mikrobiologischer Differenzierungsverfahren vergleichbar. Bisher vorgestellte Raman-spektroskopische Untersuchungen

dienten der Kalibrierung der Support-Vektor-Maschine. Dazu wird eine gewisse Anzahl von quasi bekannten Raman-Spektren zur Erstellung des Klassifikationsmodells mit Hilfe der Support-Vektor-Maschine verwendet, bei denen eine Zuordnung zum jeweiligen Bakterien- oder Hefestamm mit einfließt. Die verbleibenden Raman-Spektren werden unter Verwendung des vorher gewonnenen Modells klassifiziert und als Ergebnis dieses Kalibrierdatensatzes erhält man die sogenannte mittlere Erkennungsrate. Ziel weiterer Studien ist die Identifizierung von Raman-Spektren unbekannter, im Reinraum detektierter Mikroorganismen. Infolgedessen ist ein unabhängiger, aus 130 Raman-Spektren bestehender Datensatz von 16 verschiedenen Bakterienstämmen erstellt worden. Diese Stämme sind in dem Kalibrierdatensatz bereits enthalten. Diese Raman-Spektren wurden separat aufgenommen und dann mit dem Kalibrierdatensatz den entsprechenden Stämmen und Arten zugeordnet. Von 130 Raman-Spektren können 125 richtig identifiziert werden (Tab. 2 in [MH6]). Davon können 96.2% (125/130 Raman-Spektren) auf Stammebene und 98.5% (128/130 Raman-Spektren) auf Artebene korrekt zugeordnet werden.
Durch die Kopplung der Mikro-Raman-Spektroskopie mit der Weißlicht- und Fluoreszenzmikroskopie sowie der Support-Vektor-Maschine kann ein entscheidender Schritt zur zuverlässigen Online-Detektion und Identifizierung von Bioaerosolen gemacht werden. Die exzellente Unterscheidung von Arten und Stämmen, sogar für einzelne Bakterien, eröffnet neben der Reinraumproduktion vielversprechende Anwendungen in der Lebensmitteltechnologie und Medizin, bei der eine schnelle Erregeridentifizierung ohne zusätzliche vorherige Kultivierung zur Zellanreicherung erreicht werden kann. [MH6], [122–124]

Die vorangegangenen Ergebnisse zeigen, dass die Raman-Spektroskopie in Verbindung mit multivariater statistischer Datenanalyse, speziell der Support-Vektor-Maschine, ein einzigartiges Potential zur Klassifizierung von komplexen heterogenen Datensätzen besitzt. Die Mikro-Raman-Spektroskopie mit einer Raman-Anregungswellenlänge im sichtbaren Spektralbereich stellt einen geeigneten Ansatz für eine schnelle und vertrauenswürdige, nicht zerstörende Online-Identifizierung von einzelnen Mikroorganismen, wie Bakterien- und Hefezellen dar. Im Gegensatz zu dieser phänotypischen Differenzierung von einzelnen Zellen ist mit Hilfe der UVRR-Spektroskopie bezüglich hoher Sensititivität und Spezifität eine genotypische Unterscheidung von Bakterien und Hefen, bisher nur an Zellschichten, möglich. Um das Vermögen der UV-Resonanz-Raman-Spektroskopie als automatisierte genotypische Klassifizierungsmethode auf Einzelzellniveau auszunutzen, bedarf es weiterer Forschung.

1.2.2 Analyse von Blutzellen mittels Fluoreszenzmarkierung und Mikro-Raman-Spektroskopie für die Liquordiagnostik

Die Gehirn-Rückenmarks-Flüssigkeit (CSF) ist Hauptuntersuchungsgegenstand in der Diagnose von akuten und chronischen Krankheiten des Zentral-Nervensystems, beispielsweise bei der Identifizierung von bakteriellen, viralen oder durch Pilze hervorgerufene Infektionen, wie der bakteriellen Meningitis [125]. Die Gehirn-Rückenmarks-Flüssigkeit von gesunden Erwachsenen enthält normalerweise keine Erythrozyten und bis zu 5 Leukozyten pro μl. Der Wechsel von der gesunden klaren und farblosen Erscheinung des CSF zu einer veränderten Färbung und Trübung indiziert eine Liquordiagnose. Bei der Diagnostik zellulärer Bestandteile ist nicht nur die Identifizierung des Erregers bedeutend, sondern auch die Beurteilung der Leukozytenzahl und -arten über eine Zellzählung und Differenzierung in der ansonsten zellarmen Gehirn-Rückenmarks-Flüssigkeit.

Die Liquordiagnostik für die Diagnose von bakteriellen Infektionskrankheiten beruht u. a. auf der bakteriellen Differenzierung nach einer Kultivierung, wenn Bakterienzellen im Ausstrichpräparat ersichtlich sind. Gegenwärtige CSF-Diagnostikmethoden basieren in der Regel auf durchflusszytometrischen Analysen [126–128] und morphologischer Analyse, falls notwendig, nach einer Färbung von spezifischen Strukturen in fixierten Zellen [129].

Mittels Durchflusszytometrie können zwar Proben auch geringer Zellzahlen [130] bis auf das Niveau einzelner B- und T-Lymphozyten-Typen analysiert werden, allerdings nur mittels Immunophänotypisierung, die ihrerseits Probleme bereiten kann. Beispielsweise können dabei zu hohe Antikörperkonzentrationen zu vermehrter unspezifischer Färbung führen, zu geringe Konzentrationen hingegen zu einer nichtquantitativen Markierung vorhandener Epitope [131]. Auch eine hohe Autofluoreszenz der Zellen kann störend wirken. Verzichtet man auf die Immunofluoreszenztechniken bei der Durchflusszytometrie, ist die Befundlage rein auf morphologischen Eigenschaften des Zellbildes einer CSF-Probe nicht eindeutig: Hier kann eine granulozytäre Pleozytose (erhöhte Granulozytenzahl) für ein bakterielles Geschehen sprechen, jedoch findet sich dieser Befund auch bei Parasiten (Eosinophilie) oder in der Akutphase viraler Entzündungen wieder [132]. Weitere Hauptprobleme der labormedizinischen Diagnostik sind eine geringe Sensititivität (Gram-Färbung von Mikroorganismen korreliert mit der bakteriellen Konzentration) [133–135] und eine begrenzte Spezifität (bei malignen Blutzellen). Durch die Notwendigkeit einer hohen Zellzahl ist eine Anreicherung von bestimmten Zellpopulationen durch Kultivierung unabdingbar (Mikroorganismenkultivierung, klonale Anreicherung von Blutzellen) [136]. Weitere Schwierigkeiten der CSF-Diagnostik bestehen in der Abhängigkeit von der manuellen

CSF-Zytologie, die für die quantitative und qualitative Analyse von Blutzellen notwendig ist. Diese basiert auf der individuellen Variabiltät der Untersucher und einer hohen Personalbindung. Diese Faktoren stellen eine Beschränkung einer schnellen Identifizierung dar und können zu einer Therapieverzögerung führen.

Zur Überwindung dieser diagnostischen Komplikationen stellt die Mikro-Raman-Spektroskopie einen alternativen, verlässlichen methodologischen Ansatz für eine schnelle Charakterisierung und Differenzierung von biologischen Systemen dar. Die Raman-Spektroskopie kann zur Erforschung von einzelnen Zellen bzw. Makromolekülen mit einer räumlichen Auflösung im Submikrometerbereich herangezogen werden, da diese sogenannte *fingerprint*-Informationen über die chemische Zusammensetzung und Strukur im subzellulären Bereich liefert. Erste Raman-spektroskopische Untersuchungen an Körperzellen können eine Differenzierung zwischen Zellplasma und Zellkern an eosinophilen Granulozyten aufzeigen [137]. Auf Grundlage der Mikro-Raman-Spektroskopie wurden *Imaging*-Experimente erfolgreich in vielen Studien zur Aufklärung biologischer Prozesse durchgeführt, um Aussagen über die Verteilung und Zusammensetzung von Biomolekülen in noch lebenden Blutzellen treffen zu können [138–143]. Weiterhin sind mittels resonanter Mikro-Raman-Spektroskopie und *Mapping*-Experimenten intrazelluläre Reaktionen basierend auf dem NADPH-Oxidase-System in neutrophilen Granulozyten als Reaktion auf äußere Stimuli studiert worden [142, 144–148]. Durch verschiedene SERS-*Imaging*-Experimente können diverse Zielkomponenten in lebenden Einzelzellen verfolgt werden [149, 150].

Im Rahmen des DFG-Projektes PO 563/7-1 'Raman-spektroskopische Differenzierung und Identifizierung körpereigener Zellen und Mikroorganismen im Liquor für die medizinische Diagnostik' liegt der Schwerpunkt in der Entwicklung einer neuartigen Raman-spektroskopischen Analysemethode zur Erforschung von zellulären Bestandteilen in der Gehirn-Rückenmarks-Flüssigkeit bei bakterieller Meningitis. Dieses Verfahren soll eine rasche und zuverlässige Identifizierung von darin enthaltenen einzelnen Zellen wie Bakterien und Blutzellen auf Einzelzellniveau ermöglichen, die möglichst zeitnah zur Probennahme der Gehirn-Rückenmarks-Flüssigkeit erfolgen sollte. In enger Zusammenarbeit mit Prof. Dr. Thomas Deufel und Dr. Dr. Michael Kiehntopf vom Institut für Klinische Chemie und Laboratoriumsdiagnostik am Universitätsklinikum Jena und Prof. Dr. Eberhard Straube aus dem Institut für Medizinische Mikrobiologie werden spektroskopische Methoden weiterentwickelt bzw. die Grundlagen innovativer Techniken erforscht, die zu einer schnellen und zuverlässigen Identifizierung einzelner Bakterien- bzw. Blutzellen befähigt sind. Damit schwingungs-spektroskopische Methoden zur Differenzierung von Blutzellen aus dem CSF bei bakterieller Meningitis eingesetzt werden können, ist

zunächst ein Schwerpunkt dieser Arbeiten, die räumliche Verteilung und Lokalisierung der Inhaltsstoffe in Blutzellen mittels Mikro-Raman-Spektroskopie aufzuklären. Weiterhin wird über molekulare Informationen eine Charakterisierung der chemischen Zusammensetzung der zellulären Bestandteile vorgenommen. Im Rahmen dieser Forschungsarbeiten wird eine Kartierung mittels nicht-resonanter Raman-*Mapping*-Experimente bei einer Anregungswellenlänge von 532 nm auf zellulärer Ebene an einzelnen Leukozyten in Mikrometerauflösung durchgeführt. Da die Gehirn-Rückenmarks-Flüssigkeit nur wenige zelluläre Komponenten enthält, erfolgt mittels Zytozentrifugation eine Zellanreicherung. Abb. 1 (A) in [MH7] zeigt ein Mikroskopbild von Blutzellen, die durch Zytozentrifugation auf einen Quarzträger aufgetragen worden. Durch Vergleich der morphologischen Zellformen mit den in Abb. 1 (B) in [MH7] dargestellten Raman-Spektren verschiedener Blutzellen wird deutlich, dass keine eindeutige Zuordnung der Blutzelltypen in Erythrozyten und Leukozyten bzw. Leukozytenuntergruppen möglich ist. In der routinemäßig eingesetzten CSF-Diagnostik erfolgt die Differenzierung der verschiedenen Leukozytensubtypen mittels Pappenheim-Färbung über Form und Größe der angefärbten Granula (Abb. 2 (A) in [MH7]). Allerdings wird das Raman-Signal der Blutzellen von der Fluoreszenz der eingesetzten Farbstoffe überdeckt (Abb. 2 (B) in [MH7]). Um die Blutzellen sensitiv und selektiv in ihrer biologischen Umgebung zu lokalisieren und zu erforschen, wird die Fluoreszenzmarkierung in Kombination mit der Mikro-Raman-Spektroskopie angewendet. Diese Technik eröffnet das einzigartige Potential einer exakten und schnellen Zellidentifizierung von einer an sich zellarmen Gehirn-Rückenmarks-Flüssigkeit. Durch die Verwendung fluoreszenzmarkierter Antikörper ergibt sich die Möglichkeit, mit einem hohen Grad an Spezifität in einer Menge nicht fluoreszierender Zellen, spezifische Blutzellsubtypen direkt zu lokalisieren und zu identifizieren (Abb. 3 in [MH7]), während die Raman-Spektroskopie zusätzlich noch molekülspezifische *fingerprint*-Informationen enthält. In diesem Zusammenhang werden in einem ersten Schritt aus Vollblut isolierte Blutzellen als Modellsystem charakterisiert, die mit einem am Fluoreszenzfarbstoff FITC (Fluoreszeinisothiocyanat) gekoppelten Antikörper anti-CD15 markiert sind. Zielstellung liegt hierbei in der Erforschung von entscheidenden methodologischen Parametern bezüglich der Auswahl an fluoreszenzgefärbten Antikörpern, um eine spezifische Markierung diverser Blutzelltypen in Kombination mit der Raman-Spektroskopie zu ermöglichen. Diese Ergebnisse sollen dann auf die native CSF-Umgebung übertragen werden. Abb. 4 (A) und (B) in [MH7] stellt ein Hellfeldbild mit dem entsprechenden Fluoreszenzbild von, mit anti-CD15 Antikörper und FITC-konjugierten, markierten Leukozyten dar. Diese Leukozyten wurden zuvor durch die Behandlung mit einem Lysepuffer, der die Lyse von Erythrozyten bewirkt, aus Vollblut isoliert. Ein Vergleich der entsprechenden Raman-Spektren (Abb. 4

(C) in [MH7]) zeigt, dass die Raman-Spektren abhängig von der ausgewählten Messposition sind, d. h. man erhält unterschiedliche Raman-Spektren, je nachdem ob man die Zelle im Zentrum bzw. am Rand anvisiert. Es hat sich herausgestellt, dass die Raman-Spektren unabhänig davon sind, ob die Zellen fluoreszenzmarkiert sind oder nicht; man erhält ähnliche Raman-Spektren bei Verwendung des mit FITC konjugierten Antikörpers anti-CD15. Durch Vergleich des Raman-Spektrums des reinen FITC-gekoppelten anti-CD15 Antikörpers mit dem Mittelwert-Raman-Spektrum von fluoreszenzmarkierten Leukozyten (Abb. 5 in [MH7]) wird deutlich, dass dieser das Raman-Spektrum von fluoreszenzmarkierten Zellen nicht überlagert oder störend beeinflusst.

In einem weiteren Schritt werden Blutzellen untersucht, die aus der nativen Umgebung - der Gehirn-Rückenmarks-Füssigkeit - isoliert worden sind (Abb. 6 (A) in [MH7]). Es kann gezeigt werden, dass die aus Proteinen und Salzen bestehende CSF-Matrix die Anwendbarkeit der Raman-Spektroskopie nicht störend beeinflusst. Durch die Ramanspektroskopische Zellkartierung in lateraler und axialer Richtung kann die räumliche Verteilung von verschiedenen Makromolekülen wie DNA/RNA, Proteinen bzw. Lipiden (Abb. 6 (B) und (C) in [MH7]) innerhalb der Zellen visualisiert und aufgeklärt werden. Abb. 6 (D) in [MH7] zeigt deren rämliche Verteilung anhand von Falschfarbenbildern, die durch Integration über die Raman-Intensitäten der Marker-Banden von DNA/RNA, Protein bzw. Lipiden berechnet worden. Da diese Marker-Banden oft durch Überlagerung von anderen Signalen nicht unbedingt so deutlich ausgeprägt sind, wie in Abb. 6 (C) in [MH7] dargestellt, werden multivariate statistische Datenanalysemethoden zusätzlich zur Auswertung herangezogen. Mit Hilfe zweier unüberwachter chemometrischer Klassifizierungsverfahren, der hierarchischen Clusteranalyse (Abb. 7 (D) in [MH7]) und der Hauptkomponentenanalyse (Abb. 7 (E) in [MH7]), kann eine Differenzierung zwischen sub-mikroskopischen Komponenten innerhalb einer einzelnen Blutzelle, am Beispiel von Granulozyten, vorgenommen werden.

Im Rahmen dieses Projektes wird ein neuer Ansatz zur Analyse von einzelnen, aus der Gehirn-Rückenmarks-Flüssigkeit isolierten Blutzellen gezeigt, bei dem einmalig die simultane Anwendung der Raman-Spektroskopie nach vorangegangener spezifischer Fluoreszenzmarkierung an derselben Probe vereint ist. Diese Methode eröffnet ein neuartiges Potential zur Gewährleistung einer korrekten und schnellen Identifizierung von während einer bakteriellen Meningitis im CSF vorkommenden Blutzellen, das als biomedizinischer Assay in der klinischen Diagnostik Anwendung finden kann. [MH7]
Die verschiedenen Subtypen von Blutzellen varriieren in ihrer Zusammensetzung an subzellulären Bestandteilen wie Proteinen, DNA/RNA, Kohlenhydraten, Lipiden oder der

Anwesenheit von endogenen Farbstoffen. Aus diesem Grund sollte es bei zukünftigen Forschungsarbeiten möglich sein, mit Hilfe der Raman-Spektroskopie und chemometrischer Datenanalyse zwischen einzelnen Blutzellsubtypen durch Vergleich mit Raman-Spektren in einer Datenbank unterscheiden zu können. Aufgrund der subzellulären Heterogenität ist es nicht ausreichend, eine Blutzelle analog zu einzelnen Bakterienzellen mit einem einzigen Raman-Spektrum zu charakterisieren. Es müssen vielmehr alle möglichen Raman-Spektren bezüglich der vorhandenen subzellulären Strukturen in der Datenbank hinterlegt sein. Hierbei ist es angedacht, weitere fluoreszenzmarkierte Antikörper zur Erfassung von diversen Blutzellsubtypen, wie Monozyten oder Lymphozyten, zu testen bzw. um eine Aussage über zusätzliche Parameter, wie beispielsweise den Aktivierungsgrad von Granulozyten, treffen zu können. Bei letzterer Anwendung bietet sich für zukünftige Untersuchungen insbesondere von neutrophilen, eosinophilen und basophilen Granulozyten, eine Anregungswellenlänge von 414 nm zur Durchführung von Resonanz-Raman-*Mapping*-Experimenten an, da die in diesen Zellen lokalisierten Hämoproteine in diesem Wellenlängenbereich Absorptionsmaxima besitzen. Des Weiteren müssen die gefundenen methodologischen Parameter auf das Zielsystem, den im CSF auffindbaren Zellen, übertragen werden, die es ermöglichen mit einem geeigneten chemometrischen Klassifizierungsalgorithmus unbekannte Zellen zu identifizieren.

1.2.3 UV-Resonanz-Raman-spektroskopische Klassifizierung von Blutplasmaproben für die medizinische Diagnostik

Bei verschiedenen Krankheiten ist die Proteinzusammensetzung im Blutplasma verändert. Daher bietet die relative Quantifizierung von Blutplasmabestandteilen die Möglichkeit, Informationen über neue diagnostische und prognostische Faktoren zu erhalten. Ziel dieser Arbeit ist die Evaluierung eines neuen Verfahrens zur medizinischen Diagnose von entzündungsassoziierten Erkrankungen mittels Blutplasmaproben zwischen Gesunden und Kranken mit thrombotischer Mikroangiopathie (TMA) [151–153]. Nach bisherigem Wissensstand besteht bei Patienten mit entzündungs-assoziierten Gerinnungsstörungen, wie der thrombotischen Mikroangiopathie, eine deutliche Veränderung in der Konzentration, Aktivität bzw. allgemein in der molekularen Zusammensetzung von aus Multimeren aufgebauten Gerinnungsproteinen. Man findet bei an TMA erkrankten Personen von Willebrand Faktor (VWF)-Multimere [154] mit erhöhtem Molekulargewicht vor. Momentan wird durch Studien die Evaluation der abgestimmten Balance zwischen dem multimeren

Akutphase-Protein von Willebrand Faktor und dessen inaktivierenden Enzyms in den Brennpunkt des Interessens gelegt [155–160]. Allerdings benötigen gegenwärtige Diagnosemethoden zur Bestimmung der Multimerzusammensetzung des VWFs mittels elektrophoretischer Trennung und Immunoblotting-Technik bis zu mehreren Tagen [161, 162]. Somit sind diese Methoden für ein therapeutisches Monitoring ungeeignet. Weiterhin ist die Vergleichbarkeit und Reproduzierbarkeit dieser Methoden unzureichend [163]. Um umgehend einen therapeutischen Plasmaaustausch einleiten zu können, sind daher schnellere und zuverlässige Diagnosemethoden erforderlich.

Schwingungs-spektroskopische Diagnosemethoden erlangen als vielversprechende Alternativmethoden bei der routinemäßigen klinischen Analyse von verschiedenen Körperflüssigkeiten immer mehr an Bedeutung. So können die Zusammensetzung und/oder die Konzentration von diversen Markersubstanzen wie Glukose, Triglyceriden oder Proteinen bestimmt werden, um daraus Rückschlüsse auf den Gesundheitszustand des Probanden ziehen zu können. Die qualitative und quantitative Ermittlung der Zusammensetzung verschiedener Biomoleküle bzw. die Klassifizierung zwischen gesunden und kranken Patienten erfolgt anhand der spektrochemischen Daten aus Urin-, Serum- oder Blutplasmaproben basierend auf der IR- [87,88,164,165] oder Raman-Spektroskopie mit Anregung im nahen infraroten Spektralbereich [26, 29, 30, 60].

Im Rahmen dieses Forschungsprojektes mit Dr. Ralf Claus von der Klinik für Anästhesiologie und Intensivtherapie des Universitätsklinikums Jena wird ein neues, auf der Raman-Spektroskopie beruhendes, Verfahren zur Blutplasmaanalyse vorgestellt. Zielstellung liegt in der Erforschung einer Methode, um eine schnelle, zeitnahe Diagnose einer Gerinnungsstörung zu gewährleisten, die eine Abgrenzung zu auf einer Infektion beruhenden Krankheit, wie Sepsis, ermöglicht bzw. die zum therapeutischen Monitoring dieser Erkrankungen dienen kann. In dieser Studie werden erstmals kryopräzipitierte Blutplasmaproben von gesunden Spendern und Patienten mit thrombotischer Mikroangiopathie mit Hilfe der Resonanz-Raman-Spektroskopie mit einer Anregung im UV-Wellenlängenbereich charakterisiert. Aufgrund der Anwesenheit von hoch aktiven Markerproteinen, den von Willebrand Faktor-Multimeren in Patientenproben, erfolgt eine Klassifizierung von Kranken und Gesunden. Die Kryopräzipitation stellt ein gängiges Verfahren zur Anreicherung von VWF-Multimeren in den Blutplasmaproben dar [166, 167]. VWF-Multimere können durch die Raman-Anregung im tiefen UV-Wellenlängenbereich sensitiv und selektiv in ihrer biologischen Umgebung erforscht werden. Die dafür genutzte Wellenlänge von 244

nm des frequenzverdoppelten Argon-Ionen-Lasers liegt im Bereich der starken, elektronischen Absorptionsbanden von aromatischen Aminosäuren der untersuchten Makromoleküle. Diese UV-Anregungswellenlänge führt neben der Resonanzverstärkung dieser Moleküle auch zu einer erheblichen intrinsischen Verstärkung der Streuintensität, wodurch eine selektive Verstärkung von Proteinschwingungen erfolgt. UV-Laserstrahlung besitzt eine relativ hohe Energiedichte, wodurch biologische Proben sehr leicht photochemisch bzw. photothermisch zerstört werden können. Um diese photochemische Zerstörung der Probe zu unterbinden bzw. zu minimieren, wird die Probe während der Messung gegenüber dem Laserstrahl verschoben. In Abb. 2 in [MH8] ist der Einfluss der Spektrenqualität in Abhängigkeit der Stärke der Probenverbrennung dargestellt. Da sich mit zunehmender Verbrennung der Probe das Signal-Rausch-Verhältnis entscheidend verschlechtert, wird die Notwendigkeit der kontinuierlichen Probenverschiebung gegenüber dem Laserstrahl während der Messung ersichtlich. In Abb. 1 in [MH8] sind UVRR-Spektren von Blutplasmakryopräzipitaten gesunder Spender und von Kranken mit TMA dargestellt, die spektrale Unterschiede in der relativen Intensität diverser Raman-Banden aufweisen. Durch die Vermessung von in Kryropräzipitaten in erhöhter Konzentration vorkommender Plasmakomponenten (VWF, Faktor VIII, VWF-Faktor VIII-Komplex, Fibrinogen) (Abb. 3 (A) in [MH8]), sowie verschiedenen aromatischen Aminosäuren (Abb. 2 (B) in [MH9]), endogenen Farbstoffen (Abb. 4 (A) in [MH8]) und Lipoprotein (Abb. 4 (B) in [MH8]), können die Zusammensetzung sowie Unterschiede in den Raman-Spektren von Gesunden und Kranken bestimmt werden. Aufgrund der hohen Sensitivität dieser Methode war es möglich, durch die Detektion von erhöhten Anteilen an Lipoproteinen bei gewissen Proben von Gesunden, Präparationsfehler aufzudecken (Abb. 3 in [MH8]). Aufgrund der Komplexität der UV-Resonanz-Raman-Spektren von gesunden Spendern und an thrombotischer Mikroangiopathie erkrankten Patienten können durch multivariate Klassifikationsmethoden, der hierarchischen Clusteranalyse (Abb. 5 in [MH8]) und der Hauptkomponentenanlyse (Abb. 4 (B) in [MH9]), eine effektive und spezifische Differenzierung zwischen Gesunden und Kranken vorgenommen werden, womit diese Methode ein aussichtsreiches Werkzeug für therapeutisches Monitoring darstellt.

In dieser Studie wird gezeigt, dass sich die UV-Resonanz-Raman-Spektroskopie zur Analyse von Blutplasma und darin enthaltenen Bestandteilen als eine innovative Methode ohne komplexe und aufwändige prä-analytische Prozeduren darstellt. Am Beispiel einer entzündungsassoziierten Erkrankung von Patienten mit einer thrombotischen Mikroangiopathie kann mittels chemometrischer Datenanalysemethoden, wie der hierarchischen Clusteranalyse oder Hauptkomponentenanalyse, eine Differenzierung zwischen gesunden Spendern und im Allgemeinen von Patienten mit einer Entzündung vorgenommen werden.

Zukünftige Forschungen zielen darauf ab, Patienten mit einer systemischen Entzündungsreaktion SIRS (engl.: *systemic inflammatory response syndrome*) zu identifizieren. Hierbei ist das Ziel durch das Aufstellen einer Referenzdatenbank und die Verwendung einer überwachten Klassifizierungsmethode, eine unbekannte Probe anhand des Klassifizierungsmodells nicht nur als gesund oder erkrankt einzustufen. Vielmehr soll das Stadium einer entzündungsassozierten Erkrankung festgestellt werden. Folglich wäre eine therapeutische Überwachung bzgl. Medikamentenwirkung durchführbar. Diese Datenbank kann mit zusätzlichen, aus elektrophoretischen Methoden gewonnenen Daten, ergänzt werden, um die Sicherheit der Diagnose zu erhöhen. Des Weiteren gibt es die Möglichkeit die Datenbank mit Referenzdaten, von auf einer Infektion beruhenden Krankheit, wie Sepsis, zu erweitern. Ziel hierbei ist es, anhand dieser Referenzdatenbank neben der Feststellung des Stadiums der Krankheit, eine Abgrenzung bezüglich SIRS und zusätzlicher Beteiligung von Mikroorganismen (z. B. bei Blutvergiftung (Sepsis)) vorzunehmen. Da sich beide Krankheitsgeschehen durch ähnliche klinische Symptome wie Fieber, Tachykardie, Tachypnoe und Leukozytose auszeichnen, und somit eine Blutvergiftung mit gegenwärtig eingesetzen Methoden oft zu spät diagnostiziert wird (Letalität von bis zu 50% [168]), wäre dies ein wichtiger Schritt in der Sepsisdiagnostik. [MH8, MH9]

1.2.4 Minimal-invasive Geschlechtsbestimmung von Vögeln mittels UV-Resonanz-Raman-Spektroskopie

Eine weitere Anwendung der UV-Resonanz-Raman-Spektroskopie kann, aufgrund der erhöhten Selektivität und Sensitivität für Protein- und DNA/RNA-Schwingungen, neben der Identifizierung von verschiedenen Gesundheitszuständen, in der minimal-invasiven Identifizierung des Geschlechts von Vögeln bestehen. Die Bestimmung des Vogelgeschlechts ist bei Vogelzüchtern für die Schaffung von Brutpaaren oder Schwärmen wichtig, um eine erfolgreiche Vogelvermehrung bzw. Züchtung zu gewährleisten. Für die Geflügelindustrie ist die Feststellung des Vogelgeschlechts aufgrund unterschiedlicher Fütterungsgewohnheiten aus ökonomischen Gründen entscheidend. Im Gegensatz zu Säugetieren besitzen Vögel keine äußerlich sichtbaren Geschlechtsorgane. In vielen Fällen ist eine Unterscheidung zwischen männlichen und weiblichen Vögeln anhand sekundärer phänotypischer Merkmale, wie beispielsweise morphologischer Unterschiede über die Körpergröße, Stirnhöcker, Gefiederfärbung oder Federlänge möglich, bwz. kann diese anhand verschiedener Verhaltenscharakteristika, wie dem Paarungsverhalten oder Stimm- und Lautbildung, getroffen

werden. In nicht seltenen Fällen bereitet diese Entscheidung jedoch Schwierigkeiten bzw. eine Geschlechtsbestimmung kann speziell im embryonalen Stadium, bei jungen Vögeln oder bestimmten Vogelarten gar nicht oder zumindest nicht zuverlässig vorgenommen werden. Bei Vogelarten, bei denen sich männliche von weiblichen Vögeln nur marginal unterscheiden, kommen molekulargenetische [89,90] oder endoskopische Verfahren [91,92] zum Einsatz. Bei diesen Verfahren erfolgt eine Blutabnahme bzw. die Tiere müssen zuvor betäubt werden, was einerseits zusätzlichen Aufwand erfordert, andererseits sind die Tiere bei dieser Behandlung einer extremen Stresssituation ausgesetzt.

Ein vielversprechender, schonender Ansatz stellt die UV-Resonanz-Raman-Spektroskopie dar, die eine minimal-invasive Geschlechtsbestimmung von Vögeln anhand einer im Wachstum befindlichen Feder ermöglicht. Diese neuartige Methode wurde in Kooperation mit Dr. Thomas Bartels von der Klinik für Vögel und Reptilien der Universität Leipzig für die Vogelart des Haushuhns (*Gallus gallus domesticus*) erforscht. Da männliche im Vergleich zu weiblichen Hühnern eine um etwa 2% höhere DNA-Menge aufweisen [169], ist die UVRR-Spektroskopie aufgrund der Sensitivität und Selektivität für DNA- und Proteinschwingungen eine geeignete Methode. Das im Federkiel enthaltene Zellmaterial wird auf einem geeigneten Träger ausgedrückt. Die Untersuchungen erfolgen mit einer Raman-Anregungswellenlänge von 244 nm. Zur Minimierung der photochemischen bzw. -thermischen Zerstörung der Probe aufgrund der hohen Energiedichte von UV-Strahlung wird die Probe während der Einwirkung des Laserstrahls zur Raman-Spektren-Aufnahme bewegt.

In dieser Studie wird gezeigt, dass die UV-Resonanz-Raman-Spektroskopie einen geeigneten minimal-invasiven Ansatz zur zuverlässigen Geschlechtsbestimmung von Vögeln, speziell für das Haushuhn, ohne aufwändige Probenpräparation darstellt. Abb. 1 in [MH10] zeigt ein Schema der Prozedur. Durch die Vermessung von in einer Feder enthaltenen proteinogenen und DNA-haltigen Bestandteilen (Abb. 3 in [MH10]) kann die Zusammensetzung der Federpulpaextrakte charakterisiert werden und eine qualitative Beurteilung bezüglich der Geschlechtsunterschiede in den Raman-Spektren vorgenommen werden. Tab. 1 in [MH10] enthält eine Übersicht zur Raman-Bandenzuordnung. In Abb. 2 in [MH10] sind Mittelwert-UVRR-Spektren von männlichen und weiblichen Federpulpaextrakten dargestellt. Die Gegenüberstellung mit dem Differenz-Spektrum veranschaulicht die minimalen Unterschiede in den UVRR-Spektren beider Geschlechter. Es zeigt sich, dass die größten Abweichungen im Bereich von 1450 bis 1650 cm^{-1} liegen. Um die Unterschiede in den Resonanz-Raman-Spektren von männlichen und weiblichen Federpulpaextrakten zu analysieren, erfolgt eine Geschlechtsdifferenzierung mittels verschiedener

statistischer Klassifikationsalgorithmen. Unter Verwendung eines überwachten Klassifikationsverfahrens, der Support-Vektor-Maschine, können anhand des berechneten Klassifikationsmodells alle Spektren bzw. zu klassifizierende unbekannte Proben, zu 95% dem entsprechenden Geschlecht korrekt zugeordnet werden. (Tab. 2 und 3 in [MH10])

Zur Feststellung von entscheidenden spektralen Bereichen, die zur Geschlechtsdifferenzierung relevant sind, erfolgt eine Hauptkomponentenanalyse. Das dreidimensionale Diagramm des PCA-*Scores*-Plot der ersten drei Hauptkomponenten ist in Abb. 4 in [MH10] dargestellt. 83% der Datensatzvariation können durch die ersten drei Hauptkomponenten beschrieben werden. Diese drei Hauptkomponenten sind für eine zuverlässige Unterscheidung zwischen männlichem und weiblichem Federpulpamaterial des Haushuhns ausreichend. Wie in Abb. 4 in [MH10] ersichtlich, streuen die zwei Raman-Spektren-Gruppen der Federpulpaextrakte der Männchen und Weibchen sehr und überlagern sich teilweise. Als mögliche Ursachen können Variationen in der Zusammensetzungen der relativen DNA- und Proteinmenge, sowie infolge der Probenpräparation stark untereinander abweichende Probeninhomogenitäten festgestellt werden (Abb. 5 (A) in [MH10]). Weiterhin erfolgt trotz Probenverschiebung unter dem Laserstrahl durch die UV-Licht Bestrahlung eine Verbrennung und somit photochemischen Zerstörung der Probe (Abb. 5 (B) in [MH10]). Diese Faktoren führen zu einer Verschlechterung des Signal-Rausch-Verhältnises der Raman-Spektren und somit sind beide Geschlechter im *Scores*-plot nicht eindeutig voneinander abgrenzbar. Anhand der in Abb. 6 in [MH10] dargestellten Ladungsplots können 13, für eine Geschlechtsbestimmung entscheidende, Spektralbereiche zwischen 1660 und 1336 cm^{-1} identifiziert werden. Die in diesem Bereich auftretenden Raman-Banden resultieren nicht nur von reinen DNA-Signalen, sondern ergeben sich aus einer Überlagerung von Protein- und DNA-Signalen.

Diese Studie zur Geschlechtsbestimmung von Vögeln zeigt die einzigartige Kapazität der UVRR-Spektroskopie, die sich im Gegensatz zu herkömmlich eingesetzten Methoden dadurch auszeichnet, dass diese durch die Analyse einer im Wachstum befindlichen Feder nur minimal-invasiv sowie einfach zu realisieren ist. Zukünftige Forschungen im Rahmen dieses Projektes zielen auf eine Erweiterung der UV-Resonanz-Raman-spektroskopischen Referenzdatenbank ab, so dass außer dem Haushuhn weitere Vogelarten wie das Truthuhn (*Meleagris gallopavo*) oder verschiedene Großpapageienarten bzgl. des Geschlechts einfach und schnell klassifiziert werden können. Im Zuge des Projektes soll ein Schwerpunkt auf die Geschlechtsbestimmung von jungen Vögeln in der Geflügelindustrie gelegt werden. Hierbei ist das Ziel, die Genauigkeit der Geschlechtsbestimmung in dem Bereich der kommerziellen Akzeptanz von 98.5% zu erhöhen. Hauptaugenmerk soll hierbei

auf einer Optimierung der Probenpräparation und Vermessung der Proben liegen, die es ermöglicht noch homogenere und weniger durch Photodegradation beeinträchtigte Spektren zu erzeugen. Eine Erweiterung der Methode, um das Geschlecht der Tiere bereits am Ei festzustellen, ist auch denkbar. Damit ließe sich das routinemäßige Töten männlicher Küken im Rahmen der Legehennenzucht vermeiden. [MH10]

Literaturverzeichnis

[1] Schmidt, W.: *Optische Spektroskopie - Eine Einführung.* Weinheim, New York, Chichester, Brisbane, Singapore, Toronto : Wiley-VHC, 2000. – 373 S

[2] Carey, P. R.: *Biochemical Applications of Raman and resonance Raman spectroscopy.* New York : Academic Press, 1982. – 262 S

[3] Mantsch, H. H. (Hrsg.) ; Chapman, D. (Hrsg.): *Infrared Spectroscopy of Biomolecules.* New York, Chichester, Brisbane, Toronto, Singapore : Wiley-Liss Inc., 1996. – 359 S

[4] Mantsch, H. H. ; Choo-Smith, L.-P. ; Shaw, R. A.: Vibrational spectroscopy and medicine: an alliance in the making. In: *Vib. Spectrosc.* 30 (2002), Nr. 1, S. 31–41

[5] Naumann, D.: FT-infrared and FT-Raman spectroscopy in biomedical research. In: Gremlich, Hans-Ulrich (Hrsg.) ; Yan, Bing (Hrsg.): *Infrared and Raman Spectroscopy of Biological Materials.* New York, Basel : Marcel Deccer, Inc., 2001, S. 323–378

[6] Notingher, I. ; Jones, J. R. ; Verrier, S. ; Bisson, I. ; Embanga, P. ; Edwards, P. ; Polak, J. M. ; Hench, L. L.: Application of FTIR and Raman spectroscopy to characterization of bioactive materials and living cells. In: *Spectroscopy* 17 (2003), Nr. 2 & 3, S. 275–288

[7] Notingher, I. ; Verrier, S. ; Haque, S. ; Polak, J. M. ; Hench, L. L.: Spectroscopic study of human lung epithelial cells (A549) in culture: Living cells versus dead cells. In: *Biopolymers* 72 (2003), Nr. 4, S. 230–240

[8] Petrich, W.: Mid-infrared and Raman spectroscopy for medical diagnostics. In: *Appl. Spectrosc. Rev.* 36 (2001), Nr. 2 & 3, S. 181–237

[9] Shaw, R. A. ; Mantsch, H. H.: Vibrational biospectroscopy: from plants to animals to humans. A historical perspective. In: *J. Mol. Struct.* 481 (1999), S. 1–13

[10] Schrader, B.: *Infrared and Raman Spectroscopy - Methods and Applications.* Weinheim, New York, Basel, Cambridge, Tokyo : Wiley-VCH, 1995. – 786 S

[11] Tu, A. T.: *Raman spectroscopy in biology: Principles and Applications.* New York : John Wiley & Sons, 1982. – 447 S

[12] Maquelin, K. ; Choo-Smith, L.-P. ; van Vreeswijk, T. ; Endtz, H. P. ; Smith, B. ; Bennett, R. ; Bruining, H. A. ; Pupples, G. J.: Raman spectroscopic method for identification of clinical relevant microorganisms growing on solid culture medium. In: *Anal. Chem.* 72 (2000), Nr. 1, S. 12–19

[13] Maquelin, K. ; Choo-Smith, L. P. ; Kirschner, C. ; Ngo Thi, N. A. ; Naumann, D. ; Puppels, G. J.: Vibrational spectroscopic studies of microorganisms. In: Chalmers, J. M. (Hrsg.) ; Griffiths, P. R. (Hrsg.): *Handbook of Vibrational Spectroscopy* Bd. 5. Chichester : John Wiley & Sons Ltd., 2002, S. 3308–3334

[14] Naumann, D.: Infrared spectroscopy in microbiology. In: Meyers, R. A. (Hrsg.): *Encyclopedia of Analytical Chemistry.* Chichester : John Wiley & Sons, 2000 (Biomedical Spectroscopy), S. 102–131

[15] Notingher, I. ; Hench, L. L.: Raman microspectroscopy: a noninvasive tool for studies of individual living cells in vitro. In: *Expert Rev. Med. Devices* 3 (2006), Nr. 2, S. 215–234

[16] Baena, J. R. ; Lendl, B.: Raman spectroscopy in chemical bioanalysis. In: *Curr. Opin. Chem. Biol.* 8 (2004), Nr. 5, S. 534–539

[17] Choo-Smith, L. P. ; Edwards, H. G. M. ; Endtz, H. P. ; Kros, J. M. ; Heule, F. ; Barr, H. ; Robinson, Jr. ; Bruining, H. A. ; Puppels, G. J.: Medical applications of Raman spectroscopy: from proof of principle to clinical implementation. In: *Biopolymers* 67 (2002), Nr. 1, S. 1–9

[18] Hanlon, E. B. ; Manoharan, R. ; Koo, T.-W. ; Shafer, K. E. ; Motz, J. T. ; Fitzmaurice, M. ; Kramer, J. r. ; Itzkan, I. ; Dasari, R. R. ; Feld, M. S.: Prospects for in vivo Raman spectroscopy. In: *Phys. Med. Biol.* 45 (2000), S. R1–R59

[19] Keller, S. ; Löchte, T. ; Dippel, B. ; Schrader, B.: Quality control of food with near-infrared-excited Raman spectroscopy. In: *Fresen. J. Anal. Chem.* 346 (1993), S. 863–867

[20] Notingher, I. ; Verrier, S. ; Romanska, H. ; Bishop, A. E. ; Polak, J. M. ; Hench, L. L.: In situ characterization of living cells by Raman spectroscopy. In: *Spectroscopy* 16 (2002), Nr. 2, S. 43–51

[21] Pappas, D. ; Smith, B. W. ; Winefordner, J. D.: Raman spectroscopy in bioanalysis. In: *Talanta* 51 (2000), Nr. 1, S. 131–144

[22] Petry, R. ; Schmitt, M. ; Popp, J.: Raman spectroscopy - a prospective tool in the life sciences. In: *ChemPhysChem* 4 (2003), Nr. 1, S. 14–30

[23] Puppels, G. J. ; Bakker Schut, T. C. ; Casper, P. J. ; Wolthuis, R. ; van Aken, M. ; van der Laarse, A. ; Bruining, H. A. ; Buschmann, H. P. J. ; Shim, M. G. ; Wilson, B. C.: In vivo Raman spectroscopy. In: Lewis, I. R. (Hrsg.) ; Edwards, H. G. M. (Hrsg.): *Handbook of Raman Spectroscopy - Practical Spectroscopy* Bd. 28. New York : Marcel Dekker, 2001, S. 549–574

[24] Schrader, B. ; Dippel, B. ; Erb, I. ; Keller, S. ; Lochte, T. ; Schulz, H. ; Tatsch, E. ; Wessel, S.: NIR Raman spectroscopy in medicine and biology: results and aspects. In: *J. Mol. Struct.* 481 (1999), S. 21–32

[25] Yang, H. ; Irudayaraj, J.: Rapid detection of foodborne microorganisms on food surface using Fourier transform Raman spectroscopy. In: *J. Mol. Struct.* 646 (2003), Nr. 1-3, S. 35–43

[26] Berger, A. J. ; Koo, T.-W. ; Itzkan, I. ; Horowitz, G. ; Feld, M. S.: Multicomponent blood analysis by near-infrared Raman spectroscopy. In: *Appl. Optics* 38 (1999), Nr. 13, S. 2916–2926

[27] Clark, R. J. H. ; Hester, R. E.: Spectroscopy of biological systems (Advances in Spectroscopy). Chichester : John Wiley & Sons, 1986, S. 570

[28] Notingher, I. ; Bisson, I. ; Bishop, A. E. ; Randle, W. L. ; Polak, J. M. P. ; Hench, L. L.: In situ spectral monitoring of mRNA translation in embryonic stem cells during differentiation in vitro. In: *Anal. Chem.* 76 (2004), Nr. 11, S. 3185–3193

[29] Qu, J. Y. ; Shao, L.: Near-infrared Raman instrument for rapid and quantitative measurements of clinically important analytes. In: *Rev. Sci. Instrum.* 72 (2001), Nr. 6, S. 2717–2723

[30] Rohleder, D. ; Kocherscheidt, G. ; Gerber, K. ; Kiefer, W. ; Kohler, W. ; Mocks, J. ; Petrich, W.: Comparison of mid-infrared and Raman spectroscopy in the quantitative analysis of serum. In: *J. Biomed. Opt.* 10 (2005), Nr. 3, S. 031108/031101–031108/031110

[31] Spiro, T. G.: *Biological applications of Raman spectroscopy.* Bd. 1-3. New York : John Wiley & Sons, 1988. – 1324 S

[32] Greve, J. ; Puppels, G. J.: Raman microscopy of single whole cells. In: Hester, R. E. (Hrsg.) ; Clark, R. J. H. (Hrsg.): *Biomol. Spectrosc.* Bd. 20A. 1. Chichester : John Wiley & Sons, 1992, S. 231–265

[33] Krafft, C. ; Knetschke, T. ; Siegner, A. ; Funk, R. H. W. ; Salzer, R.: Mapping of single cells by near infrared Raman microspectroscopy. In: *Vib. Spectrosc.* 32 (2003), Nr. 1, S. 75–83

[34] Puppels, G. J. ; Bakker Schut, T. C. ; Sijtsema, N. M. ; Grond, M. ; Maraboeuf, F. ; de Grauw, C. G. ; Figdor, C. G. ; Greve, J.: Development and application of Raman microsspectroscopic and Raman imaging techniques for cell biological studies. In: *J. Mol. Struct.* 347 (1995), S. 477–484

[35] Salzer, R. ; Steiner, G. ; Mantsch, H. H. ; Mansfield, J. ; Lewis, E. N.: Infrared and Raman imaging of biological and biomimetic samples. In: *Fresen. J. Anal. Chem.* 366 (2000), Nr. 6-7, S. 712–726

[36] Beebe, K. R. ; Pell, R. J. ; Seasholtz, M. B.: *Chemometrics - A practical guide.* New York : John Wiley & Sons, Inc., 1998. – 348 S

[37] Danzer, K. ; Hobert, H. ; Fischbacher, C. ; Jagemann, K.-U.: *Chemometrik*. Berlin, Heidelberg : Springer Verlag, 2001. – 405 S

[38] Henrion, R. ; Henrion, G.: *Multivariate Datenanalyse*. Berlin, Heidelberg : Springer Verlag, 1994. – 261 S

[39] Otto, M.: *Chemometrics - Statistics and computer application in analytical chemistry*. Weinheim : Wiley-VCH, 1999. – 314 S

[40] Jackson, J. E.: *A user's guide to principal components*. New York : John Wiley & Sons, Inc., 1991 (Wiley's series in probability and mathematical statistics. Applied probability and statistics). – 569 S

[41] Jolliffe, I. T.: *Principal Component Analysis*. New York : Springer Verlag, 2002 (Springer Series in Statistics). – 487 S

[42] Scherer, A.: *Neuronale Netze - Grundlagen und Anwendungen*. Braunschweig, Wiesbaden : Vieweg Verlag, 1997 (Comput. Intell.). – 249 S

[43] Rösch, P. ; Harz, M. ; Krause, M. ; Petry, R. ; Peschke, K.-D. ; Burkhardt, H. ; Ronneberger, O. ; Schüle, A. ; Schmauz, G. ; Riesenberg, R. ; Wuttig, A. ; Lankers, M. ; Hofer, S. ; Thiele, H. ; Motzkus, H.-W. ; Popp, J.: Online monitoring and identification of bioaerosol (OMIB). In: Popp, Jürgen (Hrsg.) ; Strehle, Marion (Hrsg.): *Biophotonics. Visions for Better Health Care*. Weinheim : Wiley-VCH, 2006, S. 596

[44] Schölkopf, B. ; Smola, A. J.: *Learning with kernels: Support Vector Machines, Regularization, Optimization, and Beyond*. Cambridge, Massachusetts, London, England : The MIT Press, 2002. – 626 S

[45] Goodacre, R. ; Timmins, E. M. ; Burton, R. ; Kaderbhai, N. ; Woodward, A. M. ; Kell, D. B. ; Rooney, P. J.: Rapid identification of urinary tract infection bacteria using hyperspectral whole-organism fingerprinting and artificial neural networks. In: *Microbiology* 144 (1998), S. 1157–1170

[46] Harz, M. ; Neugebauer, U. ; Rösch, P. ; Popp, J.: Raman spectroscopy identification of bacterial cells. In: *GIT Laboratory Journal, Europe* 10 (2006), Nr. 3, S. 26–28

[47] Huang, W. E. ; Griffiths, R. I. ; Thompson, I. P. ; Bailey, M. J. ; Whiteley, A. S.: Raman microscopic analysis of single microbial cells. In: *Anal. Chem.* 76 (2004), Nr. 15, S. 4452–4458

[48] Krause, M. ; Radt, B. ; Rösch, P. ; Popp, J.: The investigation of single bacteria by means of fluorescence staining and Raman spectroscopy. In: *J. Raman Spectrosc.* 38 (2007), S. 369–372

[49] Maquelin, K. ; Choo-Smith, L. P. ; Endtz, H. P. ; Bruining, H. A. ; Puppels, G. J.: Rapid identification of candida species by confocal Raman microspectroscopy. In: *J. Clin. Microbiol.* 40 (2002), Nr. 2, S. 594–600

[50] Schuster, K. C. ; Reese, I. ; Urlaub, E. ; Gapes, J. R. ; Lendl, B.: Multidimensional information on the chemical composition of single bacterial cells by confocal Raman microspectroscopy. In: *Anal. Chem.* 72 (2000), Nr. 22, S. 5529–5534

[51] Xie, C. ; Mace, J. ; Dinno, M. A. ; Li, Y. Q. ; Tang, W. ; Newton, P. J.: Identification of single bacterial cells in aqueous solution using confocal laser tweezers Raman spectroscopy. In: *Anal. Chem.* 77 (2005), Nr. 14, S. 4390–4397

[52] Madigan, M. T. ; Martinko, J. M. ; Parker, J.: *Brock Mikrobiologie*. Heidelberg Berlin : Spektrum Akademischer Verlag GmbH, 2000. – 1175 S

[53] Schlegel, H. G.: *Allgemeine Mikrobiologie*. Stuttgart : Georg Thieme Verlag, 1992. – 634 S

[54] Gremlich, H.-U. (Hrsg.) ; Yan, B. (Hrsg.): *Infrared and Raman Spectroscopy of Biological Materials*. New York, Basel : Marcel Dekker, Inc., 2001. – 581 S

[55] Huang, Y.-S. ; Karashima, T. ; Yamamoto, M. ; Hamaguchi, H.: Molecular-level pursuit of yeast mitosis by time- and space-resolved Raman spectroscopy. In: *J. Raman Spectrosc.* 34 (2003), Nr. 1, S. 1–3

[56] Short, K. W. ; Carpenter, S. ; Freyer, J. P. ; Mourant, J. R.: Raman spectroscopy detects biochemical changes due to proliferation in mammalian cell cultures. In: *Biophys. J.* 88 (2005), Nr. 6, S. 4274–4288

[57] Xie, C. ; Dinno, M. A. ; Li, Y-S.: Near-infrared Raman spectroscopy of single optically trapped biological cells. In: *Opt. Lett.* 27 (2002), Nr. 4, S. 249–251

[58] Xie, C. ; Li, Y.-Q. ; Tang, W. ; Newton, R. J.: Study of dynamical process of heat denaturation in optically trapped single microorganisms by near-infrared Raman spectroscopy. In: *J Appl. Phys.* 94 (2003), Nr. 9, S. 6138–6142

[59] Xie, Changan ; Goodman, Charles ; Dinno, Mumtaz A. ; Li, Yong-Qing: Real-time Raman spectroscopy of optically trapped living cells and organelles. In: *Opt. Soc. Amer.* 12 (2004), Nr. 25, S. 6208–6214

[60] Qu, J. ; Suria, D. ; Wilson, B. C.: Applications of laser Raman spectroscopy in concentration measurements of multiple analytes in human body fluids. In: *Proc. SPIE-Int. Soc. Opt. Eng.* 3253 (1998), Nr. Biomedical Sensing and Imaging Technologies, S. 72–76

[61] Schrader, B. ; Hoffmann, A. ; Keller, S.: Near-infrared Fourier transform Raman spectroscopy: facing absorption and background. In: *Spectrochim. Acta A* 47A (1991), Nr. 9-10, S. 1135–1148

[62] McHale, J. L.: Resonance Raman spectroscopy. In: Chalmers, J. M. (Hrsg.) ; Griffiths, P. R. (Hrsg.): *Handbook of Vibrational Spectroscopy* Bd. 1. Chichester : John Wiley & Sons Ltd., 2002, S. 534–556

[63] Asher, S. A.: UV resonance Raman spectroscopy for analytical, physical, and biophysical chemistry. Part 1. In: *Anal. Chem.* 65 (1993), Nr. 2, S. 59A–66A

[64] Asher, S. A.: UV resonance Raman spectroscopy for analytical, physical, and biophysical chemistry. Part 2. In: *Anal. Chem.* 65 (1993), Nr. 4, S. 201A–210A

[65] Storrie-Lombardi, M. C. ; Hug, W. F. ; McDonald, G. D. ; Tsapin, A. I. ; Nealson, K. H.: Hollow cathode ion lasers for deep ultraviolet Raman spectroscopy and fluorescence imaging. In: *Rev. Sci. Instrum.* 72 (2001), Nr. 12, S. 4452–4459

[66] Fodor, S. P. A. ; Rava, R. P. ; Hays, T. R. ; Spiro, T. G.: Ultraviolet resonance Raman spectroscopy of the nucleotides with 266-, 240-, 218-, and 200-nm pulsed laser excitation. In: *J. Am. Chem. Soc.* 107 (1985), Nr. 6, S. 1520–1529

[67] Fodor, S. P. A. ; Spiro, T. G.: Ultraviolet resonance Raman spectroscopy of DNA with 200-266-nm laser excitation. In: *J. Am. Chem. Soc.* 108 (1986), Nr. 12, S. 3198–3205

[68] Wen, Z. Q. ; Thomas, Jr.: UV resonance Raman spectroscopy of DNA and protein constituents of viruses: assignments and cross sections for excitations at 257, 244, 238 and 229 nm*. In: *Biopolymers* 45 (1998), S. 247–256

[69] Tuma, R. ; Bamford, J. H. K. ; Bambord, D. H. ; Russell, M. P. ; Thomas Jr., G. J.: Structure, interactions and dynamics of PRD1 virus I. Coupling of subunit folding and capsid assembly. In: *J. Mol. Biol.* 257 (1996), Nr. 1, S. 87–101

[70] Wu, Q. ; Nelson, W. H. ; Elliot, S. ; Sperry, J. F. ; Feld, M. ; Dasari, R. ; Manoharan, R.: Intensities of E. coli nucleic acid Raman spectra excited selectively from whole cells with 251-nm light. In: *Anal. Chem.* 72 (2000), Nr. 13, S. 2981–2986

[71] Asher, S. A. ; Ludwig, M. ; Johnson, C. R.: UV resonance Raman excitation profiles of the aromatic amino acids. In: *J. Am. Chem. Soc.* 108 (1986), Nr. 12, S. 3186–3197

[72] Lopez-Diez, E. C. ; Goodacre, R.: Characterization of microorganisms using UV resonance Raman spectroscopy and chemometrics. In: *Anal. Chem.* 76 (2004), Nr. 3, S. 585–591

[73] Nelson, W. H. ; Sperry, J. F.: UV resonance Raman spectroscopic detection and identification of bacteria and other microorganisms. In: Nelson, W. H. (Hrsg.): *Modern techniques for rapid microbiological analysis.* New York : VCH Publishers, Inc., 1991, S. 97–143

[74] Nelson, W. H. ; Manoharan, R. ; Sperry, J. F.: UV resonance Raman Studies of bacteria. In: *Appl. Spectrosc. Rev.* 27 (1992), Nr. 1, S. 67–124

[75] Rava, R. P. ; Spiro, T. G.: Resonance enhancement in the ultraviolet Raman spectra of aromatic amino acids. In: *J. Phys. Chem.* 89 (1985), Nr. 10, S. 1856–1861

[76] Thomas, Jr.: Raman spectroscopy of protein and nucleic acid assemblies. In: *Annu. Rev. Biophys. Biomol. Struct.* 28 (1999), S. 1–27

[77] Wu, Q. ; Hamilton, T. ; Nelson, W. H. ; Elliott, S. ; Sperry, J. F. ; Wu, M.: UV Raman spectral intensities of E. Coli and other bacteria excited at 228.9, 244.0, and 248.2 nm. In: *Anal. Chem.* 73 (2001), Nr. 14, S. 3432–3440

[78] Chadha, S. ; Nelson, W. H. ; Sperry, J. F.: Ultraviolet micro-Raman spectrograph for the detection of small numbers of bacterial cells. In: *Rev. Sci. Instrum.* 64 (1993), S. 3088–3093

[79] Jarvis, R. M. ; Goodacre, R.: Ultra-violet resonance Raman spectroscopy for the rapid discrimination of urinary tract infection bacteria. In: *FEMS Microbiol. Lett.* 232 (2004), Nr. 2, S. 127–132

[80] Asher, S. A. ; Ianoul, A. ; Mix, G. ; Boyden, M. N. ; Karnoup, A. ; Diem, M. ; Schweitzer-Stenner, R.: Dihedral ψ angle dependence of the amide III vibration: A uniquely sensitive UV resonance Raman secondary structural probe. In: *J. Am. Chem. Soc.* 123 (2001), Nr. 47, S. 11775–11781

[81] Chi, Z. ; Chen, X. G. ; Holtz, J. S. W. ; Asher, A.: UV resonance Raman-selective amide vibrational enhancement: quantitative methodology for determining protein secondary structure. In: *Biochemistry* 37 (1998), Nr. 9, S. 2854–2864

[82] Lippert, J. L. ; Tyminski, D. ; Desmeules, P. J.: Determination of the secondary structure of proteins by laser Raman spectroscopy. In: *J. Am. Chem. Soc.* 98 (1976), Nr. 22, S. 7075–7080

[83] Mikhonin, A. V. ; Myshakina, N. S. ; Bykov, S. V. ; Asher, S. A.: UV Resonance raman determination of polyproline II, extended 2.51-helix, and b-sheet Y angle energy landscape in poly-L-lysine and poly-L-glutamic acid. In: *J. Am. Chem. Soc.* 127 (2005), Nr. 21, S. 7712–7720

[84] Wen, Z. Q. ; Overman, S. A. ; Bondre, P. ; Thomas, Jr.: Structure and organization of bacteriophage Pf3 probed by Raman and ultraviolet resonance Raman spectroscopy. In: *Biochemistry* 40 (2001), Nr. 2, S. 449–458

[85] Neugebauer, U.: *Characterization of bacteria, antibiotics of the fluoroquinolone type and their biological targets DNA and gyrase utilizing the unique potential of vibrational spectroscopy*, Friedrich-Schiller-Universität Jena, Dissertation, 2007. – 265 S

[86] Gaus, K.: *Klassifizierung von Milchsäurebakterien aus Joghurt mit schwingungsspektroskopischen Methoden*, Friedrich-Schiller-Universität Jena, Diplomarbeit, 2005. – 149 S

[87] Petrich, W. ; Staib, A. ; Otto, M. ; Somorjai, R. L.: Correlation between the state of health of blood donors and the corresponding mid-infrared spectra of the serum. In: *Vib. Spectrosc.* 28 (2002), Nr. 1, S. 117–129

[88] Petibois, C. ; Cazorla, G. ; Cassaigne, A. ; Deleris, G.: Application of FT-IR spectrometry to determine the global metabolic adaptations to physical conditioning in sportsmen. In: *Appl. Spectrosc.* 56 (2002), Nr. 10, S. 1259–1267

[89] Bermudez-Humaran, L. G. ; Garcia-Garcia, A. ; Leal-Garza, C. H. ; Riojas-Valdes, V. M. ; Jaramillo-Rangel, G. ; Montes-De-Oca-Luna, R.: Molecular sexing of monomorphic endangered Ara birds. In: *J. Exp. Zool.* 292 (2002), Nr. 7, S. 677–680

[90] Griffiths, R. ; Double, M. C. ; Orr, K. ; Dawson, R. J. G.: A DNA test to sex most birds. In: *Mol. Ecol.* 7 (1998), Nr. 8, S. 1071–1075

[91] Prus, S. E. ; Schmutz, S. M.: Comparative efficiency and accuracy of surgical and cytogenetic sexing in psittacines. In: *Avian Dis.* 31 (1987), Nr. 2, S. 420–424

[92] Satterfield, W. C.: Avian endoscopy. In: *Vet. Clin. N. Am.-Small Anim. Pract.* 20 (1990), Nr. 5, S. 1353–1367

[93] Valet, O. K.: Automatische Partikelanalyse: Schnelle Materialbestimmung von Mikrometerpartikeln. In: *GIT Labor-Fachzeitschrift* 45 (2001), S. 533–534

[94] Jones, R. N.: Resistance patterns among nosocomial pathogens. In: *Chest* 119 (2001), Nr. 2, S. 397S–404S

[95] Maquelin, K. ; Kirschner, C. ; Choo-Smith, L. P. ; Ngo-Thi, N. A. ; van Vreeswijk, T. ; Stammler, M. ; Endtz, H. P. ; Bruining, H. A. ; Naumann, D. ; Puppels, G. J.: Prospective study of the performance of vibrational spectroscopies for rapid identification of bacterial and fungal pathogens recovered from blood cultures. In: *J. Clin. Microbiol.* 41 (2003), Nr. 1, S. 324–329

[96] Maquelin, K. ; Kirschner, C. ; Choo-Smith, L. P. ; van den Braak, N. ; Endtz, H. P. ; Naumann, D. ; Puppels, G. J.: Identification of medically relevant microorganisms by vibrational spectroscopy. In: *J. Microbiol. Meth.* 51 (2002), Nr. 3, S. 255–271

[97] Vanderberg, L. A.: Detection of biological agents: Looking for bugs in all the wrong places. In: *Appl. Spectrosc.* 54 (2000), Nr. 11, S. 376A–385A

[98] Holland, R. D. ; Wilkes, J. G. ; Ralli, F. ; Sutherland, J. B. ; Persons, C. C. ; Voorhees, K. J. ; Lay, J. O. J.: Rapid identification of intact whole bacteria based on spectral patterns using matrix-assisted laser desorption/ionization with time-of-flight mass spectrometry. In: *Rapid Commun. Mass. Sp.* 10 (1996), S. 1227–1232

[99] Al-Khaldi, S. F. ; Mossoba, M. M.: Gene and bacterial identification using high-throughput technologies: genomics, proteomics, and phenomics. In: *Nutrition* 20 (2004), Nr. 1, S. 32–38

[100] Bej, A. K. ; Mahbubani, M. H. ; Dicesare, J. L. ; Atlas, R. M.: Polymerase chain reaction-gene probe detection of microorganisms by using filter-concentrated samples. In: *Appl. Environm. Microbiol.* 57 (1991), Nr. 12, S. 3529–3534

[101] Belgrader, P. ; Benett, W. ; Hadley, D. ; Richards, J. ; Stratton, P. ; Mariella, R. ; Milanovich, F.: PCR detection of bacteria in seven minutes. In: *Science* 284 (1999), Nr. 5413, S. 449–450

[102] Ivnitski, D. ; Abdel-Hamid, I. ; Atanasov, P. ; Wilkins, E.: Biosensors for detection of pathogenic bacteria. In: *Biosens. Bioelectron.* 14 (1999), Nr. 7, S. 599–624

[103] Hauer, B. ; Eipel, H.: Flow cytometry: useful tool for analyzing bacterial populations cell by cell. In: Shapiro, James A. (Hrsg.) ; Dworkin, Martin (Hrsg.): *Bacteria as Multicellular Organisms.* New York, Oxford : Oxford University Press, Inc., 1997, S. 273–291

[104] Luppa, P. B. ; Sokoll, L. J. ; Chan, D. W.: Immunosensors - principles and applications to clinical chemistry. In: *Clin. Chim. Acta* 314 (2001), Nr. 1-2, S. 1–26

[105] Shapiro, H. M.: Microbial analysis at the single-cell level: tasks and techniques. In: *J. Microbiol. Meth.* 42 (2000), S. 3–16

[106] Oliveira, K. ; Procop, G. W. ; Wilson, D. ; Coull, J. ; Stender, H.: Rapid identification of Staphylococcus aureus directly from blood cultures by fluorescence in situ hybridization with peptide nucleic acid probes. In: *J. Clin. Microbiol.* 40 (2002), Nr. 1, S. 247–251

[107] Freydiere, A. M. ; Guinet, R. ; Boiron, P.: Yeast identification in the clinical microbiology laboratory: Phenotypical methods. In: *Med. Mycol.* 39 (2001), Nr. 1, S. 9–33

[108] Choo-Smith, L. P. ; Maquelin, K. ; Van Vreeswijk, T. ; Bruining, H. A. ; Puppels, G. J. ; Thi, N. A. N. ; Kirschner, C. ; Naumann, D. ; Ami, D. ; Villa, A. M. ; Orsini, F. ; Doglia, S. M. ; Lamfarraj, H. ; Sockalingum, G. D. ; Manfait, M. ; Allouch, P. ; Endtz, H. P.: Investigating microbial (micro)colony heterogeneity by vibrational spectroscopy. In: *Appl. Environm. Microbiol.* 67 (2001), Nr. 4, S. 1461–1469

[109] Helm, D. ; Labischinski, H. ; Schallehn, G. ; Naumann, D.: Classification and identification of bacteria by Fourier-transform infrared spectroscopy. In: *J. Gen. Microbiol.* 137 (1991), Nr. Pt 1), S. 69–79

[110] Naumann, D. ; Helm, D. ; Labischinski, H.: Microbiological characterizations by FT-IR spectroscopy. In: *Nature* 351 (1991), S. 81–82

[111] Naumann, D. ; Helm, D. ; Labischinski, H. ; Giesbrecht, P.: The characterization of microorganisms by Fouier-Transform infrared spectroscopy (FT-IR). In: Nelson, W. H. (Hrsg.): *Modern techniques for rapid microbiological analysis.* New

York : VCH Publisher, 1991 (Modern techniques for rapid microbiological analysis), S. 43–96

[112] Ngo-Thi, N. A. ; Kirschner, C. ; Naumann, D.: Characterization and identification of microorganisms by FT-IR microspectrometry. In: *J. Mol. Struct.* 661-662 (2003), S. 371–380

[113] Schmitt, J. ; Flemming, H.-C.: FTIR-spectroscopy in microbial and material analysis. In: *Int. Biodeter. Biodegr.* 41 (1998), Nr. 1, S. 1–11

[114] Wenning, M. ; Seiler, H. ; Scherer, S.: Fourier-transform infrared microspectroscopy, a novel and rapid tool for identification of yeasts. In: *Appl. Environm. Microbiol.* 68 (2002), Nr. 10, S. 4717–4721

[115] Kirschner, C. ; Maquelin, K. ; Pina, P. ; Thi, N. A. N. ; Choo-Smith, L. P. ; Sockalingum, G. D. ; Sandt, C. ; Ami, D. ; Orsini, F. ; Doglia, S. M. ; Allouch, P. ; Mainfait, M. ; Puppels, G. J. ; Naumann, D.: Classification and identification of enterococci: A comparative phenotypic, genotypic, and vibrational spectroscopic study. In: *J. Clin. Microbiol.* 39 (2001), Nr. 5, S. 1763–1770

[116] Naumann, D. ; Keller, S. ; Helm, D. ; Schultz, C. ; Schrader, B.: FT-IR spectroscopy and FT-Raman spectroscopy are powerful Analytical tools for the noninvasive characterization of intact microbial cells. In: *J. Mol. Struct.* 347 (1995), S. 399–405

[117] Naumann, D.: Infrared and NIR Raman Spectroscopy in Medical Microbiology. In: Mantsch, H. H. (Hrsg.) ; Jackson, M. (Hrsg.): *Infrared Spectroscopy: New Tool in Medicine: Proc. SPIE* Bd. 3257. Bellingham,Washington, 1998, S. 245–257

[118] Hutsebaut, D. ; Maquelin, K. ; De Vos, P. ; Vandenabeele, P. ; Moens, L. ; Puppels, G. J.: Effect of culture conditions on the achievable taxonomic resolution of Raman spectroscopy disclosed by three bacillus species. In: *Anal. Chem.* 76 (2004), Nr. 21, S. 6274–6281

[119] Schuster, K. C. ; Urlaub, E. ; Gapes, J. R.: Single-cell analysis of bacteria by Raman microscopy: spectral information on the chemical composition of cells and on the heterogeneity in a culture. In: *J. Microbiol. Meth.* 42 (2000), Nr. 1, S. 29–38

[120] Gaus, K. ; Rösch, P. ; Petry, R. ; Peschke, K. D. ; Ronneberger, O. ; Burkhardt, H. ; Baumann, K. ; Popp, J.: Classification of lactic acid bacteria with UV-resonance Raman spectroscopy. In: *Biopolymers* 82 (2006), Nr. 4, S. 286–290

[121] Neugebauer, U. ; Schmid, U. ; Baumann, K. ; Holzgrabe, U. ; Ziebuhr, W. ; Kozitskaya, S. ; Kiefer, W. ; Schmitt, M. ; Popp, J.: Characterization of bacterial growth and the influence of antibiotics by means of UV resonance Raman spectroscopy. In: *Biopolymers* 82 (2006), Nr. 4, S. 306–311

[122] Popp, J. ; Rösch, P. ; Harz, M. ; Schmitt, M. ; Peschke, K. D. ; Ronneberger, O. ; Burkhardt, H.: Raman-Spectroscopy for a rapid identification of single microorganisms. In: *Proc. SPIE-Int. Soc. Opt. Eng.* 6180 (2006), Nr. Photonics, Devices, and Systems III, S. 6180/6241–6180/6249

[123] Rösch, P. ; Harz, M. ; Schmitt, M. ; Peschke, K. D. ; Ronneberger, O. ; Burkhardt, H. ; Motzkus, H.-W. ; Lankers, M. ; Hofer, S. ; Thiele, H. ; Popp, J.: Rapid identification of single microbes by various Raman spectroscopic techniques. In: *Proc. SPIE-Int. Soc. Opt. Eng.* 6093 (2006), Nr. Biomedical Vibrational Spectroscopy III: Advances in Research and Industry, S. 6093/6078–6093/6088

[124] Rösch, P. ; Harz, M. ; Krause, M. ; Popp, J.: Fast and reliable identification of microorganisms by means of Raman spectroscopy. In: *Proc. SPIE-Int. Soc. Opt. Eng.* 6633 (2007), S. 6633/6631A

[125] Gray, L. D. ; Fedorko, D. P.: Laboratory diagnosis of bacterial meningitis. In: *Clin. Microbiol. Rev.* 5 (1992), Nr. 2, S. 130–145

[126] Aune, M. W. ; Sandberg, S.: Automated counting of white and red blood cells in the cerebrospinal fluid. In: *Clin. Lab. Haematol.* 22 (2000), Nr. 4, S. 203–210

[127] Hoffmann, J. J. M. L. ; Janssen, W. C. M.: Automated counting of cells in cerebrospinal fluid using the CellDyn-4000 hematology analyzer. In: *Clin. Chem. Lab. Med.* 40 (2002), Nr. 11, S. 1168–1173

[128] Soogarun, S. ; Sirimongkolsakul, S. ; Wiwanitkit, V. ; Siritantikorn, A. ; Pimsane, K. ; Srivijarn, R.: Leukocyte counts in cerebrospinal fluid with the automated hematology analyzer, Technicon H*3. In: *Clin. Lab.* 48 (2002), Nr. 11-12, S. 623–629

[129] Brando, B. ; Barnett, D. ; Janossy, G. ; Mandy, F. ; Autran, B. ; Rothe, G. ; Scarpati, B. ; D'Avanzo, G. ; D'Hautcourt, J. L. ; Lenkei, R. ; Schmitz, G. ; Kunkl, A. ; Chianese, R. ; Papa, S. ; Gratama, J. W.: Cytofluorometric methods for assessing absolute numbers of cell subsets in blood. European Working Group on Clinical Cell Analysis. In: *Cytometry* 42 (2000), Nr. 6, S. 327–346

[130] Subira, D. ; Castanon, S. ; Aceituno, E. ; Hernandez, J. ; Jimenez-Garofano, C. ; Jimenez, A. ; Jimenez, A. M. ; Roman, A. ; Orfao, A.: Flow cytometric analysis of cerebrospinal fluid samples and its usefulness in routine clinical practice. In: *Am. J. Clin. Pathol.* 117 (2002), S. 952–958

[131] Thomas, L.: *Labor und Diagnose: Indikation und Bewertung von Laborbefunden für die medizinische Diagnostik*. Frankfurt/Main : TH-Books Verlagsgesellschaft mbH, 2005. – 2016 S

[132] Rauer, S. ; Stich, O. ; Bogdan, C.: Microbiological diagnostics in the CSF. In: *Laboratoriumsmedizin* 29 (2005), Nr. 6, S. 434–438

[133] La Scolea, Jr. ; Dryja, D.: Quantitation of bacteria in cerebrospinal fluid and blood of children with meningitis and its diagnostic significance. In: *J. Clin. Microbiol.* 19 (1984), Nr. 2, S. 187–190

[134] Mylonakis, E. ; Hohmann, E. L. ; Calderwood, S. B.: Central nervous system infection with listeria monocytogenes. 33 years' experience at a general hospital and review of 776 episodes from the literature. In: *Medicine* 77 (1998), Nr. 5, S. 313–336

[135] Tunkel, A. R. ; Hartman, B. J. ; Kaplan, S. L. ; Kaufman, B. A. ; Roos, K. L. ; Scheld, W. M. ; Whitley, R. J.: Practice guidelines for the management of bacterial meningitis. In: *Clin. Infect. Dis.* 39 (2004), Nr. 9, S. 1267–1284

[136] Ibrahim, S. F. ; van den Engh, G.: High-speed cell sorting: fundamentals and recent advances. In: *Curr. Opin. Biotech.* 14 (2003), Nr. 1, S. 5–12

[137] Puppels, G. J. ; Mul, F. F. M. d. ; Otto, C. ; Greve, J. ; Robert-Nicoud, M. ; Arndt-Jovin, D. J. ; Jovin, T. M.: Studying single living cells and chromosomes by confocal Raman microspectroscopy. In: *Nature* 347 (1990), S. 301–303

[138] Puppels, G. J. ; Garritsen, H. S. P. ; Segers-Nolten, G. M. J. ; De Mul, F. F. M. ; Greve, J.: Raman microspectroscopic approach to the study of human granulocytes. In: *Biophys. J.* 60 (1991), Nr. 5, S. 1046–1056

[139] Ramanauskaite, R. B. ; Segers-Nolten, I. G. M. J. ; de Grauw, K. J. ; Sijtsema, N. M. ; van der Maas, L. ; Greve, J. ; Otto, C. ; Figdor, C. G.: Carotenoid levels in human lymphocytes, measured by Raman microspectroscopy. In: *Pure Appl. Chem.* 69 (1997), Nr. 10, S. 2131–2134

[140] Shen, Z. X. ; Shu, H. ; Qiu, D. W. ; Qin, L. ; Tang, S. H.: Resonant and non-resonant Raman spectra of human neutrophil and eosinophil cells. In: *Asian J. Spectrosc.* 1 (1997), S. 215–224

[141] Uzunbajakava, N. ; Lenferink, A. ; Kraan, Y. ; Willekens, B. ; Vrensen, G. ; Greve, J. ; Otto, C.: Nonresonant Raman imaging of protein distribution in single human cells. In: *Biopolymers* 72 (2003), S. 1–9

[142] van Manen, H.-J. ; Uzunbajakava, N. ; van Bruggen, R. ; Roos, D. ; Otto, C.: Resonance Raman imaging of the NADPH oxidase subunit cytochrome b558 in single neutrophilic granulocytes. In: *J. Am. Chem. Soc.* 125 (2003), Nr. 40, S. 12112–12113

[143] van Manen, H.-J. ; Kraan, Y. M. ; Roos, D. ; Otto, C.: Resonance Raman imaging of the NADPH oxidase subunit cytochrome b558 in single neutrophilic granulocytes. In: *Proc.Nat. Academ. Sciences United States Am.* 102 (2005), Nr. 29, S. 10159–10164

[144] van Manen, H.-J. ; Kraan, Y.M. ; Roos, D. ; Otto, C.: Intracellular chemical imaging of heme-containing enzymes involved in innate immunity using resonance Raman microscopy. In: *J. Phys. Chem. B* 108 (2004), Nr. 48, S. 18762–18771

[145] van Manen, H.-J. ; van Bruggen, R. ; Roos, D. ; Otto, C.: Single-cell optical imaging of the phagocyte NADPH oxidase. In: *Antioxidants Redox Signaling* 8 (2006), Nr. 9, 10, S. 1509–1522

[146] Sijtsema, N. M. ; Wouters, S. D. ; DeGrauw, C. J. ; Otto, C. ; Greve, J.: Confocal direct imaging Raman microscopy: design and applications in biology. In: *Appl. Sepctrosc.* 52 (1998), Nr. 3, S. 348–355

[147] Sijtsema, N. M. ; Tibbe, A. G. J. ; Segers-Nolten, I.G.M.J. ; Verhoeven, A.J. ; Weening, R.S. ; Greve, J. ; Otto, C.: Intracellular reactions in single human granulocytes upon phorbol myristate acetate activation using confocal Raman microspectroscopy. In: *Biophys. J.* 78 (2000), Nr. 5, S. 2606–2613

[148] Otto, C. ; Sijtsema, N. M. ; Greve, J.: Confocal Raman microspectroscopy of the activation of single neutrophilic granulocytes. In: *Eur. Biophys. J. Biophys. Lett.* 27 (1998), Nr. 6, S. 582–589

[149] Chalmers, J. M. (Hrsg.) ; Griffith, P. R. (Hrsg.): Chichester : John Wiley & Sons Ltd., 2002 (Handbook of Vibrational Spectroscopy.). – 3862 S

[150] Eliasson, C. ; Loren, A. ; Engelbrektsson, J. ; Josefson, M. ; Abrahamsson, J. ; Abrahamsson, K.: Surface-enhanced Raman scattering imaging of single living lymphocytes with multivariate evaluation. In: *Spectrochim. Acta A* 61 (2005), S. 755–760

[151] Budde, U. ; Schneppenheim, R.: Von Willebrand factor cleaving protease and thrombotic microangiopathy. In: *Laboratoriumsmedizin* 28 (2004), Nr. 6, S. 506–513

[152] Ono, T. ; Mimuro, J. ; Madoiwa, S. ; Soejima, K. ; Kashiwakura, Y. ; Ishiwata, A. ; Takano, K. ; Ohmori, T. ; Sakata, Y.: Severe secondary deficiency of von Willebrand factor-cleaving protease (ADAMTS13) in patients with sepsis-induced disseminated intravascular coagulation: Its correlation with development of renal failure. In: *Blood* 107 (2006), Nr. 2, S. 528–534

[153] Remuzzi, G. ; Ruggenenti, P. ; Bertani, T.: Thrombotic microangiopathies. In: Brenner, B. M. (Hrsg.): *Renal pathology: with clinical and functional correlations.* Philadelphia : JB Lippincott Company, 1994, S. 1154

[154] Sadler, J. E.: Biochemistry and genetics of von Willebrand factor. In: *Annu. Rev. Biochem.* 67 (1998), S. 395–424

[155] Arya, M. ; Anvari, B. ; Romo, G. M. ; Cruz, M. A. ; Dong, J.-F. ; McIntire, L. V. ; Moake, J. L. ; Lopez, J. A.: Ultralarge multimers of von Willebrand factor form spontaneous high-strength bonds with the platelet glycoprotein Ib-IX complex: Studies using optical tweezers. In: *Blood* 99 (2002), Nr. 11, S. 3971–3977

[156] Kaufman, R. J. ; Pipe, S. W.: Regulation of factor VIII expression and activity by von Willebrand factor. In: *Thromb. Haemostasis* 82 (1999), Nr. 2, S. 201–208

[157] Mannucci, P. M. ; Canciani, M. T. ; Forza, I. ; Lussana, F. ; Lattuada, A. ; Rossi, E.: Changes in health and disease of the metalloprotease that cleaves von Willebrand factor. In: *Blood* 98 (2001), Nr. 9, S. 2730–2735

[158] Prucha, M. ; Ruryk, A. ; Boriss, H. ; Moeller, E. ; Zazulla, R. ; Herold, I. ; Claus, R. A. ; Reinhart, K. A. ; Deigner, P. ; Russwurm, S.: Expression profiling: toward an application in sepsis diagnostics. In: *Shock* 22 (2004), Nr. 1, S. 29–33

[159] Reiter, R. A. ; Varadi, K. ; Turecek, P. L. ; Jilma, B. ; Knoebl, P.: Changes in ADAMTSI3 (von-Willebrand-factor-cleaving protease) activity after induced release of von Willebrand factor during acute systemic inflammation. In: *Thromb. Haemostasis* 93 (2005), Nr. 3, S. 554–558

[160] Ruggeri, Z. M.: Von Willebrand factor, platelets and endothelial cell interactions. In: *J. Thromb. Haemostasis* 1 (2003), Nr. 7, S. 1335–1342

[161] Gerritsen, H. E. ; Turecek, P. L. ; Schwarz, H. P. ; Lammle, B. ; Furlan, M.: Assay of von Willebrand factor (vWF)-cleaving protease based on decreased collagen binding affinity of degraded vWF: a tool for the diagnosis of thrombotic thrombocytopenic purpura (TTP). In: *Thromb. Haemostasis* 82 (1999), Nr. 5, S. 1386–1389

[162] Gerritsen, H. E. ; Robles, R. ; Lammle, B. ; Furlan, M.: Partial amino acid sequence of purified von Willebrand factor-cleaving protease. In: *Blood* 98 (2001), Nr. 6, S. 1654–1661

[163] Studt, J. D. ; Budde, U. ; Schneppenheim, R. ; Eisert, R. ; von Depka Prondzinski, M. ; Ganser, A. ; Barthels, M.: Quantification and facilitated comparison of von Willebrand factor multimer patterns by densitometry. In: *Am. J. Clin. Pathol.* 116 (2001), Nr. 4, S. 567–574

[164] Deleris, G. ; Petibois, C.: Applications of FT-IR spectrometry to plasma contents analysis and monitoring. In: *Vib. Spectrosc.* 32 (2003), Nr. 1, S. 129–136

[165] Wang, J. ; Sowa, M. ; Mantsch, H. H. ; Bittner, A. ; Heise, H. M.: Comparison of different infrared measurement techniques in the clinical analysis of biofluids. In: *TrAC, Trends in Analytical Chemistry* 15 (1996), Nr. 7, S. 286–296

[166] Hornsey, V. S. ; Krailadsiri, P. ; MacDonald, S. ; Seghatchian, J. ; Williamson, L. M. ; Prowse, C. V.: Coagulation factor content of cryoprecipitate prepared from methylene blue plus light virus-inactivated plasma. In: *Brit. J. Haematol.* 109 (2000), Nr. 3, S. 665–670

[167] Rock, G. ; Berger, R. ; Lange, J. ; Tokessy, M. ; Palmer, D. S. ; Giulivi, A.: A novel, automated method of temperature cycling to produce cryoprecipitate. In: *Transfusion* 41 (2001), Nr. 2, S. 232–235

[168] Cohen, J.: The immunopathogenesis of sepsis. In: *Nature* 420 (2002), Nr. 6917, S. 885–891

[169] Tiersch, T. R.: Identification of sex in chickens by flow cytometry. In: *World Poult. Sci. J.* 59 (2003), Nr. 01, S. 24–31

Kapitel 2

Veröffentlichungen

Im Folgenden sind die Nachdrucke der im Rahmen der Dissertation erschienenen Publikationen aufgeführt. Die Urheberrechte sind jeweils auf dem Deckblatt angegeben.

2.1 UV Raman spectroscopy - A technique for biological and mineralogical *in situ* planetary studies. [MH1]

N. Tarcea, M. Harz, P. Rösch, T. Frosch, M. Schmitt, H. Thiele, R. Hochleitner, J. Popp

Spectrochimica Acta Part A **2007**, 68, 1029-1035.

Available online at www.sciencedirect.com
ScienceDirect
Spectrochimica Acta Part A 68 (2007) 1029–1035
SPECTROCHIMICA ACTA PART A
www.elsevier.com/locate/saa

UV Raman spectroscopy—A technique for biological and mineralogical *in situ* planetary studies

Nicolae Tarcea [a], Michaela Harz [a], Petra Rösch [a], Torsten Frosch [a], Michael Schmitt [a], Hans Thiele [b], R. Hochleitner [d], Jürgen Popp [a,c,*]

[a] *Institut für Physikalische Chemie, Friedrich-Schiller-Universität Jena, Helmholtzweg 4, D-07743 Jena, Germany*
[b] *Kayser-Threde GmbH, Munich, Germany*
[c] *Institut für Photonische Technologien e.V., Albert-Einstein-Str. 9, D-07745 Jena, Germany*
[d] *Mineralogische Staatssammlung München, Munich, Germany*

Accepted 10 June 2007

Abstract

We report on the great advantages of using deep UV Raman system for *in situ* planetary applications. Among them are to be mentioned: (I) higher scattering efficiency compared to VIS–IR Raman excitation wavelengths, (II) electronic resonance effects which increase the intrinsically weak Raman signal thus improving the S/N ratio of the detected Raman signals and (III) spectral separation of Raman and fluorescence signals.

All these advantages are making UV Raman a valuable technique for *in situ* planetary applications. Mineral as well as biological samples were analyzed using Raman deep UV excitation and the results are presented. For the mineral samples a comparison with excitation in the NIR–VIS spectral regions is made. The impact of fluorescence on Raman data acquisition at different laser excitation wavelengths is assessed. Making use of the resonance effects, spectra of microorganisms were recorded with a high S/N ratio, allowing afterwards a very precise identification and classification (to the strain level) of the measured samples.

Keywords: UV Raman spectroscopy; Meteroites; Microorganism

1. Introduction

Raman spectroscopy [1] is a powerful method used to determine the complete chemical composition of unprepared surfaces. This method is equally well suited and applicable for the detection of minerals, organic substances, and water. This qualifies Raman spectroscopy as a valid technique for space applications. A Raman instrument can contribute to resolving various questions in the field of planetary research [2–8], e.g., the search for signs of extinct and/or extant life on Mars as well as to identify hazards for future human missions. The search for extant life needs to look for traces of sugars, phospholipids, amino acids, nucleotides (ATP/ADP). The search for extinct life, on the other hand, requires looking for organic residuals of biological origin like fossils or related geochemical and mineralogical bio-signatures. The envisaged future planetary missions require space-born instruments, which are highly miniaturized and which require as little power as possible. Space-born Raman spectrometers fulfilling these characteristics have been developed in the past years [9–13] for future Mars missions.

Raman scattering is a very inefficient process with roughly one in 10^7 scattered photons carrying the needed information. The Raman signal yield and the gained information can be maximized by carefully choosing the excitation laser wavelength in a normal Raman experiment. Raman scattering is only one of several other physical processes that might take place when light interacts with matter. Some of these processes compete with the Raman process (e.g., absorption) or/and are interfering with the detection of the weak Raman signal (e.g., fluorescence). To avoid the problem of fluorescence, two approaches are normally used. One is to lower the energy of the incoming photon such that the excitation of the molecule in an electronic state does not take place. Therefore the wavelengths of the laser used for excitation lie in the NIR region of the spectrum (from 785 nm up to 1064 nm). With this approach for most of the samples

* Corresponding author.
E-mail address: juergen.popp@uni-jena.de (J. Popp).

1386-1425/$ – see front matter © 2007 Elsevier B.V. All rights reserved.
doi:10.1016/j.saa.2007.06.051

(especially the biological samples) the fluorescence excitation is avoided. Avoiding fluorescence in this way for the minerals does not prove to be very efficient since in minerals there is always a certain amount of rare-earth elements impurities which do have the excited electronic levels at relatively low energies.

The second approach used for minimizing the interference of fluorescence with the Raman signal is to use excitation wavelengths in the deep UV region. At these wavelengths the fluorescence is excited but no fluorescence interference exists when excitation is at wavelengths below about 250 nm [14]. A typical Raman spectral range of 4000 cm^{-1} occurs in less than 30 nm above the excitation wavelength at 250 nm. This provides complete spectral separation of Raman and fluorescence emission bands resulting in high signal to noise measurements.

In addition to having spectrally well-separated Raman and fluorescence signals, if the Raman excitation occurs within an electronic resonance band of a material then the scattering cross-section can be highly improved. Diamond, nitrites and nitrates, and many other organic and inorganic materials have strong absorption bands in the deep UV and exhibit resonance enhancement of Raman bands when excited in the deep UV [14]. This resonance effect gives extraordinary results when biological samples are to be investigated [14].

Although the Raman spectrum acts like a clear fingerprint for mineral samples and simple organics, for bacterial identification the Raman spectral fingerprint is 'blurred' by the overlapping of Raman signals generated by all bacterial constituents. Conventional bacterial identification methods currently used are based on morphological evaluation of the microorganisms and their ability to grow in various media under different conditions [15]. Depending on the type of bacteria, the identification process may take at least one day but generally much longer [16,17]. Other analytical methods such as mass spectroscopy, polymerase chain reaction (PCR), flow cytometry, or fluorescence spectroscopy were developed, which allow for a fast and reliable identification [15,16] but their application for remote based instruments (e.g., *in situ* planetary science) is not readily possible because of the miniaturization of equipment such a deployment requires.

Vibrational spectroscopy of biological samples provides information about the chemical composition of all cell components. Naumann et al. [18–21] showed that IR and Raman spectroscopy can be used to classify bacteria and yeasts. Due to the high spatial resolution of approximately 1 μm micro-Raman spectroscopy can be used both on bulk samples [22,23] and on single bacterial cells [24,25]. For eukaryotic cells like yeast cells line scans over the cells are necessary in order to overcome the spatial heterogeneity of the cells [23,26].

In order to enhance the Raman signals a special technique, the so-called surface enhanced Raman spectroscopy (SERS), with various different SERS-substrates or SERS microchips in combination with antibodies is also used for bacterial investigation [27–30].

A different method of enhancing Raman signals is resonance Raman spectroscopy. Using UV excitation direct investigation of macromolecules such as DNA or proteins becomes possible [31–35]. This allows for the measurement of microorganisms with high reproducibility [36,37]. The first attempts of a UV-resonance Raman spectroscopic identification were performed on bacteria on a genera level [32] and of the bacillus group [38].

In addition, when comparing the available Raman signal for both cases of NIR and UV excitation an increase of approximately two orders of magnitude in the Raman scattered photons can be obtained by moving from NIR (at 785 nm) to the UV spectral region (248 nm). The Raman cross-section itself is dependent on the excitation wavelength to the inverse fourth power resulting in higher Raman intensity with shorter wavelength laser excitation. The size of the sampling spot for micro-Raman experiments is proportional to the wavelength of the laser beam. A better spatial resolution for Raman mapping experiments is achieved when the excitation laser has a shorter wavelength.

All of these advantages make deep UV Raman spectroscopy a valuable technique for planetary *in situ* applications. The technical readiness needed for implementing this approach into a space-qualified instrument is currently under investigation and the results are to be published. The MIRAS 2 project run by the Institute of Chemical-Physics at the University of Jena and Kayser-Threde GmbH in Munich and financed by the German Space Agency is analyzing a possible instrument design for a deep UV Raman spectrometer.

2. Materials and methods

The capabilities of deep UV Raman excitation were investigated for two different sample systems—mineral samples (MARS meteorites) and biological systems (microorganisms). For the mineral samples comparisons between deep UV Raman excitation and excitation at other laser wavelengths were made (excitation wavelengths used were 244, 257, 532, 633 and 830 nm). The microorganisms were investigated with only the deep UV excitation using the Raman resonance effect for recording spectra with a good S/N ratio. A good S/N ratio was needed for a reliable automatic identification and classification of the microorganisms using multivariate analysis.

2.1. Spectroscopic instrumentation

UV (for mineral samples) and UV-resonance (for biological samples) Raman spectra were collected using a micro-Raman setup (HR800, Horiba/Jobin-Yvon) with a focal length of 800 mm, a 40× anti-reflection coated objective (LMU UVB) with a numerical aperture of 0.5 and a 2400 lines/mm grating. The entrance slit was 150 μm wide. Excitation wavelength of a frequency doubled line of an argon-ion laser (Innova 300, FReD) at 244 nm was used. Raman-scattered light was detected by a nitrogen-cooled CCD-camera with an accumulation time set to 120 s. Samples were prepared as dried films on silica plates according to the procedure described by Naumann et al. [19,39] and rotated at 6 rpm, moving it in *x*, *y*-direction after each rotation. For the *x*/*y*-scans the meteorites were moved relative to the fixed laser spot with help of a motorized stage.

The comparative VIS/NIR Raman spectra on mineral samples were taken with a micro-Raman setup (HR LabRam, Horiba/Jobin-Yvon, focal length of 800 mm, a 300-lines/mm grating) equipped with an Olympus IX70 microscope, a video camera, and an air-cooled CCD detector operating at 220 K. A Nikkon LPlan SLWD 20×/0.35 objective focused the laser light on the meteorites. Validation of the wavenumber axis was performed by using the well known Raman signals from TiO_2 (anatase). The excitation wavelengths are the 633 nm of a HeNe laser, the 532 nm line of a frequency doubled Nd:YAG laser (Coherent Compass) and the 830 nm of external cavity semiconductor laser (TEC100 Raman, Sacher Lasertechnik) were used.

2.2. Mineral samples

The mineral samples studied are materials that are known to contain compounds with strong fluorescence and are also of relevance for space missions (i.e., measurements were performed on three Martian meteorites: SAU 008, DAG 735 and Zagami). The three meteorites are named after their find locations—Sayh al Uhaymir in Oman, Dar Al Ghani in Libya, and Zagami in Nigeria. The Zagami meteorite is the only observed to fall. The finds SAU 008 and DAG 735 show some degree of terrestrial alteration and secondary mineralization such as the formation of calcite along cracks. Primarily, all three Martian meteorites belong to the group of shergottites, i.e., they are basalts that are mainly composed of pyroxenes (augite, pigeonite) and plagioclase with minor phosphates and opaques (ilmenite, chromite, sulfide). In addition, SAU 008 and DAG 735 contain porphyric olivine megacrystals. All three Martian meteorites are heavily shocked, resulting in the complete conversion of crystalline plagioclase into diaplectic glass, the so-called maskelynite. For Raman measurement, the surfaces of these Martian meteorites were polished. Five different laser wavelengths have been used for excitation: 244, 257, 532, 633 and 830 nm. With each wavelength, 441 Raman spectra were recorded from the same 200 μm × 200 μm area on each of the meteor's polished cut. By employing the point measurement technique and the point counting procedure [4], the mineral phases on the surface of the rock were identified. The measured spots were organized in a 21 × 21 sampling matrix, with a sampling step size of 10 μm.

2.3. Microorganisms growing conditions

The microorganisms were chosen according to the conditions present in clean rooms. The microorganisms *Micrococcus luteus* (DSM 348 and 20030), *Micrococcus lylae* (DSM 20315 and 20318), *Bacillus subtilis* (DSM 10 and 347), *Bacillus pumilus* (DSM 27 and 361), *Bacillus sphaericus* (DSM 28 and 396), *Escherichia coli* (DSM 423, 426, 429, 498, 499, 501, 613, 1058, 2769 and 5208), *Staphylococcus cohnii* (DSM 6669, 6718, 6719 and 20260), *Staphylococcus epidermidis* (195 and 2682; DSM 1798, 3269, 3270 and 20042; ATCC 515 and 35984) and *Staphylococcus warneri* (DSM 20036 and 20316) were purchased from the "Deutsche Sammelstelle für Mikroorganismen und Zellkulturen" and from the Institut für Infektionsbiologie, Universität Würzburg. They were cultivated on a standard or nutrition agar (*Micrococcus* and *Bacillus*, *E. coli*) or CA or CASO (*Staphylococcus*) at 30 °C for 1 day. The bacteria were harvested from the agar plates washed twice in water and then dried in vacuum on fused silica plates.

2.4. Multivariate analysis

The analysis of Raman spectra was performed in two steps. First, the spectra were pre-processed. Second, a support vector machine (SVM) was used for classification (for more details see refs. [22,42]).

3. Results and discussion

3.1. Mineral samples

In order to be able to compare the wavelength dependent Raman measurements with each other it has to be guaranteed that exactly the same sample spots on the meteorites are investigated for all 5 Raman excitation wavelengths. Therefore we used a special micro grid made out of a silicon wafer attached above the meteorites. By doing so we were always able to record Raman spectra within the same 200 × 200 μm fields. Thereby these fields were scanned with a stepsize of 10 μm leading to 441 measurement points for the investigated grid field. This procedure was performed for all 5 Raman excitation wavelengths (244, 257, 532 and 633 nm). For each Raman scan the number of Raman spectra containing no information to be used for a mineral analysis due to a strong fluorescence background or the appearance of no Raman bands was determined [45]. Representative Raman spectra measured with different laser excitation wavelengths on the three meteorite samples are shown in Fig. 1. The amount of major mineral phases (pyroxene, plagioclase, and olivine) as well as minor phases (ilmenite, chromite, calcite, phosphates) was assessed. In general, the data gathered with excitation at 244 and 257 nm show very low backgrounds, which allows a good S/N ratio for recording of the Raman features (Fig. 1). Each spectrum was evaluated with respect to its content of useful information for a mineral analysis. The statistic of this evaluation is presented in Table 1. For all three samples (DAG 735, SAU 008, and Zagami) the same general behaviour is observed. The number of unsuccessful measurements is smaller when employing excitation lasers in UV. Also, the number of spectra that suffer from fluorescent background interference is significantly smaller when using these wavelengths for Raman experiments. The reason for the high number of failed measurements on Zagami when using VIS–NIR excitation (∼50% in Fig. 2) is due to an extremely fluorescent shock vein, which according to recent investigations is glassy [40,41]. Measurements with 244 and 257 nm laser indicate a high contribution of feldspar component to the melt vein.

It is observed that the spectra measured with excitation in VIS and NIR are qualitatively worse than the ones measured in UV. With excitation in visible–NIR region, most of the time

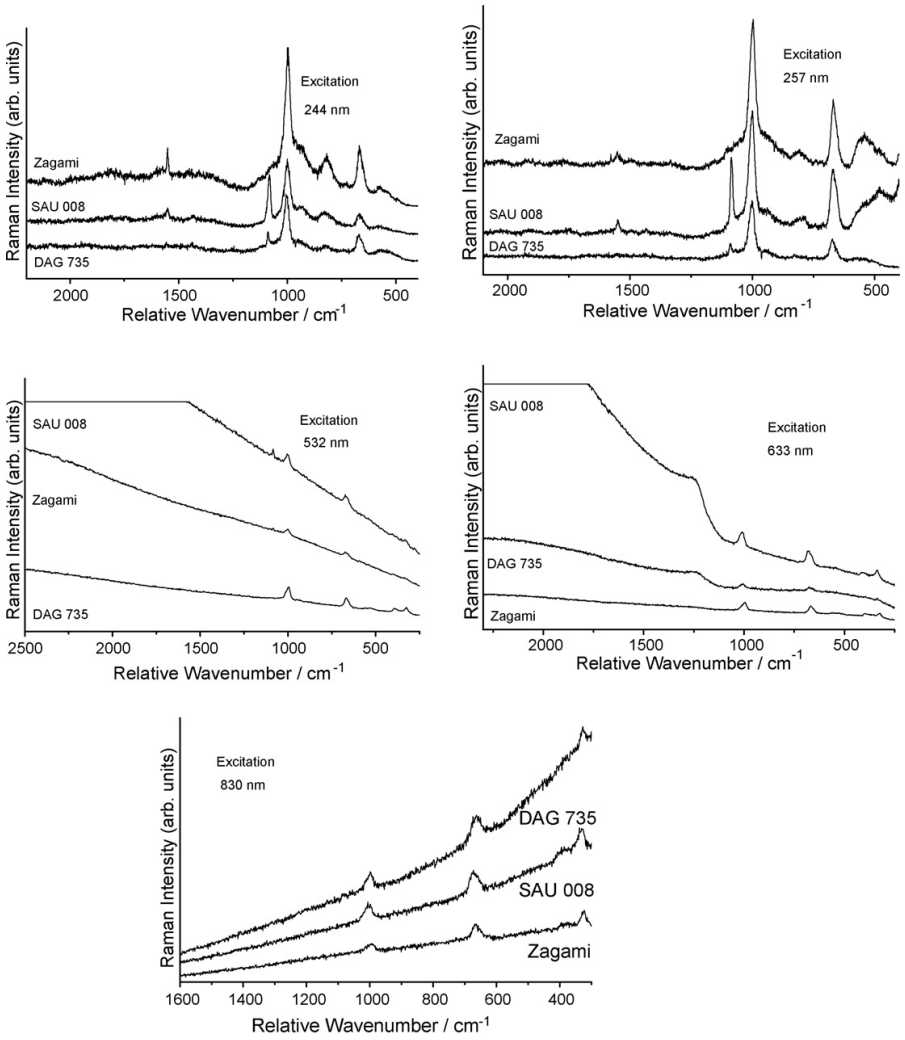

Fig. 1. Representative Raman spectra measured with different laser excitation wavelengths (244, 257, 532, 633 and 830 nm) on the three meteorite samples (DAG 735, SAU 008 and Zagami).

the high fluorescence background is covering the Raman bands that quickly saturate the detector, and does not allow for the measurement of faint Raman features by using longer integration time intervals.

3.2. Microorganisms

For chemotaxonomic identification of bacteria several macromolecules, e.g., proteins, cytochromes and nucleic acids, are widely used [43]. Among these macromolecules DNA is of particular interest. Using Raman excitation wavelengths in the ultraviolet region selectively enhances Raman signals of proteins and DNA/RNA. Fig. 2 shows a UV-resonance Raman spectrum of *S. warneri* DSM 20316. The signals can mainly be assigned to DNA bases as well as aromatic amino acids. The C=C stretching vibration of the aromatic amino acids tyrosine (Tyr), tryptophan (Trp) and phenylalanine (Phe) can be found at 1612 cm^{-1}. In addition, the ring breathing vibrations of Tyr arises at 1361 cm^{-1} and those of Trp and Phe at a broad band at 1010 cm^{-1}. The combined C=C and C=N stretching vibrations of guanine (G) and adenine (A) are located at 1570 cm^{-1}. The pyrimidin ring vibration of guanine and adenine gives rise to a very strong signal at 1481 cm^{-1}. The signal of thymine can be found at 1361 cm^{-1}. A combination of adenine, thymine and tyrosine whereas the combination of adenine, guanine and uracil exhibit broad bands at approximately 1328 and 1230 cm^{-1}, respectively.

Because the Raman signals of the DNA bases guanine, adenine, cytosine and thymine as well as the RNA base uracil are resonantly enhanced it is possible to correlate the UV-resonance Raman spectra with the GC value [44]. The GC value is defined

Table 1
Number of measurement points containing no useful information for the three meteorites DAG 735, SAU 008 and Zagami

	Number of points containing no useful information
DAG 735	
244 nm	26
257 nm	5
532 nm	436
633 nm	412
830 nm	438
SAU 008	
244 nm	1
257 nm	0
532 nm	405
633 nm	304
830 nm	308
Zagami	
244 nm	0
257 nm	4
532 nm	185
633 nm	344
830 nm	340

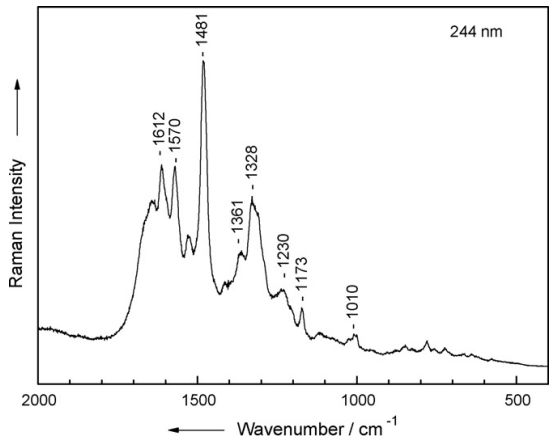

Fig. 2. UV-resonance Raman spectrum of *S. warneri* DSM 20316 (λ_{ex} = 244 nm).

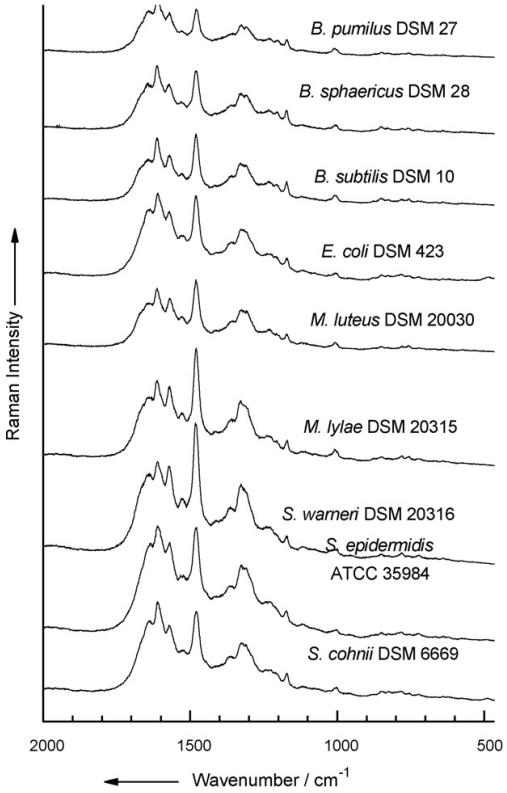

Fig. 3. UV-resonance Raman spectra of different bacterial strains (λ_{ex} = 244 nm).

as the ratio of guanine and cytosine to all DNA bases. The GC value may range from 30% for *Streptococcus* species and to over 70% for some *Micrococcus* species and can be used as taxonomic criteria because it is species specific [43].

For the analysis, bacteria were measured as dried films on fused silica plates. Because ultraviolet laser radiation may cause photo degradation of the sample the incident laser intensity should be kept to a minimum. In order to minimize sample damage, the sample was rotated and simultaneously moved in *x* and

Table 2
Classification of bacterial UV-resonance Raman spectra (λ_{ex} = 244 nm)

Name	Number of strains	Total number of spectra	Number of wrong classified strain spectra	Recognition rate for strains (%)	Number of wrong classified species spectra	Recognition rate for species (%)
Bacillus pumilus	2	112	0	100	0	100
Bacillus sphaericus	2	95	1	98.8	0	100
Bacillus subtilis	2	97	0	100	0	100
Escherichia coli	10	271	8	96.4	0	100
Micrococcus luteus	2	107	0	100	0	100
Micrococcus lylae	2	64	0	100	0	100
Staphylococcus cohnii	4	111	0	100	0	100
Staphylococcus epidermidis	8	239	2	99.22	1	99.6
Staphylococcus warneri	2	54	0	100	0	100
	34	1150		98.7		99.9

y-direction. With this method approximately 10^5 bacterial cells contribute to one UV-resonance Raman spectrum. This amount of cells is comparable with a micro-colony after about 5 h of cultivation.

Fig. 3 displays UV-resonance Raman spectra of different strains from nine bacterial species. The excitation wavelength was 244 nm and the integration time for each spectrum 120 s. The UV-resonance Raman spectra mainly show signals from DNA bases and additional from aromatic amino acids such as phenylalanine, tryptophan or tyrosine. For a significant dataset, 1150 UV-resonance Raman spectra from nine species with 34 strains were recorded.

The classification was performed using a support vector machine (SVM) with a non-linear RBF kernel (cost value 1×10^6; γ-value 5.1×10^{-7}). The UV-resonance Raman spectra were pre-treated by median filtering (9 pt) and vector normalization. Table 2 displays the results of the classification. The lowest average recognition rate on strain level can be found for *E. coli* with 96.4%. The other species show much higher recognition rates. For species level only *Staphylococcus epidermidis* with an average recognition rate of 99.6% differs from the other species.

4. Conclusion

The experiments presented within this study convincingly demonstrate the great capabilities of deep UV Raman spectroscopy.

For the identification of mineral phases the number of unsuccessful measurements is clearly smaller when employing excitation lasers in UV. The number of spectra which suffer from fluorescent background interference is also significantly smaller when using these wavelengths for Raman experiments.

Bacterial identification with UV-resonance Raman spectroscopy was performed with a recognition rate of nearly 99% on strain level. Raman signals from macromolecules like DNA/RNA or proteins can be selectively enhanced by means of UV resonance Raman spectroscopy. The selective enhancement of the cellular DNA/RNA content allows for a correlation with the GC value and therefore for a genotaxonomic classification of bacteria.

Acknowledgements

We gratefully acknowledge financial support by the German Aerospace Centre (project number DLR 50OW0502) and by research project FKZ 13N8369 within the framework ‘Biophotonic’ from the Federal Ministry of Education and Research, Germany (BMBF).

References

[1] J. Popp, W. Kiefer, Fundamentals of Raman spectroscopy, in: Encyclopedia of Analytical Chemistry, Wiley, 2000, pp. 13104–13142.
[2] P.A. Estec, J.J. Kovach, P. Waldstein, C. Karr Jr., Proc. Lunar Sci. Conf. 3 (1972) 3047–3067.
[3] E.J. Isreal, R.E. Arvidson, A. Wang, J.D. Pasteris, B.L. Jolliff, J. Geophys. Res. [Planets] 102 (E12) (1997) 28705–28716.
[4] L.A. Haskin, A. Wang, K.M. Rockow, B.L. Jolliff, R.L. Korotev, K.M. Viskupic, J. Geophys. Res. [Planets] 102 (E8) (1997) 19293–19306.
[5] R.L. Korotev, A. Wang, L.A. Haskin, B.L. Jolliff, in: Lunar and Planetary Science Conference, Lunar Planet. Sci. XXIX (1998) 1797–1798.
[6] H.G.M. Edwards, D.W. Farwell, M.M. Grady, D.D. Wynn-Williams, P. Wright 1, Planet. Space. Sci. 47 (1999) 353–363.
[7] J. Popp, N. Tarcea, W. Kiefer, M. Hilchenbach, N. Thomas, S. Hofer, T. Stuffler, European Space Agency, [Special Publication] SP, SP-496(Exo-/Astro-Biology), 2001, 193–196.
[8] A. Wang, B.L. Joliiiff, L.A. Haskin, J. Geophys. Res. [Planets] 104 (E4) (1999/2001) 8509–8519.
[9] D.L. Dickensheets, D.D. Wynn-Williams, H.G.M. Edwards, C. Schoen, C. Crowder, E.M. Newton, J. Raman Spectrosc. 31 (7) (2000) 633–635.
[10] J. Popp, N. Tarcea, M. Schmitt, W. Kiefer, R. Hochleitner, G. Simon, M. Hilchenbach, S. Hofer, T. Stuffler, Proceedings of the Second European Workshop on Exo/Astrobiology, 2002, pp. 339–402.
[11] M.C. Storrie-Lombardi, A.I. Tsapin, G.D. McDonald, H. Sun, K.H. Nealson, Book of Abstracts, 217th ACS National Meeting, Anaheim, California, March 21–25, GEOC-069, 1999.
[12] N. Tarcea, J. Popp, M. Schmitt, W. Kiefer, T. Stuffler, S. Hofer, G. Simon, R. Hochleitner, M. Hilchenbach, Geophys. Res. Abstr. 5 (2003) 12030.
[13] A. Wang, L.A. Haskin, Microbeam Analysis 2000, Institute of Physics Conference Series, 165, 2000, pp. 103–104.
[14] W.H. Nelson, J.F. Sperry, UV resonance Raman spectroscopic detection and identification of bacteria and other microorganisms, in: W.H. Nelson (Ed.), Modern Techniques for Rapid Microbiological Analysis, VCH Publisher, New York, 1991, pp. 97–143.
[15] D. Ivnitski, I. Abdel-Hamid, P. Atanasov, E. Wilkins, Biosens. Bioelectr. 14 (1999) 599–624.
[16] S.F. Al-Khaldi, M.M. Mossoba, Nutrition 20 (2004) 32–38.
[17] A.M. Freydiere, R. Guinet, P. Boiron, Med. Mycol. 39 (2001) 9–33.
[18] D. Naumann, Infrared and NIR Raman spectroscopy in medical microbiology, in: H.H. Mantsch, M. Jackson (Eds.), Infrared Spectroscopy: New Tool in Medicine Proceedings of SPIE, Bellingham, Washington, 1998, pp. 245–257.
[19] D. Naumann, in: R.A. Meyers (Ed.), Encyclopedia of Analytical Chemistry, John Wiley & Sons, Chichester, 2000, pp. 102–131.
[20] D. Naumann, D. Helm, H. Labischinski, Nature 351 (1991) 81–82.
[21] D. Naumann, D. Helm, H. Labischinski, P. Giesbrecht, in: W.H. Nelson (Ed.), Modern Techniques for Rapid Microbiological Analysis, VCH Publisher, New York, 1991, pp. 43–96.
[22] P. Rösch, M. Harz, M. Schmitt, K.-D. Peschke, O. Ronneberger, H. Burkhardt, H.-W. Motzkus, M. Lankers, S. Hofer, H. Thiele, J. Popp, Appl. Environ. Microbiol. 71 (2005) 1626–1637.
[23] P. Rösch, M. Harz, K.-D. Peschke, O. Ronneberger, H. Burkhardt, J. Popp, Biopolymers 82 (2006) 312–316.
[24] M. Harz, P. Rösch, K.-D. Peschke, O. Ronneberger, H. Burkhardt, J. Popp, Analyst 130 (2005) 1543–1550.
[25] P. Rösch, M. Harz, K.-D. Peschke, O. Ronneberger, H. Burkhardt, A. Schüle, G. Schmautz, M. Lankers, S. Hofer, H. Thiele, H.-W. Motzkus, J. Popp, Anal. Chem. 78 (2006) 2163–2170.
[26] P. Rösch, M. Harz, M. Schmitt, J. Popp, J. Raman Spectrosc. 36 (2005) 377–379.
[27] R.M. Jarvis, A. Brooker, R. Goodacre, Anal. Chem. 76 (2004) 5198–5202.
[28] R.M. Jarvis, R. Goodacre, Anal. Chem. 76 (2004) 40–47.
[29] L. Zeiri, B.V. Bronk, Y. Shabtai, J. Czege, S. Efrima, Colloid Surf. A: Physicochem. Eng. Asp. 208 (2002) 357–362.
[30] L. Zeiri, B.V. Bronk, Y. Shabtai, J. Eichler, S. Efrima, Appl. Spectrosc. 58 (2004) 33–40.
[31] S. Chadha, R. Manoharan, P. Moenne Loccoz, W.H. Nelson, W.L. Peticolas, J.F. Sperry, Appl. Spectrosc. 47 (1993) 38–43.
[32] R.M. Jarvis, R. Goodacre, FEMS Microbiol. Lett. 232 (2004) 127–132.
[33] R. Manoharan, E. Ghiamati, S. Chadha, W.H. Nelson, J.F. Sperry, Appl. Spectrosc. 47 (1993) 2145–2150.
[34] R. Manoharan, E. Ghiamati, R.A. Dalterio, K.A. Britton, W.H. Nelson, J.F. Sperry, J. Microbiol. Meth. 11 (1990) 1–15.

[35] Q. Wu, T. Hamilton, W.H. Nelson, S. Elliott, J.F. Sperry, M. Wu, Anal. Chem. 73 (2001) 3432–3440.
[36] K.A. Britton, R.A. Dalterio, W.H. Nelson, D. Britt, J.F. Sperry, Appl. Spectrosc. 42 (1988) 782–788.
[37] R.A. Dalterio, W.H. Nelson, D. Britt, J.F. Sperry, Appl. Spectrosc. 41 (1987) 417–422.
[38] E.C. Lopez-Diez, R. Goodacre, Anal. Chem. 76 (2004) 585–591.
[39] D. Naumann, in: H.-U. Gremlich, B. Yan (Eds.), Infrared and Raman Spectroscopy of Biological Materials, Marcel Dekker, New York, 2001, pp. 323–378.
[40] F. Langenhorst, J.-P. Poirier, Earth Planet. Sci. Lett. 176 (2000) 259–265.
[41] F. Langenhorst, J.-P. Poirier, Earth Planet. Sci. Lett. 184 (2000) 37–55.
[42] C.C. Chang, C.J. Lin, LIBSVM: A Library for Support Vector Machines, 2004.
[43] M.T. Madigan, J.M. Martinko, J. Parker, Brock Mikrobiologie, Spektrum Akademischer Verlag, Heidelberg, 2002.
[44] W.H. Nelson, R. Manoharan, J.F. Sperry, Appl. Spectrosc. Rev. 27 (1992) 67–124.
[45] T. Frosch, N. Tarcea, M. Schmitt, H. Thiele, F. Langenhorst, J. Popp, Anal. Chem. 79 (2007) 1101–1108.

2.2 Micro-Raman spectroscopic identification of bacterial cells of the genus Staphylococcus and dependence on their cultivation conditions. [MH2]

M. Harz, P. Rösch, K.-D. Peschke, O. Ronneberger, H. Burkhardt, J. Popp

Analyst **2005**, 130, 1543-1550.

PAPER www.rsc.org/analyst | The Analyst

Micro-Raman spectroscopic identification of bacterial cells of the genus *Staphylococcus* and dependence on their cultivation conditions

M. Harz,[a] P. Rösch,[a] K.-D. Peschke,[b] O. Ronneberger,[b] H. Burkhardt[b] and J. Popp*[a]

Received 1st June 2005, Accepted 31st August 2005
First published as an Advance Article on the web 30th September 2005
DOI: 10.1039/b507715j

Microbial contamination is not only a medical problem, but also plays a large role in pharmaceutical clean room production and food processing technology. Therefore many techniques were developed to achieve differentiation and identification of microorganisms. Among these methods vibrational spectroscopic techniques (IR, Raman and SERS) are useful tools because of their rapidity and sensitivity. Recently we have shown that micro-Raman spectroscopy in combination with a support vector machine is an extremely capable approach for a fast and reliable, non-destructive online identification of single bacteria belonging to different genera. In order to simulate different environmental conditions we analyzed in this contribution different *Staphylococcus* strains with varying cultivation conditions in order to evaluate our method with a reliable dataset. First, micro-Raman spectra of the bulk material and single bacterial cells that were grown under the same conditions were recorded and used separately for a distinct chemotaxonomic classification of the strains. Furthermore Raman spectra were recorded from single bacterial cells that were cultured under various conditions to study the influence of cultivation on the discrimination ability. This dataset was analyzed both with a hierarchical cluster analysis (HCA) and a support vector machine (SVM).

Introduction

Fast and exact identification of microorganisms is becoming an important challenge in various fields of research and industry, *e.g.*, reliable and rapid methods are needed for the characterization of relevant microorganisms in medical diagnostics, pharmaceutical production or food processing technology. Routine bacterial identification of pathogenic microorganisms is largely based on a morphological evaluation of the microorganism, growing them in various media and a set of biochemical tests.[1] Consequently, this procedure takes at least a few hours or even longer than a day.[2] Therefore novel and fast analytical techniques are necessary, making an extensive, reliable and fast identification of microbes possible. Concerning these requirements, new analysis methods such as mass spectrometry, polymerase chain reaction (PCR), flow cytometry or fluorescence spectroscopy were developed.[1,2] Alternatively vibrational spectroscopic techniques such as Fourier transform infrared spectroscopy (FT-IR)[3–7] and Raman spectroscopy[8–11] in combination with chemometric procedures[12,13] or neural networks (NN)[14,15] are suitable tools for the rapid identification of bacteria.[5] The IR and vibrational spectra provide biochemical information on the molecular composition of the studied microorganisms.[3,8] Spectral signals can be used to differentiate between several microbial species and strains in bulk material or micro colonies.[16–21]

Recently we have shown that micro-Raman spectroscopy in combination with a support vector machine is an extremely capable approach for a fast and reliable, non-destructive online identification of single bacteria belonging to different genera.[22] It could be shown that for the identification of single bacterial cells, one Raman spectrum is sufficient if a powerful database and appropriate evaluation software are available. In contrast yeasts as eukaryotes differ from prokaryotes such as bacteria in their molecular composition. They exhibit certain organelles and therefore they show a spatial heterogeneity. Hence one spectrum is not enough to describe the whole yeast cell. Using a mean spectrum over several measured positions inside the yeast cell it is feasible to distinguish yeasts on a single cell level.[23]

With the help of this technique it is possible to identify both bacteria and yeasts on a single cell level by means of micro-Raman spectroscopy. By investigating microorganisms under real environmental conditions the origin of these cells is unknown, *e.g.* nutrition, temperature or cell age. In order to simulate this situation, in this contribution different *Staphylococcus* strains with varying cultivation conditions were analyzed in order to evaluate this method with a reliable database. The species *Staphylococcus cohnii*, *Staphylococcus epidermidis* and *Staphylococcus warneri* were grown under different cultivation conditions such as nutrition, temperature and culture age. This dataset is analyzed both with a supervised and an unsupervised technique.

In a first attempt, micro-Raman measurements were performed to obtain spectra from bulk material to prove the principal feasibility of the method. For a distinct

[a]*Institut für Physikalische Chemie, Friedrich-Schiller-Universität Jena, Helmholtzweg 4, 07743 Jena, Germany. E-mail: juergen.popp@uni-jena.de; Fax: +49 3641 948302; Tel: +49 3641 948320*
[b]*Lehrstuhl für Mustererkennung und Bildverarbeitung, Institut für Informatik, Albert-Ludwigs-Universität Freiburg, Georges-Koehler-Allee Geb. 052, D-79110 Freiburg, Germany*

identification of the strains a chemometric data analysis was performed.

In further experiments micro-Raman spectra were recorded from single bacterial cells grown under the same conditions as bulk material for a discrimination at a species and strain level. Since signals of single bacteria have more distinctive variabilities[22–26] than those of bulk material a complete dataset including all possible variations of cultivation conditions is needed. A varying culturing environment leads to a variance in the biochemical composition of a microbial cell and could therefore affect the ability to discriminate and identify the investigated species.[27–29] Therefore Raman spectra were recorded from single bacterial cells that were grown under several cultivation conditions with respect to the nutrient medium, incubation temperature and culturing age. These spectra were used to discriminate and classify bacterial species and strains and to analyze the effect of growth dependent distributions of the biochemical compositions of bacterial cells on the distinction capability.

Experimental

Sample preparation

The microorganisms of the species *Staphylococcus cohnii* DSM 6669, DSM 6718, DSM 6719 and DSM 20260, *Staphylococcus warneri* DSM 20036 and DSM 20316 and *Staphylococcus epidermidis* DSM 1798 were obtained from DSMZ (Deutsche Sammelstelle für Mikroorganismen und Zellkulturen). *Staphylococcus epidermidis* ATCC 35984 (American Type Culture Collection) was purchased from the Institut für Infektionsbiologie, Universität Würzburg.

Bacterial cells were cultivated on CA (corynebacterium agar) or CASO (trypticase soy yeast extract medium) plates under varying cultivation conditions with respect to nutrient medium, growing time and temperature. Table 1 gives an overview of the investigated bacteria. In initial experiments the micro-Raman measurements were performed for bulk samples and single bacterial cells cultured on CA-agar or CASO-agar at a temperature of 37 °C following the recommended conditions listed in the DSMZ. For further single bacterial experiments the strains were grown on different media to that listed in the DSMZ. In an additional experiment bacteria were grown on the suggested media but under a different temperature of 30 °C instead of 37 °C.

For a Raman analysis the grown cells were taken from the agar plates and smeared by a diluting loop on a fused silica plate. Fig. 1 shows an image of single bacterial cells smeared on a fused silica plate. The dark roundly shaped features correspond to single bacterial cells. The light features are caused by the blurred extra cellular matrix of the bacteria.

Table 1 Selected bacteria strains for micro-Raman spectroscopy with sample labels

Sample	
S. cohnii subsp. cohnii DSM 6669	A
S. cohnii subsp. urealyticum DSM 6718	B
S. cohnii subsp. urealyticum DSM 6719	C
S. cohnii subsp. cohnii DSM 20260	D
S. warneri DSM 20036	E
S. warneri DSM 20316	F
S. epidermidis ATCC 35984	G
S. epidermidis DSM 1798	H

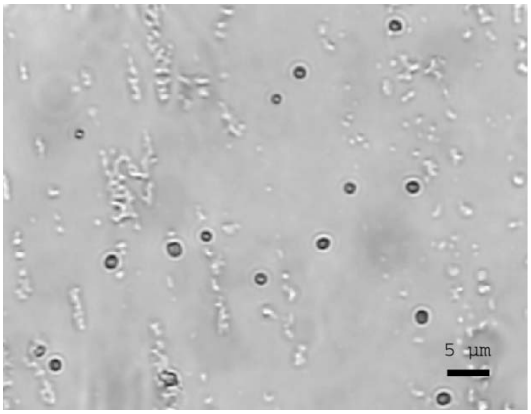

Fig. 1 Microscopic image of a smear of single bacterial cells of *S. cohnii* DSM 6669 on a fused silica plate. The dark roundly shaped features correspond to single bacterial cells and the light features to the blurred extra cellular matrix of the bacteria.

Spectroscopic instrumentation

The Raman spectra of the bacteria were recorded with a micro-Raman setup (HR LabRam invers system, Jobin Yvon, Horiba). Raman scattering was excited by a frequency doubled Nd:YAG laser at a wavelength of 532 nm with a laser power of about 10 mW incident on the sample. The laser beam was focused on individual cells or a bacterial layer by means of a Leica PLFluoar x100/0.75 microscope objective down to a spot diameter of approximately 0.7 µm which is sufficient to resolve single bacteria from the background. The dispersive spectrometer has an entrance slit of 100 µm, a focal length of 800 mm and is equipped with a grating of 300 lines mm^{-1}. The Raman scattered light was detected by a CCD camera operating at 220 K.

Raman spectra of bacterial bulk samples were measured with an integration time of about 10–190 s depending on the fluorescence background. Thereby for each spectrum a new area of the bulk sample was investigated. For the single cell analysis for every spectrum a new cell was measured and an acquisition time of 60 s was used. The data were acquired over the course of several days. For the calibration procedure of the spectrometer a routine check was performed on a daily basis using titanium dioxide as a reference control.

Chemotaxonomic analysis

An unsupervised classification method, hierarchical cluster analysis, was applied to analyze both the bulk spectra and the single bacterial spectra cultivated under recommended conditions. This was done with the program OPUS IDENT from Bruker. Spectral preprocessing was also performed with the OPUS software from Bruker (first derivative, 13 points). For a distinct identification of single bacteria grown under different

cultivation conditions a supervised classification method, a support vector machine, was used.[22,30]

Results and discussion

Raman spectra from bulk samples

In a first attempt, Raman measurements within a multilayer region of the smear were recorded in order to obtain Raman bulk spectra. Raman spectra of bacterial bulk samples are often masked by the appearance of fluorescence. About 148 spectra of the bulk material were recorded. Fig. 2 shows one representative micro-Raman spectrum of a bacterial layer for each *Staphylococcus* strain. It can be seen that the spectra are very similar and reveal a high fluorescence background. The spectrum of *S. cohnii* DSM 6669 (A) exhibits more pronounced signals over the whole spectral region in contrast to the other spectra of *S. cohnii* DSM 6718 (B), *S. cohnii* DSM 6719 (C), *S. cohnii* DSM 20260 (D), *S. warneri* DSM 20036 (E), *S. warneri* DSM 20316 (F), *S. epidermidis* ATCC 35984 (G) and *S. epidermidis* DSM 1798 (H). In the Raman spectrum of *S. cohnii* DSM 6669 (A) there are three dominant bands at 746 cm^{-1}, 1125 cm^{-1} and 1575 cm^{-1}. The peak around 1125 cm^{-1} could be assigned to the ν (C–O–C) stretching vibration from symmetric glycosidic linkages[31] or to ν (C–N) and ν (C–C) stretching vibrations.[11] The peak at 1575 cm^{-1} might be due to the δ (NH) deformation vibration and the ν (CN) stretching vibration.[31,32] These bands are not so pronounced in the spectra of the other examined bacterial bulk samples. However the prominent C–H stretching band region in the range of 2700–3100 cm^{-1} with the ν (CH_2) asymmetric stretching vibration around 2935 cm^{-1} exhibits similar intensities for all investigated strains (Fig. 2). This major C–H stretching band and the peak in the region of 1440–1460 cm^{-1} corresponding to a δ (CH_2) scissoring vibration originate from the CH bindings in lipids, proteins and carbohydrates.[32] Another important peak in the range of 1650–1680 cm^{-1} could be attributed to the amide I band.[32] Table 2 provides an overview of the observed Raman bands of the investigated bacterial cells together with a tentative assignment.

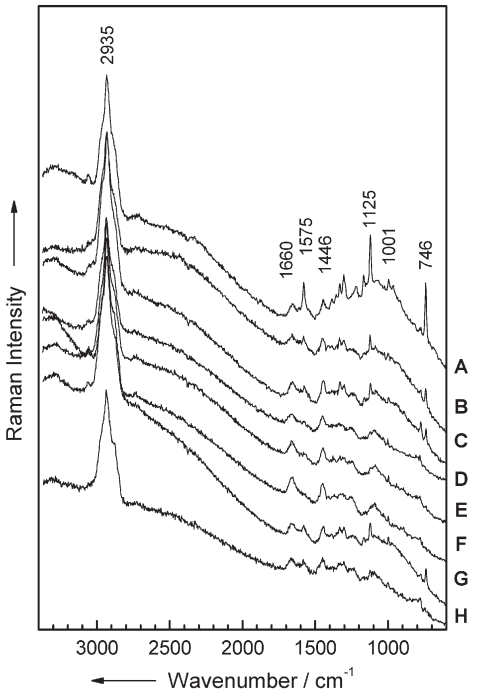

Fig. 2 Raman spectra of bacterial bulk samples of different *Staphylococcus* strains that were smeared on fused silica plates, recorded with an excitation wavelength of 532 nm. The investigated bacterial strains were *S. cohnii* DSM 6669 (A), *S. cohnii* DSM 6718 (B), *S. cohnii* DSM 6719 (C), *S. cohnii* DSM 20260 (D), *S. warneri* DSM 20036 (E), *S. warneri* DSM 20316 (F), *S. epidermidis* ATCC 35984 (G) and *S. epidermidis* DSM 1798 (H) cultured under the recommended conditions listed in the DSMZ.

Table 2 Raman bands observed in spectra of bacterial cells and tentative assignment

Wavenumber/cm^{-1}	Assignment[a]	Reference
~722	ρ (CH_2)	32
746		
~778	Cytosine, uracil ring stretching	11
850	ν (CC) Ring breathing	32
	ν (COC) 1,4-Glycosidic link	32
1001	ν (CC) Aromatic ring breathing (phenylalanine)	20
1125	ν (COC) Symmetric glycosidic link	31
	ν (C–N) and ν (C–C)	11
1200–1280	Amide III	31, 32
~1327	δ (C–H)	20
1440–1460	δ (CH_2) Scissoring	31, 32
1575	Amide II	31, 32
	Guanine, adenine ring stretching	11
1650–1680	Amide I	32
2935	ν (CH_2) Asymmetric	32
3060	ν (CH) Olefinic	32

[a] δ: Deformation vibration, ν: stretching vibration, ρ: rocking vibration.

In order to classify the analyzed bacteria an unsupervised method, hierarchical cluster analysis, was performed. The spectra were pretreated by calculating the first derivative of the Raman spectra to eliminate disturbing baseline contributions. Furthermore the spectral range for the classification was changed and then investigated in order to evaluate the most suitable classes. The best results were obtained by carrying out the hierarchical cluster analysis in the spectral range between 850–1750 cm^{-1} and 2650–3150 cm^{-1}. The spectral distances between every spectrum were calculated with the Normalization to Reproduction Level algorithm. This method is based on a vector normalization that is calculated separately for each spectral range. Furthermore several spectral ranges can be weighted independently with a reproduction level. Hence the spectral distances are expressed in units of the reproduction level. Ward's Technique was used to calculate the spectral distances between a newly created cluster and all the other spectra or clusters. With the help of this cluster algorithm the most similar groups are not clustered but feasible most homogeneous clusters are formed. Fig. 3 shows the dendrogram of the resulting classification of the bulk samples based on 137 spectra of the eight different strains. The labels A to H for each cluster correspond to the

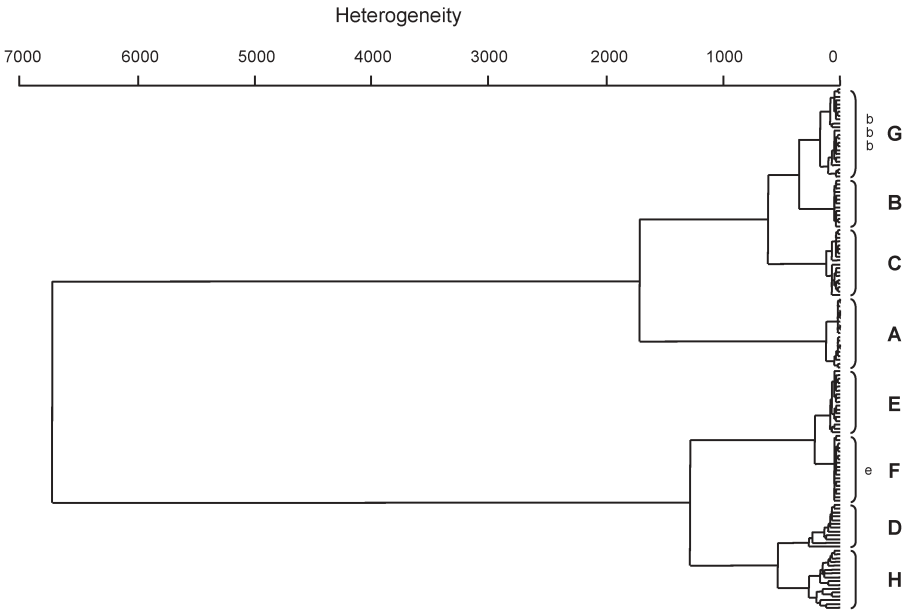

Fig. 3 Cluster analysis of the first derivative spectra using the wavenumber range 850–1750 cm^{-1} and 2650–3150 cm^{-1}. The dendrogram of Raman spectra resulting from HCA was calculated with the spectra of bacterial bulk samples of *S. cohnii* DSM 6669 (A), *S. cohnii* DSM 6718 (B), *S. cohnii* DSM 6719 (C), *S. cohnii* DSM 20260 (D), *S. warneri* DSM 20036 (E), *S. warneri* DSM 20316 (F), *S. epidermidis* ATCC 35984 (G) and *S. epidermidis* DSM 1798 (H). The bacterial bulk samples were cultivated under the recommended culture condition listed in the DSMZ.

one in Table 1. The smaller the spectral distances the more similar are the spectra. A discrimination on the strain level could be achieved. Nearly all spectra of one strain are classified to the same cluster and are well separated from the others. Altogether there is a distinction into two main clusters. One cluster consists of four strains that are *S. cohnii* DSM 6669 (A), *S. cohnii* DSM 6718 (B), *S. cohnii* DSM 6719 (C) and *S. epidermidis* ATCC 35984 (G). The other group is formed by *S. cohnii* DSM 20260 (D), *S. epidermidis* DSM 1798 (H), *S. warneri* DSM 20036 (E) and *S. warneri* DSM 20316 (F). Nevertheless the distinction into two clusters does not reflect the relationship between the species *S. cohnii*, *S. warneri* and *S. epidermidis* within subclusters. In Fig. 3 the incorrectly grouped spectra are displayed with small letters, where the small characters have the same attribution to the different strains as capital letters. Three spectra of *S. cohnii* subsp. urealyticum DSM 6718 (b) were incorrectly grouped to *S. epidermidis* ATCC 35984 (G). They were assigned to another species. Furthermore one spectra of *S. warneri* DSM 20036 (e) was not clustered to the equivalent strain but was grouped to the appropriate species. Nevertheless an identification accuracy of 97.0% (133/137) on the strain level could be obtained, while three of the four spectra were not clustered to the appropriate species leading to a distinction precision of 97.7% (134/137) on the species level.

Beside the hierarchical cluster analysis, a supervised method, the support vector machine, was applied to classify the analyzed bacteria. In contrast to the hierarchical cluster analysis, where spectra with spikes were excluded for the clustering, every measured spectrum was used for the classification by means of the support vector machine. Before classification *via* the support vector machine Raman spectra were preprocessed by running median filtering and by centering. The running median filter is realized as a window that moves over each spectrum while replacing the data point at the center of the window by the median calculated over all points that are covered by the window. The size of the window was chosen to be 9 spectral points. By the centering step the mean value of all feature points over all spectra was set to 0 and the standard deviation was set to 1. This was done to homogenize the distribution in all dimensions in the feature space. The classification is based on the wavenumber region of 330–3600 cm^{-1}. For the classification a nonlinear SVM with a Radial Basis Function (RBF)-Kernel was applied and for our data the one-*versus*-one test was used for training and classification. Only two parameters needed to be adjusted for SVM classification. Firstly, a value that controlled the local support of the radial basis function, called the gamma value and secondly, a cost value that punishes outliers during the training process. For the experiments the gamma value was set to 3.5×10^{-7} while the cost value was set to 2.6×10^{6}. For an estimation of the classification error probability of the final system (which used all N recorded spectra as training set) the leave-one-out error was chosen, which uses $N - 1$ samples as a training set. The reported ''average recognition rate'' is the arithmetic mean of the recognition rates for each strain and species and therefore equalizes the varying number of samples per strain and species in our database. Accomplishing a classification with 148 spectra of the eight different strains from three species, we obtain 141 correctly identified spectra on the strain level (average recognition rate: 94.9%) and 144 correctly identified spectra on the species level (average

Table 3 Recognition rate for Raman spectra of bulk material

Sample	Total number of spectra	Number of wrongly classified strain spectra	Recognition rate for strains (%)	Number of wrongly classified species spectra	Recognition rate for species (%)
S. cohnii subsp. cohnii DSM 6669	20	2	90	1	98.9
S. cohnii subsp. urealyticum DSM 6718	16	1	93.8	0	100
S. cohnii subsp. urealyticum DSM 6719	18	1	94.4	0	100
S. cohnii subsp. cohnii DSM 20260	13	1	92.3	1	92.3
S. warneri DSM 20036	20	0	100	0	100
S. warneri DSM 20316	20	1	95	1	95
S. epidermidis ATCC 35984	25	0	100	0	100
S. epidermidis DSM 1798	16	1	93.8	1	93.8
Average recognition rate			**94.9**		**97.0**

recognition rate: 97.0%). All results are summarized in Table 3. It can be shown that the support vector machine for the classification of our dataset leads to a similar identification accuracy to a hierarchical cluster analysis. However by means of the support vector machine, spectra with spikes could also be used for identification because the data were median filtered.

Raman spectra from single cells

The Raman spectra of the bulk material result from the averaged signal over several bacteria. For the identification of single bacterial cells individual variations have to be taken into account. Therefore it is essential to investigate how different parameters influence the identification ability of microorganisms on a single cell level. Hence to create a reliable dataset the influence of several factors like nutrition, temperature and growing time need to be considered. Thus bacterial cells grown under several cultivation conditions with respect to the nutrient medium (CA-agar or CASO-agar), incubation temperature (30 °C or 37 °C) and culture age were investigated.

First, micro-Raman spectra of single bacteria grown under the DSMZ listed recommended conditions were recorded and used to discriminate and classify bacterial species and strains. Fig. 4 shows representative micro-Raman spectra of eight different strains. The Raman spectra of single cells show characteristic differences compared with the corresponding bulk spectra plotted in Fig. 2. They reveal a lower fluorescence background and additional signals in the range of 720–890 cm^{-1} and 950–1120 cm^{-1} due to the fused silica plate because of the very low sample volume of a single cell. Furthermore a peak at 1001 cm^{-1} corresponding to the ring breathing vibration of the amino acid phenylalanine[20] is more intense in the single cell spectra than in the bulk spectra. It is noteworthy that the three dominant bands at 746 cm^{-1}, 1125 cm^{-1} and 1575 cm^{-1} which appear in the bulk spectrum of *S. cohnii* DSM 6669 (A) (Fig. 2) are marginal or absent in the corresponding single bacterial spectrum (Fig. 4). However an additional band at 778 cm^{-1} that could be attributed to a cytosine and uracil ring stretching vibration[11] can be seen.

For a hierarchical cluster analysis the resulting dendrogram was calculated for the spectral range between 850–1750 cm^{-1} and 2650–3150 cm^{-1}. The spectral distances between every spectrum were calculated with the Normalization to Reproduction Level algorithm and the clustering was based on Ward's Technique. The spectra containing spikes were not considered for the classification. The dendrogram of the resulting classification of single bacteria spectra based on 143 spectra of eight different *Staphylococcus* strains cultivated under the same conditions as bacterial layers is shown in Fig. 5. There are two major clustering branches in the dendrogram. The first cluster consists of *S. warneri* DSM 20036 (E) and *S. warneri* DSM 20316 (F).

The second cluster is made up of two subgroups: one group consists of the four *S. cohnii* strains: *S. cohnii* DSM 6669 (A), *S. cohnii* DSM 6718 (B), *S. cohnii* DSM 6719 (C) and *S. cohnii* DSM 20260 (D) and the other subcluster contains *S. epidermidis* ATCC 35984 (G) and *S. epidermidis* DSM 1798 (H). Hence within this latter group, a clear separation

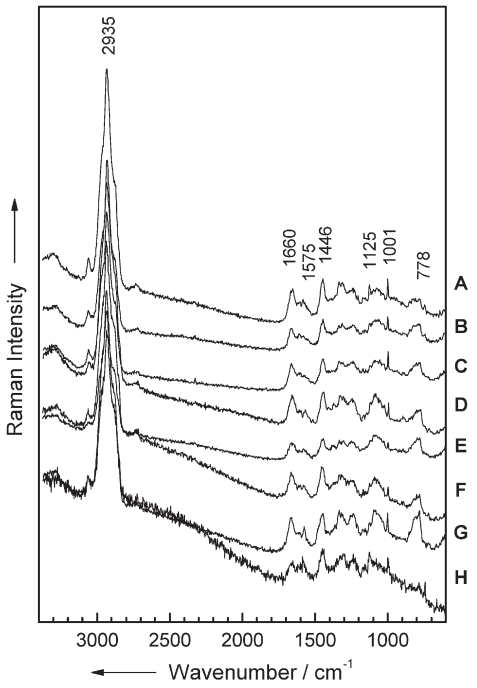

Fig. 4 Raman spectra of single bacterial cells of different *Staphylococcus* strains that were smeared on quartz plates recorded for an excitation wavelength of 532 nm. The analyzed bacterial strains were *S. cohnii* DSM 6669 (A), *S. cohnii* DSM 6718 (B), *S. cohnii* DSM 6719 (C), *S. cohnii* DSM 20260 (D), *S. warneri* DSM 20036 (E), *S. warneri* DSM 20316 (F), *S. epidermidis* ATCC 35984 (G) and *S. epidermidis* DSM 1798 (H) cultured under the recommended condition listed in the DSMZ.

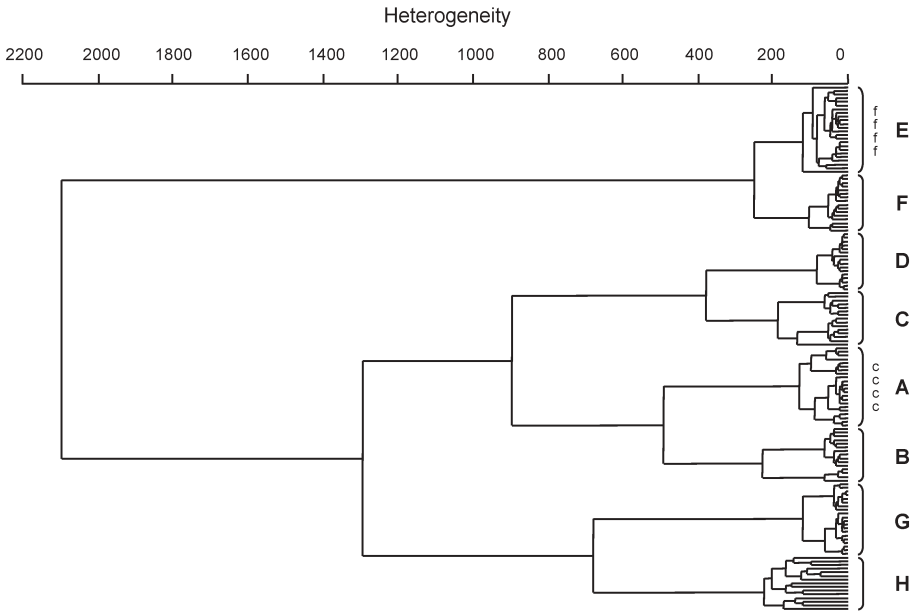

Fig. 5 Cluster analysis on the first derivative spectra for the wavenumber range 850–1750 cm^{-1} and 2650–3150 cm^{-1}. The dendrogram of Raman spectra resulting from HCA was determined with the spectra of single bacterial cells of *S. cohnii* DSM 6669 (A), *S. cohnii* DSM 6718 (B), *S. cohnii* DSM 6719 (C), *S. cohnii* DSM 20260 (D), *S. warneri* DSM 20036 (E), *S. warneri* DSM 20316 (F), *S. epidermidis* ATCC 35984 (G) and *S. epidermidis* DSM 1798 (H). The single bacterial cells were cultivated under the recommended culture conditions listed in the DSMZ.

between the species *S. cohnii* and *S. epidermidis* can be seen. The dendrogram exhibits a good separation of each strain and in contrast to the classification of the bulk samples also a discrimination of the species. As a result there is a distinction on the strain level and on the species level. The divisions into subclusters reflect the relationship between the species *S. cohnii*, *S. warneri* and *S. epidermidis* in contrast to the classification of the bulk spectra. This could be the consequence of the lower background signal of the single cell spectra compared to the bulk spectra. Nevertheless eight samples out of 143 were not clustered to the correct strain. In Fig. 5 the incorrectly grouped spectra are displayed with small letters, where the small characters have the same attribution to the different strains as capital letters. Four spectra of *S. warneri* DSM 20316 (f) were incorrectly grouped to *S. warneri* DSM 20036 (E) however they were assigned to the same species. Furthermore four spectra of *S. cohnii* subsp. urealyticum DSM 6719 (c) were not clustered to the correctt strain, but they were grouped to the appropriate species. Nevertheless an identification accuracy of 94.9% (135/143) on the strain level could be obtained while all spectra were clustered to the appropriate species leading to a distinction precision of 100% on the species level.

These experiments were performed on single bacterial cells cultivated under the recommended culture conditions listed in the DSMZ. However in real applications we do not know the origin of the bacteria. So it was necessary to analyze the effect of different growing circumstances to increase the possible variability of bacteria in authentic applications. The effect of culturing conditions on the identification capability of single bacterial cells for some representative examples was investigated. Therefore bacterial cells were cultivated on different media to those listed in the DSMZ; strains that are recommended to be grown on CA were grown in this experiment on CASO and *vice versa*. In an additional experiment, bacteria were grown under a lower temperature than that recommended from the DSMZ; here the strains were grown at 30 °C.

Fig. 6A shows for each *Staphylococcus* strain representative Raman spectra of *S. cohnii* DSM 20260 and of *S. warneri* DSM 20316 obtained after culturing under several growing conditions. The spectra of the single cells from cultures grown under a lower temperature (30 °C instead of 37 °C) exhibit nearly the same background signal with bands as broad as the bacterial spectra grown under 37 °C. The same effect is observable in the Raman spectra of bacteria grown on CASO-agar instead of a CA-agar and reversed respectively. In general Raman spectra recorded from cells cultured under different conditions exhibit nearly equivalent Raman bands. This is exemplarily shown in Fig. 6A for *S. cohnii* DSM 20260 and for *S. warneri* DSM 20316. All spectra exhibit a characteristic band at 778 cm^{-1}. This peak occurs almost always for *S. warneri* DSM 20036 and *S. warneri* DSM 20316 grown on CASO-agar at 37 °C and CA-agar at 30 °C. This peak cannot be found for the bacteria of *S. cohnii* DSM 6669, *S. cohnii* DSM 6719 and *S. cohnii* DSM 20260 under several growing circumstances.

Additionally the influence of the growing time on the Raman spectrum of single *S. epidermidis* ATCC 35984 cells was evaluated. The first Raman spectra were recorded after only 6 hours incubation time. New samples were prepared and measured in intervals of 6 hours to a total incubation time of

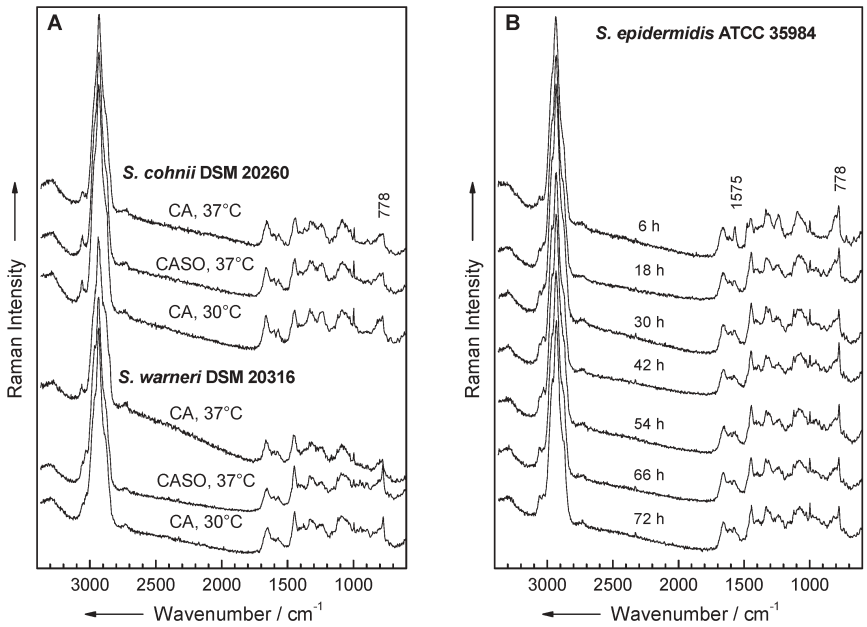

Fig. 6 A: Representative Raman spectra of single cells of *S. cohnii* DSM 20260 and *S. warneri* DSM 20316 obtained after growth on CA-agar or CASO-agar at 37 °C and CA-agar at 30 °C are shown. B: Raman spectra of single *S. epidermidis* ATCC 35984 cells cultured on CASO-agar at 37 °C were recorded for different growth times as indicated.

72 hours. In Fig. 6B representative Raman spectra of single *S. epidermidis* ATCC 35984 cells are displayed that were measured after growing on CASO-agar for different incubation times as indicated. Micro-Raman spectra recorded from cells cultured under these conditions exhibit nearly the same Raman bands, but there is one band in the region about 1575 cm^{-1} that decreases with increasing culturing time. This effect was also observable by examining single *S. epidermidis* ATCC 35984 cells grown on CA-agar at 37 °C and for a lower temperature of 30 °C, not shown here. In contrast to the other strains, every spectrum of *S. epidermidis* ATCC 35984 exhibits a band at 778 cm^{-1} independently of the culture conditions. It can be observed that the spectra of single bacterial cells from older cultures exhibit a better SNR. For an unambiguous analysis on a single cell level, these variations need to be taken into account by including these variations into the applied database for the chemotaxonomic identification.

When this complex data set was applied to the HCA, no clear separation of the species in separate clusters was possible, nor were clusters formed that are based on the same nutrient medium or incubation temperature. Recently we have shown that micro-Raman spectroscopy in connection with a support vector machine is able to identify single bacteria on a strain level.[22] Therefore a support vector machine was used to achieve a classification of single bacteria spectra grown under different culturing conditions. The classification was based on the same pretreatment of the spectra and the same parameters as were used for the identification of bulk material while the gamma value was set to 1×10^{-6} and the cost value to 1×10^{6}. Performing a classification with 1280 spectra of the eight different strains from three species we obtain 1248 correctly identified spectra on the strain level (average recognition rate: 94.1%) and 1266 correctly identified spectra on the species level (average recognition rate: 97.6%). The lowest recognition rate for strains is for *S. cohnii* DSM 6718 with 83.6% and for species for *S. cohnii* DSM 6718 with 90.2%. All results are summarized in Table 4. With these results it can be shown that micro-Raman spectroscopy in combination with support vector machines could be an appropriate approach for a rapid identification of single bacterial cells on the strain level.

Conclusions

In this contribution a chemotaxonomic study of a micro-Raman spectroscopic identification of bacterial bulk material and single cells of different species within the genus *Staphylococcus* is presented. In our experiments, spectra of bulk samples reveal a higher fluorescence background signal in comparison to the corresponding single cell spectra but nevertheless a distinction of strains is possible when applying a support vector machine and a hierarchical cluster analysis although the relationship on the species level is not reflected correctly with the latter method.

When going from a bulk environment to a single cell analysis, individual cell variations need to be considered in order to prove the ability to discriminate single bacteria on a strain level. For this reason, different culturing methods, which include various growing times, temperatures and different agar types, are used to maximize the variation in the single strains. When applying a hierarchical cluster analysis to single bacteria spectra where the strains were grown under one culture condition a distinction of the species is possible

Table 4 Recognition rate for Raman spectra of single bacteria that were grown under different culture conditions

Sample	Total number of spectra	Number of wrongly classified strain spectra	Recognition rate for strains (%)	Number of wrongly classified species spectra	Recognition rate for species (%)
S. cohnii subsp. cohnii DSM 6669	62	0	100	0	100
S. cohnii subsp. urealyticum DSM 6718	61	10	83.6	6	90.2
S. cohnii subsp. urealyticum DSM 6719	63	8	87.3	2	96.8
S. cohnii subsp. cohnii DSM 20260	65	3	95.4	0	100
S. warneri DSM 20036	65	2	96.9	1	98.5
S. warneri DSM 20316	67	7	89.6	3	95.5
S. epidermidis ATCC 35984	785	2	99.7	2	99.7
S. epidermidis DSM 1798	112	0	100	0	100
Average recognition rate			**94.1**		**97.6**

and reflects the relationship of species and subspecies. After cultivating bacteria under various methods a hierarchical cluster analysis was not successful for classification. Therefore a support vector machine was used to identify the whole dataset. By applying 1280 spectra for the classification an average recognition rate of 94.1% on the strain level and 97.6% on the species level was achieved. These results make us hopeful that the combination of Raman spectroscopy with a support vector machine is an extremely capable method of identifying single bacteria of different cultivation conditions not only on the species level but also on the strain level.

For the identification of single bacteria by means of Raman spectroscopy and support vector machines for real applications the origin of the cells is often unknown. As could be shown, varying cultivation conditions have an influence on the Raman spectra, nevertheless for our dataset the identification of the single cell spectra with a support vector machine is suitable.

Acknowledgements

The funding of the research project FKZ 13N8365 and 13N8369 within the framework 'Biophotonik' from the Federal Ministry of Education and Research, Germany (BMBF) is gratefully acknowledged.

References

1 D. Ivnitski, I. Abdel-Hamid, P. Atanasov and E. Wilkins, *Biosens. Bioelectron.*, 1999, **14**, 599–624.
2 S. F. Al-Khaldi and M. M. Mossoba, *Nutrition*, 2004, **20**, 32–38.
3 D. Naumann, D. Helm and H. Labischinski, *Nature*, 1991, **351**, 81–82.
4 D. Helm, H. Labischinski, G. Schallehn and D. Naumann, *J. Gen. Microbiol.*, 1991, **137**, 69–79.
5 D. Naumann, S. Keller, D. Helm, C. Schultz and B. Schrader, *J. Mol. Struct.*, 1995, **347**, 399–405.
6 D. Naumann, in *Encyclopedia of Analytical Chemistry*, ed. R. A. Meyers, John Wiley & Sons, Chichester, 2000, pp. 102–131.
7 C. Kirschner, K. Maquelin, P. Pina, N. A. N. Thi, L. P. Choo-Smith, G. D. Sockalingum, C. Sandt, D. Ami, F. Orsini, S. M. Doglia, P. Allouch, M. Mainfait, G. J. Puppels and D. Naumann, *J. Clin. Microbiol.*, 2001, **39**, 1763–1770.
8 G. J. Puppels, W. Colier, J. H. F. Olminkhof, C. Otto, F. F. M. De Mul and J. Greve, *J. Raman Spectrosc.*, 1991, **22**, 217–25.
9 J. Greve and G. J. Puppels, in *Biomolecular Spectroscopy*, ed. R. E. Hester and R. J. H. Clark, John Wiley & Sons, Chichester, 1992, pp. 231–265.
10 S. J. Webb, *Phys. Rep.*, 1980, **60**, 201–24.
11 K. Maquelin, C. Kirschner, L. P. Choo-Smith, N. van den Braak, H. P. Endtz, D. Naumann and G. J. Puppels, *J. Microbiol. Methods*, 2002, **51**, 255–71.
12 B. K. Lavine, *Anal. Chem.*, 1998, **70**, 209R–228R.
13 E. C. Lopez-Diez and R. Goodacre, *Anal. Chem.*, 2004, **76**, 585–591.
14 R. Goodacre, R. Burton, N. Kaderbhai, E. M. Timmins, A. Woodward, P. J. Rooney and D. B. Kell, *NATO ASI Ser., Ser. 1*, 2000, **30**, 111–136.
15 R. Goodacre, E. M. Timmins, R. Burton, N. Kaderbhai, A. M. Woodward, D. B. Kell and P. J. Rooney, *Microbiology (Reading, UK)*, 1998, **144**, 1157–1170.
16 N. A. Ngo-Thi, C. Kirschner and D. Naumann, *J. Mol. Struct.*, 2003, **661–662**, 371–380.
17 N. A. Ngo Thi, C. Kirschner and D. Naumann, in *Spectroscopy of Biological Molecules: New Directions, 8th European Conference*, ed. J. Greve, G. J. Puppels and C. Otto, Kluwer Academic Publishers, Dordrecht, 1999, pp. 557–558.
18 L.-P. Choo-Smith, K. Maquelin, H. P. Endtz, H. A. Bruining and G. J. Puppels, in *Spectroscopy of Biological Molecules: New Directions, 8th European Conference*, ed. J. Greve, G. J. Puppels and C. Otto, Kluwer Academic Publishers, Dordrecht, 1999, pp. 537–540.
19 L. P. Choo-Smith, K. Maquelin, T. Van Vreeswijk, H. A. Bruining, G. J. Puppels, N. A. N. Thi, C. Kirschner, D. Naumann, D. Ami, A. M. Villa, F. Orsini, S. M. Doglia, H. Lamfarraj, G. D. Sockalingum, M. Manfait, P. Allouch and H. P. Endtz, *Appl. Environ. Microbiol.*, 2001, **67**, 1461–1469.
20 K. Maquelin, L.-P. Choo-Smith, T. van Vreeswijk, H. P. Endtz, B. Smith, R. Bennett, H. A. Bruining and G. J. Pupples, *Anal. Chem.*, 2000, **72**, 12–19.
21 P. Rösch, M. Schmitt, W. Kiefer and J. Popp, *J. Mol. Struct.*, 2003, **661–662**, 363–369.
22 P. Rösch, M. Harz, K.-D. Peschke, O. Ronneberger, H. Burkhardt, H.-W. Motzkus, M. Lankers, S. Hofer, H. Thiele and J. Popp, *Appl. Environ. Microbiol.*, 2005, **71**, 1626–1637.
23 P. Rösch, M. Harz, M. Schmitt and J. Popp, *J. Raman Spectrosc.*, 2005, **36**, 377–379.
24 K. C. Schuster, E. Urlaub and J. R. Gapes, *J. Microbiol. Methods*, 2000, **42**, 29–38.
25 K. C. Schuster, I. Reese, E. Urlaub, J. R. Gapes and B. Lendl, *Anal. Chem.*, 2000, **72**, 5529–5534.
26 W. E. Huang, R. I. Griffiths, I. P. Thompson, M. J. Bailey and A. S. Whiteley, *Anal. Chem.*, 2004, **76**, 4452–4458.
27 H. C. van der Mei, D. Naumann and H. J. Busscher, *Infrared Phys. Technol.*, 1996, **37**, 561–564.
28 D. Hutsebaut, K. Maquelin, P. De Vos, P. Vandenabeele, L. Moens and G. J. Puppels, *Anal. Chem.*, 2004, **76**, 6274–6281.
29 P. K. Sharma, A. Das, K. H. Rao, K. A. Natarajan and K. S. E. Forssberg, *Process Metall.*, 2001, **11B**, 589–598.
30 V. N. Vapnik, *The Nature of Statistical Learning Theory*, Springer Verlag, New York, 1995.
31 H. G. M. Edwards, N. C. Russell, R. Weinstein and D. D. Wynn-Williams, *J. Raman Spectrosc.*, 1995, **26**, 911–916.
32 A. C. Williams and H. G. M. Edwards, *J. Raman Spectrosc.*, 1994, **25**, 673–677.

2.3 Chemotaxonomic identification of single bacteria by micro-Raman spectroscopy: Application to clean-room-relevant biological contaminations. [MH3]

P. Rösch, M. Harz, M. Schmitt, K.-D. Peschke, O. Ronneberger, H. Burkhardt, H.-W. Motzkus, M. Lankers, S. Hofer, H. Thiele, J. Popp

Applied and Environmental Microbiology **2005**, 71, 1626-1637.

APPLIED AND ENVIRONMENTAL MICROBIOLOGY, Mar. 2005, p. 1626–1637 Vol. 71, No. 3
0099-2240/05/$08.00+0 doi:10.1128/AEM.71.3.1626–1637.2005

Chemotaxonomic Identification of Single Bacteria by Micro-Raman Spectroscopy: Application to Clean-Room-Relevant Biological Contaminations

Petra Rösch,[1] Michaela Harz,[1] Michael Schmitt,[1] Klaus-Dieter Peschke,[2] Olaf Ronneberger,[2] Hans Burkhardt,[2] Hans-Walter Motzkus,[3] Markus Lankers,[4] Stefan Hofer,[5] Hans Thiele,[5] and Jürgen Popp[1]*

Institut für Physikalische Chemie, Friedrich-Schiller-Universität Jena, Jena,[1] Lehrstuhl für Mustererkennung und Bildverarbeitung, Institut für Informatik, Albert-Ludwigs-Universität Freiburg, Freiburg,[2] Schering AG[3] and rap.ID Particle Systems GmbH,[4] Berlin, and Kayser-Threde GmbH, Munich,[5] Germany

Received 10 June 2004/Accepted 29 September 2004

Microorganisms, such as bacteria, which might be present as contamination inside an industrial food or pharmaceutical clean room process need to be identified on short time scales in order to minimize possible health hazards as well as production downtimes causing financial deficits. Here we describe the first results of single-particle micro-Raman measurements in combination with a classification method, the so-called support vector machine technique, allowing for a fast, reliable, and nondestructive online identification method for single bacteria.

Microbial contamination not only is a medical problem but also plays a large role in pharmaceutical clean-room production and food-processing technology. For all these fields, a fast and nonambiguous identification of pathogenic and nonpathogenic microorganisms is required. Conventional bacterial identification methods are based on morphological evaluation of the microorganisms and their ability to grow in various media under different conditions (23). Depending on the type of bacteria, the identification process may take at least 1 day but generally takes much longer (2). Bacterial detection methods have to be rapid and very sensitive because even a single pathogenic organism may be an infectious dose (23). To address the requirements, new analysis methods such as mass spectroscopy, PCR, flow cytometry and fluorescence spectroscopy were developed, allowing a fast and reliable identification (2, 23).

An alternative approach to the analysis of microorganisms is the application of vibrational spectroscopic techniques (infrared [IR] and Raman spectroscopy), which have a long tradition since the vibrational spectrum displays a fingerprint of the chemical composition of each bacterium (35). While an IR spectroscopic investigation of microorganisms requires a few hundred cells from controlled cultivation conditions for an analysis and a drying step (37), this is not necessary when applying Raman spectroscopy (36). In particular, when only a small sample amount is available, a special Raman technique called SERS spectroscopy (surface-enhanced Raman scattering spectroscopy) is especially suited. For an investigation of bacteria, various different SERS substrates or SERS microchips in combination with antibodies were tested (14, 15, 19, 24, 25, 53, 54, 63). By applying UV-resonance Raman spectroscopy, direct investigation of macromolecules such as proteins or DNA becomes possible. However, this Raman technique involves extensive experimental costs and extremely careful sample handling (4, 7, 8, 13, 18, 26, 28–30, 38, 39, 58, 59). In 1990, Puppels et al. developed a confocal Raman microscope, capable of recording Raman spectra of single human cells and polytene chromosomes (42). Since then, many biological phenomena in single human cells have been studied by Puppel's group; e.g., Raman spectra of the cell nucleus and the cell cytoplasm in human white blood cells were obtained (43–46). Various groups have reported the classification of bacteria by means of Raman spectroscopy (3, 11, 12, 17, 27, 31–34, 47). Very recently, Maquelin et al. (31) performed for the first time a clinical Fourier transform IR and near-IR–Raman study of bacterial contamination in blood cultures by using microcolonies obtained after 6 to 8 h of cultivation. Other papers have reported Raman and SERS investigations of single yeast cells, bacteria, or spores (1, 10, 21, 60–62). Various investigations of cell components of single bacteria or spores by means of Raman spectroscopy have also been reported (16, 20, 22, 40, 50, 51). In this paper we describe, to the best of our knowledge for the first time, a fast, nondestructive, and very reliable approach to the identification of bacteria on a single-microparticle level by means of a combination of a micro-Raman analysis together with a data classification approach, the so-called support vector machine (SVM) technique.

MATERIALS AND METHODS

Spectroscopic instrumentation. The Raman spectra were obtained with a micro-Raman setup (HR LabRam invers, Jobin-Yvon-Horiba). The spectrometer has an entrance slit of 100 μm and a focal length of 800 mm and is equipped with a 300-lines/mm grating. As excitation wavelengths, the 532-nm line of a frequency-doubled Nd:YAG laser (Coherent Compass) with a laser power of 10 mW incident on the sample were used. The Raman-scattered light was detected by a charge-coupled-device camera operating at 220 K. A Leica PLFluoar 100×

* Corresponding author. Mailing address: Institut für Physikalische Chemie, Friedrich-Schiller-Universität Jena, Helmholtzweg 4, D-07743 Jena, Germany. Phone: (49-3641) 948320. Fax: (49-3641) 948302. E-mail: Juergen.popp@uni-jena.de.

objective focused the laser light onto the samples (ca. 0.7-μm focus diameter). An integration time of 60 s was used both for the bulk and single-bacterium spectra. For the spatially resolved measurements, an *x*/*y* motorized stage (Merzhäuser) with a minimal possible step size of 0.1 μm was used. The *z* displacement was controlled by a piezo-transducer on the objective.

Bacteria and growth conditions. The microorganisms were chosen according to the conditions present in clean rooms. The microorganisms *Micrococcus luteus* (DSM 348 and DSM 20030), *Micrococcus lylae* (DSM 20315 and DSM 20318), *Bacillus subtilis* (DSM 10 and DSM 347), *Bacillus pumilus* (DSM 27 and DSM 361), *Bacillus sphaericus* (DSM 28 and DSM 396), *Escherichia coli* (DSM 423, DSM 498, and DSM 499), *Staphylococcus cohnii* (DSM 6669, DSM 20260, DSM 6718, and DSM 6719), *Staphylococcus warneri* (DSM 20036 and DSM 20316), and *Staphylococcus epidermidis* (RP 62A) were purchased from the Deutsche Sammelstelle für Mikroorganismen und Zellkulturen and from the Institut für Infektionsbiologie, Universität Würzburg. They were cultivated on a standard or nutrition agar (*Micrococcus* and *Bacillus*) or on caseine-peptone soymeal-peptone agar (*Staphylococcus*) for different growing conditions, such as growing time and temperature, respectively. To simulate samples from clean rooms, the Raman measurements were directly performed on single cells from smears on fused silica plates.

SVMs. The analysis of Raman spectra was performed in two steps: (i) preprocessing of the spectra and (ii) classification by using SVMs. The preprocessing was tested by different methods such as baseline correction, normalization, first derivative, and median filtering. Normalization for bulk data and median filtering for both bulk and single-bacterium analysis have obtained the best results. The classification was based on the regions from 850 to 1,750 and 2,650 to 3,150 cm^{-1}. The limits of those regions were chosen by using the optimization procedure of linear SVMs described below.

The classification step was achieved by using SVM. These large-margin classifiers are widely used in pattern analysis and are already well understood (5, 57). It has been shown that standard SVMs perform as well as or better than neural networks (NN) even in domains such as hand-written character recognition, where several years of research were spent to optimize the NN for a certain problem (48).

Since a classification task can always be broken down into several two-class problems (using a one-versus-one approach), a SVM solves only a two-class problem. The basic idea is as follows. The traditional approach to classification usually tries to build a model during the training step for each class independently from the other classes. The classifier then tests how well an unknown spectrum matches the different models and assigns the spectrum to the best-fitting one. This could also be interpreted as first using the two models for calculating a border between the two classes and second testing on which side of this border the spectrum lies. The idea of an SVM is therefore to combine these two steps and directly model the border between the two classes. This omits modeling of irrelevant parts and therefore needs much less training data. Since there are many possible hyperplanes, which separate the two classes in the feature space (Fig. 1A), the distance to the training samples is introduced as a quality criterion. With this criterion, there is only one global optimum—the hyperplane with the largest margin—which could reliably be found in the training process. This is a big advantage of SVMs compared to NN, where several suboptimal solutions are found during the training process. The samples that are touched by the margin of the hyperplane are called "support vectors." Therefore, for training and classification, only these support vectors are necessary, while all other vectors could be removed from the training set without changing the result. If an SVM is trained, for example, to classify yeasts and bacteria, it will select the most yeast-like bacteria and the most bacterium-like yeasts as support vectors and will use only those to classify an unknown microorganism. The optimal separation plane with the largest margin and the support vectors (adjacent training samples marked by circles) are shown in Fig. 1B. In cases where the training set includes outliers, i.e., samples that are beyond the separating plane, a cost value is introduced to give those data points a disadvantage. In that way, SVM can model a real-world training data set very efficiently.

For classification, we used an SVM template library that was developed at our institute and is based on the libsvm library (9). Due to the high dimensionality of the data, the border could be defined by a linear function yielding a linear SVM. Applying other (nonlinear) SVMs to the classification problem did not improve the recognition result significantly. We tried one-versus-one and one-versus-rest test setups separately; we found that for our data, the one-versus-one test performed slightly better. Therefore, all the reported results were acquired with a linear SVM and a one-versus-one method for training and classification, while the cost value was set to 90,000.

The output of linear SVMs can be interpreted geometrically, so that one can find out which parts of the spectrum were used for the classification by looking at the direction of the normal vector of the separating hyperplane. In that way, one can identify relevant and irrelevant peaks; this is one of the main advantages of using SVM for classification of spectral data.

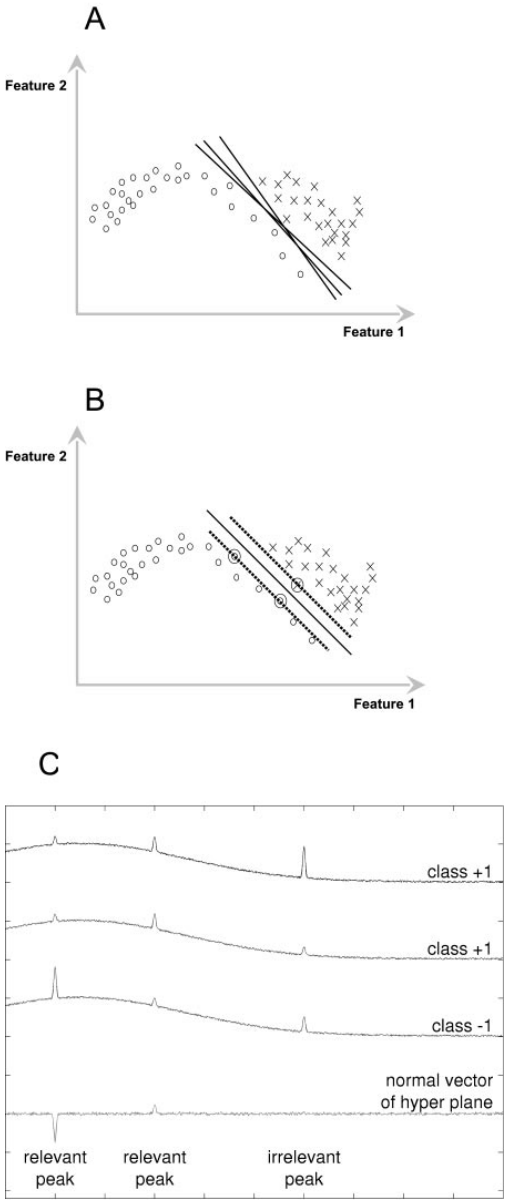

FIG. 1. (A) Possible planes for separating the two classes. (B) The optimal separation plane has the largest margin and is defined only by the adjacent training samples. Support vectors are marked by circles. (C) Classification of simulated spectra. The SVM automatically detects relevant and irrelevant peaks. The third peaks of class +1 differ in size, and so compared to the third peak in class −1, those peaks contain no discriminative information and are irrelevant for the SVM classification.

This is shown in a simple simulation in Fig. 1C, where three spectra (two of

class +1 and one of class −1) and a plot of the normal vector are given. For the spectra, only the first two peaks contain relevant information, while the third does not. Training an SVM with those three spectra, the SVM will automatically find the relevant parts of the spectrum and ignore the irrelevant parts. The height of the peaks in the hyperplane plot shows how important this peak is for the classification, whereas the sign of the peak tells whether it belongs to class +1 or class −1.

Leave-one-out test. For the estimation of the classification error probability of the final system (which will use all recorded spectra as the training set), the leave-one-out error was chosen (which uses $N - 1$ samples as the training set) instead of the widely used "holdout method" (which uses only a certain fraction, e.g., 50%, of the samples as the training set). While it is mathematically proven that the leave-one-out error is an "almost unbiased" estimate for the real classification error probability (49), the holdout method is proven to always return a biased (too high) estimate of the classification error probability (55). (The term "almost" refers to the fact that the leave-one-out error provides an estimate for training on sets of size $N - 1$ rather than N [49].)

Since the a priori probability for the occurrence of each cell species may vary from clean room to clean room, the reported "average recognition rate" is always the arithmetic mean of the recognition rates for each species and therefore equalizes the varying number of samples per species in our database.

RESULTS AND DISCUSSION

In clean-room applications not only the composition of dust but also the number of particles differ from those in the regular environment (56). Usually, production in the pharmaceutical industry takes place in class A or B clean rooms (3,500 0.5-μm particles per m^3 and 0 5-μm particles per m^3). The main components of dust are metal particles, rubber abrasion, skin, hair, and a few microorganisms. Conventional investigation methods count the total number of particles or the colony-building units (56). A complete investigation of the origin of particle contamination would be extremely beneficial, since this would lead to a rapid identification of the source of the contamination. Since clean-room conditions differ from a natural environment, bacteria that can be found in a clean room depend on the purpose for which the room is being used. Furthermore, the total number of bacteria is fairly small, and only a limited number of species are detected compared to a natural environment (H.-W. Motzkus, personal communication).

Bulk spectra. Since the origin of the microorganisms present in a clean room is unknown, a single-bacterium analysis requires careful testing of various parameters such as different culture media or growth times. In the experiments described below, typical clean-room samples are modeled as smears of various microorganisms on fused silica plates. In a first approach, 20 different strains of nine bacterial species which are typical of clean-room contaminants (Motzkus, personal communication) were chosen. Among the chosen bacteria, both colored and noncolored species can be found. Colored bacteria can be easily identified by the presence of carotenoids, which is the pigment in most colored microorganisms. However, this does not allow a distinct identification of the species or strain that is present. Identification of the noncolored bacteria is expected to be even more difficult. Different regions can be found on such a smear: (i) multilayer regions, which can be used to record bulk spectra, and (ii) regions with isolated single cells, where single-bacterium investigations can be performed.

In a first attempt, Raman measurements within a multilayer region on the smear were recorded in order to obtain bulk Raman spectra. Figure 2 shows the Raman spectra of nine different strains, typical of each species. The spectra were recorded with an integration time of 60 s on different multilayer regions on the plate (10 to 20 repetitions [Table 1]). The spectrum of the colored strain (*M. luteus* DSM 20030) is dominated by the carotene bands at 1,525, 1,154, and 1,002 cm^{-1}. Almost no vibrations due to the cell matrix can be seen. For the noncolored strains, the Raman spectra of the four genera are very similar. The Raman spectrum of *E. coli* DSM 499 reveals higher intensities of the amid-I band than do the spectra of the *Bacillus* strains, as well as a very intense C-H band (around 2,900 cm^{-1}). The three *Bacillus* strains (*B. subtilis* DSM 10, *B. pumilus* DSM 361, and *B. sphaericus* DSM 28) exhibit very similar spectra. The signal-to-noise ratio of the three *Staphylococcus* spectra is very low, which is due to the high fluorescence background of these strains (*S. warneri* DSM 20316, *S. cohnii* DSM 20260, and *S. epidermidis* RP 62 A). For a distinct identification of the strains, a reliable data analysis method is required. Therefore, a chemometric data analysis was performed.

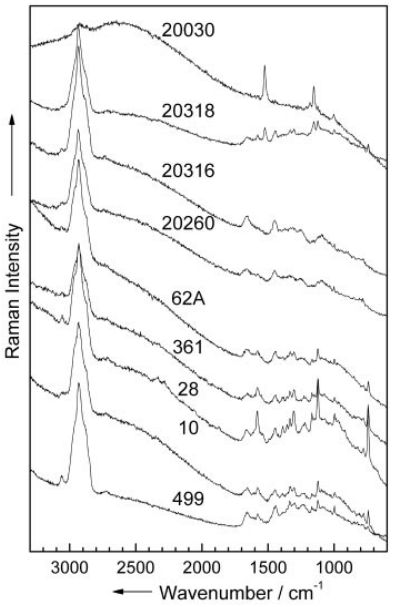

FIG. 2. Micro-Raman spectra of nine different strains (bulk). The numbers in the figure are the strain numbers.

Data analysis of bulk spectra. Since the Raman intensities differ between two successive measurements due to slightly different experimental conditions, a normalization procedure is required. The Raman spectra were normalized on the intensity of the CH peak because this signal represents the total amount of organic compounds in the cells. Not only is the C-H vibration characteristic of one special component, as, for example, fatty acids, but also it corresponds to the sum of all saturated organic material. (Note that it has been found that using C-H vibrations for normalization yields the best results of classification and testing.)

The recognition rate (median filtering, normalization, linear SVM, leave-one-out test) shows very good results (98.0%; Table 1) for all bacterial strains. Of the 339 Raman spectra, 7

TABLE 1. Recognition rate for bulk Raman spectra of various bacterial strains

Strain	Total no. of spectra	No. of wrongly classified strain spectra	Recognition rate for strains (%)	No. of wrongly classified species spectra	Recognition rate for species (%)
B. pumilus DSM 27	12	0	100.0	0	100.0
B. pumilus DSM 361	12	0	100.0	0	100.0
B. sphaericus DSM 28	14	0	100.0	0	100.0
B. sphaericus DSM 396	16	1	93.8	0	100.0
B. subtilis subsp. *subtilis* DSM 10	16	0	100.0	0	100.0
B. subtilis subsp. *spizizenii* DSM 347	10	0	100.0	0	100.0
E. coli DSM 423	12	0	100.0	0	100.0
E. coli DSM 498	20	1	95.0	0	100.0
E. coli DSM 499	20	0	100.0	0	100.0
M. luteus DSM 348	12	0	100.0	0	100.0
M. luteus DSM 20030	20	0	100.0	0	100.0
M. lylae DSM 20315	21	0	100.0	0	100.0
M. lylae DSM 20318	22	0	100.0	0	100.0
S. cohnii subsp. *cohnii* DSM 6669	20	2	90.0	2	90.0
S. cohnii subsp. *cohnii* DSM 20260	13	1	92.3	1	92.3
S. cohnii subsp. *urealyticum* DSM 6718	16	0	100.0	0	100.0
S. cohnii subsp. *urealyticum* DSM 6719	18	1	94.4	0	100.0
S. epidermidis RP 62A	25	0	100.0	0	100.0
S. warneri DSM 20036	20	1	95.0	1	95.0
S. warneri DSM 20316	20	0	100.0	0	100.0
Average recognition rate			98.0		98.9

were misclassified; e.g., within *E. coli*, one DSM 498 strain spectrum was not classified correctly but was assigned as a spectrum of *E. coli* DSM 499 (i.e., the species was identified correctly whereas the assigned strain was wrong). Therefore, the overall identification at the species level reveals 98.9%. These results nicely prove that a reliable identification can be obtained for microcultures. However, it requires up to 6 h to obtain those microcultures by cultivation. It would be greatly preferable to identify single bacteria by means of micro-Raman spectroscopy. Therefore, experiments with isolated single cells were performed to test if a reliable identification of the bacteria is possible on the single-cell level.

Single-cell spectra. Bulk Raman spectra are the result of an averaging over several bacteria. However, for isolated single bacteria, individual variations within the various cells need to be considered. Before performing a single-bacterium analysis, various experiments are needed to investigate if and how different parameters influence the identification of microorganisms on the single-cell level. As already mentioned, no information about the origin of the bacteria is available. Therefore, to create a reliable data set, the variation of different parameters, e.g., nutrition, temperature, and growth time, needs to be considered. Furthermore, it is also necessary to investigate the spatial heterogeneity within a single microorganism, i.e., whether there are any variations within the Raman spectra if the laser focus slightly shifts on the investigated single bacterium.

Raman mapping (heterogeneity effect). Figure 3A shows a micrograph of an isolated single *B. sphaericus* DSM 28 cell on a fused silica plate. Figure 3B displays a Raman spectrum of this bacterium in comparison with a background spectrum, which was recorded beside the microorganism. To test if the Raman spectrum depends on the spatial position of the focus within the bacterium, Raman mapping experiments over the area displayed by the white square in Fig. 3A were performed. For the mapping experiments, a step size of 0.3 by 0.3 μm^2 (total, 20 by 28 points) was chosen. These parameters are smaller than the spatial resolution of the Raman microscope (0.7 μm) but were chosen to increase the spatial overlap of the Raman mapping experiments. Each spectrum was measured with an integration time of 120 s, which leads to a total measuring time of 20 h. To minimize the background of fused silica, a pinhole of 500 μm was used.

Figure 3C shows three Raman images of the three representative bands labeled in Fig. 3B, namely, the C-H stretch vibrations at ~2,900 cm^{-1} (a), the amide I vibration at ~1,650 cm^{-1} (b), and the CH_2 deformation vibration at ~1,420 cm^{-1} (c). As can be clearly seen in the Raman images, no dependency on the spatial position of the measurement could be observed; i.e., the bacterium shows spatial homogeneity. This can be explained by the fact that bacteria normally have no compartments. Some bacteria might contain vesicles where, for example, sulfur or poly-β-hydroxybutyric acid is stored. As was shown by Schuster et al. (50, 51), Raman spectra of single *Clostridium* cells differ with different amounts of starchlike granulose. When line scans over the cell axis were used, no variations with the measuring position could be observed. Another example of structured bacteria involves resistant dominant bodies (spores), which are known to be more complex than vegetative cells since they exhibit several layers, which are schematically displayed in Fig. 4A. The marker substance of bacterial spores is calcium dipicolinate (CaDPA; the structure is shown in Fig. 4B). In Fig. 4C, two spectra of isolated *B. sphaericus* DSM 28 cells (vegetative cell and spore) are displayed. Distinct differences due to CaDPA can be observed in the spectra. The Raman spectrum of the spore shows a band at 1,651 cm^{-1}, which is due to the amide I band. The very intense signals at 1,565, 1,440, 1,383, and 1,007 cm^{-1} can be assigned to CaDPA (6, 16, 18, 30, 41, 53). According to Carmona (6), the vibration at 1,007 cm^{-1} can be assigned to the ring-breath-

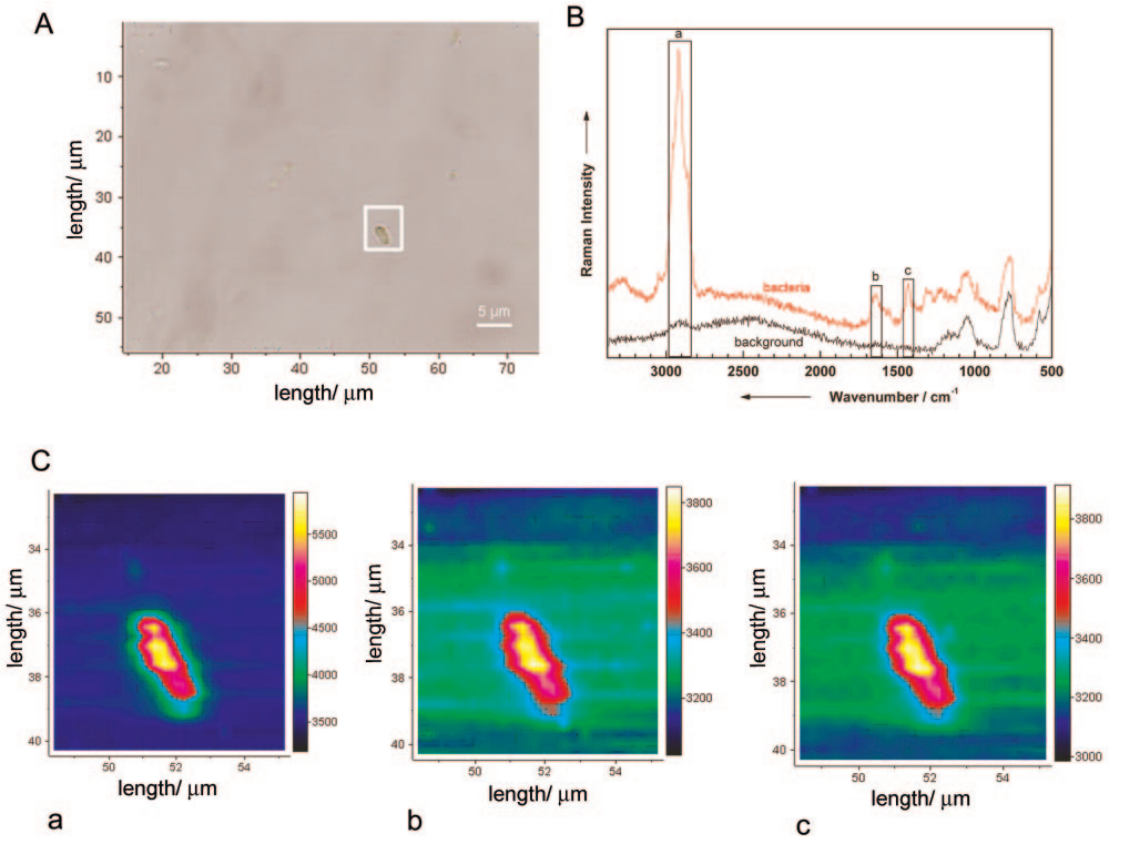

FIG. 3. Raman mapping experiment of a single bacterium (*B. sphaericus* DSM 28). (A) Micrograph of a single bacterium. The white frame indicates the mapping area (0.3 by 0.3 μm^2) for taking the Raman images shown in panel C. (B) Micro-Raman spectra from selected positions within the marked scan area. The marked bands are used to calculate the Raman images plotted in panel C. (C) Raman maps for three different wavenumber regions labeled in panel B: a, 2,851 to 2,964 cm^{-1}; b, 1,604 to 1,671 cm^{-1}; and c, 1,410 to 1,455 cm^{-1}. For details, see the text.

ing vibration of the pyridine ring. The C-O-C stretching vibration can be observed at 1,385 cm^{-1}, whereas both signals at 1,440 and 1,565 cm^{-1} can be assigned to ring vibrations.

Since bacterial spores are highly heterogeneous (Fig. 4A), it is expected that the Raman spectra of such spores will depend on the spatial position where the Raman spectrum was recorded. Figure 5A shows a microphotograph of several vegetative cells and two spores of *B. sphaericus* DSM 28. Spores, which are highly refractive bodies, can be distinguished from vegetative cells under a light microscope (Fig. 5A). In Fig. 5B, Raman spectra taken at four different spatial positions within the white square are shown. The spectrum at the bottom corresponds to a background spectrum, while the other spectra are from a vegetative cell or at two different positions within the spore, respectively. As already shown in Fig. 4C, the spectra of vegetative cells and spores differ due to the different concentrations of CaDPA. Additionally, the Raman spectra of the spore recorded at two different positions show subtle variations. This becomes even more obvious in Fig. 5D, where various confocal Raman images are shown. The images were recorded over the area displayed by the white square shown in the microphotograph in Fig. 5A. Furthermore, a depth profiling has been performed by measuring the images at three different depths shown in the schematic sketch in Fig. 5C. For the three-dimensional Raman mapping, a lateral and axial spatial resolution of 0.5 µm was used, which leads to a total volume of 22 by 16 by 3 points. Each spectrum was measured with an integration time of 300 s, resulting in a total time of approximately 90 h. For the confocal measurements, a hole of 200 µm and a slit of 50 µm was used. The laser power at the sample was ca. 2.5 mW. The images a1, a2, and a3 map the intensity of the C-H stretch vibrations (2,871 to 2,991 cm^{-1} in Fig. 5B, region a) recorded for the three different depth positions 1, 2, and 3, as shown in Fig. 5C inside the mapping area. As can be seen from the Raman spectra (Fig. 5B), C-H stretch vibrations can be found in both vegetative cells and spores. However, when looking at the confocal Raman images displayed in Fig. 5D (a1, a2, and a3), it is evident that spores exhibit a higher degree of ellipticity because at depth position 1 the CH intensity can be found only at positions where the spores are located (image a1 in Fig. 5D). For positions 2 and 3, CH intensity also occurs where the vegetative cells can be

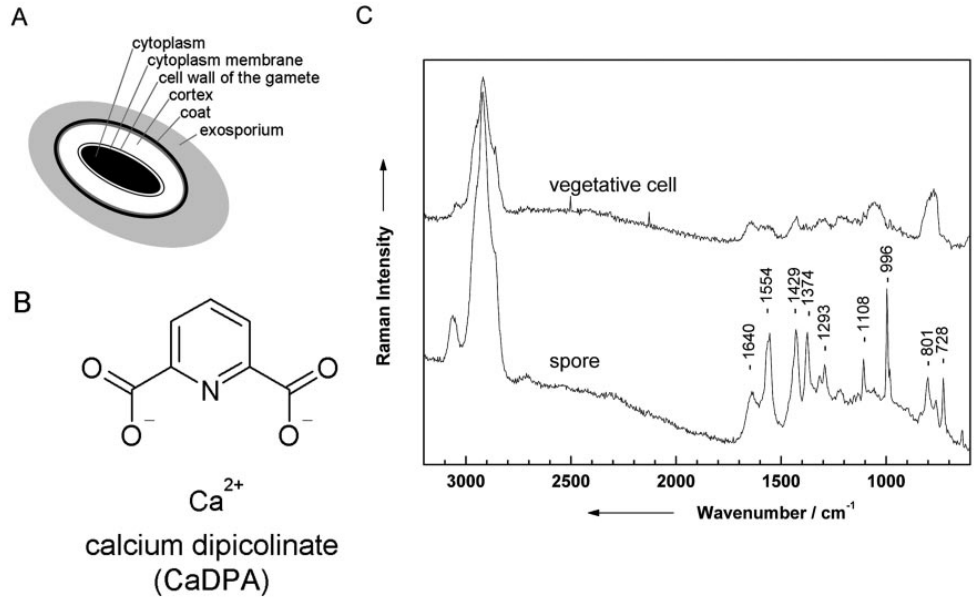

FIG. 4. (A) Schematic diagram of a spore. (B) Chemical structure of CaDPA, which is a marker substance and can be found in all spores. (C) Raman spectra of a vegetative cell and a spore of *B. sphaericus* DSM 28.

found (images a2 and a3 in Fig. 5D). This becomes even more obvious when mapping a Raman band which can be only found in the Raman spectrum of the spores. Images b1, b2, and b3 in Fig. 5D map the intensity of the ring-breathing mode of the pyridine ring of CaDPA (993 to 1,034 cm^{-1} in Fig. 5B, region b), which is a characteristic component of spores and which does not appear in vegetative cells. Images b1, b2, and b3 in Fig. 5D map the spores exclusively. The spore images recorded by integrating over the C-H stretch vibrations (a1, a2, and a3 in Fig. 5D) show subtle differences from the images obtained by integrating over the pyridine ring breathing mode (b1, b2, and b3 in Fig. 5D). CaDPA can be found only within the cortex layer of the spore (Fig. 4A). The C-H stretch vibrations result from all biological components (proteins, lipids, DNA, etc.) within the vegetative cells or spores, respectively. Their distribution within the spores differs from that of CaDPA.

To establish an automatic analytical procedure for the identification of single bacteria by means of Raman spectroscopy, these observations have to be taken into account; i.e., to identify heterogeneous bacteria such as single spores, measurements at three to five different positions should be performed (S. Hofer et al., 23 February 2004, German Patent Office).

Cultivation conditions. Another issue which might be of relevance for an analysis at the single-cell level is that of different nutritional conditions. This has also been tested by measuring Raman spectra of various single bacteria of different strains (not shown here) in different culture media and included in the identification data set.

Furthermore, the influence of the growth time on the Raman spectrum needs to be evaluated. Figure 6 shows representative Raman spectra of single *B. subtilis* DSM 10 (Fig. 6A) and *M. luteus* DSM 348 (Fig. 6B) cells recorded for different growth times as indicated. The spectra of single cells from very young cultures exhibit a low signal-to-noise ratio with broad bands, while Raman spectra of cells of older cultures show sharp distinct signals. These signals belong to vegetative cells and not to spores (compare Fig. 4C). For an unambiguous analysis on the single-cell level, these variations have to be taken into account, being included in the applied database for the chemometric identification (see below).

M. luteus is a colored bacterium, in which the pigment comes from the presence of the carotenoid sarcinaxanthin exhibiting an absorption maximum around 500 nm. Therefore, the Raman spectra of *M. luteus* recorded for an excitation wavelength of 532 nm are resonantly enhanced. The strong bands at 1,532, 1,157, and 1,005 cm^{-1} (Fig. 6B) are due to C═C stretch, C—C stretch, and C—CH_3 deformation modes of sarcinaxanthin. As can be seen in Fig. 6B, the concentration of this chromophore varies with the cultivation age. For 32 h, the lowest concentration of sarcinaxanthin can be observed, while for 45 h, a maximum is reached. Overall, the concentration distribution of sarcinaxanthin does not show a linear relationship to cultivation age.

Photobleaching. The concentration variation of colored bacteria is accompanied by bleaching effects, which occur exclusively when working with a single colored bacterium and when the Raman excitation laser lies within the absorption band of the bacterium's chromophore. This is illustrated in Fig. 7A, where Raman spectra of a single *M. luteus* cell (cell marked by a circle in Fig. 7B, showing a microphotograph of several *M. luteus* DSM 348 cells) are plotted for three different irradiation times, as indicated. Each Raman spectrum was recorded with

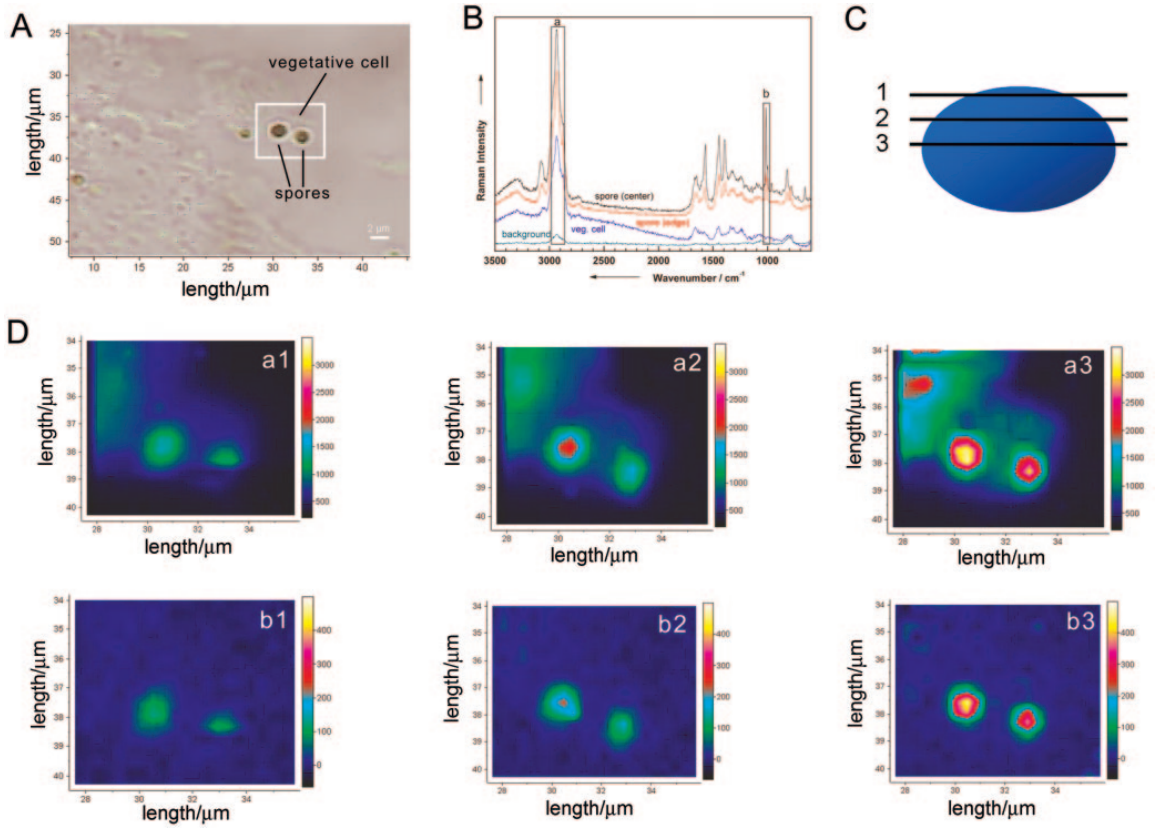

FIG. 5. Raman mapping experiment on single spores and vegetative cells (*B. sphaericus* DSM 28). (A) Micrograph of two spores surrounded by vegetative cells. The white frame indicates the mapping area. (B) Micro-Raman spectra from selected positions within the marked scan area. The spectrum at the bottom corresponds to a background spectrum, while the other spectra are taken from a vegetative cell or at two different positions within the spore, respectively. The marked bands are used to calculate the Raman images plotted in panel D. (D) Raman maps for the two different wavenumber regions labeled in panel B (a, 2,871 to 2,991 cm^{-1}; b, 993 to 1,034 cm^{-1}) for three different depths positions indicated by the three horizontal lines within the schematic sketch of a spore shown in panel C. Position 3, −1.0 µm; position 2, −0.5 µm; position 1, 0 µm. For details, see the text.

an integration time of 60 s. The top spectrum shows the initial Raman spectrum, while the two other spectra were recorded directly after irradiating the same single *M. luteus* bacterium after 60 and 360 s, respectively, with the 532-nm laser. The intensity of the carotenoid bands at 1,532, 1,157, and 1,005 cm^{-1} decreases with increasing irradiation time. Figure 7C shows the dependency of the intensity of three different bands labeled by a, b, and c in Fig. 7A as a function of the irradiation time. As can be clearly seen from the marked signals, only the mode corresponding to the C═C stretch vibration of sarcinaxanthin at 1,532 cm^{-1} (band a), which is resonantly enhanced, shows a time dependency. The intensities of the other two bands, b and c, which are not chromophore vibrations, are almost unaffected by the irradiation process. These measurements have been repeated several times, and the same time behavior could always be observed; i.e., this irradiation time behavior is absolutely reproducible. However, this bleaching effect of the chromophore modes is advantageous for a single-cell analysis, since after the bleaching has taken place, only the characteristic Raman bands due to the cell matrix are left. This is especially important since many bacteria produce pigment structures of the carotenoid type and since the production of these structures depends strongly on the cultivation and growth state. Thus, pigmentation of bacteria alone is generally useless for microbiological identification, but when it is used in combination with the information about the cell matrix obtained after bleaching, an exact identification can be made.

All these results demonstrate that the above-mentioned parameters, such as heterogeneity, growth time, bleaching effects, and nutrition conditions, might lead to more or fewer variations within the Raman spectra of single cells. Most of those variations have already been included in our database as well as in our classification procedure for an unambiguous assignment of bacteria on a single-cell level.

Single-cell identification. In Fig. 8, examples of micro-Raman spectra of single cells of nine representative different species are shown, with an integration time of 60 s per spectrum. The spectra show characteristic differences from the

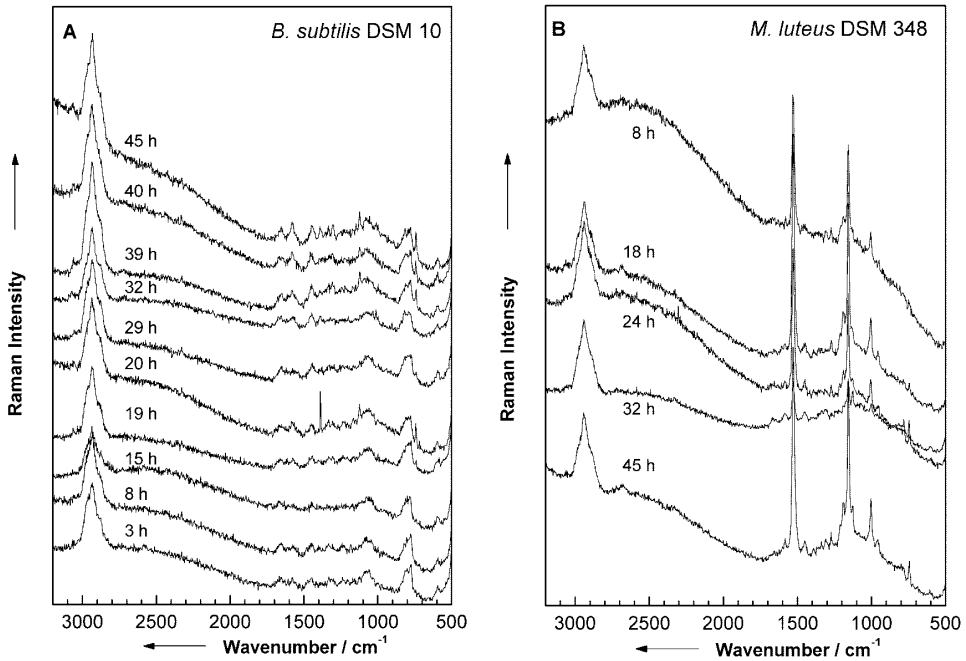

FIG. 6. (A) Raman spectra of single *B. subtilis* cells recorded for different growth times as indicated. (B) Raman spectra of single colored *M. luteus* bacteria for various growth times as indicated.

corresponding bulk spectra plotted in Fig. 2: a lower background, a lower signal-to-noise ratio, or additional signals due to the fused silica plate (asterisk in Fig. 8), which all occur from the very low sample volume of 0.5 μm^3 (*Micrococcus* and *Staphylococcus*) to 2.5 μm^3 (*Bacillus* and *E. coli*) of a single bacterium. The poor signal-to-noise ratio for each Raman spectrum of the various single cells is a result of the short integration time. However, the quality of the single-cell spectra shown in Fig. 8 is sufficient for an identification of the bacteria by means of an SVM (see below) (Table 2). Since time is a critical issue for the analysis of clean-room samples, the overall investigation time should be kept as short as possible.

Additionally, some other features appear in the spectra, e.g., additional protein signals at 1,655 and 1,452 cm^{-1} in the spectra of *M. luteus* DSM 20030. The differences in the three Raman spectra of *Bacillus* strains as well as the *E. coli* spectrum are less pronounced than for to the corresponding bulk spectra plotted in Fig. 2. The three *Staphylococcus* spectra as well as the *M. lylae* spectrum are of much better quality than the bulk spectra in Fig. 2.

For an identification, spectra from single vegetative cells of different agar types and growth times are used and each single bacterium is represented by one spectrum; however, for *M. luteus*, three spectra recorded in a row were always used for the identification. Performing a classification with 2,257 spectra of the 20 different strains from nine species (median filtering, no normalization, linear SVM, leave-one-out test), we obtain 2,136 correctly identified spectra at the strain level (average recognition rate, 89.2%) and 2,180 correctly identified spectra at the species level (average recognition rate, 93.6%). The lowest recognition rate for strains was obtained for *B. sphaericus* DSM 362, with 76.7%, and that for species was for *B. sphaericus* DSM 27, with 82.5%. All the results at the single-cell level are summarized in Table 2. The decrease in recognition rate for single cells compared to the bulk samples was mostly because of less characteristic spectra and low signal-to-noise ratios.

With this first approach, it can be shown that micro-Raman spectroscopy in connection with SVMs is capable of rapid identification of bacteria at the single-cell level. When going from a bulk environment to a single-cell analysis, several points need to be considered. For this reason, different culture methods, which include different growth times and different agar types, are used to maximize the variation in the single strains. Furthermore, possible heterogeneity effects within single cells were evaluated, and it could be shown that single bacteria exhibit a spatial homogeneity. This is not the case for spores. If spores or bacteria with, for example, poly-β-hydroxybutyric acid inclusions are included in the data set, more than one sample spot is necessary. It is possible, for example, to identify the principal axis of spores and to measure three times along this axis. For an investigation of single colored bacteria, where the Raman laser is resonant with the electronic absorption of the pigment, possible bleaching effects must be taken into account. However, it could be shown that such bleaching effects are advantageous since, after the bleaching process, only the Raman bands corresponding to the cell matrix necessary for an unambiguous identification of single cells are left. Over-

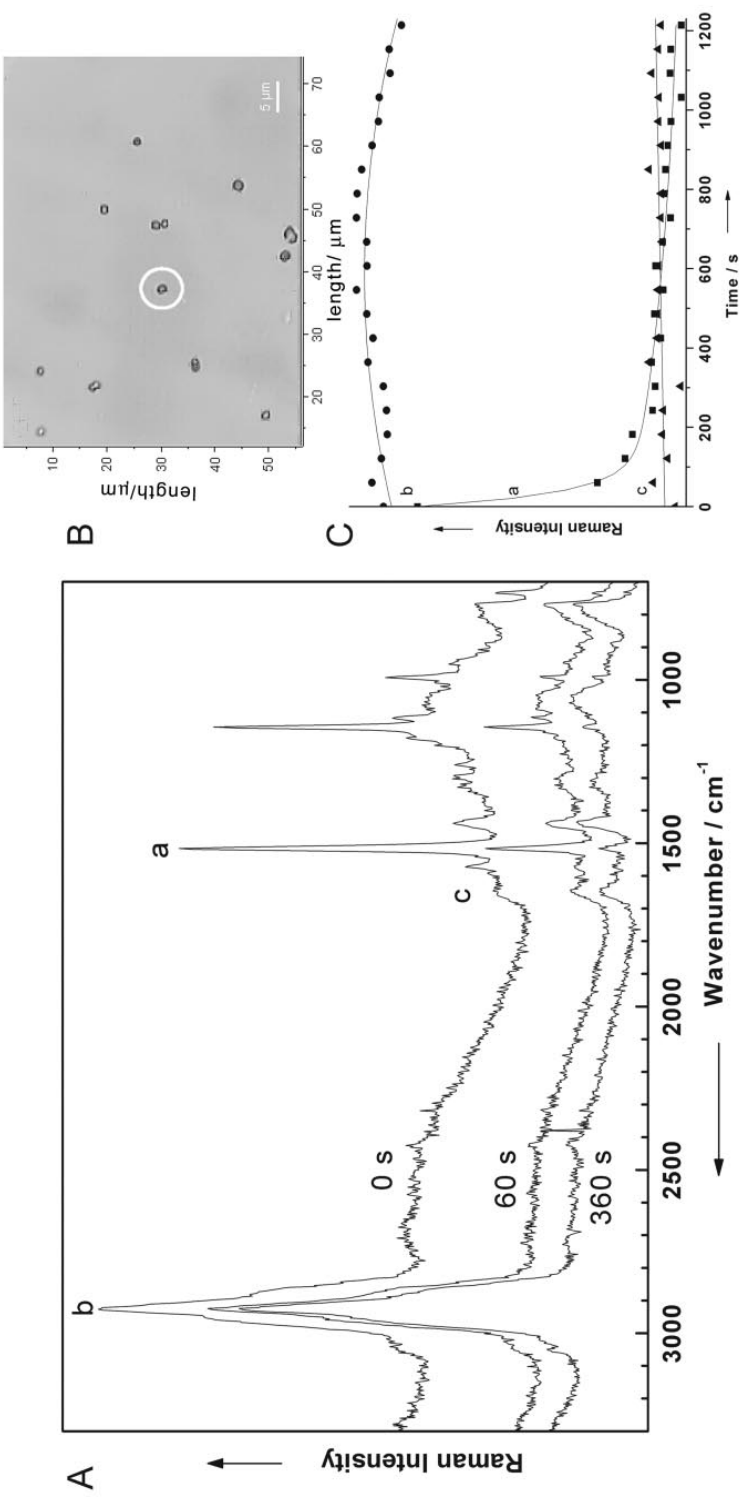

FIG. 7. (A) Micro-Raman spectra of *M. luteus* DSM 348 recorded after irradiating the single *M. luteus* cell at 0, 60, and 360 s with the 532-nm laser, which is resonant with an electronic absorption of the chromophore sacinaxanthin of this microorganism. (B) Micrograph of various single *M. luteus* bacteria. The cell with which the Raman spectra in panel A was obtained is marked by a circle. (C) Dependency of the three bands labeled a, b, and c in panel A on the irradiation time. Only the band which corresponds to the C═C stretch vibration of the protection pigment sacinaxanthin of *M. luteus* shows a bleaching effect, while the other two vibrations, namely, the C-H vibration (b) and the amide-I band (c), are almost not affected by irradiation with 532 nm. For details, see the text.

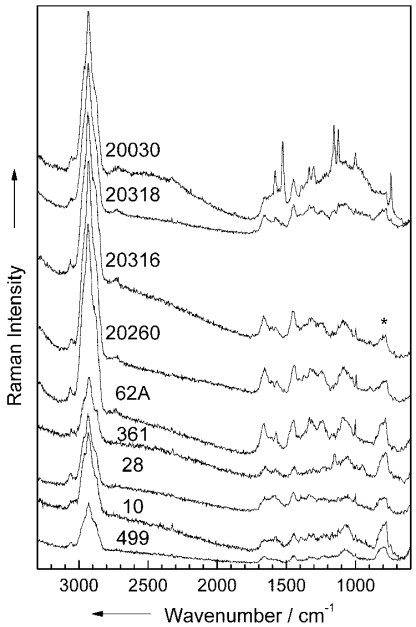

FIG. 8. Micro-Raman spectra of single living bacteria of nine different strains. The numbers in the figure are the strain numbers. *, fused silica.

all, a total of 2,257 Raman spectra of single cells were used to differentiate among 20 strains belonging to nine different species, and a recognition rate of 89.2% for strains and 93.6% for species using an SVM technique could be achieved. These results make us hopeful that by increasing the number of species, a reliable database allowing for a rapid identification of bacteria in clean rooms can be established.

Within the scope of the main research "Biophotonic" supported by the German Ministry of Education and Research, we are currently developing a technique for the rapid detection of airborne biological contaminations within clean rooms (S. Hofer et al., 23 February 2004, German Patent Office). In this technique, the airborne microparticles are deposited on special filters and, in a successive monitoring step, the particles are differentiated into biological and nonbiological particles by means of fluorescence detection. Once the biological particles have been identified on the filter, the actual identification step by means of Raman spectroscopy and SVM can take place. The investigated basic principles of this method are supported by the companies Kayser-Threde (Munich) and RapId (Berlin). With these companies, a first functional model has already been realized.

The presented method can be readily used for all fields where a limited number of bacteria need to be identified. The ultimate goal of our work, however, is a generalization of the technique to all applications, e.g., food-processing technologies and medical applications, where microorganism contaminations are troublesome. To reach this goal, the diversity of microorganism needs to be extended.

ACKNOWLEDGMENTS

Funding of research project FKZ 13N8369, 13N8365, and 13N8379 within the framework "Biophotonik" from the Federal Ministry of Education and Research, Germany (BMBF), is gratefully acknowledged.

We thank W. Kiefer for helpful scientific discussions. We are most grateful to D. Naumann and G. Puppels for many helpful and fruitful discussions and for the thorough review of the manuscript.

TABLE 2. Recognition rate for Raman spectra of single bacteria

Strain	Total no. of spectra	No. of wrongly classified strain spectra	Recognition rate for strains (%)	No. of wrongly classified species spectra	Recognition rate for species (%)
B. pumilus DSM 27	57	11	80.7	10	82.5
B. pumilus DSM 361	43	10	76.7	5	88.4
B. sphaericus DSM 28	53	8	84.9	5	90.6
B. sphaericus DSM 396	42	7	83.3	7	83.3
B. subtilis subsp. *subtilis* DSM 10	306	10	96.7	8	97.4
B. subtilis subsp. *spizizenii* DSM 347	42	8	81.0	3	92.9
E. coli DSM 423	51	4	92.2	3	94.1
E. coli DSM 498	21	1	95.2	0	100.0
E. coli DSM 499	20	3	85.0	1	95.0
M. luteus DSM 348	619	1	99.8	1	99.8
M. luteus DSM 20030	48	7	85.4	4	91.6
M. lylae DSM 20315	20	0	100.0	0	100.0
M. lylae DSM 20318	20	2	90.0	2	90.0
S. cohnii subsp. *cohnii* DSM 6669	67	3	95.5	2	97.0
S. cohnii subsp. *cohnii* DSM 20260	65	2	96.9	0	100.0
S. cohnii subsp. *urealyticum* DSM 6718	65	14	78.5	7	89.2
S. cohnii subsp. *urealyticum* DSM 6719	63	8	87.3	2	96.8
S. epidermidis RP 62A	517	6	98.8	6	98.8
S. warneri DSM 20036	67	6	91.0	4	94.0
S. warneri DSM 20316	71	10	85.2	7	90.1
Average recognition rate			89.2		93.6

REFERENCES

1. **Alexander, T. A., P. M. Pellegrino, and J. B. Gillespie.** 2003. Near-infrared surface-enhanced-Raman-scattering (SERS) mediated identification of single optically trapped bacterial spores. Proc. SPIE **5085:**91–100.
2. **Al-Khaldi, S. F., and M. M. Mossoba.** 2004. Gene and bacterial identification using high-throughput technologies: genomics, proteomics, and phenomics. Nutrition **20:**32–38.
3. **Berger, A. J., and Q. Zhu.** 2003. Identification of oral bacteria by Raman microspectroscopy. J. Mod. Optics **50:**2375–2380.
4. **Britton, K. A., R. A. Dalterio, W. H. Nelson, D. Britt, and J. F. Sperry.** 1988. Ultraviolet resonance Raman spectra of Escherichia coli with 222.5–251.0 nm pulsed laser excitation. Appl. Spectrosc. **42:**782–788.
5. **Burges, C. J. C.** 1998. A tutorial on support vector machines for pattern recognition. Data Mining Knowledge Disc. **2:**121–167.
6. **Carmona, P.** 1980. Vibrational spectra and structure of crystalline dipicolinic acid and calcium dipicolinate trihydrate. Spectrochim. Acta Ser. A **36:**705–712.
7. **Chadha, S., R. Manoharan, P. Moenne-Loccoz, W. H. Nelson, W. L. Peticolas, and J. F. Sperry.** 1993. Comparison of the UV resonance Raman spectra of bacteria, bacterial cell walls, and ribosomes excited in the deep UV. Appl. Spectrosc. **47:**38–43.
8. **Chadha, S., W. H. Nelson, and J. F. Sperry.** 1993. Ultraviolet micro-Raman spectrograph for the detection of small numbers of bacterial cells. Rev. Sci. Instrum. **64:**3088–3093.
9. **Chang, C.-C., and C.-J. Lin.** 2001. LIBSVM: a library for support vector machines. [Online.] http://www.csie.ntu.edu.tw/~cjlin/libsvm.
10. **Chan, J. W., A. P. Esposito, C. E. Talley, C. W. Hollars, S. M. Lane, and T. Huser.** 2004. Reagentless identification of single bacterial spores in aqueous solution by confocal laser tweezers Raman spectroscopy. Anal. Chem. **76:**599–603.
11. **Choo-Smith, L. P., K. Maquelin, H. P. Endtz, H. A. Bruining, and G. J. Puppels.** 1999. A novel method for rapid identification of micro-organisms using confocal Raman microspectroscopy. Spectrosc. Biol. Mol. New Dir. **8:**537–540.
12. **Choo-Smith, L. P., K. Maquelin, T. Van Vreeswijk, H. A. Bruining, G. J. Puppels, N. A. N. Thi, C. Kirschner, D. Naumann, D. Ami, A. M. Villa, F. Orsini, S. M. Doglia, H. Lamfarraj, G. D. Sockalingum, M. Manfait, P. Allouch, and H. P. Endtz.** 2001. Investigating microbial (micro)colony heterogeneity by vibrational spectroscopy. Appl. Environ. Microbiol. **67:**1461–1469.
13. **Dalterio, R. A., W. H. Nelson, D. Britt, and J. F. Sperry.** 1987. An ultraviolet (242 nm excitation) resonance Raman study of live bacteria and bacterial components. Appl. Spectrosc. **41:**417–422.
14. **Efrima, S., and B. V. Bronk.** 1998. Silver colloids impregnating or coating bacteria. J. Phys. Chem. Ser. B **102:**5947–5950.
15. **Efrima, S., B. V. Bronk, and J. Czege.** 1999. Surface-enhanced Raman spectroscopy of bacteria coated by silver. Proc. SPIE **3602:**164–171.
16. **Esposito, A. P., C. E. Talley, T. Huser, C. W. Hollars, C. M. Schaldach, and S. M. Lane.** 2003. Analysis of single bacterial spores by micro-Raman spectroscopy. Appl. Spectrosc. **57:**868–871.
17. **Fehrmann, A., M. Franz, A. Hoffmann, L. Rudzik, and E. Wust.** 1995. Dairy product analysis: identification of microorganisms by mid-infrared spectroscopy and determination of constituents by Raman spectroscopy. J. AOAC Int. **78:**1537–1542.
18. **Ghiamati, E., R. Manoharan, W. H. Nelson, and J. F. Sperry.** 1992. UV resonance Raman spectra of *Bacillus* spores. Appl. Spectrosc. **46:**357–364.
19. **Grow, A. E., L. L. Wood, J. L. Claycomb, and P. A. Thompson.** 2003. New biochip technology for label-free detection of pathogens and their toxins. J. Microbiol. Methods **53:**221–233.
20. **Huang, W. E., R. I. Griffiths, I. P. Thompson, M. J. Bailey, and A. S. Whiteley.** 2004. Raman microscopic analysis of single microbial cells. Anal. Chem. **76:**4452–4458.
21. **Huang, Y.-S., T. Karashima, M. Yamamoto, and H.-O. Hamaguchi.** 2003. Molecular-level pursuit of yeast mitosis by time- and space-resolved Raman spectroscopy. J. Raman Spectrosc. **34:**1–3.
22. **Huang, Y.-S., T. Karashima, M. Yamamoto, T. Ogura, and H.-O. Hamaguchi.** 2004. Raman spectroscopic signature of life in a living yeast cell. J. Raman Spectrosc. **35:**525–526.
23. **Ivnitski, D., I. Abdel-Hamid, P. Atanasov, and E. Wilkins.** 1999. Biosensors for detection of pathogenic bacteria. Biosens. Bioelectron. **14:**599–624.
24. **Jarvis, R. M., A. Brooker, and R. Goodacre.** 2004. Surface-enhanced Raman spectroscopy for bacterial discrimination utilizing a scanning electron microscope with a Raman spectroscopy interface. Anal. Chem. **76:**5198–5202.
25. **Jarvis, R. M., and R. Goodacre.** 2004. Discrimination of bacteria using surface-enhanced Raman spectroscopy. Anal. Chem. **76:**40–47.
26. **Jarvis, R. M., and R. Goodacre.** 2004. Ultra-violet resonance Raman spectroscopy for the rapid discrimination of urinary tract infection bacteria. FEMS Microbiol. Lett. **232:**127–132.
27. **Kirschner, C., K. Maquelin, P. Pina, N. A. N. Thi, L. P. Choo-Smith, G. D. Sockalingum, C. Sandt, D. Ami, F. Orsini, S. M. Doglia, P. Allouch, M. Mainfait, G. J. Puppels, and D. Naumann.** 2001. Classification and identification of enterococci: a comparative phenotypic, genotypic, and vibrational spectroscopic study. J. Clin. Microbiol. **39:**1763–1770.
28. **Lopez-Diez, E. C., and R. Goodacre.** 2004. Characterization of microorganisms using UV resonance Raman spectroscopy and chemometrics. Anal. Chem. **76:**585–591.
29. **Manoharan, R., E. Ghiamati, R. A. Dalterio, K. A. Britton, W. H. Nelson, and J. F. Sperry.** 1990. UV resonance Raman spectra of bacteria, bacterial spores, protoplasts, and calcium dipicolinate. J. Microbiol. Methods **11:**1–15.
30. **Manoharan, R., E. Ghiamati, S. Chadha, W. H. Nelson, and J. F. Sperry.** 1993. Effect of cultural conditions of deep UV resonance Raman spectra of bacteria. Appl. Spectrosc. **47:**2145–2150.
31. **Maquelin, K., C. Kirschner, L. P. Choo-Smith, N. A. Ngo-Thi, T. van Vreeswijk, M. Stammler, H. P. Endtz, H. A. Bruining, D. Naumann, and G. J. Puppels.** 2003. Prospective study of the performance of vibrational spectroscopies for rapid identification of bacterial and fungal pathogens recovered from blood cultures. J. Clin. Microbiol. **41:**324–329.
32. **Maquelin, K., C. Kirschner, L. P. Choo-Smith, N. van den Braak, H. P. Endtz, D. Naumann, and G. J. Puppels.** 2002. Identification of medically relevant microorganisms by vibrational spectroscopy. J. Microbiol. Methods **51:**255–271.
33. **Maquelin, K., L. P. Choo-Smith, H. P. Endtz, H. A. Bruining, and G. J. Puppels.** 2002. Rapid identification of Candida species by confocal Raman microspectroscopy J. Clin. Microbiol. **40:**594–600.
34. **Maquelin, K., L. P. Choo-Smith, T. V. Vreeswijk, H. P. Endtz, B. Smith, R. Bennett, H. A. Bruining, and G. J. Pupples.** 2000. Raman spectroscopic method for identification of clinically relevant microorganisms growing on solid culture medium. Anal. Chem. **72:**12–19.
35. **Naumann, D.** 2000. Infrared spectroscopy in microbiology, p. 102–131. *In* R. A. Meyers (ed.), Encyclopedia of analytical chemistry. John Wiley & Sons, Ltd., Chichester, United Kingdom.
36. **Naumann, D., D. Helm, H. Labischinski, and P. Giesbrecht.** 1991. The characterization of microorganisms by Fourier-transform infrared spectroscopy (FT-IR), p. 43–96. *In.* W. H. Nelson (ed.), Modern techniques for rapid microbiological analysis. VCH Publishers, New York, N.Y.
37. **Naumann, D., S. Keller, D. Helm, C. Schultz, and B. Schrader.** 1995. FT-IR spectroscopy and FT-Raman spectroscopy are powerful analytical tools for the noninvasive characterization of intact microbial cells. J. Mol. Struct. **347:**399–405.
38. **Nelson, W. H., and J. F. Sperry.** 1991. UV resonance Raman spectroscopic detection and identification of bacteria and other microorganisms, p. 97–143. *In* W. H. Nelson (ed.), Modern techniques for rapid microbiological analysis. VCH Publishers, New York, N.Y.
39. **Nelson, W. H., R. Manoharan, and J. F. Sperry.** 1992. UV resonance Raman studies of bacteria. Appl. Spectrosc. Rev. **27:**67–124.
40. **Pasteris, J. D., J. J. Freeman, S. K. Goffredi, and K. R. Buck.** 2001. Raman spectroscopic and laser scanning confocal microscopic analysis of sulfur in living sulfur-precipitating marine bacteria. Chem. Geol. **180:**3–18.
41. **Phillips, T. E., J. L. Sample, P. F. Scholl, and J. Miragliotta.** 2003. The use of surface enhanced Raman scattering for the detection of dipicolinic acid on silver nanoparticles. Mater. Res. Soc. Symp. Proc. **738:**227–232.
42. **Puppels, G. J., F. F. M. de Mul, C. Otto, J. Greve, M. Robert-Nicoud, D. J. Arndt-Jovin, and T. M. Jovin.** 1990. Studying single living cells and chromosomes by confocal Raman microspectroscopy. Nature **347:**301–303.
43. **Puppels, G. J., H. S. P. Garritsen, G. M. J. Segers-Nolten, F. F. M. de Mul, and J. Greve.** 1991. Raman microspectroscopic approach to the study of human granulocytes. Biophys. J. **60:**1046–1056.
44. **Puppels, G. J., H. S. P. Garritsen, J. A. Kummer, and J. Greve.** 1993. Carotenoids located in human lymphocyte subpopulations and natural killer cells by Raman microscopy. Cytometry **14:**251.
45. **Puppels, G. J., M. van Rooijen, C. Otto, and J. Greve.** 1993. Confocal Raman microscopy, p. 238–258. *In* W. T. Mason (ed.), Fluorescent and luminescent probes. Confocal Raman microspectroscopy. Academic Press, Ltd., London, United Kingdom.
46. **Puppels, G. J., T. C. Bakker Schut, N. M. Sijtsema, M. Grond, F. Maraboeuf, C. G. de Grauw, C. G. Figdor, and J. Greve.** 1995. Development and application of Raman microspectroscopic and Raman imaging techniques for cell biological studies. J. Mol. Struct. **347:**477–484.
47. **Rowe, N. J., J. Tunstall, L. Galbraith, and S. G. Wilkinson.** 2000. Lipid composition and taxonomy of [*Pseudomonas*] *echinoides*: transfer to the genus *Sphingomonas*. Microbiology **146:**3007–3012.
48. **Schölkopf, B., and A. J. Smola.** 2002. Learning with kernels, p. 215–222. MIT Press, Cambridge, Mass.
49. **Schölkopf, B., and A. J. Smola.** 2002. Learning with kernels, p. 366–380. MIT Press, Cambridge, Mass.
50. **Schuster, K. C., E. Urlaub, and J. R. Gapes.** 2000. Single-cell analysis of bacteria by Raman microscopy: spectral information on the chemical composition of cells and on the heterogeneity in a culture. J. Microbiol. Methods **42:**29–38.
51. **Schuster, K. C., I. Reese, E. Urlaub, J. R. Gapes, and B. Lendl.** 2000. Multidimensional information on the chemical composition of single bacterial cells by confocal Raman microspectroscopy. Anal. Chem. **72:**5529–5534.

52. **Shibata, H., S. Yamashita, M. Ohe, and I. Tani.** 1986. Laser Raman spectroscopy of lyophilized bacterial spores. Microbiol. Immunol. **30:**307–313.
53. **Sockalingum, G. D., H. Lamfarraj, A. Beljebbar, P. Pina, M. Delavenne, F. Witthuhn, P. Allouch, and M. Manfait.** 1999. Vibrational spectroscopy as a probe to rapidly detect, identify, and characterize micro-organisms. Proc. SPIE **3608:**185–194.
54. **Sockalingum, G. D., H. Lamfarraj, A. Beljebbar, P. Pina, P. Allouch, and M. Manfait.** 1999. Direct on-plate analysis of microbial cells: a pilot study by surface-enhanced Raman spectroscopy. Spectrosc. Biol. Mol. New Dir. **8:**599–600.
55. **Theodoridis, S., and K. Koutroumbas.** 1999. Pattern recognition, p. 339–349. Academic Press, Inc., San Diego, Calif.
56. **Valet, O.** Automatische Partikelerkennung in Reinraumtechnik. *In* D. Buerkle (ed.)., Reinraumtechnik, in press. Carl Hauser Verlag, Munich, Germany.
57. **Vapnik, V. N.** 1995. The nature of statistical learning theory. Springer Verlag, New York, N.Y.
58. **Wu, Q., T. Hamilton, W. H. Nelson, S. Elliott, J. F. Sperry, and M. Wu.** 2001. UV Raman spectral intensities of *E. coli* and other bacteria excited at 228.9, 244.0, and 248.2 nm. Anal. Chem. **73:**3432–3440.
59. **Wu, Q., W. H. Nelson, S. Elliot, J. F. Sperry, M. Feld, R. Dasari, and R. Manoharan.** 2000. Intensities of *E. coli* nucleic acid Raman spectra excited selectively from whole cells with 251-nm light. Anal. Chem. **72:**2981–2986.
60. **Xie, C., and Y.-Q. Li.** 2003. Confocal micro-Raman spectroscopy of single biological cells using optical trapping and shifted excitation difference techniques. J. Appl. Physiol. **93:**2982–2986.
61. **Xie, C., M. A. Dinno, and Y.-S. Li.** 2002. Near-infrared Raman spectroscopy of single optically trapped biological cells. Optics Lett. **27:**249–251.
62. **Xie, C., Y.-Q. Li, W. Tang, and R. J. Newton.** 2003. Study of dynamical process of heat denaturation in optically trapped single microorganisms by near-infrared Raman spectroscopy. J. Appl. Physiol. **94:**6138–6142.
63. **Zeiri, L., B. V. Bronk, Y. Shabtai, J. Czege, and S. Efrima.** 2002. Silver metal induced surface enhanced Raman of bacteria. Colloids Surf. Ser. **208:**357–362.

2.4 Raman spectroscopic identification of single yeast cells. [MH4]

P. Rösch, M. Harz, M. Schmitt, J. Popp

Journal of Raman Spectroscopy **2005**, 36, 377-379.

JOURNAL OF RAMAN SPECTROSCOPY
J. Raman Spectrosc. 2005; **36**: 377–379
Published online 1 April 2005 in Wiley InterScience (www.interscience.wiley.com). DOI: 10.1002/jrs.1312

JRS

Rapid Communication

Raman spectroscopic identification of single yeast cells

Petra Rösch, Michaela Harz, Michael Schmitt and Jürgen Popp*

Institut für Physikalische Chemie, Friedrich-Schiller-Universität Jena, Helmholtzweg 4, D-07743 Jena, Germany

Received 7 November 2004; Accepted 15 January 2005

Eukaryotes (such as yeasts) and prokaryotes (such as bacteria) differ in size, molecular complexity, etc. By definition, eukaryotic cells store their DNA in a separate internal compartment, the so-called nucleus. Owing to this molecular compartmentalization, the identification of yeast cells by vibrational spectroscopy at a single-cell level is challenging. This contribution reports on first results of micro-Raman analysis together with a hierarchical cluster analysis allowing for an online identification method for yeast cells at a single-cell level. For the classification analysis, an average spectrum from 10 different measuring points within a single yeast cell was used to overcome the heterogeneity of the yeast cells. Copyright © 2005 John Wiley & Sons, Ltd.

KEYWORDS: micro-Raman spectroscopy; yeast cells; single cell identification; eukaryotes; hierarchical cluster analysis

INTRODUCTION

The identification of yeast is of high relevance not only in the medical area (e.g. different *Candida* strains) but also for various food-relevant areas (e.g. wine, beer, bakery products). Various conventional methods, e.g. enzymatic tests, exist that allow for an identification of yeast cells in about 5 h.[1] However, these tests require a pure culture or are not available for all species.

Vibrational spectroscopy offers a different approach to identify yeast or microorganisms. Various groups have reported on the non-ambiguous identification of yeast and bacteria micro-colonies within a size range of 50–100 μm.[2–4] In order to reduce further the amount of microorganisms needed for a rapid identification or to perform measurements at the single-cell level without a cultivation step,[5] further studies on isolated yeast cells are necessary. Xie and co-workers performed measurements on single yeast cells by means of Raman spectroscopy in combination with optical tweezers.[6,7] Further studies on Raman spectroscopic monitoring of yeast mitosis[8] and a micro-Raman mapping experiment of KCN toxication of single yeast cells[9] are also known.

Yeast microorganisms belong to eukaryotes, which differ by definition from prokaryotes (such as bacteria) in their molecular clustering. Micro-Raman mapping experiments with sub-micro resolution of single bacteria cells were performed by Rösch *et al*.[5] From these Raman images, no dependence on the spatial position of measurement was observed, i.e. the bacterium shows spatial homogeneity. This can be explained by the fact that bacteria normally exhibit no compartments. However, yeast cells belong to eukaryotes and micro-Raman mapping experiments on single yeast cells performed by Huang *et al*.[8] to study the mitosis revealed inhomogeneities in the molecular distribution of the various cell components. Therefore, the identification of eukaryotic microorganisms is more complicated. In this paper, we present a micro-Raman spectroscopic approach to overcome the problems caused by compartmentalization, allowing identification of yeast cells at the single-cell level.

EXPERIMENTAL

The Raman spectra were taken with a micro-Raman setup (HR LabRam invers, Jobin-Yvon-Horiba). The spectrometer has an entrance slit of 100 μm and a focal length of 800 mm and is equipped with a 300 lines mm^{-1} grating. For excitation, 532 nm radiation from a frequency-doubled Nd : YAG laser (Coherent Compass) with a laser power of 10 mW incident on the sample was used. The Raman scattered light was detected by a charge-coupled device (CCD) camera operating at 220 K. A Leica PLFluoar ×100 objective focused the laser light on the samples (~0.7 μm focus diameter). For spatially resolved measurements, an

*Correspondence to: Jürgen Popp, Institut für Physikalische Chemie, Friedrich-Schiller-Universität Jena, Helmholtzweg 4, D-07743 Jena, Germany. E-mail: juergen.popp@uni-jena.de
Contract/grant sponsor: Federal Ministry of Education and Research, Germany (BMBF); Contract/grant number: FKZ 13N8369.

x–y motorized stage (Merzhäuser) with a minimum possible step size of 0.1 μm was used. For hierarchical cluster analysis, the OPUS IDENT program was used. The full spectral range (600–3500 cm^{-1}) in combination with vector normalization was used. Clustering was performed using normalization to reproduction level in combination with Ward's technique.

The yeast *Saccharomyces cerevisiae* (DSM 1334 and 70 449) was purchased from the Deutsche Sammelstelle für Mikroorganismen und Zellkulturen. Dry yeast was purchased from a supermarket. They were cultivated on a universal medium for yeast. Raman measurements were performed directly on single cells from smears on fused silica plates.

RESULTS AND DISCUSSION

Raman mapping experiments were performed to test the suitability of yeast cells for a single cell identification.[5] Plate 1(A) shows three Raman spectra (a–c) recorded at three different points within a single yeast cell in comparison with the background spectrum (d), which was recorded where no yeast cells could be found. In Plate 1(B) a microphotograph of two yeast cells is presented. The positions marked correspond to the location where the four Raman spectra (a)–(d) in panel (A) were taken. Raman mapping experiments over the area displayed by the white square in Plate 1(B) were performed to determine the spatial distribution of the various components within the yeast cells. Plate 1(C)–(F) show four Raman images of four representative Raman bands. The image shown in Plate 1(C) is a result of integrating over the CH stretch vibration, being a marker band for organic matter. The intensity distribution of this band mirrors the different thickness of the yeast cells. Plate 1(D) displays the intensity distribution of the C═O stretch vibration (1731–1765 cm^{-1}) marking the lipid fraction. Mapping over the amide I and the C═C lipid band (1624–1687 cm^{-1}) yields the Raman image shown in Plate 1(E). These Raman bands exhibit considerable intensity only in confined areas. The phenylenic C═C Raman band (1567–1607 cm^{-1}) can be only seen in the periphery of the cells.

By applying a micro-Raman setup, one obtains a spatial resolution of <1 μm. However, the heterogeneity of the yeast cells [see the Raman images in Plate 1(C)–(F)] makes it impossible to describe a yeast cell by a single Raman spectrum. Therefore, to reach the goal of identifying a single yeast cell, several Raman spectra recorded within a cell were used to create an average spectrum. Figure 1(A) shows three such average spectra of different yeast cells: (a) *S. cerevisiae* DSM 70 449, (b) dry yeast and (c) *S. cerevisiae* DSM 1334). The spectra are the result of averaging over 10 spectra per cell. The 10 measurements were performed at different locations inside the same cell. These average spectra were used to perform a hierarchical cluster analysis [see Fig. 1(B)]. In Fig. 1(B) the cluster for both *S. cerevisiae* DSM 1334 and DSM 70 449 shows high homogeneity. The cluster of the dry yeast is more heterogeneous than those of the two *S. cerevisiae*, but nevertheless very narrow. The two *S. cerevisiae* strains show a higher similarity to each other than to the dry yeast. As can be seen in Fig. 1(B), the average spectra cluster very well

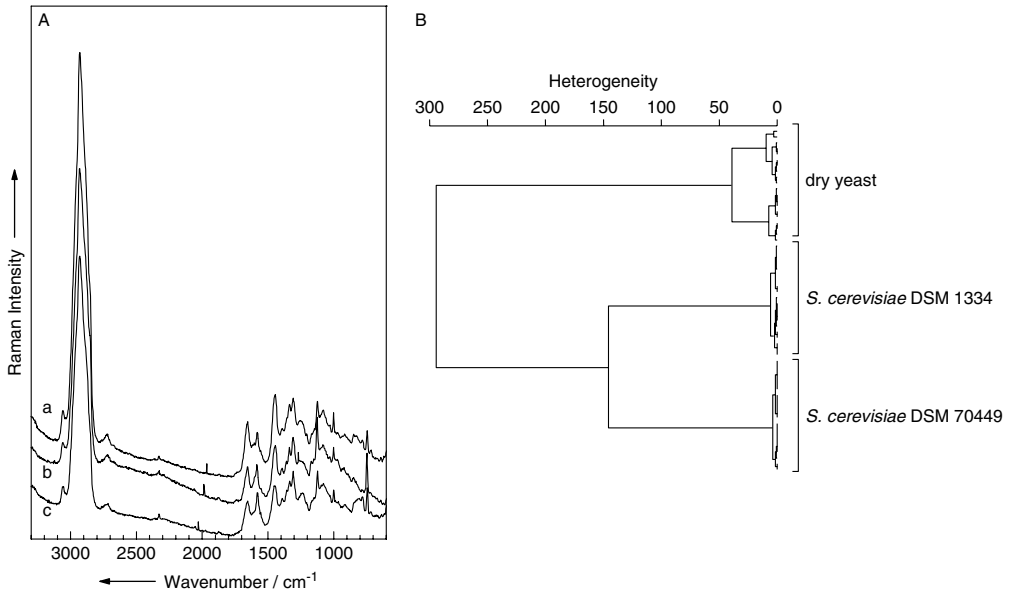

Figure 1. (A) Average Raman spectra from 10 different measuring points within a single yeast cell each for (a) *S. cerevisiae* DSM 70 449, (b) a dry yeast and (c) *S. cerevisiae* DSM 1334. (B) Hierarchical cluster analysis from the average Raman spectra.

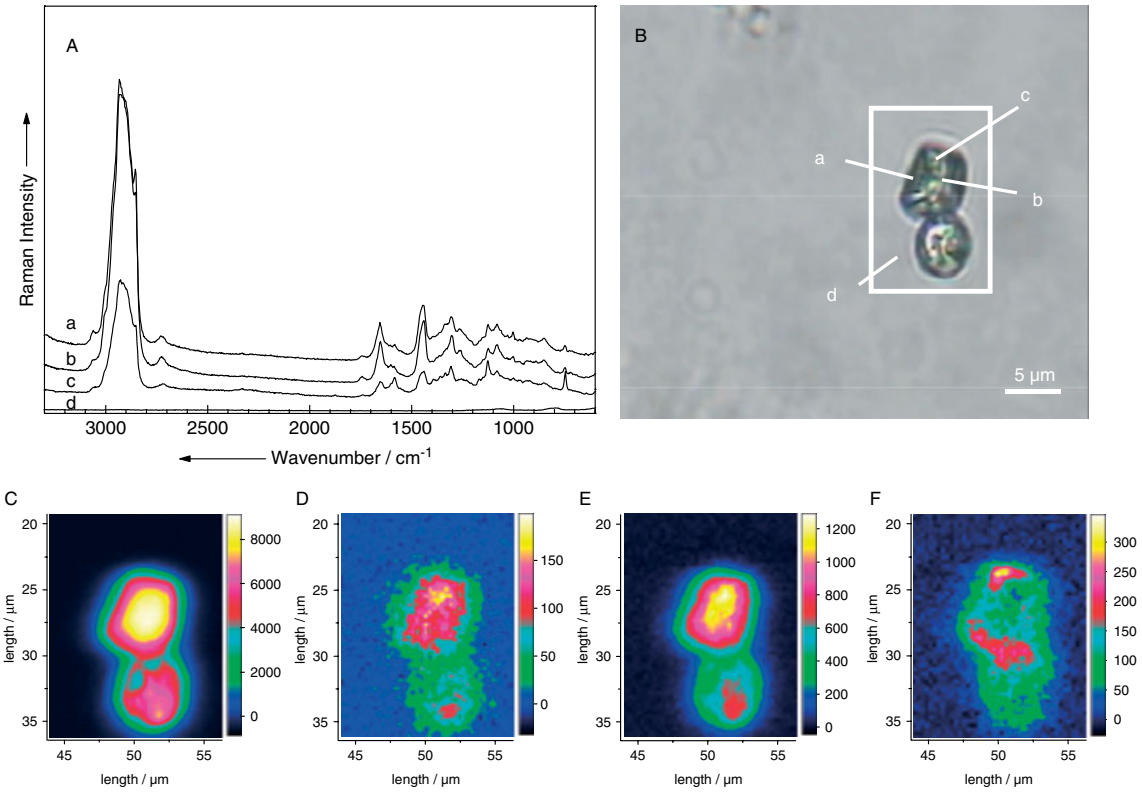

Plate 1. Raman mapping experiment on two single yeast cells (*S. cerevisiae* DSM 70 449). The Raman spectra (A) are characteristic of different regions in the cells [see microphotograph (B)]. The false color plots display these distributions for different marker bands in the cells. (C) 2849–2988; (D) 1731–1765; (E) 1624–1687; (F) 1567–1599 cm^{-1}.

and the three yeast species can be easily separated from each other.

The results presented show that by averaging over 10 more or less statistically chosen Raman spectra recorded within on different parts of a yeast cell, an identification at the single-cell level via hierarchical cluster analysis is possible. This proves that micro-Raman spectroscopy in combination with classification methods allows for a fast and reliable, non-destructive online identification of single microorganism such as single bacteria[5] and yeast. However, owing to the inhomogeneous distribution of the various components in eukaryotes, the identification procedure is more complex than that for the identification of prokaryotes.[5] In future experiments these methods should be applied to a greater set of species also for other genera.

Acknowledgment

The funding of the research project FKZ 13N8369 within the framework 'Biophotonik' by the Federal Ministry of Education and Research, Germany (BMBF) is gratefully acknowledged.

REFERENCES

1. Freydiere AM, Guinet R, Boiron P. *Med. Mycol.* 2001; **39**: 9.
2. Wenning M, Seiler H, Scherer S. *Appl. Environ. Microbiol.* 2002; **68**: 4717.
3. Ngo-Thi NA, Kirschner C, Naumann D. *J. Mol. Struct.* 2003; **661–662**: 371.
4. Maquelin K, Kirschner C, Choo-Smith LP, Ngo-Thi NA, van Vreeswijk T, Stammler M, Endtz HP, Bruining HA, Naumann D, Puppels GJ. *J. Clin. Microbiol.* 2003; **41**: 324.
5. Rösch P, Harz M, Peschke K-D, Ronneberger O, Burkhardt H, Motzkus H-W, Lankers M, Hofer S, Thiele H, Popp J. *Appl. Environ. Microbiol.* 2004; 71, in press.
6. Xie C, Li Y-q. *J. Appl. Phys.* 2003; **93**: 2982.
7. Xie C, Li Y-q, Tang W, Newton RJ. *J. Appl. Phys.* 2003; **94**: 6138.
8. Huang Y-S, Karashima T, Yamamoto M, Hamaguchi H. *J. Raman Spectrosc.* 2003; **34**: 1.
9. Huang Y-S, Karashima T, Yamamoto M, Ogura T, Hamaguchi H. *J. Raman Spectrosc.* 2004; **35**: 525.

2.5 Identification of single eukaryotic cells with micro-Raman spectroscopy. [MH5]

P. Rösch, M. Harz, K.-D. Peschke, O. Ronneberger, H. Burkhardt, J. Popp

Biopolymers **2006**, 82, 312-316.

P. Rösch[1]
M. Harz[1]
K.-D. Peschke[2]
O. Ronneberger[2]
H. Burkhardt[2]
J. Popp[1,3]

[1] *Institut für Physikalische Chemie, Friedrich-Schiller-Universität Jena, Helmholtzweg 4, 07743 Jena, Germany*

[2] *Lehrstuhl für Mustererkennung und Bildverarbeitung, Institut für Informatik, Albert-Ludwigs-Universität Freiburg,Georges-Koehler-Allee Geb. 052, D-79110 Freiburg, Germany*

[3] *Institut für Physikalische Hochtechnologie, Albert-Einstein-Str. 9, D-07745 Jena, Germany*

Identification of Single Eukaryotic Cells with Micro-Raman Spectroscopy

Received 11 November 2005; revised 22 December 2005; accepted 23 December 2005
Published online 18 January 2006 in Wiley InterScience (www.interscience.wiley.com). DOI 10.1002/bip.20449

Abstract: *For a fast identification of eukaryotic cells such as yeast species without a cultivation step it should be possible to perform the investigation on only one single cell. Since yeasts as eukaryotes are heterogeneous and their Raman spectra are therefore dependent on the measuring position, one Raman spectra is not representative of the whole cell. In this contribution we demonstrate the application of average Raman spectra of a line scan over single yeast cells. These average spectra are used for classification with the help of a support vector machine.* © 2006 Wiley Periodicals, Inc. Biopolymers 82: 312–316, 2006

This article was originally published online as an accepted preprint. The ''Published Online'' date corresponds to the preprint version. You can request a copy of the preprint by emailing the Biopolymers editorial office at biopolymers@wiley.com

Keywords: *micro-Raman spectroscopy; eukaryotic cells; yeast; single cell identification; support vector machine*

Correspondence to: J. Popp; e-mail: juergen.popp@uni-jena.de

INTRODUCTION

The identification of eukaryotic cells such as yeasts is of high relevance not only in the medical area (different *Candida* strains) but also for various food-related areas (wine, beer, and bakery products). Routine analysis of microorganisms is based on differences in nutrition and biochemical characteristics. This normally requires cultivation procedures as a cell mass of 10^6–10^8 cells is necessary. In addition to these conventional identification methods, enzymatic tests, for example, allow identification of yeast cells in about 5 h.[1]

Besides microbiologic methods, vibrational spectroscopy can be used to characterize microorganisms. First, investigations on microorganisms with FT–IR spectroscopy were performed by Naumann et al.[2,3] This method leads to good results but needs dried microbial films from microorganisms cultivated by a strict protocol.[4,5] The use of a confocal Raman setup allows the use of lower cell numbers and minimal sample preparation. With this method it was possible to identify yeast microcolonies.[6,7]

For a faster method without any cultivation step it should be possible to investigate one single cell. With micro-Raman spectroscopy, spatial resolution in the submicrometer range can be achieved, which allows the investigation of one single microbial cell. Single cell investigations of yeast were performed by Xie et al.[8–10] using an optical trap in combination with micro-Raman spectroscopy. This methods allows, e.g., the monitoring of the heat denaturation of a single trapped cell.

Recently micro-Raman mapping experiments with submicrometer resolution of single bacteria cell were performed.[11] From these Raman images no dependency on the spatial position of the measurement was observed, i.e., the bacterium shows a spatial homogeneity. This can be explained by the fact that bacteria normally exhibit no compartments. Therefore one bacterial cell can be described by a single micro-Raman spectrum.

However, yeast cells as eukaryotes show no spatial homogeneity. They have different compartments, such as the nucleus or mitochondria, that can be shown by micro-Raman mapping experiments.[12–14] Therefore, the identification of eukaryotic microorganisms on single-cell level is more complicated.

In this contribution we show a possible identification method of single yeast cells. By measuring line scans of single yeast cells, representative information of the whole cell can be achieved. Using average spectra for the classification it is possible to identify single eukaryotic cells. For a first approach different species of the genera *Saccharomyces* and *Candida* are used.

MATERIALS AND METHODS

The yeasts *Saccharomyces cerevisiae* (DSM 1334 and 70449), *Candida glabrata* (DSM 11226, 70614, and 70615), and *C. krusei* (DSM 70075 and 70086) were purchased from the Deutsche Sammelstelle für Mikroorganismen und Zellkulturen (Braunschweig, Germany). The dry yeast was purchased from a supermarket. They were cultivated on an universal medium for yeast at 25°C. The Raman measurements were directly performed on single cells from smears on fused silica plates.

The Raman spectra were taken with a micro-Raman setup (HR LabRam invers, Jobin–Yvon–Horiba, Bensheim, Germany). The spectrometer has an entrance slit of 100 μm, has a focal length of 800 mm, and is equipped with a 300-lines/mm grating. As excitation wavelengths the 532-nm line of a frequency doubled Nd:YAG laser (Coherent Compass, Dieburg, Germany) with a laser power of 10 mW incident on the sample were used. The Raman scattered light was detected by a CCD camera operating at 220 K. A Leica PLFluoar 100× objective (NA 0.75) focused the laser light onto the samples (approx. 7 μm focus diameter). For the line scans an *x*/*y* motorized stage (Merzhäuser, Wetzlar, Germany) with a minimal possible step size of 0.1 μm was used.

For classification a support vector machine (SVM) was used with a γ-value of 1.1×10^{-7} and a cost value of 3.9×10^6. For the calculation the spectral range of 330–3150 cm^{-1} was used without further preprocessing. SVM is based on statistical learning theory.[15] The SVM always solves two-class problems. For discrimination of two classes a hyperplane is defined in such a way that an optimal discrimination between the two classes can be performed.[16] The classes are only defined by the so called support vectors, which are the data points (here spectra) with the most similarity to the other class and which are used to define the hyperplane.[17]

RESULTS AND DISCUSSION

As shown previously,[11] bacteria are homogeneous, therefore one spectrum represents the whole bacterial cell. In contrast to bacteria, yeasts as eukaryotes exhibit compartments. This can be shown by Raman mapping experiments[14] in which different regions inside the cell can be displayed. Here, the Raman spectra are different depending on the investigated position inside the yeast cell.

To enable single-cell analysis of yeast cells, it is necessary to incorporate the varying information from the whole cell. One method would be the use of a microscope objective with lower magnification and

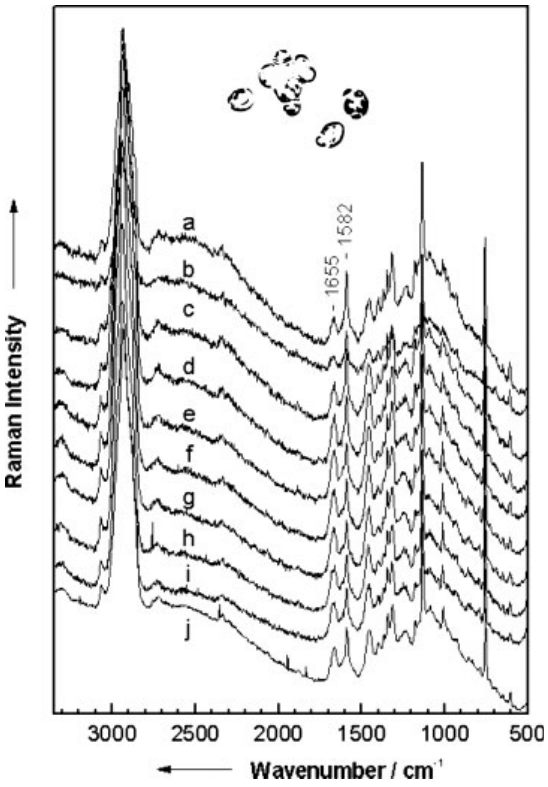

FIGURE 1 Micro-Raman spectra at different positions on a dry yeast cell (a–i); average spectrum (j). (Inset) Microphotograph of several yeast cells. The scan was performed along the main axis as indicated.

therefore lower spatial resolution. However, with this method it would not be possible to measure bacteria and yeast cells at the same time. Therefore, line scans were performed along the main axis of the cell. The inset of Figure 1 displays a microphotograph of different yeast cells from dry yeast. The dotted line indicates the line scan performed over the main axis of one cell. The micro-Raman spectra a–i are the different point spectra from the line scan. Here, the dependency of the Raman spectra on the position inside the yeast cell can be seen. The relative intensity of the signal at 1655 cm^{-1} with respect to the peak at 1582 cm^{-1} varies especially. Spectrum j is the corresponding average spectrum of the nine Raman spectra (a to i). With this method it is possible to overcome the variations inside a yeast cell and to obtain a Raman spectrum that represents the whole cell.

In Figure 2 representative average spectra of nine different yeast strains are displayed. The Raman spectra of commercial dry yeast (a) are compared to two *S. cerevisiae* strains [DSM 70499 (b), 1334 (c)]. From the genus *Candida* three strains of *C. glabrata* [DSM 11226 (d), 70614 (e) and 70615 (f)] and two of *C. krusei* [DSM 70075 (g) and 70086 (h)] were measured. In the average Raman spectra different chemical components can be identified: the signal at 1746 cm^{-1} can be assigned to the C=O double bond of esters, e.g., fatty acid esters. The amide I vibration exhibits a band at 1665 cm^{-1}, which can be seen as a shoulder of the 1655 cm^{-1} band from a C=C stretching vibration of a *cis*-isomer. Aromatic amino acids and nucleic acid bases (G, A) give rice to Raman signals at 1599 and 1582 cm^{-1}, respectively.[10,18] The broad band at 1440 cm^{-1} is due to CH_2, CH_3 deformation vibrations. Glycogen exhibits vibrations at 1362, 1337, 1124, and 1083 cm^{-1},[19] whereas the ring breathing vibrations of phenylalanine and tryptophan can be found at 1000 and 747 cm^{-1}, respectively.[10,20,21] For smaller yeast cells such as *C. krusei* DSM 70086 (h), signals from the fused silica substrate also can be observed (Figure 2, asterisk). For *S. cerevisiae* DSM 1334 (c) and the two *C. krusei* [DSM 70075 (g)

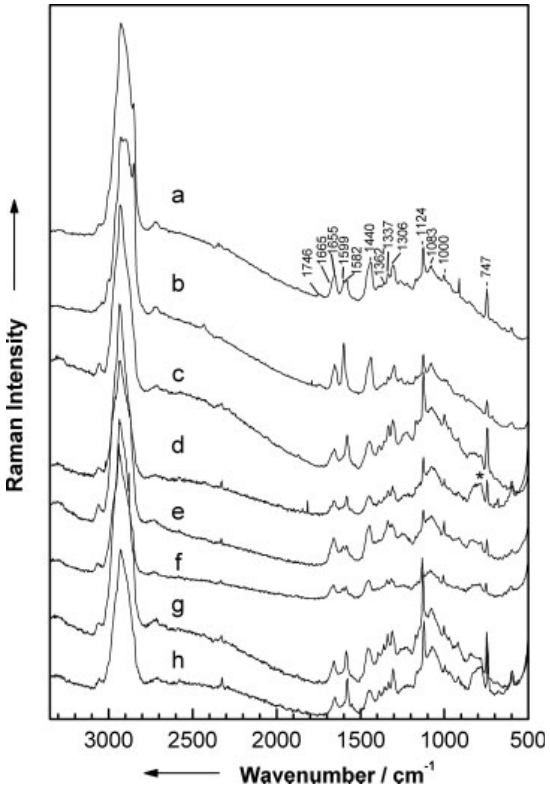

FIGURE 2 Average Raman spectra of (a) dry yeast, (b) *S. cerevisiae* DSM 70499, (c) *S. cerevisiae* DSM 1334, (d) *C. glabrata* DSM 11226, (e) *C. glabrata* DSM 70614, (f) *C. glabrata* DSM 70615, (g) *C. krusei* DSM 70075, (h) *C. krusei* DSM 70086; ∗, fuse silica.

Table I Classification of Average Raman Spectra of Single Yeast Cells with Support Vector Machine

	Number of Average Spectra	Number of Wrongly Classified Spectra at Strain Level	Recognition Rate at Strain Level (%)	Number of Wrongly Classified Spectra at Species Level	Recognition Rate at Species Level (%)
C. glabrata DSM 11226	10	1	90.0	0	100
C. glabrata DSM 70614	10	0	100	0	100
C. glabrata DSM 70615	10	4	60.0	1	90.0
C. krusei DSM 70075	10	1	90.0	0	100
C. krusei DSM 70086	10	1	90.0	0	100
S. cerevisiae DSM 1334	11	3	72.7	2	81.8
S. cerevisiae DSM 70449	13	1	92.3	1	92.3
Dry yeast	18	1	94.4	1	94.4
Average recognition rate			86.2		94.8

and 70086 (h)], the signals of glycogen are very intense. On the other hand the lipid bands can only be observed for the dry yeast (a), *C. glabrata* DSM 70614 (e), and *C. glabrata* DSM 70615 (f).

For classification of the yeast strains with the help of a support vector machine, 10 to 18 average Raman spectra of each strain were used. In Table I the recognition rate for each strain is summarized. All average Raman spectra of *C. glabrata* DSM 70614 are classified correctly (10/10), whereas the average Raman spectra of *C. glabrata* DSM 70615 show, at 60% (6/10), the lowest recognition rate of all strains. This leads to an average recognition rate of 86.2% (80/92) at strain level. Nevertheless, most of the wrongly classified spectra from *C. glabrata* DSM 70615 are classified to the correct species. At species level the strain with the lowest recognition rate is *S. cerevisiae* DSM 1334, with 81.8% (9/11). At species level an average recognition rate of 94.8% can be obtained.

CONCLUSION

Eukaryotes such as yeast cells exhibit compartments that can be observed in spatially dependent micro-Raman spectra. In this study we demonstrate that it is possible to overcome the heterogeneity problem of eukaryotes by using average Raman spectra of line scans from single cells. With this method the varying information over the cell can be included in the dataset and it is possible to use an average Raman spectrum from one cell for classification of the strain or species.

The funding of the research project FKZ 13N8365 and 13N8369 within the framework Biophotonik from the Federal Ministry of Education and Research, Germany (BMBF) is gratefully acknowledged.

REFERENCES

1. Freydiere, A. M.; Guinet, R.; Boiron, P. Med Mycol 2001, 39, 9–33.
2. Naumann, D.; Helm, D.; Labischinski, H.; Giesbrecht, P. In Modern Techniques for Rapid Microbiological Analysis; Nelson, W. H., ed.; VCH Publisher: New York, 1991; pp. 43–96.
3. Naumann, D. In Infrared and Raman Spectroscopy of Biological Materials; Gremlich, H.-U.; Yan, B., eds.; Marcel Dekker: New York, 2001; pp. 323–378.
4. Ngo-Thi, N. A.; Kirschner, C.; Naumann, D. J Mol Struct 2003, 661/662, 371–380.
5. Wenning, M.; Seiler, H.; Scherer, S. Appl Environ Microbiol 2002, 68, 4717–4721.
6. Maquelin, K.; Kirschner, C.; Choo-Smith, L. P.; Ngo-Thi, N. A.; van Vreeswijk, T.; Stammler, M.; Endtz, H. P.; Bruining, H. A.; Naumann, D.; Puppels, G. J. J Clin Microbiol 2003, 41, 324–329.
7. Ibelings, M. S.; Maquelin, K.; Endtz, H. P.; Bruining, H. A.; Puppels, G. J. Clin Microbiol Infect 2005, 11, 353–358.
8. Xie, C.; Dinno, M. A.; Li, Y.-S. Optics Lett 2002, 27, 249–251.
9. Xie, C.; Li, Y.-Q. J Appl Phys 2003, 93, 2982–2986.
10. Xie, C.; Li, Y.-Q.; Tang, W.; Newton, R. J. J Appl Phys 2003, 94, 6138–6142.
11. Rösch, P.; Harz, M.; Schmitt, M.; Peschke, K.-D.; Ronneberger, O.; Burkhardt, H.; Motzkus, H.-W.; Lankers, M.; Hofer, S.; Thiele, H.; Popp, J. Appl Environ Microbiol 2005, 71, 1626–1637.
12. Huang, Y.-S.; Karashima, T.; Yamamoto, M.; Hamaguchi, H. J Raman Spectrosc 2003, 34, 1–3.
13. Huang, Y.-S.; Karashima, T.; Yamamoto, M.; Ogura, T.; Hamaguchi, H. J Raman Spectrosc 2004, 35, 525–526.

14. Rösch, P.; Harz, M.; Schmitt, M.; Popp, J. J Raman Spectrosc 2005, 36, 377–379.
15. Vapnik, V. N. The Nature of Statistical Learning Theory; Springer Verlag: New York, 1995.
16. Schulz-Mirbach, H. 17 DAGM: Symposium Musterer-kennung, Reihe Informatik aktuell, Bielefeld, 1995; pp. 1–14.
17. Ronneberger, O.; Schultz, E.; Burkhardt, H. Aerobiologia 2002, 12, 107–115.
18. Maquelin, K.; Kirschner, C.; Choo-Smith, L. P.; van den Braak, N.; Endtz, H. P.; Naumann, D.; Puppels, G. J. J Microbiol Methods 2002, 51, 255–271.
19. De Jong, B. W. D.; De Gouveia Brazao, C. A.; Stoop, H.; Wolffenbuttel, K. P.; Oosterhuis, J. W.; Puppels, G. J.; Weber, R. F. A.; Looijenga, L. H. J.; Kok, D. J. J Urol 2004, 171, 92–96.
20. Berger, A. J.; Zhu, Q. J Modern Opt 2003, 50, 2375–2380.
21. Naumann, D. Infrared Spectroscopy: New Tool in Medicine; Proceedings of SPIE: Bellingham, WA, 1998: pp. 245–257.

Reviewing Editor: Ronald Hester

2.6 On-line monitoring and identification of bioaerosols. [MH6]

P. Rösch, M. Harz, K.-D. Peschke, O. Ronneberger, H. Burkhardt, A. Schuele, G. Schmauz, M. Lankers, S. Hofer, H. Thiele, H.-W. Motzkus, J. Popp

Analytical Chemistry **2005**, 78, 2163-2170.

Anal. Chem. **2006,** *78,* 2163−2170

On-Line Monitoring and Identification of Bioaerosols

Petra Rösch,[†] Michaela Harz,[†] Klaus-Dieter Peschke,[‡] Olaf Ronneberger,[‡] Hans Burkhardt,[‡] Andreas Schüle,[§] Günther Schmauz,[§] Markus Lankers,[∥] Stefan Hofer,[⊥] Hans Thiele,[⊥] Hans-Walter Motzkus,[#] and Jürgen Popp*[,†,▽]

Institut für Physikalische Chemie, Friedrich-Schiller-Universität Jena, Helmholtzweg 4, D-07743 Jena, Germany, Lehrstuhl für Mustererkennung und Bildverarbeitung, Institut für Informatik, Albert-Ludwigs-Universität Freiburg, Georges-Koehler-Allee Geb. 052, D-79110 Freiburg, Germany, Fraunhofer Institut für Produktionstechnik und Automatisierung, Nobelstrasse 12, D-70569 Stuttgart, Germany, rap.ID Particle Systems GmbH, Ostendstrasse 25, D-12459 Berlin, Germany, Kayser-Threde GmbH, Wolfratshauser Strasse 48, D-81379 München, Germany, Schering AG, Müllerstrasse 178, D-13353 Berlin, Germany, and Institut für Physikalische Hochtechnologie, Albert-Einstein-Strasse 9, D-07745 Jena, Germany

Fast analysis of bioaerosols in clean room environments is necessary in order to prevent contamination of pharmaceutical products, minimize machine downtimes, or both. The detection and identification of microbes will be carried out in several steps: After impaction of the aerosol on a surface, the particles are presorted with glancing light illumination and fluorescence imaging in order to distinguish between abiotic and biotic particles. Since only the biotic particles are of interest, the analysis time can be minimized due to reduction of the data set. The biotic particles are then analyzed further with Raman spectroscopy and identified with a support vector machine.

Bioaerosols play a large role in a multiplicity of different production processes. Especially the occurrence of bioaerosols in hygienic productions is normally critical since they may contaminate pharmaceuticals.[1] Therefore, aerosol particles are routinely monitored according to their number and particle size distribution, and a distinction between abiotic and biotic particles should be performed. Abiotic particles can be classified in organic and inorganic particles. Inorganic particles might derive from metal, metal oxide, building material, glass, ceramics, inorganic excipients, etc., whereas organic particles might occur from plastics, organic fibers, keratin, etc.[1] The composition of organic and inorganic particles can be analyzed by spectroscopic methods such as energy-dispersive X-ray analysis or Raman spectroscopy.[1] These methods so far only allow the identification of organic and inorganic abiotic particles.

Biotic particles, on the other hand, might be pollen, mold, yeast, bacteria, and viruses.[1] Biotic particles are conventionally analyzed by isolation and cultivation of microorganisms. The subsequent identification with conventional bacterial identification methods is based on morphological evaluation of the microorganisms and their ability to grow in various media under different conditions according to their biochemical properties.[2] Depending on the type of bacteria, the identification process may take one day but generally is much longer.[3] Various conventional methods, e.g., enzymatic tests, exist allowing for an identification of yeast cells in ∼5 h.[4] However, these tests require a pure culture or are not available for all species. Microbial detection methods have to be rapid and very sensitive because even a single pathogenic organism may be an infectious dose.[2] Concerning the requirements, new analysis methods such as mass spectroscopy, polymerase chain reaction (PCR), flow cytometry, or fluorescence spectroscopy were developed, allowing a fast and reliable identification or cell count.[2,3]

An alternative approach for the analysis of microorganisms is vibrational spectroscopic methods. IR and Raman spectroscopy reveal the spectroscopic fingerprint of microorganisms, revealing their chemical composition. Using IR spectroscopy, Naumann et al.[5−18] were able to identify bacteria by analysis of colonies of a few hundred cells from controlled cultivation conditions after a

* Corresponding author. Fax: (+49-3641) 948302. E-mail: Juergen.popp@uni-jena.de.
[†] Friedrich-Schiller-Universität Jena.
[‡] Albert-Ludwigs-Universität Freiburg.
[§] Fraunhofer Institut für Produktionstechnik und Automatisierung.
[∥] rap.ID Particle Systems GmbH.
[⊥] Kayser-Threde GmbH.
[#] Schering AG.
[▽] Institut für Physikalische Hochtechnologie.

(1) Valet, O. In *Reinraumtechnik*; Buerkle, D., Ed.; Karl Hanser Verlag: München. In press.
(2) Ivnitski, D.; Abdel-Hamid, I.; Atanasov, P.; Wilkins, E. *Biosens. Bioelectron.* **1999**, *14*, 599−624.
(3) Al-Khaldi, S. F.; Mossoba, M. M. *Nutrition* **2004**, *20*, 32−38.
(4) Freydiere, A. M.; Guinet, R.; Boiron, P. *Med. Mycol.* **2001**, *39*, 9−33.
(5) Naumann, D.; Schultz, C. P.; Helm, D. In *Infrared Spectroscopy of Biomolecules*; Mantsch, J. J., Chapman, D., Eds.; Wiley-Liss: New York, 1996; Vol. 1, pp 279−310.
(6) Schmitt, J.; Udelhoven, T.; Naumann, D.; Flemming, H. C. *Proc. SPIE−Int. Soc. Opt. Eng.* **1998**, *3257*, 236−244.
(7) Udelhoven, T.; Naumann, D.; Schmitt, J. *Appl. Spectrosc.* **2000**, *54*, 1471−1479.
(8) van der Mei, H. C.; Naumann, D.; Busscher, H. J. *Infrared Phys. Technol.* **1996**, *37*, 561−564.
(9) Ngo-Thi, N. A.; Kirschner, C.; Naumann, D. *J. Mol. Struct.* **2003**, *661−662*, 371−380.
(10) Kirschner, C.; Ngo Thi, N. A.; Naumann, D. *Spectrosc. Biol. Mol.: New Directions, Eur. Conf., 8th* **1999**, 561−562.
(11) Naumann, D. *Infrared Spectroscopy: New Tool in Medicine*; Proceedings of SPIE, Infrared and NIR Raman Spectroscopy in Medical Microbiology, Bellingham, WA, 1998; pp 245−257.
(12) Naumann, D. In *Encyclopedia of Analytical Chemistry*; Meyers, R. A., Ed.; John Wiley & Sons: Chichester, 2000; pp 102−131.

10.1021/ac0514974 CCC: $33.50
Published on Web 03/04/2006

drying step. The drying step is not necessary by applying Raman spectroscopy. Using UV-resonance Raman spectroscopy signals of macromolecules such as DNA/RNA or proteins are selectively enhanced. This allows the identification of the guanine-cytosine relation to all DNA bases of bacteria.[19−31] This technique is very sensitive but also requires hundreds to thousands of cells.

For an in-line or at-line identification of single particles, methods are required that can be used as single-cell analysis. The surface-enhanced Raman spectroscopy technique allows the detection of minimal concentrations and therefore is particularly suitable for the investigation of single microorganisms.[32−34] Since the microbes are in this case contaminated with heavy metal, e.g., silver colloid, it is not possible to use them in a second step for conventional microbiological investigations. Raman spectroscopy in combination with an optical tweezers also allows the investigation of single bacteria and spores,[35−38] but here an enormous setup is required. Conventional micro-Raman spectroscopy is reported for the investigation of single bacteria[39−42] and yeast cells[43,44] as well as spores.[45] Recently we have demonstrated the identification of single bacteria[46] and yeasts[47] on strain level by micro-Raman spectroscopy in combination with support vector machines (SVM).[48]

(13) Naumann, D. In *Infrared and Raman Spectroscopy of Biological Materials*; Gremlich, H.-U., Yan, B., Eds.; Marcel Dekker: New York, 2001; Vol. 24, pp 323−378.
(14) Naumann, D. *Infrared Phys.* **1984**, *24*, 233−238.
(15) Naumann, D.; Helm, D.; Labischinski, H. *Nature* **1991**, *351*, 81−82.
(16) Naumann, D.; Helm, D.; Labischinski, H.; Giesbrecht, P. In *Modern Techniques for Rapid Microbiological Analysis*; Nelson, W. H., Ed.; VCH Publisher: New York, 1991; pp 43−96.
(17) Naumann, D.; Keller, S.; Helm, D.; Schultz, C.; Schrader, B. *J. Mol. Struct.* **1995**, *347*, 399−405.
(18) Helm, D.; Labischinski, H.; Schallehn, G.; Naumann, D. *J. Gen. Microbiol.* **1991**, *137*, 69−79.
(19) Dalterio, R. A.; Nelson, W. H.; Britt, D.; Sperry, J. F. *Appl. Spectrosc.* **1987**, *41*, 417−422.
(20) Wu, Q.; Nelson, W. H.; Elliot, S.; Sperry, J. F.; Feld, M.; Dasari, R.; Manoharan, R. *Anal. Chem.* **2000**, *72*, 2981−2986.
(21) Chadha, S.; Manoharan, R.; Moenne.Loccoz, P.; Nelson, W. H.; Peticolas, W. L.; Sperry, J. F. *Appl. Spectrosc.* **1993**, *47*, 38−43.
(22) Ghiamati, E.; Manoharan, R.; Nelson, W. H.; Sperry, J. F. *Appl. Sepctrosc.* **1992**, *46*, 357−364.
(23) Nelson, W. H.; Manoharan, R.; Sperry, J. F. *Appl. Spectrosc. Rev.* **1992**, *27*, 67−124.
(24) Chadha, S.; Nelson, W. H.; Sperry, J. F. *Rev. Sci. Instrum.* **1993**, *64*, 3088−3093.
(25) Manoharan, R.; Ghiamati, E.; Dalterio, R. A.; Britton, K. A.; Nelson, W. H.; Sperry, J. F. *J. Microbiol. Methods* **1990**, *11*, 1−15.
(26) Nelson, W. H.; Sperry, J. F. In *Modern Techniques for Rapid Microbiological Analysis*; Nelson, W. H., Ed.; VCH Publisher: New York, 1991; pp 97−143.
(27) Wu, Q.; Hamilton, T.; Nelson, W. H.; Elliott, S.; Sperry, J. F.; Wu, M. *Anal. Chem.* **2001**, *73*, 3432−3440.
(28) Britton, K. A.; Dalterio, R. A.; Nelson, W. H.; Britt, D.; Sperry, J. F. *Appl. Spectrosc.* **1988**, *42*, 782−788.
(29) Manoharan, R.; Ghiamati, E.; Chadha, S.; Nelson, W. H.; Sperry, J. F. *Appl. Spectrosc.* **1993**, *47*, 2145−2150.
(30) Lopez-Diez, E. C.; Goodacre, R. *Anal. Chem.* **2004**, *76*, 585−591.
(31) Jarvis, R. M.; Goodacre, R. *FEMS Microbiol. Lett.* **2004**, *232*, 127−132.
(32) Alexander, T. A.; Pellegrino, P. M.; Gillespie, J. B. *Appl. Spectrosc.* **2003**, *57*, 1340−1345.
(33) Farquharson, S.; Gift, A. D.; Maksymiuk, P.; Inscore, F. E. *Appl. Spectrosc.* **2004**, *58*, 351−354.
(34) Guzelian, A. A.; Sylvia, J. M.; Janni, J. A.; Clauson, S. L.; Spencer, K. M. *Proc. SPIE−Int. Soc. Opt. Eng.* **2002**, *4577*, 182−192.
(35) Chan, J. W.; Esposito, A. P.; Talley, C. E.; Hollars, C. W.; Lane, S. M.; Huser, T. *Anal. Chem.* **2004**, *76*, 599−603.
(36) Xie, C.; Dinno, M. A.; Li, Y.-S. *Opt. Lett.* **2002**, *27*, 249−251.
(37) Xie, C.; Li, Y.-q. *J. Appl. Phys.* **2003**, *93*, 2982−2986.
(38) Xie, C.; Li, Y.-Q.; Tang, W.; Newton, R. J. *J. Appl. Phys.* **2003**, *94*, 6138−6142.

In this paper, we describe an approach for the fast, nondestructive, and very reliable analysis of bioaerosols. Here, the impacted particles were monitored with fluorescence imaging in order to obtain first information of biological particles. This steps dramatically minimizes the particle numbers to be analyzed. In a second step, only the biotic particles were analyzed and identified with micro-Raman spectroscopy in combination with SVM. This combination leads to an effective and fast tool for the identification of microorganisms on the single-cell level.

MATERIALS AND METHODS

Bacteria and Growing Conditions. The microorganisms were chosen when referenced in the UPSP or according to the conditions present in clean rooms. The microorganisms *Micrococcus luteus* (DSM 348 and 20030), *Micrococcus lylae* (DSM 20315 and 20318), *Bacillus subtilis* (DSM 10 and 347), *Bacillus pumilus* (DSM 27 and 361), *Bacillus sphaericus* (DSM 28 and 396), *Escherichia coli* (DSM 423, 429, 498, 499, 613, 1058, and 2769), *Staphylococcus cohnii* (DSM 6669, 20260, 6718, and 6719), *Staphylococcus warneri* (DSM 20036 and 20316), and *Saccharomyces cerevisiae* (DSM 1334 and 70449) were purchased from the "Deutsche Sammelstelle für Mikroorganismen und Zellkulturen". *Staphylococcus epidermidis* (ATCC 35984 and 195) were purchased from the Institut für Infektionsbiologie, Universität Würzburg. In addition, commercial dry yeast was used. They were cultivated on a standard or nutrition agar (*Micrococcus* and *Bacillus*) or on CASO and CA (*Staphylococcus*) for different growing conditions, such as time and temperature, respectively. To simulate samples from clean rooms, the Raman measurements were directly performed on single cells from smears on fused-silica plates.

Fluorescence Instrumentation. The fluorescence spectra were measured between 400 and 900 nm with a cooled CCD array spectrometer (AS&Co with Axioskop2 MAT, Zeiss) with 1024 pixels and a 248 lines/mm flat field grating. A light fiber guide launched the fluorescence signals of the samples from a fluorescence microscope via a microaperture into the spectrometer cartridge. The central wavelength of the excitation light was 365 nm.

Raman Setup. The Raman spectra were taken with a micro-Raman setup (HR LabRam invers, Jobin-Yvon-Horiba). The spectrometer has an entrance slit of 100 μm, a focal length of 800 mm, and is equipped with a 300 lines/mm grating. As excitation

(39) Huang, W. E.; Griffiths, R. I.; Thompson, I. P.; Bailey, M. J.; Whiteley, A. S. *Anal. Chem.* **2004**, *76*, 4452−4458.
(40) Schuster, K. C.; Reese, I.; Urlaub, E.; Gapes, J. R.; Lendl, B. *Anal. Chem.* **2000**, *72*, 5529−5534.
(41) Schuster, K. C.; Urlaub, E.; Gapes, J. R. *J. Microbiol. Methods* **2000**, *42*, 29−38.
(42) Pasteris, J. D.; Freeman, J. J.; Goffredi, S. K.; Buck, K. R. *Chem. Geol.* **2001**, *180*, 3−18.
(43) Huang, Y.-S.; Karashima, T.; Yamamoto, M.; Hamaguchi, H. *J. Raman Spectrosc.* **2003**, *34*, 1−3.
(44) Huang, Y.-S.; Karashima, T.; Yamamoto, M.; Ogura, T.; Hamaguchi, H. *J. Raman Spectrosc.* **2004**, *35*, 525−526.
(45) Esposito, A. P.; Talley, C. E.; Huser, T.; Hollars, C. W.; Schaldach, C. M.; Lane, S. M. *Appl. Spectrosc.* **2003**, *57*, 868−871.
(46) Rösch, P.; Harz, M.; Schmitt, M.; Peschke, K.-D.; Ronneberger, O.; Burkhardt, H.; Motzkus, H.-W.; Lankers, M.; Hofer, S.; Thiele, H.; Popp, J. *Appl. Environ. Microbiol.* **2005**, *71*, 1626−1637.
(47) Rösch, P.; Harz, M.; Schmitt, M.; Popp, J. *J. Raman Spectrosc.* **2005**, *36*, 377−379.
(48) Vapnik, V. N. *The Nature of Statistical Learning Theory*; Springer-Verlag: New York, 1995.

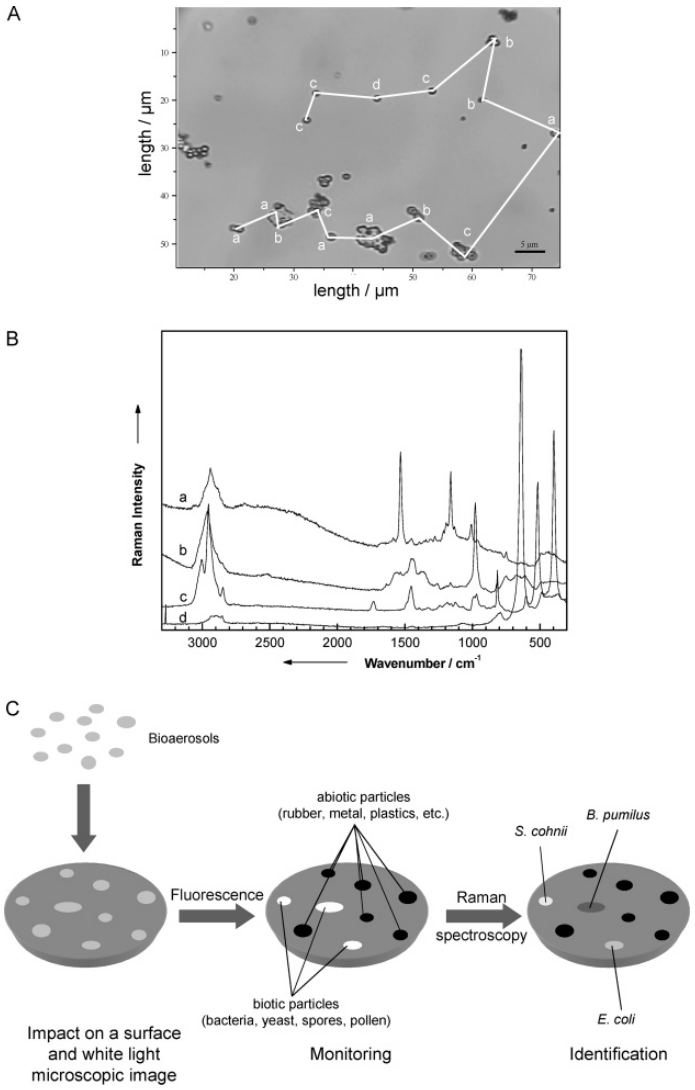

Figure 1. (A) Microscopic image of particles on a sample surface with corresponding micro-Raman spectra (B) of the particles (a, *M. luteus*; b, melamine resin; c, PMMA; d, TiO_2). (C) Schematic drawing of the OMIB identification principle.

wavelengths, the 532-nm line of a frequency-doubled Nd:YAG laser (Coherent Compass) with a laser power of 10 mW incident on the sample was used. The Raman scattered light was detected by a CCD camera operating at 220 K. A Leica PLFluoar ×100 objective focused the laser light onto the samples (~0.7-μm focus diameter). An integration time of 60 s was used for single bacteria spectra.

Preprocessing and Classification As a preprocessing step, the spectra were filtered with a median filter to remove (cosmic) spikes. Afterward, the grid points of each spectrum are reinterpolated with a bilinear interpolation. This step is necessary because the grid points of some spectra vary due to different systematic measurement conditions. All spectra were then limited to the region of 550−3300 cm^{-1}. For the classification of Raman spectra, a support vector machine is used. Compared to other classifiers (e.g., neural networks), support vector machines solve a convex optimization problem and hence give a solution that is a global optimum. Moreover, a SVM with a nonlinear (radial basis function) kernel is used, so only two parameters ($\gamma = 5 \times 10^{-6}$ and cost of 1 400 000) needed to be adjusted. For the training process, the whole data set was normalized by subtracting the mean value and dividing with the standard deviation of all spectra for each grid point. This normalization is done to homogenize the distribution of the training data. Finally, to get a robust characterization of the data set, a leave-one-out test is applied.

RESULTS AND DISCUSSION

Micro-Raman spectroscopy allows measurements in heterogeneous samples with a spatial resolution of ~1 μm. Therefore, spectra of particles of this size are easily accessible with micro-Raman spectroscopy and provide an optical fingerprint depending on their chemical composition. Figure 1A shows a microphoto-

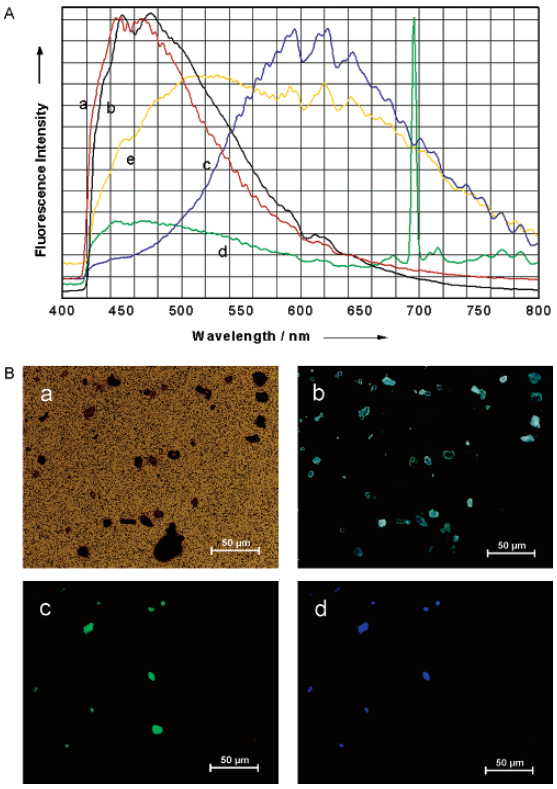

Figure 2. (A) Fluorescence spectra of single particles (λ_{ex} = 365 nm; a, *B. subtilis*; b, *M. luteus*; c, silicon carbide; d, corundum; e, titanium dioxide); (B) microscopic image of a dust sample. a, bright light; b, glancing light; c, fluorescence image (λ_{ex} = 365 nm, λ_{em} = 460 nm); d, fluorescence image (λ_{ex} = 365 nm, λ_{em} = 515 nm).

graph of four different types of particles, which are all similar in size and shape. Due to the high similarity, it is impossible to distinguish between them by optical microscopy. As test particles, beads of melamine resin and poly(methyl methacrylate) (PMMA), titanium dioxide, and *Micrococcus luteus* were chosen. These are all particles that might be found as contaminants. Exemplarily, 15 particles were chosen and their micro-Raman spectra were recorded with an integration time of 60 s each. The reference Raman spectra from the different particles are shown in Figure 1B (a, *M. luteus*; b, melamine resin; c, PMMA; d, titanium dioxide). Comparing the Raman spectra with reference data, each of the 15 particles can be assigned to the 4 groups. The particles in the microscopic image (Figure 1A) are labeled according to their Raman spectroscopic characterization (see Figure 1B).

Since each substance exhibits its own typical Raman spectrum, the method enables an unambiguous identification of single microparticles, but it is time-consuming. In typical clean room samples, a large number of particles need to be analyzed. Concerning microbiology, only the biotic particles are of interest, which can be found in the range of 10^{-2}–10^{-5} in the samples[1] depending on the type of hygienic production (pharmacy, food, cosmetics). Other sources determine the relation between air-

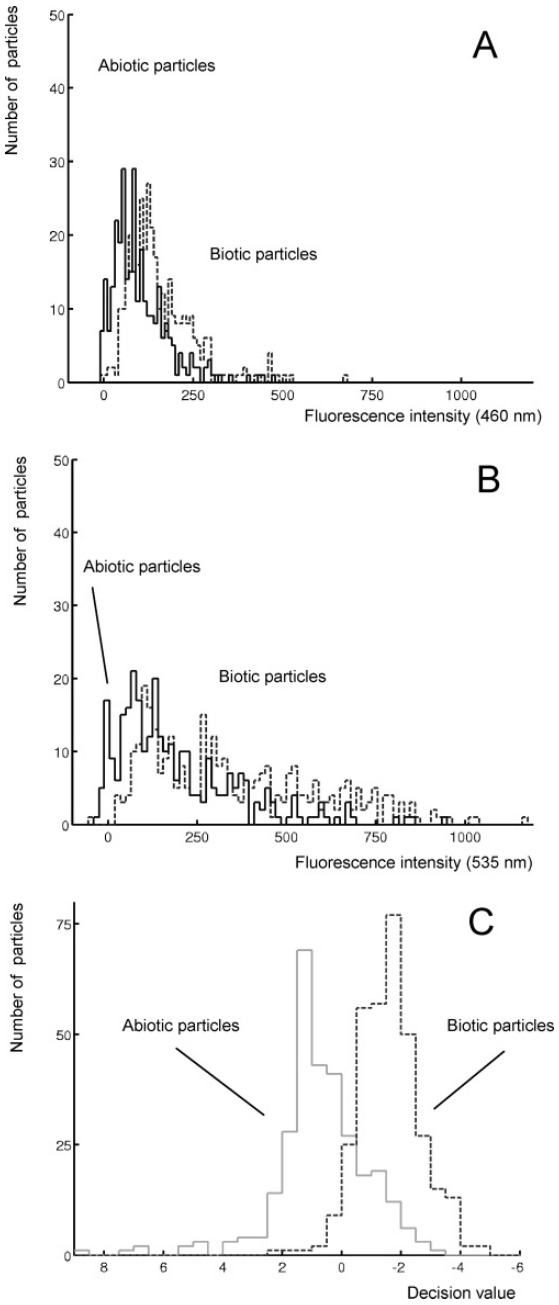

Figure 3. Intensity histograms of fluorescence images of biotic and abiotic particles for two different emission filters, centered at 460 nm (A) and one at 535 nm (B). Biotic and abiotic particles can hardly be distinguished based on the intensity histograms only. (C) Decision value histogram for biotic and abiotic particles after feature extraction. The particles can be separated more easily, based on the decision values.

borne particles and bioaerosols between 1:1000 and 1:10 000.[49] Analyzing all particles is therefore not recommended.

(49) N. N. *Empfehlung zur hygienischen Abnahmeprüfung und zur hygienischen Kontrolle nach DIN 1946 Teil 4. Hyg. Med.* **1989**, *14*, 168–170.

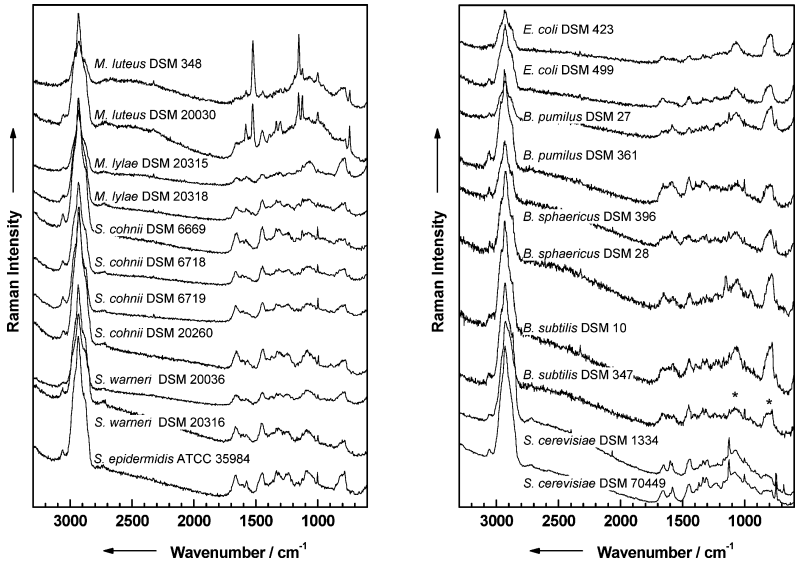

Figure 4. Raman spectra from single bacteria and yeast cells of different strains (λ_{ex} = 532 nm).

Table 1. Classification of Micro-Raman Spectra of Single Bacteria

	no. of strains	no. of spectra	no. of wrong classified strain spectra	recognition rate for strains (%)	no. of wrong classified species spectra	recognition rate for species (%)
B. pumilus	2	100	19	80.5	7	92.7
B. sphaericus	2	95	17	81.8	11	88.2
B. subtilis	2	348	12	94.0	8	96.6
E. coli	7	666	178	73.1	8	99.1
M. luteus	2	667	10	93.5	7	96.6
M. lylae	2	40	1	97.5	1	97.5
S. cohnii	4	260	20	92.2	11	95.8
S. epidermidis	2	879	9	97.6	9	97.6
S. warneri	2	138	11	92.1	4	97.2
S. cerevisiae	3	42	7	80.7	5	86.9
av recognition rate		3235		85.6		95.4

To minimize the analysis time, a sorting method is necessary to distinguish between biotic and abiotic particles. This method is schematically displayed in Figure 1C. The bioaerosol is impacted on a surface. In a first step (monitoring), biotic particles are investigated or analyzed by white light microscopy and fluorescence imaging. In this step, the position, size, and shape of the particles are determined. Here, it is possible to distinguish between biotic and abiotic particles due to the different fluorescence characteristics. This leads to a drastic decrease of the amount of particles that needs to be analyzed. The biotic particles are marked, and in a second step, micro-Raman spectra are recorded only at these positions. The Raman spectra of the biotic particles are compared with a database, resulting in the identification of the microorganisms. Reducing the number of spectra to be recorded leads to a drastic increase in analyzing velocity.

The monitoring step utilizes different fluorescence characteristics of biotic and abiotic particles. In Figure 2A, fluorescence spectra with an excitation wavelength of 365 nm from different particles are shown. As examples for biotic particles, single cells of *B. subtilis* (a) and *M. luteus* (b) are chosen exemplarily. Their spectra differ strongly from abiotic particles such as silicon carbide (c), corundum (d), or titanium dioxide (e). This difference enables the discrimination between biotic and abiotic particles. In Figure 2B, a typical sample, which contains yeast cells and dust particles with different illuminations, is shown. Normal microscopy bright light illumination (a) leads to an image in which only large particles can be found due to the roughness of the sample carrier. Using glancing illumination (b), the contrast is improved and much more particles can be detected. Fluorescence illumination with two different wavelengths (excitation 365 nm, detection (c) 460 and (d) 515 nm) leads to additional information, which allows for the localization of the yeast cells. In the fluorescence images, only the small amount of fluorescent particles can be seen. Therefore, the total amount of particles is reduced, and preferably, the biotic particles can be analyzed.

Afterward, the particle images are segmented, so that there are one dark field image and two fluorescence images available for each particle. Those three images are necessary because in some critical cases the fluorescence information only is not enough to discriminate between biotic and abiotic particles. This can be seen in Figure 3, where intensity histograms for 338 biotic

particles (*S. cohnii*, *B. sphaericus*, *M. luteus*) and 301 abiotic particles (titanium dioxide) are shown. Even when using the fluorescence images based on two filters (460 and 535 nm), no threshold can be found to separate the biotic and abiotic particles completely. To improve the discriminatory capabilities, two processing steps are applied. First, structural information is also taken into account, and second, a SVM is used as a more advanced classifier. This is achieved by calculating gray scale invariants[50,51] for each particle on the dark field and fluorescence images. Those invariants represent the particles based on their morphological structure independently of their position and orientation. Moreover, the invariants can also link the three images of each particle, so it is possible to combine spectral information contained in the different images. Two point invariants are used, with a multiplicative combination of the image points. Moreover, to take into account different sizes of structural details of the particles, a multiscale approach is applied. The invariants are used as features for discrimination between biotic and abiotic particles via a SVM classifier. The classification is based on decision values and a threshold. Figure 3C shows the decision value histograms for the same particles as above. Even when the range of the two histograms overlaps, two distinctive peaks can be seen in the plot. The amount of false classified particles can be controlled by a weight value for the classifier. In the case shown, 1.5% of the biotic particles was classified as abiotic (false negatives) whereas 34.5% of the abiotic particles was classified as biotic particles (false positives), while the weight was set to 0.3. Decreasing the amount of false negative particles increases the amount of false positives and the other way round. This means, that the separation of biotic and abiotic particles can be carried out as a tradeoff between the amount of the false positives and false negatives. This leads to a reduction of the number of particles that need to be analyzed, which finally results in a speedup of the overall processing time.

Particles marked as biotic are then analyzed in a second step by applying micro-Raman spectroscopy. We have recently shown that one Raman spectrum of a single vegetative bacterial cell is sufficient for the identification.[46] This is possible since bacteria are homogeneous and one spectrum is therefore representative for the whole cell. In Figure 4, micro-Raman spectra of different single bacterial and yeast cells with an excitation wavelength of 532 nm and an integration time of 60 s each are shown. Most of the spectra are very similar. Only the spectra of the colored bacteria *M. luteus* are dominated by signals of their pigment sarcinaxanthin. Additional signals due to the fused-silica plate (∗) can be seen in the spectra deriving from the sample holder because of the very low sample volume of a single bacterium. The poor signal-to-noise ratio, especially for the Raman spectra of the *E. coli*, is a result of the low integration time. However, the quality of the single-cell spectra shown in Figure 4 is sufficient for an identification of the bacteria by means of a support vector machine (see below and Table 1). Since time is a critical issue for the analysis of clean room samples the overall investigation time should be kept as short as possible. For identification, a pattern recognition method is necessary in order to distinguish between the different strains.

(50) Schulz-Mirbach, H. 17. *DAGM−Symposium Mustererkennung*, Reihe Informatik aktuell; Springer-Verlag, Berlin, 1995; pp 1−14.
(51) Ronneberger, O.; Schultz, E.; Burkhardt, H. *Aerobiologia* **2002**, *12*, 107−115.

Table 2. Identification of an Independent Data Set

strain	no. of spectra	correctly identified	identified as
B. subtilis DSM 347	8	8	
B. sphaericus DSM 28	8	8	
B. sphaericus DSM 396	7	7	
E. coli DSM 423	7	7	
E. coli DSM 498	7	7	
E. coli DSM 1058	20	17	*E. coli* DSM 499, 423, and 2769
M. luteus DSM 20030	6	6	
M. lylae DSM 20315	5	5	
M. lylae DSM 20318	5	5	
S. cohnii DSM 6669	8	8	
S. cohnii DSM 6718	5	5	
S. cohnii DSM 6719	5	5	
S. cohnii DSM 20260	7	7	
S. epidermidis ATCC 35984	7	7	
S. epidermidis 195	20	18	*S. warneri*, *E. coli*
S.warneri DSM 20036	5	5	
identification	130	125	

For classification, a support vector machine was used for the 3235 micro-Raman spectra of single microorganisms from 28 different strains and 10 species (see Table 1). Beside bacteria spectra, yeast spectra[47] are also included in the database. For the identification of the yeast, Raman spectra from 5 to 10 positions inside the cell were used to create a average spectrum (see Figure 4). This is necessary since yeasts as eukaryotes exhibit compartments, and therefore, the cells are heterogeneous. To reach a representative single spectrum from one cell, the average spectrum was used in the database. For the measurements, the microorganisms are always cultivated under different conditions such as temperature, nutrition, or cultivation age. In the data set, additional information such as varying pigment concentration of, for example, *M. luteus* is also included. In addition, from the Bacillus strains, besides vegetative cells Raman spectra of bacterial spores are also included in the data set. This approach can also used for cell inclusions such as poly(hydroxybutyric acid). Due to the large data set and the nonselective cultivation conditions, different states of growth should be included in the database. This was done in order to maximize the variability of the data set since the origin of unknown microorganisms will not be known in analysis samples.

Performing a classification with 3235 spectra of the 28 different strains from 10 species (median filtering, normalization, Rbf-SVM, leave-one-out test), we obtain 2951 correctly identified spectra on the strain level (average recognition rate, 85.6%) and 3164 correctly identified spectra on the species level (average recognition rate, 95.4%). All results on the single-cell level are summarized in Table 1. The lowest recognition rate on the strains is received for *E. coli* with 73.1%. On a species level, on the other hand, *E. coli* shows with 99.1% the highest recognition rate of all investigated species. Here, the lowest recognition rate is from *S. cerevisiae* with 86.9%. This leads to an average recognition rate of 95.4% on a species level.

For identification of unknown single bacteria, an independent set of different single bacteria from 16 strains, already included in the database, are measured. These spectra were recorded anonymously and then identified with the above-mentioned data

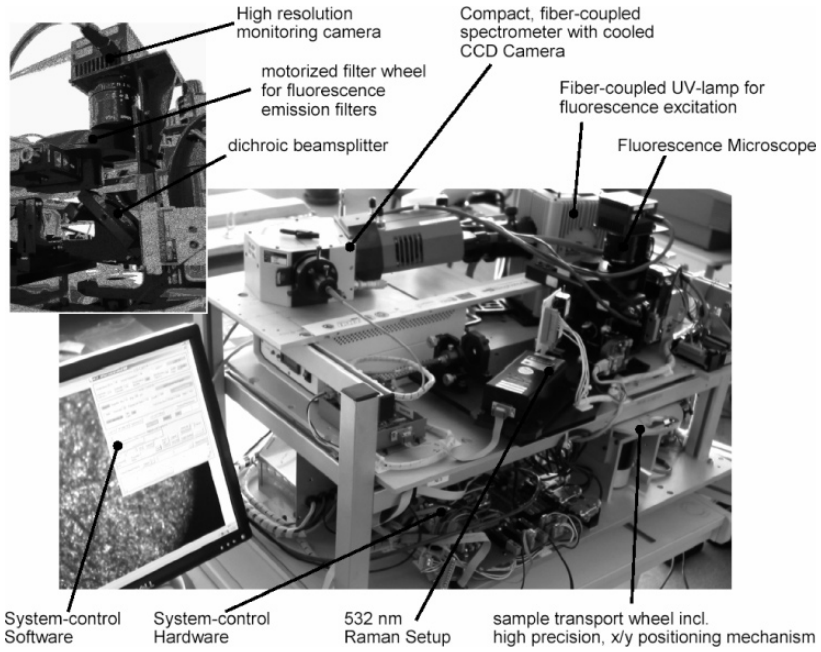

Figure 5. Fully automated OMIB laboratory demonstrator, including visual and fluorescence microscopic setup and a Raman setup with fiber-coupled spectrometer.

set (see Table 2). From 130 spectra, 125 were correctly identified. Three spectra that were known to be *E. coli* DSM 1058 are identified as different *E. coli* strains. Therefore, the correct species was always identified. Two spectra of *S. epidermidis* 195 were identified as *S. warneri* and *E. coli*, respectively, which is the wrong species or even the wrong genus. This test demonstrates that from the 130 independent Raman spectra 96.2% were identified correctly on a strain level and 98.5% on a species level. A comparison between the rate of correctly identified samples according to conventional identification methods including Gram strain, identification using PCR, and this new technique will have to be performed in order to evaluate the above-mentioned numbers. For this purpose, the measured samples will be cultivated and then identified with different microbiological methods.

The spectroscopic identification method is realized as an analytical instrument in which the monitoring and identification routine is integrated and performed automatically. Only the sample holder is inserted manually. Figure 5 shows the setup where both the monitoring step with glancing light illumination and the Raman identification are inserted. The upper left inset shows a closeup of the microscopic setup, which is used for visible inspection of the sample surface and for fluorescence monitoring. The filter wheel allows us to rotate various fluorescence emission filters into the optical path of the microscope to discriminate between different fluorescence behavior of the particles. The dichroic beam splitter, shown in the inset, folds the Raman optical train on the optical axis of the optical train of the microscope. This confocal setup allows us to focus the Raman excitation laser beam at a precisely known position in the field of view of the microscope. The sample transport wheel transports the sample filter roughly under the focus plane of the confocal Raman microscope. A high-precision actuator grabs the sample and allows us to position it relative to the microscope and Raman focus, respectively, with a high accuracy and repeatability in x and y. If a particle is detected as a potentially relevant bioparticle through microscopy (size, shape) and fluorescence microscopy (fluorescence emission), the sample stage moves this particular particle exactly under the Raman focus spot. The measurement procedure implemented in the demonstrators hard and software subsequently automatically measures Raman spectra of all particles, which were found to be of relevance. Number, size, shape, fluorescence behavior, and Raman spectrum are stored in a log file and allow us to derive statistical information about the contamination on the sample. Additionally when this data set is transferred to the support vector machine, the individual particles can be identified with high precision. Through the automation of the whole process, a large number of particles can be monitored in a short time and the identification of individual bioparticles within this process is a matter of a few minutes.

CONCLUSIONS

With these investigations, we provide the scientific background for a fully automated device, which allows identification of bacterial contamination in clean room environment on a single-cell level. The combination of fluorescence imaging and Raman spectroscopy allows for a reduction in the amount of particles that need to be analyzed. Therefore, the total investigation time can be minimized. For commercial application in clean room environment, in addition to the above-mentioned strains, strains isolated directly in the clean rooms need to be implemented in order to adapt the data

set to the particular requirement. With these strains, both the microscopic images (glancing light illumination and fluorescence images) and the Raman spectra of the particular particles are necessary for the data set. An extension of the reference data set will lead to a special adaptation on the particular application and allow the detection of outliers (e.g., unknown microbes) that are not known to the data set. With these data, it will be possible to provide a fast and easy to handle tool for the monitoring of clean room contamination.

ACKNOWLEDGMENT

Funding of the research project FKZ 13N8365, 13N8366, 13N8369, and 13N8379 within the framework 'Biophotonik' from the Federal Ministry of Education and Research, Germany (BMBF) is gratefully acknowledged.

Received for review August 19, 2005. Accepted December 13, 2005.

AC0514974

2.7 Analysis of single blood cells for liquor diagnostics *via* a combination of fluorescence staining and micro-Raman spectroscopy. [MH7]

M. Harz, M. Kiehntopf, S. Stöckel, P. Rösch, T. Deufel, J. Popp

Analyst **2008**, *published online* (DOI:10.1039/b716132h).

The Analyst
RSC Publishing
Journals The Analyst Advance Articles DOI: 10.1039/b716132h

Analyst, 2008 | DOI: 10.1039/b716132h | Paper

Analysis of single blood cells for CSF diagnostics *via* a combination of fluorescence staining and micro-Raman spectroscopy

Michaela Harz†[a], Michael Kiehntopf†[b], Stephan Stöckel[a], Petra Rösch[a], Thomas Deufel[b] and Jürgen Popp*[ac]

[a]*Institute of Physical Chemistry, Friedrich-Schiller-Universität Jena, Helmholtzweg 4, D-07743 Jena, Germany. E-mail: juergen.popp@uni-jena.de; Fax: +49 3641 948302; Tel: +49 3641 948320*

[b]*Institute of Clinical Chemistry and Laboratory Diagnostics, Friedrich-Schiller-Universität Jena, Erlanger Allee 101, D-07747 Jena, Germany*

[c]*Institute of Photonic Technologies, Albert-Einstein-Straße 9, D-07745 Jena, Germany*

Received 18th October 2007, Accepted 24th April 2008

First published on the web 28th May 2008

This contribution provides a new approach for single blood cell analysis in cerebrospinal fluid (CSF) with the possibility of utilizing simultaneously on the same sample the unique capabilities of the two methods fluorescence staining and Raman spectroscopy. By doing so this technique enables the potential of accurate and rapid cell identification in order to determine cell parameters immediately (*e.g.* the study of the level of activation or phagocytosis activity of single blood cells). Fluorescence labeling of blood cells offers the great possibility of differentiating easily between the subtypes of white blood cells, while Raman spectroscopy reveals molecular fingerprint information with a spatial resolution down to the diffraction limit. Compared to an unstained cell, the presented results nicely demonstrate that the selected fluorescence dye does not influence the Raman spectrum of a labeled blood cell notably. By the combined application of Raman spectroscopy and statistical data analysis a distinction between white blood cell substructures could be performed. Since several blood cell types also differ in the amount of their cell components, differentiation between several blood cell types is also possible when one blood cell is described in the database by several Raman spectra according their presented sub-microscopic structures. This capability with the possibility of accurate and rapid blood cell identification in cerebrospinal fluid is extremely promising for implementation in clinical diagnostics.

Introduction

The cerebrospinal fluid (CSF) is the major specimen in the diagnosis of acute and chronic diseases of the central nervous system (*e.g.* for the identification of bacterial, viral or fungal infections of the central nervous system such as bacterial meningitis).[1] CSF of healthy adults contains no erythrocytes and up to five leukocytes per microliter. The change of the healthy clear and colorless appearance of the CSF to a differing color and turbidity warrants investigation according to the analysis of its cellular components. That includes cell counts and differentiation of liquor cells. Furthermore, CSF analysis incorporates bacterial differentiation for the diagnosis of infectious diseases after cultivation if bacterial cells are present in the smear. Recent CSF diagnosis is based on flow cytometric analysis[2–4] and morphological analysis, if necessary after staining of specific structures in a fixed cell.[5] A basic problem of laboratory medical diagnosis is low sensitivity (*e.g.* Gram staining of micro-organisms correlates with the bacterial concentration).[6–8] Further difficulties are the limited specificity (by malignant blood cells) and the requirement of a huge number of cells, making enrichment of particular cell populations necessary by cultivation (*e.g.* micro-organisms, clonal enrichment of blood cells).[9] Furthermore, the diagnosis depends on manual CSF cytology for quantitative and qualitative analysis of blood cells based on an individual personnel variability and a high staff binding. Altogether there is a restriction of rapid identification such that these diagnostic difficulties can result in a therapy delay.

To overcome these diagnostic complications micro-Raman spectroscopy is a capable alternative and reliable approach of rapidly characterizing biological samples since it yields structural fingerprint information of the investigated sample.[10] Raman spectroscopy offers important advantages as an analytical tool. The combination of a Raman setup with a microscope offers the possibility of achieving a high spatial resolution in the range of 1 μm. By doing so, mapping experiments of several structures within one eukaryotic cell[11,12] or even the examination of bacteria on a single cell level[13–16] becomes possible. A confocal Raman arrangement enables the Raman signal from a small volume element in the sample to be separated from the signals originating from the surrounding material.[17,18] While the Raman effect suffers from its low sensitivity, a variety of Raman signal-enhancing methods exists, where the two most important ones are surface-enhanced Raman scattering (SERS) and UV-resonance Raman (UVRR) spectroscopy. Applying UVRR spectroscopy for the analysis of biological samples Raman signals of aromatic amino acids of proteins and DNA are selectively enhanced. Furthermore, owing to the resonance enhancement the scattering intensity increases up to 10^6, making UVRR an extremely useful approach to study samples containing high amounts of protein such as human plasma[19] and/or DNA.[20]

The first Raman investigations on human cells were performed on eosinophil granulocytes, showing the possibility of differentiating between cell plasma and nucleus.[21] Further Raman studies were accomplished for the identification of several

cell components in granulocytes and lymphocytes.[22–25]

A lot of studies dealt with Raman investigations on erythrocytes. Hereby Raman spectra are reported for single red blood cells in the oxygenated and deoxygenated state using different excitation wavelengths.[26–29] Furthermore, the Raman micro-imaging technique was utilized for the identification of markers for heme aggregation.[30] The results of polarized Raman measurements indicate that a distinct ordering of hemes exists in the functional red blood cell.[31] Further Raman studies were performed on erythrocytes for the *in situ* localization of the malaria pigment hemozoin.[32]

Moreover, several Raman analysis approaches for the determination of the distribution of DNA[33] and RNA[34] in embryonic stem cells as well as the distribution of proteins and DNA in apoptotic cells are known.[35]

The aim of the work presented within this study is to elucidate if it is possible to characterize cells by means of fluorescence staining to differentiate between cells in combination with Raman spectroscopy to gain additional molecular information on the investigated cells. Our major interest in the analysis of CSF concerns a fast differentiation between single blood cell types independently of the investigating person. In many cases CSF contains just a small number of cells, while specific populations may be increased during some diseases, *e.g.* meningitis. Conventional diagnostic strategies are characterized by several shortcomings, in particular by inter-individual variations between manually performed CSF cytology. The development and evaluation of non-microscopic, automated diagnostic procedures is thus strongly required. To that purpose we used a Raman spectroscopic approach which focuses first on the analysis of blood cells isolated out of whole blood as a model system to determine several important methodological parameters, *e.g.* for fluorescence staining and the choice of antibodies for specific labeling of several cell types. In a next step this knowledge will be transferred to our target system CSF.

Fluorescence microscopy has become an essential tool in cell biology and the biomedical sciences due to attributes that are not readily available in phase contrast microscopy. In this contribution, in a first attempt, fluorescence labeling of a clinical specimen of blood is required since unstained samples lead to a low contrast yielding uncertain and unreliable results. Selective fluorescence staining allows the direct visualization and detection of specific blood cells depending on the applied antibody. The application of an array of fluorescence labels has the potential for the conduction of parallel measurements where different probes can concurrently identify several target molecules simultaneously. Furthermore, such a multiplex approach made it possible to identify cells and sub-microscopic cellular components with a high degree of specificity in the midst of non-fluorescing probes.[36]

The application of Raman spectroscopy subsequent to specific fluorescence staining results in a powerful biomedical assay since the molecular composition of subcellular compartments within a cell can be easily localized by means of the specific Raman fingerprint.

Experimental

Sample preparation

Samples were prepared in the Institute of Clinical Chemistry and Laboratory Diagnostics of the Friedrich-Schiller-Universität Jena, Germany. Samples of whole blood were prepared as smears or spotted onto fused silica plates. Samples extracted from CSF were brought onto fused silica plates by cytocentrifugation in order to achieve cell enrichment.

Fluorescence observation

The localization and evaluation of the success of the fluorescence labeling process concerning completeness and intensity was performed with the fluorescence microscope Axio Imager Z1 (Carl Zeiss AG, Germany) equipped with the camera AxioCam HR 8193, the ocular PI 10×/25 and the objective EC Apiplan-Apochromate 50×/0.95 HD DIC.

Spectroscopic instrumentation

Micro-Raman spectra were obtained with a micro-Raman setup (HR LabRAM invers system, Horiba/Jobin-Yvon) equipped with a 300 lines mm^{-1} grating and an inverse microscope (Olympus BX41). For Raman excitation a frequency doubled Nd:YAG laser (Coherent), providing 532 nm with a laser power of about 10 mW incident on the sample, was used. The Raman scattered light of single blood cells was collected by a Leica PLFluoar objective (100×/NA = 0.75) and detected by a thermoelectrically cooled charge coupled device (CCD) camera operating at 220 K.

The localization of the fluorescence-labeled blood cells is realized by means of Olympus U-MWIBA3 fluorescence filters (excitation: BP 460–495 nm and emission: BA 510–550 nm). Micro-Raman experiments were performed on single cells within an accumulation time between 10 and 60 s depending on the Raman signal intensity of the investigated cell.

Results and discussion

In this contribution the first characterization of unstained and fluorescence-stained blood cells by means of Raman spectroscopy is presented. In a first set of experiments blood cells isolated from whole blood were studied as a model system to determine decisive parameters for a successful combination of fluorescence-labeled antibodies and Raman spectroscopy. Secondly, blood cells extracted from their real environment – the CSF – were investigated to prove if the CSF matrix influences the applicability of Raman spectroscopy.

Since CSF is normally poor in numbers of cellular components, samples were prepared by cytocentrifugation for cell enrichment. Fig. 1(A) shows a representative microscopic image of cells extracted from CSF that were brought onto a fused silica plate by cytocentrifugation. Fig. 1(B) presents characteristic Raman spectra for several measuring positions of different cells shown in the image of 1(A). As can be seen the cells show several morphological shapes and the Raman spectra recorded at positions (d) and (e) differ significantly in intensity and band profile compared to the Raman spectra (a)–(c). The Raman signatures of the latter cells exhibit differences among each other, albeit slightly, due to the biochemical heterogeneity of these cells. Their Raman spectra (a)–(c) can be attributed to leukocytes. The Raman spectra (d) and (e)

feature typical characteristics of spectra arising from erythrocytes, although both cell exhibit different shapes. The Raman excitation wavelength of 532 nm leads to resonantly-enhanced signals due to the hemoglobin chromophore. The resonance Raman-enhanced bands at 1588, 1127 and 745 cm^{-1} can be assigned to several symmetric and asymmetric stretching vibrations of C_α of the pyrrole ring in combination with the bridge atom C_m between the rings.[28,29] Switching the Raman excitation wavelength in the non-resonance region of the hemoproteins in erythrocytes or leukocytes, Raman spectra are comparable or did not contain any significant information.

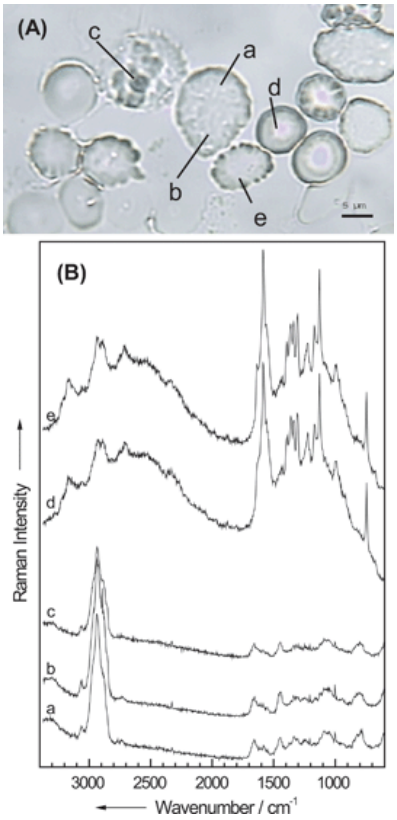

Fig. 1 (A) Microscopic image of blood cells extracted from CSF brought onto a fused silica plate by cytocentrifugation. **(B)** Two groups of Raman spectra of blood cells with different shape but similar spectra. Raman spectra of leukocytes (a–c) compared with Raman spectra of erythrocytes (d and e).

In routine diagnostic procedures different subtypes of leukocytes were identified by CSF cytology after Pappenheim-staining of the cells. In Fig. 2(A) a microscopic image of such stained cells of CSF is depicted. The cells can be well distinguished by the size and the shape of the colored granules. However, as can be seen in Fig. 2(B) the fluorescence of the applied dyes masks the Raman signal of the cells for a Raman excitation wavelength of 532 nm. Hence, Pappenheim-stained leucocytes are unsuitable to be investigated by Raman spectroscopy with an excitation wavelength of around 532 nm.

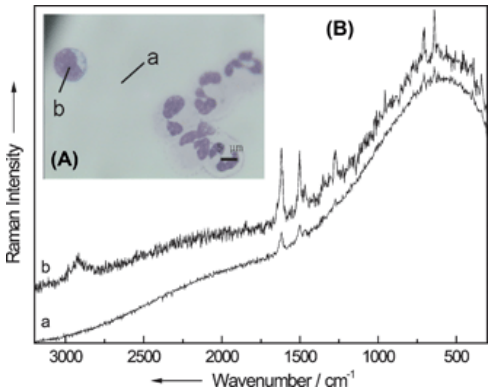

Fig. 2 (A) Bright-light image of Pappenheim-stained blood cells isolated from CSF. **(B)** Raman spectra of a Pappenheim-stained blood cell (b) compared with a

background Raman spectrum of the dye (a).

In order to differentiate between leukocytes, fluorescence labeling was applied to whole blood to determine several parameters for fluorescence staining and Raman spectroscopic measurements. In Fig. 3(A) a microscopic image of a smear of whole blood is shown that is dominated by erythrocytes (a) and just a few leukocytes (b and c). It is not possible to easily differentiate between the subtypes of the white blood when they are unstained. In order to distinguish between the white blood cells we used fluorescence staining, applying CD-15 fluorescein isothiocyanate (FITC)-labeled antibodies. CD-15 antibodies can be used for identifying granulocytes (>95%) including neutrophils and eosinophils. In addition, CD-15 is expressed in varying degrees on monocytes. CD-15 is not expressed on erythrocytes, platelets, lymphocytes or basophils. On the basis of the natural existence of white blood cells in blood, mostly neutrophils and just a few monocytes will be stained with FITC-CD-15 antibodies. Fig. 3(B) shows the fluorescence image of one stained (FITC-CD-15) leukocyte (b) as well of one unstained (c) leukocyte.

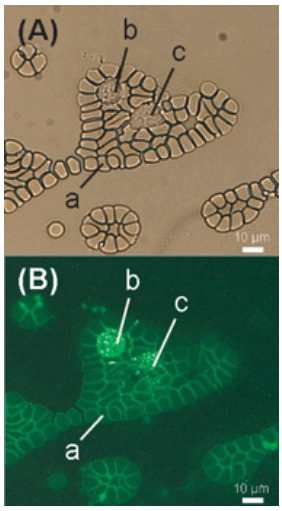

Fig. 3 Bright-light image **(A)** and fluorescence image **(B)** of blood cells of a smear of whole blood that is dominated by erythrocytes (a) and some fluorescence-stained (FITC-CD-15) (b) and unstained leukocytes (c).

For an exclusive characterization of white blood cells, blood samples were treated with lysis buffer where the erythrocytes were lysed and removed prior to CD-15 fluorescence staining. This sample preparation allows for, besides a specific fluorescence labeling of leukocytes, achieving additional molecular Raman information on the isolated leukocytes. In Fig. 4(A) a bright-light image is shown and compared with the fluorescence image in Fig. 4(B) of fluorescence-stained (FITC-CD-15) white blood cells spotted onto a fused silica plate.

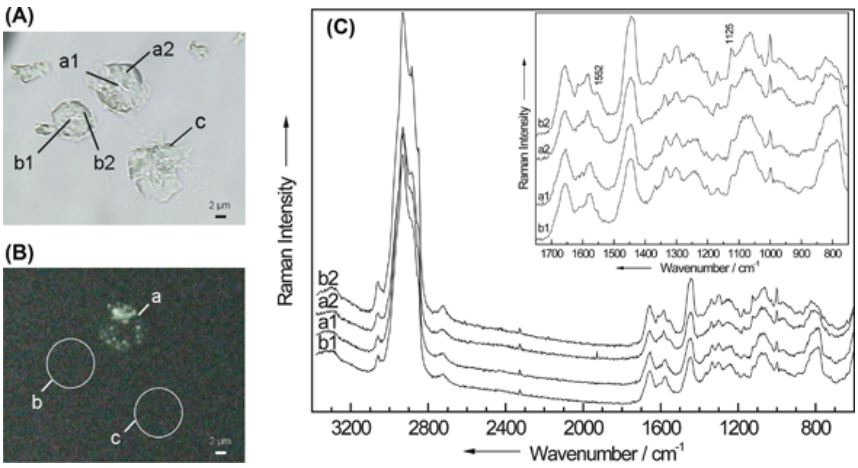

Fig. 4 Sample of whole blood treated with lysis buffer to remove erythrocytes. **(A)** Bright-light image of white blood cells extracted from whole blood treated with lysis buffer spotted onto a fused silica plate. **(B)** Fluorescence image of white blood cells extracted from whole blood treated with lysis buffer spotted onto a fused silica plate; white circles mark unstained blood cells. **(C)** Raman spectra of a fluorescence-stained (FITC-CD-15) leukocyte (a) compared

with an unstained leukocyte (b).

In the microscopic image [Fig. 4(A)], besides the two cells (a) and (b) additional cell fragments can be found as well as a lysed cell (c). In the fluorescence image [Fig. 4(B)] just one cell (a) in the middle is fluorescent while the two other cells are not (b and c) (indicated with a circle). Several Raman spectra of a fluorescence-stained (a1 and a2) and unstained cell (b1 and b2) at different measuring points were recorded. These Raman signals are shown in Fig. 4(C) where the corresponding Raman spectra are compared. There are two major spectral groups where the Raman spectra are dependent on the measuring position but independent of whether the cell is unstained or fluorescence stained. The Raman bands at 1552 and 1125 cm^{-1} exhibit different intensities in the spectra (a2) and (b2) compared to (a1) and (b1). These two Raman bands can be attributed to enhanced contributions of proteins. The mode of 1125 cm^{-1} can be assigned to C–N and C–C stretching vibrations of proteins.[37,38] The peak around 1552 cm^{-1} results from the C_2–C_3 stretching mode of the pyrrole ring from tryptophan.[39] To corroborate the assumption that the fluorescence stain used (FITC) leaves the Raman spectrum of fluorescence FITC-CD-15 antibody-labeled leukocyte unaltered, its influence was investigated by measuring the fluorescence-labeled FITC-CD-15 antibody directly. For Raman analysis, the fluorescence-labeled FITC-CD-15 antibody was spotted onto fused silica plates and dried before measurement. Initially its Raman spectrum is masked by the fluorescence of the dye (Fig. 5c). After a prolonged laser exposure the fluorescence of the fluorescence-labeled FITC-CD-15 antibody is quenched and bands of this antibody of the class IgM are visualized. Fig. 5b represents the corresponding Raman spectrum of the FITC-CD-15 antibody that is compared with an average Raman spectrum of five FITC-CD-15-labeled leukocytes in Fig. 5a. FITC-CD-15 antibodies deliver similar signals as FITC-CD-15-labeled leukocytes, except for an additional band at 936 cm^{-1} that does not appear in the average Raman spectrum of the FITC-CD-15-labeled leukocytes. Nevertheless, the fluorescence-stained FITC-CD-15 antibody is used in practice with a much lower concentration than in this experiment. Therefore, this label has no interfering influence on the Raman spectrum of the leukocytes independently if it is present in solution or bound to the cell surface.

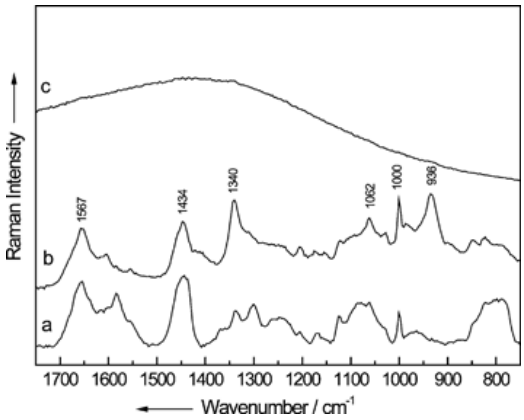

Fig. 5 Influence of the fluorescence stain FITC on the Raman spectrum of a fluorescence FITC-CD-15 antibody-labeled leukocyte: **a**: average Raman spectrum of five FITC-CD-15-labeled leukocytes; **b**: Raman spectrum of a fluorescence-labeled FITC-CD-15 antibody after fluorescence quenching with treatment by laser exposure; **c**: Raman spectrum of a fluorescence-labeled FITC-CD-15 antibody masked by the fluorescence of the fluorescence dye.

These investigations showed that Raman spectroscopy can be applied to fluorescence-stained blood cells. Selective fluorescence staining allows for the direct localization and identification of blood cell types with a high degree of specificity in the midst of numerous cells. The application of Raman spectroscopy subsequently provides additional molecular information about subcellular compartments within a cell. However, Raman spectra are very often masked by the competing process of fluorescence, having a higher intensity of about ten orders of magnitude. The fluorescence dye FITC has an absorption maximum of 495 nm and an emission maximum at 517 nm. Since the absorption maximum of the fluorescent dye is about 37 nm away from the Raman laser excitation wavelength of 532 nm, no fluorescence of the dye is excited. Therefore, well-resolved, fluorescence-free Raman spectra can be recorded of fluorescence-labeled blood cells. Thus we could demonstrate that by using an appropriate fluorescence dye and a Raman excitation wavelength far away from the absorption region of the dye, it is possible to gain Raman spectra of labeled cells without any interference by the dye itself.[40]

In a next step we investigated leukocytes isolated from CSF to determine the spatial distribution of the various components within the cell by means of Raman mapping experiments. Furthermore, we studied whether or not the native CSF environment proves to be an appropriate matrix for measuring cells by Raman spectroscopy. In Fig. 6(A), a microscopic image of two unstained CSF-leukocytes brought onto a silica plate by cytocentrifugation is shown. Raman point mapping experiments were performed by recording Raman spectra in the red marked area. The corresponding Raman spectra are shown for the wavenumber region of 2500–3300 cm^{-1} in Fig. 6(B) and for the fingerprint region between 600 and 1800 cm^{-1} in Fig. 6(C). It can be seen that the Raman spectra depend on the measuring position within the cell. Three different kinds of Raman spectra, characteristic of various regions in the cell, were observed that can be assigned to certain molecular substances. Raman spectrum (a) corresponds to a DNA spectrum that shows typical Raman DNA bands at 725,

781, 1334, 1373, 1480 and 1575 cm^{-1}. Raman spectrum (b) shows characteristics of a Raman spectrum obtained when analyzing lipids with pronounced bands at 1301, 1437, 1654 and 1744 cm^{-1}, and spectrum (c) can be assigned to proteins with marker bands at 1001, 1447 and 1553 cm^{-1}. The bands around 1654 and 1250 cm^{-1} are due to the amide I and amide III bands. In Fig. 6(D), false color plots showing the distribution of different marker bands within the cell are depicted. To map the DNA distribution the Raman band in the range of 1559–1584 cm^{-1} was integrated, showing that the left cell exhibits a segmented cell nucleus and differs morphologically from the right cell which possesses a compact intracellular nucleus. Probably, both cells can be attributed to granulocytes since granulocytes are the dominant blood cell types during bacterial meningitis, and granulocytes change from the compact cell shape to a segmented shape when they grow old.

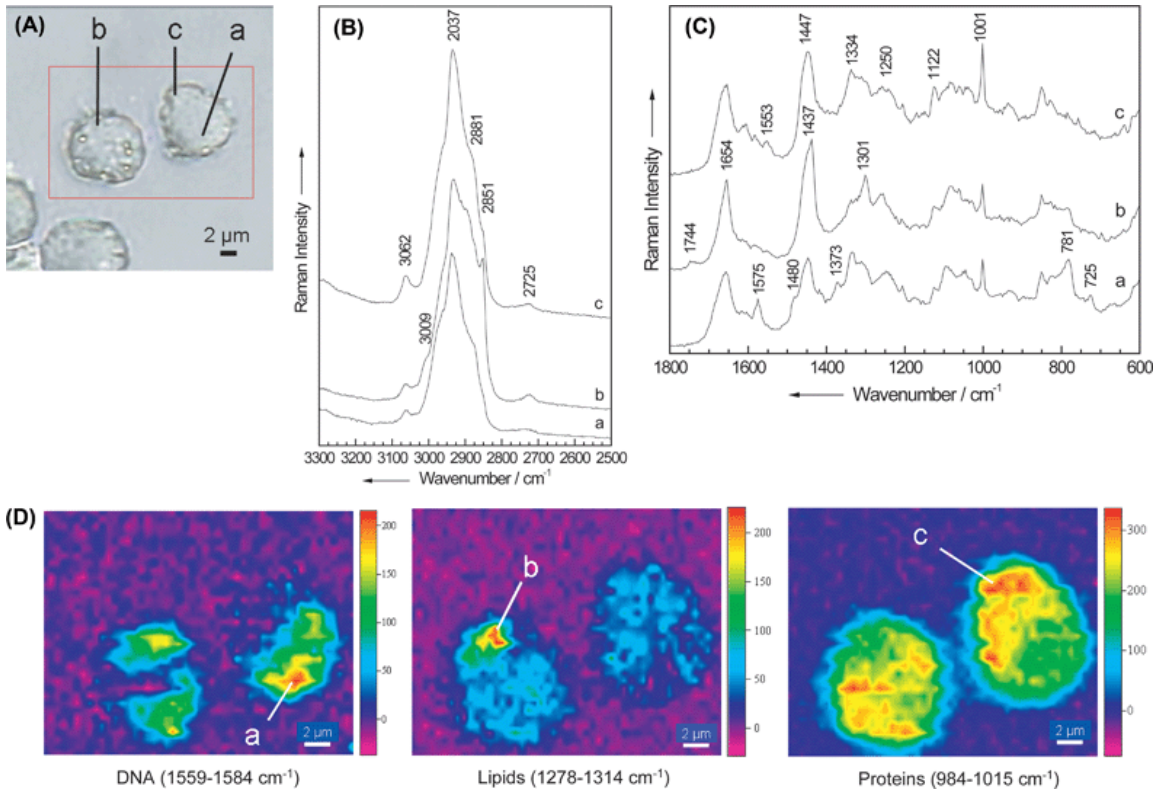

Fig. 6 Raman mapping experiment on two single leukocytes extracted from CSF. **(A)** Microscopic image of blood cells brought onto a fused silica plate by cytocentrifugation. **(B)** and **(C)** Corresponding Raman spectra for the spectral region of 2500–3300 cm^{-1} **(B)** and for the fingerprint region of 600–1800 cm^{-1} **(C)**. **(D)** The false color plots display these distributions for different marker bands in the cell base on baseline-corrected spectra. DNA: 1559–1584 cm^{-1}; lipids: 1278–1314 cm^{-1}; proteins: 984–1015 cm^{-1}.

In the middle of Fig. 6(D) a false color plot depicting the lipid distribution within the cell (integrated wavenumber region: 1278–1314 cm^{-1}) can be seen while the image on the right-hand side presents the false color plot of proteins by integrating over the phenylalanine and tryptophan bands in the range of 984–1015 cm^{-1}.

The false color plots presented above demonstrate the spatial distribution of the various components of proteins, DNA and lipids within the leukocytes by integrating over the respective marker bands. Often these marker bands are superpositioned by neighboring signals and therefore the intensity information may be obscured. For an increased informational value a chemometric analysis is required. Hence two chemometric analysis methods, namely hierarchical cluster analysis (HCA) and principal component analysis (PCA), were applied to the Raman spectra of the leukocyte (extracted from CSF) marked by the red square in Fig. 7(A) placed on a quartz plate.

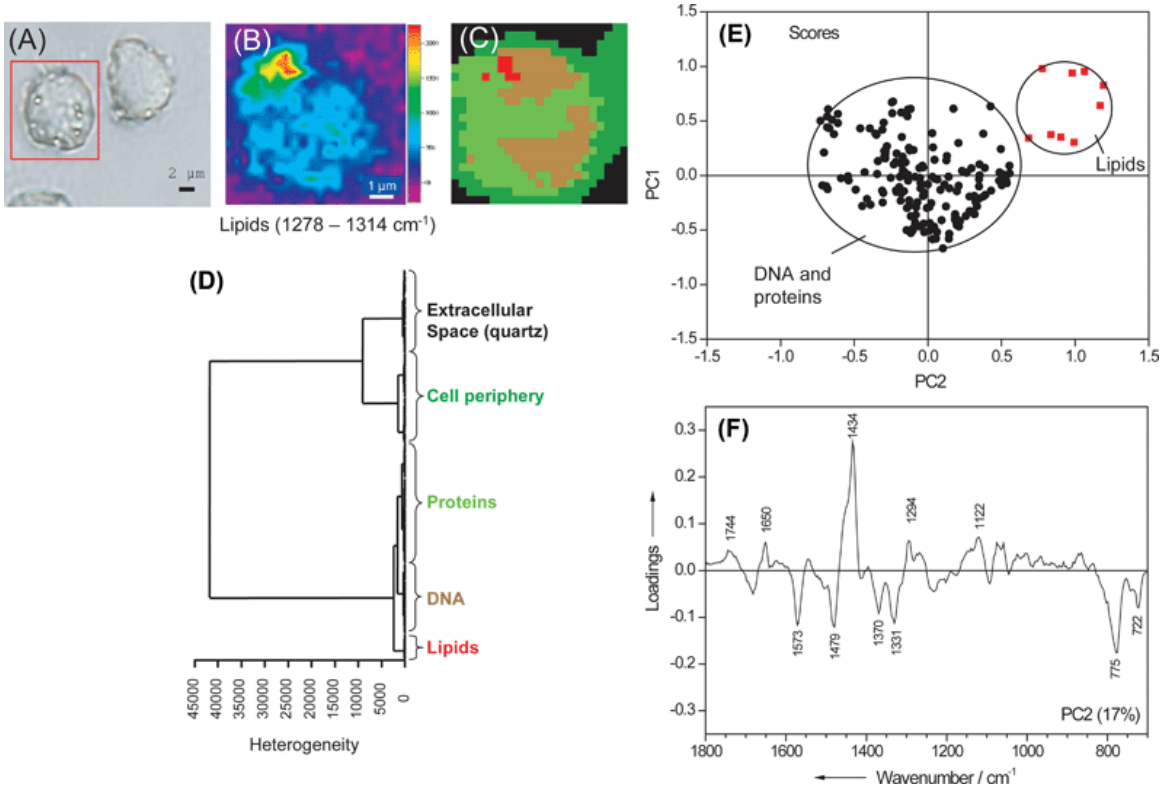

Fig. 7 Raman mapping experiment on two single leukocytes extracted from CSF. **(A)** Microscopic image of a chemometrically analyzed leukocyte extracted from CSF and brought onto a quartz plate. The area enclosed by the red square was used for chemometric analysis. **(B)** Corresponding false color plot constructed in the 1301 cm^{-1} band of lipids. **(C)** Corresponding HCA image partitioned into five clusters correlating with the extracellular space (black), cell periphery (dark green), cytoplasm (protein-rich domains; light green), nucleus (DNA-rich domains; light brown) and lipid-rich regions (red). **(D)** Hierarchical cluster analysis of the left leukocyte; the dendrogram displays a clear separation between the extracellular space and cell periphery as well as from DNA, proteins and lipid-rich domains. This classification served as a basis for the HCA image (C). **(E)** Scores plot of the first two principal components PC1 (53% of the total variance) and PC2 (17% of the total variance) of the Raman spectra of different positions within the left leukocyte. **(F)** Loading plot of the second principal component PC2 (17% of the total variance) highlighting regions associated with large loadings.

Prior to the chemometric analysis of the Raman spectra, the first derivative of the spectra (Savitzky–Golay, 13 smoothing points) was calculated to realize both a background correction and a signal-to-noise ratio enhancement. The final data pre-processing step consisted of a vector normalization of the spectra. With this pre-treated data set, HCA was employed and the spectral region of 660–1816 cm^{-1} and 2747–3162 cm^{-1} was chosen for a classification of the spectra. For the hierarchical cluster analysis the program package 'Opus Ident 3.1' (Bruker Optics, Ettlingen, Germany) was used accounting with the Normalization to Reproduction Level method and Ward's algorithm for calculating the spectral distances and cluster grouping. Fig. 7(D) shows the result of the hierarchical cluster analysis of the leukocyte displayed in the red square in Fig. 7 (A). The dendrogram displays a clear separation between the extracellular space (quartz background) and the cell periphery. Furthermore, DNA-rich regions (nucleus) and protein-rich regions (cytoplasm) are well divided from the lipid-rich domains.

To prove the classification correctness an HCA image displayed in Fig. 7(C) was constructed from the dendrogram of the hierarchical cluster analysis, thereby visualizing areas with high Raman similarities. The cluster of the extracellular space (black) and the cell periphery (dark green) delimit the cell from the surroundings in good accordance with the microscopic image in Fig. 7(A). Additionally, the spatial distribution of the three intracellular components is displayed. High concentrations and therefore strong contributions from the corresponding marker bands to the Raman spectra are found for proteins, DNA and lipids in the light green, brown and red clusters, respectively. The resemblance to the intensity-correlated false color plots in Fig. 6(D) and Fig. 7(B) is apparent.

For a principal component analysis (PCA) the software 'The Unscrambler®' (CAMO Process AS; Version 9.2,

Reutlingen, Germany) was applied. This software uses a cross-validation to verify the results. For PCA, calculation spectra of the extracellular space (quartz background) and spectra with a poor signal-to-noise ratio were removed from the data set prior to chemometric analysis on the basis of an intensity threshold of the band at 2932 cm^{-1} of around 5000 counts. Hereby, the original and vector-normalized Raman spectra were used for calculation. The spectral regions of 660–1816 and 2747–3162 cm^{-1} were chosen. After this calculation, further spectra of the cell periphery were excluded concerning the grouping in the scores plot (not shown here). With the remaining Raman spectra a recalculation was performed. Fig. 7(E) displays the scores plot of the first two principal components PC1 (53% of the total variance) and PC2 (17% of the total variance) of the Raman spectra of different positions within the leukocyte shown in the red square in Fig. 7(A). It is possible to separate lipid-rich domains from DNA and proteins within the cell along the axis of the second principal component PC2. The loading plot provides information on the variables (wavenumbers of the spectrum) that are important for group separation. The loading plot of the second principal component PC2 (17% of the total variance) highlighting regions associated with large loadings is presented in Fig. 7(F). The spectral regions of 1122, 1294, 1434, 1650 and 1744 cm^{-1} show positive loadings and are correlated with lipid information. The wavenumber regions with the negative loadings of 722, 775, 1331, 1370, 1479 and 1573 cm^{-1} represent both DNA and proteins bands.

In summary, the Raman mapping experiments of erythrocyte-free CSF samples showed that the CSF matrix does not influence the Raman measurements. Moreover, the chemometric evaluation by means of a hierarchical cluster analysis and principal component analysis showed that it is possible to characterize a single leukocyte concerning the distribution of the intracellular components of proteins and DNA from lipid-rich domains within a cell. With the HCA a further separation of proteins, DNA and lipid domains from the cell periphery and the extracellular space (quartz background) could be demonstrated. For further investigations, blood cells in CSF will be fluorescence-stained and labeled with specific antibodies to create a database capable of differentiating and identifying fluorescence-labeled blood cells by means of Raman spectroscopy in combination with statistical data evaluation.

Conclusions

This contribution reports on a successful application of selective fluorescence staining for the identification of blood cells in combination with Raman spectroscopy to gain additional information on the composition of subcellular components within a cell. Since the absorption maximum of the fluorescence dye (495 nm) is at least 37 nm away from the Raman laser excitation wavelength (532 nm) it is possible to record unaltered Raman spectra of fluorescence-stained blood cells isolated from whole blood that are not masked by fluorescence.

Firstly, blood cells isolated from whole blood were studied as a model system to determine several parameters for selective fluorescence labeling and analysis by means of Raman spectroscopy. For further characterization and differentiation, additional fluorescence stains linked to different antibodies have to be tested which allow for specifically staining other blood cells such as monocytes or lymphocytes. This will facilitate the setup of a database containing Raman characteristics of several cell types, enabling specific differentiation of certain types of blood cells.

The results presented above demonstrate that the CSF environment has no crucial influence on the Raman measurements. By means of hierarchical cluster analysis and principal component analysis a single leukocyte could be characterized regarding the intracellular distribution of proteins and DNA that could be separated from lipid-rich domains within the cell. Moreover, by means of the HCA an additional separation between the extracellular space (quartz background) and the cell periphery from proteins, DNA and lipid domains could be achieved. However, next to the differentiation of sub-microscopic components within a single blood cell, a separation between white blood cell types by means of a combination of Raman spectroscopy and multivariate statistical data analysis is also possible when these different cell structures can be compared with a database since several blood cell types differ in their amounts of inner microscopic components such as proteins, DNA/RNA, carbohydrates, lipids or the presence of endogenous dyes. Hereby one blood cell has to be described not only by one but by several Raman spectra according to their presented sub-microscopic structures.

For further investigations, fluorescence labeling of specific blood cell types with several antibodies will be applied to our target system CSF. After successfully applying the former approach (fluorescence labeling of blood cells isolated from whole blood) in the real CSF environment, Raman spectroscopic analysis will be performed on unknown blood cells isolated from CSF for identification by means of multivariate chemometric methods based on well-trained data sets. In future work we will also study the rather highly complex eukaryotic cell growth process, since the database for the identification of unknown blood cells has to contain not only several cell types but also different ages of such cells. Furthermore, additional information such as the level of activation or phagocytosis activity of distinct cells (*e.g.* monocytes, granulocytes) may be gained.

Acknowledgements

We gratefully acknowledge financial support from the Deutsche Forschungsgemeinschaft (DE 307/7-1 and PO 563/7-1).

References

1 L. D. Gray and D. P. Fedorko, *Clin. Microbiol. Rev.*, 1992, **5**, 130–145 [Links].

2 M. W. Aune and S. Sandberg, *Clin. Lab. Haematol.*, 2000, **22**, 203–210.

3 J. J. M. L. Hoffmann and W. C. M. Janssen, *Clin. Chem. Lab. Med.*, 2002, **40**, 1168–1173 [Links].

4 S. Soogarun, S. Sirimongkolsakul, V. Wiwanitkit, A. Siritantikorn, K. Pimsane and R. Srivijarn, *Clin. Lab.*, 2002, **48**, 623–629.

5 B. Brando, D. Barnett, G. Janossy, F. Mandy, B. Autran, G. Rothe, B. Scarpati, G. D'Avanzo, J. L. D'Hautcourt, R. Lenkei, G. Schmitz, A. Kunkl, R. Chianese, S. Papa and J. W. Gratama, *Cytometry*, 2000, **42**, 327–346 [Links].

6 L. J. La Scolea, Jr. and D. Dryja, *J. Clin. Microbiol.*, 1984, **19**, 187–190 [Links].

7 E. Mylonakis, E. L. Hohmann and S. B. Calderwood, *Medicine (Baltimore)*, 1998, **77**, 313–336.

8 A. R. Tunkel, B. J. Hartman, S. L. Kaplan, B. A. Kaufman, K. L. Roos, W. M. Scheld and R. J. Whitley, *Clin. Infect. Dis.*, 2004, **39**, 1267–1284 [Links].

9 S. F. Ibrahim and G. Van Den Engh, *Curr. Opin. Biotechnol.*, 2003, **14**, 5–12 [Links].

10 R. Petry, M. Schmitt and J. Popp, *ChemPhysChem*, 2003, **4**, 14–30 [Links].

11 P. Rösch, M. Harz, K. D. Peschke, O. Ronneberger, H. Burkhardt and J. Popp, *Biopolymers*, 2006, **82**, 312–316 [Links].

12 P. Rösch, M. Harz, M. Schmitt and J. Popp, *J. Raman Spectrosc.*, 2005, **36**, 377–379 [Links].

13 M. Harz, P. Rösch, K. D. Peschke, O. Ronneberger, H. Burkhardt and J. Popp, *Analyst*, 2005, **130**, 1543–1550 [Links].

14 P. Rösch, M. Harz, K.-D. Peschke, O. Ronneberger, H. Burkhardt, A. Schuele, G. Schmauz, M. Lankers, S. Hofer, H. Thiele, H.-W. Motzkus and J. Popp, *Anal. Chem.*, 2006, **78**, 2163–2170 [Links].

15 P. Rösch, M. Harz, M. Schmitt, K.-D. Peschke, O. Ronneberger, H. Burkhardt, H.-W. Motzkus, M. Lankers, S. Hofer, H. Thiele and J. Popp, *Appl. Environ. Microbiol.*, 2005, **71**, 1626–1637 [Links].

16 P. Rösch, M. Schmitt, W. Kiefer and J. Popp, *J. Mol. Struct.*, 2003, **661–662**, 363–369 [Links].

17 L. Baia, K. Gigant, U. Posset, R. Petry, G. Schottner, W. Kiefer and J. Popp, *Vib. Spectrosc.*, 2002, **29**, 245–249 [Links].

18 L. Baia, K. Gigant, U. Posset, G. Schottner, W. Kiefer and J. Popp, *Appl. Spectrosc.*, 2002, **56**, 536–540 [Links].

19 M. Harz, R. A. Claus, C. L. Bockmeyer, M. Baum, P. Rösch, K. Kentouche, H. P. Deigner and J. Popp, *Biopolymers*, 2006, **82**, 317–324 [Links].

20 U. Neugebauer, U. Schmid, K. Baumann, U. Holzgrabe, W. Ziebuhr, S. Kozitskaya, W. Kiefer, M. Schmitt and J. Popp, *Biopolymers*, 2006, **82**, 306–311 [Links].

21 G. J. Puppels, F. F. M. De Mul, C. Otto, J. Greve, M. Robert-Nicoud, D. J. Arndt-Jovin and T. M. Jovin, *Nature*, 1990, **347**, 301–303 [Links].

22 G. J. Puppels, H. S. P. Garritsen, G. M. J. Segers-Nolten, F. F. M. De Mul and J. Greve, *Biophys. J.*, 1991, **60**, 1046–1056 [Links].

23 R. B. Ramanauskaite, I. G. M. J. Segers-Nolten, K. J. de Grauw, N. M. Sijtsema, L. Van Der Maas, J. Greve, C. Otto and C. G. Figdor, *Pure Appl. Chem.*, 1997, **69**, 2131–2134 [Links].

24 Z. X. Shen, H. Shu, D. W. Qiu, L. Qin and S. H. Tang, *Asian J. Spectrosc.*, 1997, **1**, 215–224.

25 H.-J. van Manen, N. Uzunbajakava, R. van Bruggen, D. Roos and C. Otto, *J. Am. Chem. Soc.*, 2003, **125**, 12112–12113 [Links].

26 R. Gessner, C. Winter, P. Rösch, M. Schmitt, R. Petry, W. Kiefer, M. Lankers and J. Popp, *ChemPhysChem*, 2004, **5**, 1159–1170 [Links].

27 B. R. Wood, P. Caspers, G. J. Puppels, S. Pandiancherri and D. McNaughton, *Anal. Bioanal. Chem.*, 2007, **387**, 1691–1703 [Links].

28 B. R. Wood and D. McNaughton, *J. Raman Spectrosc.*, 2002, **33**, 517–523 [Links].

29 B. R. Wood, B. Tait and D. McNaughton, *Biochim. Biophys. Acta*, 2001, **1539**, 58–70 [Links].

30 B. R. Wood, L. Hammer, L. Davis and D. McNaughton, *J. Biomed. Opt.*, 2005, **10**, 014005 [Links].

31 B. R. Wood, L. Hammer and D. McNaughton, *Vib. Spectrosc.*, 2005, **38**, 71–78 [Links].

32 T. Frosch, S. Koncarevic, L. Zedler, M. Schmitt, K. Schenzel, K. Becker and J. Popp, *J. Phys. Chem. B*, 2007, **111**, 11047 [Links].

33 I. Notingher, I. Bisson, J. M. Polak and L. L. Hench, *Vib. Spectrosc.*, 2004, **35**, 199–203 [Links].

34 I. Notingher, I. Bisson, A. E. Bishop, W. L. Randle, J. M. P. Polak and L. L. Hench, *Anal. Chem.*, 2004, **76**, 3185–3193 [Links].

35 N. Uzunbajakava, A. Lenferink, Y. Kraan, E. Volokhina, G. Vrensen, J. Greve and C. Otto, *Biophys. J.*, 2003, **84**, 3968–3981 [Links].

36 J. S. Ploem, in *Fluorescent and Luminescent Probes for Biological Activity* ed. W. T. Mason, Academic Press, San Diego, CA, 1993, ch. 1.

37 C. Krafft, T. Knetschke, A. Siegner, R. H. W. Funk and R. Salzer, *Vib. Spectrosc.*, 2003, **32**, 75–83 [Links].

38 I. Notingher, S. Verrier, S. Haque, J. M. Polak and L. L. Hench, *Biopolymers*, 2003, **72**, 230–240 [Links].

39 T. Kitagawa and S. Hirota, in *Handbook of Vibrational Spectroscopy. Volume 5: Applications in Life, Pharmaceutical and Natural Sciences*, ed. J. M. Chalmers and P. R. Griffiths, John Wiley & Sons, Chichester, 2002, pp. 3426–3446.

40 M. Krause, B. Radt, P. Rösch and J. Popp, *J. Raman Spectrosc.*, 2007, **38**, 369–372 [Links].

Footnote

† Authors contributed equally to this study.

2.8 UV-resonance Raman spectroscopic study of human plasma of healthy donors and patients with thrombotic microangiopathy. [MH8]

M. Harz, R. A. Claus, C. L. Bockmeyer, M. Baum, P. Rösch, K. Kentouche, H.-P. Deigner, J. Popp

Biopolymers **2006**, 82, 317-324.

M. Harz[1]
R. A. Claus[2]
C. L. Bockmeyer[2]
M. Baum[1]
P. Rösch[1]
K. Kentouche[3]
H.-P. Deigner[4]
J. Popp[1]

[1] *Institute of Physical Chemistry, Friedrich-Schiller-University Jena, Helmholtzweg 4, D-07743 Jena, Germany*

[2] *Department for Anesthesiology and Intensive Care Medicine, Friedrich-Schiller-University Jena, Erlanger Allee 101, D-07747 Jena, Germany*

[3] *Department of Paediatrics, Friedrich-Schiller-University Jena, Kochstraße 4, D-07743 Jena, Germany*

UV-Resonance Raman Spectroscopic Study of Human Plasma of Healthy Donors and Patients with Thrombotic Microangiopathy

[4] *Biomedicinal Chemistry, School of Chemical Sciences and Pharmacy, University of East Anglia, Norwich, United Kingdom*

Received 11 November 2005; revised 1 February 2006; accepted 17 February 2006
Published online 27 February 2006 in Wiley InterScience (www.interscience.wiley.com).
DOI 10.1002/bip.20489

Abstract: *Various diseases shift the composition of human plasma; hence, the relative quantification of plasma constituents offers the opportunity to use the dynamic and complex composition of plasma to gain information on novel diagnostic and prognostic factors. Since plasma contains, besides water, mostly proteins, UV-resonance Raman spectroscopy (UVRR) seems to be a suitable method for investigating plasma. With this method the signals of aromatic amino acids and proteins are selectively enhanced. In this study an UV-resonance Raman approach was used for the investigation of human plasma of healthy volunteers and patients with thrombotic microangiopathy. For comparison, selected plasma components were analyzed for a more detailed characterization of cryoprecipitates from human plasma.* © 2006 Wiley Periodicals, Inc. Biopolymers 82: 317–324, 2006

This article was originally published online as an accepted preprint. The "Published Online" date corresponds to the preprint version. You can request a copy of the preprint by emailing the Biopolymers editorial office at biopolymers@wiley.com

Keywords: *cryoprecipitated human plasma; plasma components; UV-resonance Raman spectroscopy (UVRR)*

Correspondence to: J. Popp; e-mail: juergen.popp@uni-jena.de
M. Harz and R. A. Claus contributed equally to this study.

INTRODUCTION

There is a wide array of pathophysiological conditions that can be present with a luminal platelet aggregation leading to a microangiopathic phenotype, all of which are characterized by thrombocytopenia, organ failure, and hemolytic anemia.[1] The pathologic substrate of most critical relevance is the thrombotic plaque in the microcirculation, composed mainly of aggregated platelets with a small amount of fibrin but huge amounts of von Willebrand factor (VWF). VWF is an adhesive and multimeric plasma glycoprotein required for normal hemostasis. The agglutinative properties of VWF are a critical function of its size, since the larger the molecule, the more active it is in promoting platelet adhesion or spontaneous aggregation, resulting in a thrombophilic state.[2] The proteolytic activity of the protease ADAMTS-13 results in limited degradation of the VWF. However, e.g., in patients with severe infections, disseminated intravascular coagulation, or the catastrophic antiphospholipid antibody syndrome, decreased activity of ADAMTS-13, severe thrombocytopenia and an elevated thrombotic microangiopathy (TMA) ratio has been observed,[3–5] resulting in the appearance of unusually large VWF multimers in plasma, e.g., after endotoxin challenge in healthy volunteers.[6] At present, these unusually large multimers of VWF in plasma were identified using electrophoretic methods,[7] however there were disadvantages, such as time-consuming analysis as well as insufficient reproducibility and comparability between laboratories. For rapid diagnosis to expedite earlier initiation of a beneficial plasma exchange as therapy of choice, faster analytical techniques are needed.

From this point of view vibrational spectroscopy can be regarded as a suitable method. The possibilities of the application of Fourier transform infrared spectroscopy (FT–IR)[8,9] and Raman spectroscopy[10–12] have already been demonstrated successfully to investigate plasma or serum samples. Also the ability to measure important properties of plasma has been shown using Raman spectroscopy with an excitation wavelength in the near infrared.[13]

Because of its protein constituents, UV-resonance Raman spectroscopy is a method of choice for analyzing plasma in contrast to the above mentioned methods, because UV-resonance Raman spectroscopy signals from molecules, like aromatic amino acids and proteins, are selectively enhanced.[14–16]

Blood contains plasma and corpuscular components such as erythrocytes, leukocytes, and platelets. The plasma, however, consists of about 92–94% water, 6–8% proteins, and other components such as salts, carbohydrates, and fats. Highly abundant proteins of human plasma are albumin (60–80%), immunglobulin (20–40%), and fibrinogen (4%). Since the plasma samples were cryoprecipitated for measurement, the plasma composition deviates from pure plasma. Cryoprecipitated plasma consists mostly of the proteins of clotting factor VIII, VWF, and fibrinogen as well as glucose. In contrast, albumin and immunglobulins are reduced.[17,18]

In this study an UV-resonance Raman approach was used for the characterization of human plasma samples of healthy donors and patients with thrombotic microangiopathy of different origin. Furthermore, we analyzed spectra of cryoprecipitated plasma components such as factor VIII, VWF of different lengths, and fibrinogen; aromatic amino acids tryptophan, tyrosine, and phenylalanine; and glucose as well as β-carotene, hemoglobin, bilirubin, whole blood, and lipoprotein to study the plasma composition and differences in plasma spectra of healthy donors and patients. Because of the complexity of the spectra, the different features of plasma samples of healthy donors and patients are not easy to detect at a glance, making it necessary to conduct a hierarchical cluster analysis to distinguish between them.

MATERIALS AND METHODS

Preanalytical Sample Preparation

Upon approval of the local ethical committee, 200 μL citrated plasma from healthy controls as well as from patients with thrombotic microangiopathy of different origin diagnosed by a residual proteolytic activity of ADAMTS13 $< 20\%$ as determined by the method of Gerritsen et al.[19] was cryoprecipitated by thawing on ice for 45 min after freezing at -80°C for about 6 h. Afterward the samples were centrifugated at 15,000g for 30 min at 4°C. The supernatant was discarded and the cryoprecipitated pellet was resolubilized in a total volume of 200 μL phosphate-buffered saline (PBS) solution. For UV–Raman analysis, the cryoprecipitated protein mixture was spotted onto fused silica plates and dried in vacuo.

The plasma components were purchased by Sigma–Aldrich (Taufkirchen, Germany). Recombinant factor VIII was purchased from Baxter (Vienna, Australia). The substances were diluted in water or PBS in appropriate concentrations and spotted onto fused silica plates and dried in vacuo. For comparison of VWF multimers differing in length and thrombophilic activity, we used two different VWF specimens: (i) ultralarge VWF was obtained from recombinant protein synthesis[20] and (ii) low-molecular-weight VWF was obtained by limited proteolysis of *rh*VWF by ADAMTS13 at mild denaturating conditions (1.5 *M* urea) in the presence of Ba^{2+} over 2 h as described previously.[20]

Spectroscopic Instrumentation

The UVRR data were collected on a micro-Raman instrument (HR 800, Horiba/Jobin Yvon, Bensheim, Germany)

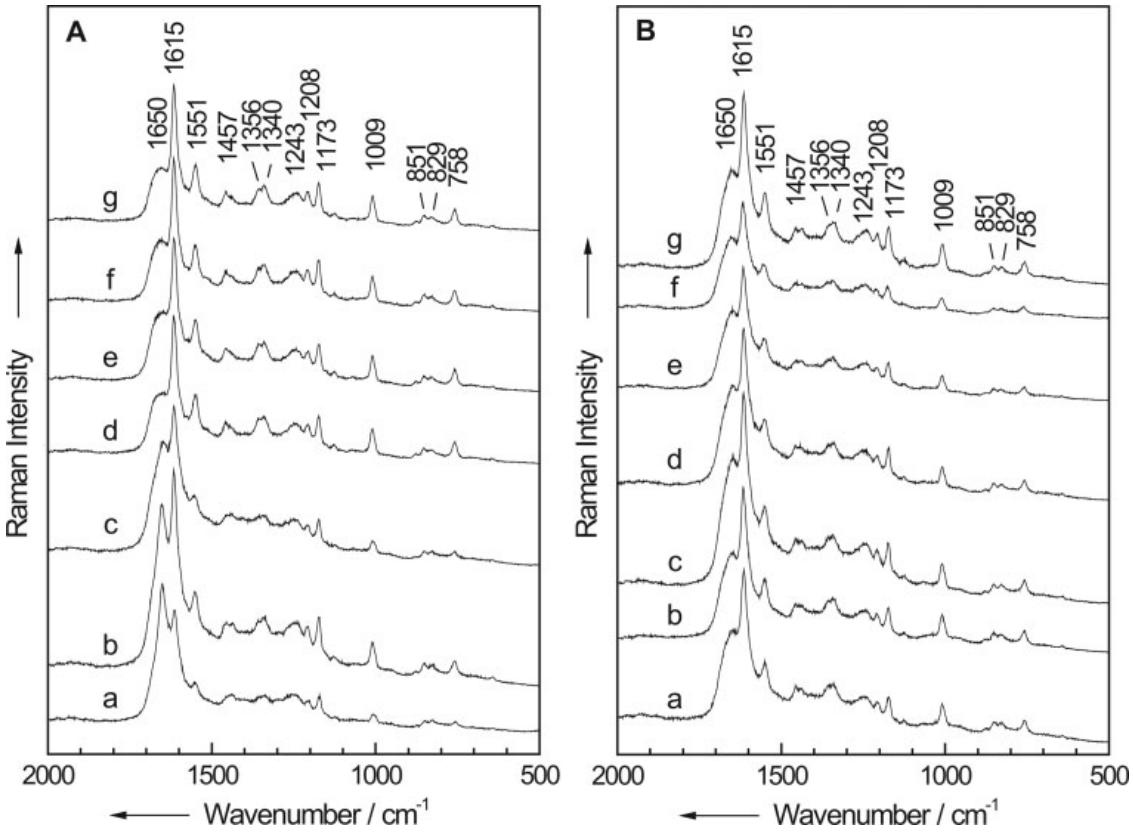

FIGURE 1 UV-resonance Raman spectra of human plasma samples from healthy donors (A) and patients with thrombotic microangiopathy (B).

equipped with a 2400 groove mm^{-1} grating and a cryogenically cooled CCD detector. An intracavity frequency doubled argon ion laser (Innova 300, FReD, Coherent, Dieburg, Germany) provided the 243.993 nm continuous wave laser lines. Approximately 1 mW was delivered to the sample. The wavenumber accuracy of the HR800 spectrometer is 4 cm^{-1}. Incident light on the sample and 180° backscattered light was collected by a broadband antireflection–coated UV microspot objective (LMU UVB, 40×/0.50) with a working distance of 1 mm. Photochemical decomposition was limited by rotating the blood plasma samples at 6 rpm on a turning knob, whereby the turning knob was moved in the *xy*-direction after each turn. A video camera, which is sensitive in the UV and the visible spectral range, was used for positioning of the samples under the microscope. The spectrometer's entrance hole was set to 300 μm. An accumulation time of 100–240 s was chosen for each spectrum.

Chemotaxonomic Analysis

An unsupervised classification method, the hierarchical cluster analysis, was applied to differentiate between cryoprecipitated plasma samples of healthy controls and patients with TMA, which was performed by the use of the program OPUS IDENT from Bruker (Ettlingen, Germany).

RESULTS AND DISCUSSION

In Figure 1, various UV-resonance Raman spectra of plasma samples of healthy donors (A) and patients with thrombotic microangiopathy (B) are represented, illustrating considerable variations in the absolute and relative intensities of the bands of 1551, 1615, and 1650 cm^{-1} between patients with TMA and healthy donors. Differences of the absolute intensities are due to the inhomogeneous distribution and variations in thickness resulting from surface tension across the plasma spot. Variation in the background intensities can be attributed to mild pyrolysis of the sample despite moving the sample during measurement. Figure 2 illustrates the influence of photochemical degradation of the plasma samples during measurement with an accumulation time of 2 min. When the sample was rotated and moved in the *xy*-direction after each turn during spectrum recording, the best resolution of the spectrum was demonstrated compared with that obtained when the sample was rotated and not moved in the *xy*-direction (Figure 2b) and when the sample was measured by keeping the laser beam

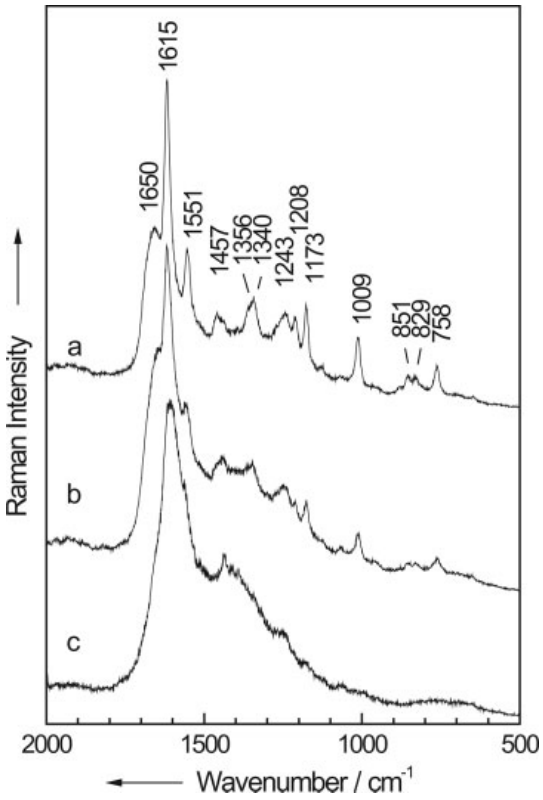

FIGURE 2 UV-resonance Raman spectra of human plasma samples of healthy donors. During measurement with an accumulation time of 2 min, the sample was rotated and moved in the *xy*-direction after each turn (a), the sample was rotated and not moved in the *xy*-direction (b), and the sample was measured by keeping the laser beam position fixed on the sample (c).

position fixed on the sample (Figure 2c). Therefore the samples were rotated and moved during measurement to minimize the photochemical decomposition of the plasma samples.

Additionally, there is a significant change in the relative intensities of the two principal bands at 1615 and 1650 cm^{-1} for healthy donors. Most of the samples show an increased intensity at 1615 cm^{-1} compared with the signal at 1650 cm^{-1}. The signal at 1551 cm^{-1} is due to vibrations of tryptophan and the amide II vibration. The amide II vibration reflects the N–H bending coupled with the C–N stretching mode. The signal at 1615 cm^{-1} can be attributed to in-plane ring stretching vibrations of aromatic amino acids. The band at 1650 cm^{-1} can be assigned to the amide I vibration, the C–O stretching, and N–H in-plane bending vibration, and the amino acid phenylalanine. The amide III mode is located at 1243 cm^{-1} and results from the N–H and C–C_α vibration.

To characterize cryoprecipitated human plasma and to elucidate the differences of the relative intensity of the bands at 1615 and 1650 cm^{-1} for healthy controls, different plasma components such as high-abundance proteins were investigated. Figure 3A represents UV-resonance Raman spectra of a plasma sample of a healthy donor (a) opposed to clotting factor VIII (b), ultralarge VWF multimers (c), proteolyzed VWF (d), fibrinogen (e), and glucose (f). Glucose exhibits various bands. The two prominent bands at 1334 and 1124 cm^{-1} can contribute slightly to the plasma spectrum. The spectrum of fibrinogen (e) reveals nearly the same bands as a plasma sample, featuring some differences in the relative intensities of the three bands at 1551, 1615, and 1650 cm^{-1}. Furthermore proteolyzed VWF fragments (d) that give an intense band at 1009 cm^{-1} and some small signals at 1176, 1543, 1580, 1616, and 1650 cm^{-1} were analyzed. Ultralarge VWF multimers (c) were investigated that are present in a complex with factor VIII in patients' plasma samples. This spectrum looks also similar to that of the plasma sample, although the bands are less intense. The spectrum of clotting factor VIII (b) shows two prominent bands at 874 and 1446 cm^{-1} and various weaker peaks at 1145, 1250, 1320, 1366, 1567, and 1567 cm^{-1}.

In Figure 3B, UV-resonance Raman spectra of blood plasma of a healthy donor (a), PBS (b), tryptophan (c), tyrosine (d), and phenylalanine (e) are illustrated. The plasma samples were resolubilized in PBS, hence PBS was measured to exclude distortion arising from the buffer. The spectrum of PBS (b) shows an intense signal at 960 cm^{-1} and some small bands at 860, 1092, and 1134 cm^{-1}. These bands are not detectable in the human plasma spectrum, excluding an attributable role of PBS in the assay system. Since using UV-resonance Raman spectroscopy signals from aromatic amino acids are discriminatory enhanced, three important amino acids, tryptophan, tyrosine, and phenylalanine, were analyzed. Tryptophan (c) exhibits characteristic bands at 758 and 1009 cm^{-1} due to symmetric benzene/pyrrole in-phase and out-of-phase breathing modes. The signals at 1340 and 1356 cm^{-1} can be attributed to the vibration resulting from the fermi resonance between the N_1–C_8 stretching in the pyrrole ring and combination bands of the out-of-plane bending. The signal of the C–C stretching vibration of the pyrrole ring is located at 1551 cm^{-1}. The C=C stretching mode of all aromatic acids gives a band at 1615 cm^{-1}.[14–16] The symmetric ring stretching mode of tyrosine (d) is located with an intense band at 829 cm^{-1} connected with a shoulder at 851 cm^{-1}. The signal at 1173 cm^{-1} can be assigned to the in-plane C–H bending vibration. The band at

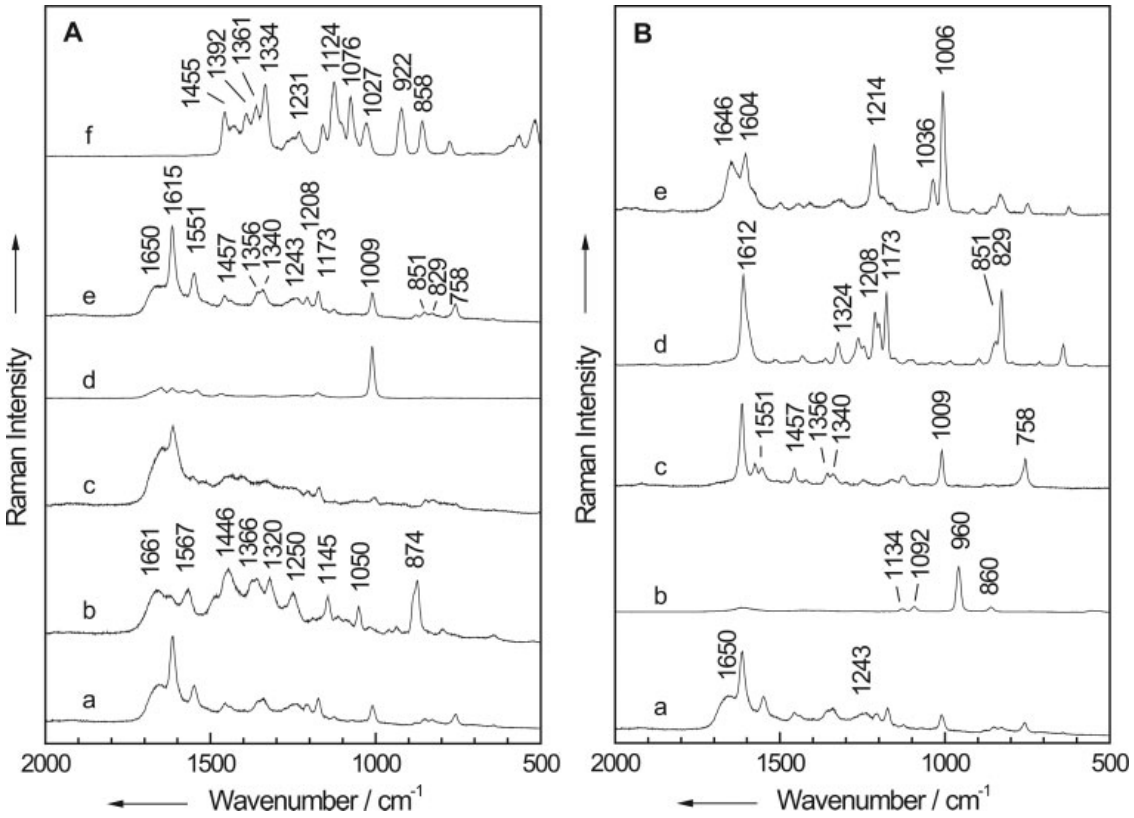

FIGURE 3 (A) UV-resonance Raman spectra of a human plasma sample from a healthy donor (a), recombinant factor VIII (b), ultralarge VWF multimers (c), proteolyzed VWF fragments (d), fibrinogen (e), and glucose (f). (B) UV-resonance Raman spectra of blood plasma from a healthy donor (a), PBS (b), tryptophan (c), tyrosine (d), and phenylalanine (e).

1208 cm^{-1} can be attributed to the ring C–C_β stretching mode of tyrosine and phenylalanine (e). The signal of tyrosine at 1615 and of phenylalanine at 1604 cm^{-1} is due to the in-plane ring stretching vibration. An additional band of phenylalanine is seen for the ring breathing mode at 1006 cm^{-1}. Comparing the signals of plasma components with those of cryoprecipitated human plasma, the most common peaks arise from the amino acids tryptophan, tyrosine, and phenylalanine.

Some plasma samples differed in intensity of yellowness. This effect could be caused by different endogenous dyes. Therefore β-carotene was studied because it is often responsible for pigmentation in biological samples such as human plasma. Furthermore whole blood was measured to investigate whether these variations were caused by other components of whole blood, such as cellular components. The dye hemoglobin from erythrocytes and its degradation product bilirubin were also investigated. Figure 4A illustrates UV-resonance Raman spectra of a human plasma sample of a healthy donor (a), whole blood (b), β-carotene (c), hemoglobin (d), and bilirubin (e). The spectra of whole blood, hemoglobin, and bilirubin do not reflect an increased band at 1650 cm^{-1} as seen in some plasma samples. These components show an intense band at 1615 cm^{-1}. Hence these variations of the relative intensities between the 1615 and 1650 cm^{-1} peaks do not occur because of the availability of some different blood components in the plasma sample. β-Carotene shows one dominant broad band at 1640 cm^{-1} (c). This signal does not occur at the spectrum of human plasma. Thus β-carotene does not contribute decisively to the human plasma spectra; it only contributed to the peak at 1650 cm^{-1} with a slight shoulder.

In addition to the various dyes, high-density lipoprotein from human plasma as a lead structure for human lipoproteins was investigated to clarify the differences in the relative intensities between the 1615

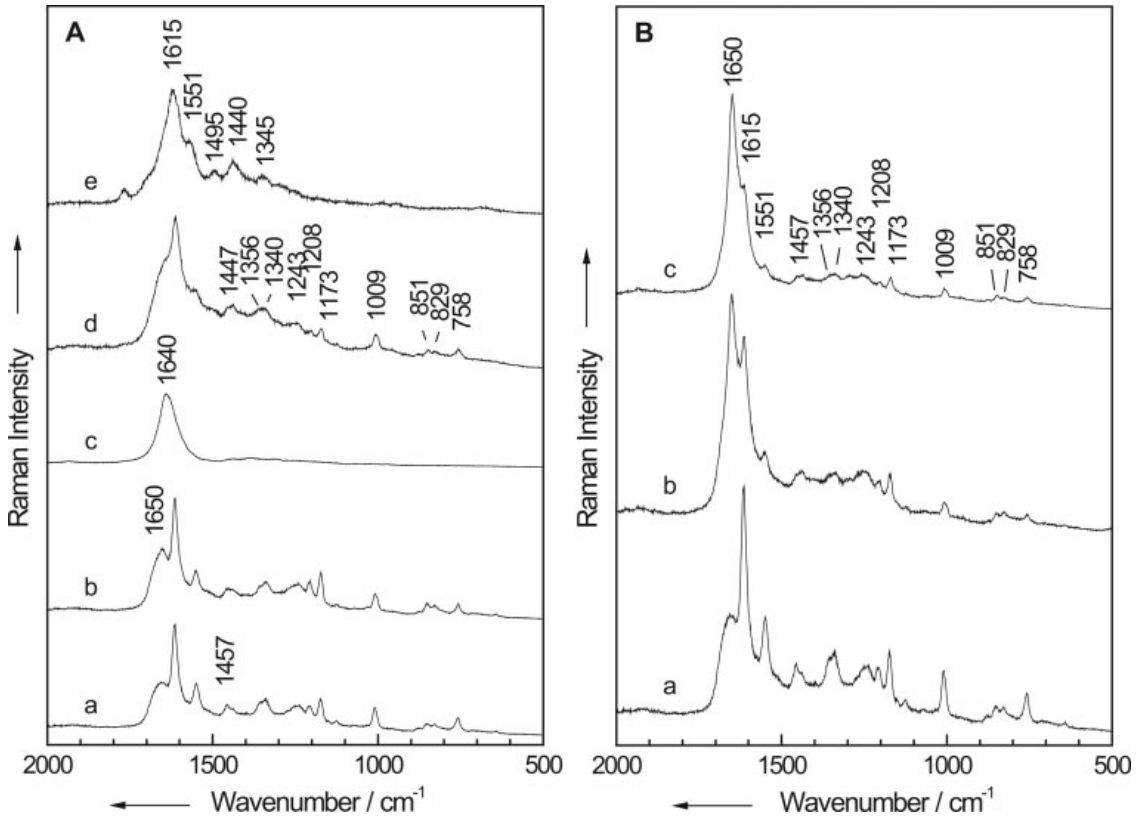

FIGURE 4 (A) UV-resonance Raman spectra of a human plasma sample from a healthy donor (a), whole blood (b), β-carotene (c), hemoglobin (d), and bilirubin (e). (B) UV-resonance Raman spectra of blood plasma from a healthy donor showing an increased intensity at 1615 cm^{-1} compared with the signal of 1650 cm^{-1} (a), human plasma samples from a healthy donor showing an decreased intensity at 1615 cm^{-1} relative to the signal of 1650 cm^{-1} (b), and high-density lipoprotein from human plasma (c).

and 1650 cm^{-1} peaks. In Figure 4B, UV-resonance Raman spectra of blood plasma of a healthy donor showing increased intensity at 1615 cm^{-1} compared with the signal at 1650 cm^{-1} (a), a human plasma sample of a healthy donor showing decreased intensity at 1615 cm^{-1} relative to the signal at 1650 cm^{-1} (b), and lipoprotein (c) are represented. Lipoproteins exhibit an increased intensity at 1650 cm^{-1} compared with the signal at 1615 cm^{-1}. Therefore the plasma samples with the raised band at 1650 cm^{-1} offer a high content of lipoproteins. Normally lipids should not be present with high concentrations in the cryoprecipitated plasma. Plasma sample spectra with an absence of the increased band at 1650 cm^{-1} may serve as a method for quality control of sample preparation.

To classify the analyzed plasma samples of healthy donors and patients with thrombotic microangiopathy, an unsupervised classification method, the hierarchical cluster analysis, was performed. Only spectra without an increased peak at 1650 cm^{-1} were used for classification. The spectra were pretreated by vector normalization and the spectral range between 600 and 1800 cm^{-1} was chosen for classification. The spectral distances between each spectrum were calculated with the standard method. Ward's technique was used to calculate the spectral distances between a newly created cluster and all of the other spectra or identified clusters. Figure 5 shows the dendrogram of the resultant classification of the cryoprecipitated plasma samples based on 175 spectra of 8 healthy controls and 10 different patients' samples. The smaller the spectral distances in the dendrogram the more similar are the spectra. The dendrogram shows a clear separation of healthy controls and patients; however the spectrum of one healthy control was falsely classified to the patients' cluster for unknown reasons. This spectrum is indicated in the figure by an asterisk.

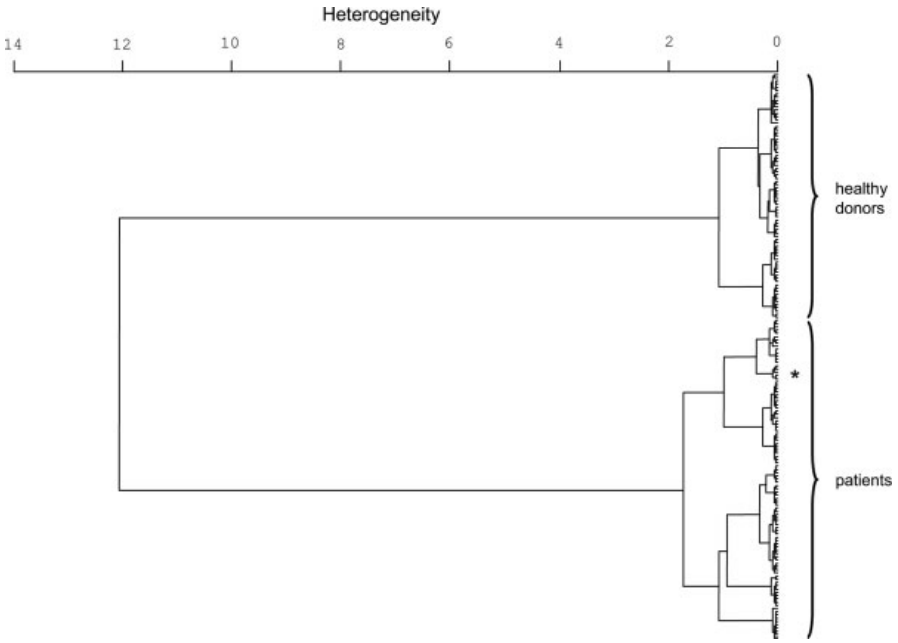

FIGURE 5 Dendrogram resulting from hierarchical cluster analysis of plasma sample spectra from healthy controls and patients with thrombotic microangiopathy based on the spectral range of 600–1800 cm^{-1}. The asterisk indicates one misclassified spectrum of a healthy donor as a patient.

CONCLUSION

This study demonstrates that UV-resonance Raman spectroscopy is a valuable tool for the investigation of human plasma samples and its components without complex and laborious preanalytical procedures because signals from proteins are selectively enhanced using an excitation wavelength in the UV. With this methodological approach the components contributing to the major signals in human plasma were identified as aromatic amino acids, particularly as tryptophan, tyrosine, and phenylalanine. Additional bands can be attributed to amide I, II, and III vibrations. This study demonstrates that the differences of the intensity ratio of the bands at 1615 and 1650 cm^{-1} for patients with thrombotic microangiopathy are not caused by components of whole blood in the plasma sample or endogenous dyes such as β-carotene, hemoglobin, or bilirubin, however, they could be attributed to lipoproteins. Plasma samples with the raised band at 1650 cm^{-1} offer a high content of lipoproteins. Hence spectra of plasma samples with an absence of the increased band at 1650 cm^{-1} may serve as a method for quality control of sample preparation.

The hierarchical cluster analysis demonstrates the possibility for differentiation of cryoprecipitated plasma samples of healthy controls and patients with thrombotic microangiopathy. Therefore the present UV-Raman spectroscopic approach provides the potential not only for the characterization but also for the rapid and early discrimination of human plasma of healthy donors and patients with thrombotic microangiopathy by means of different statistical data algorithms for classification of unknown samples and correlation with electrophoretic methods.

We gratefully acknowledge the funding of the research project FKZ 13N8369 within the framework "Biophotonic" from the Federal Ministry of Education and Research, Germany (BMBF). Human recombinant VWF protein was a generous gift of Prof. Schneppenheim, UKJ Hamburg. Tutorials for electrophoretical separation of VWF multimers by Prof. U. Budde, Labor Arndt & Partner, Hamburg, Germany are gratefully acknowledged.

REFERENCES

1. Remuzzi, G.; Ruggenenti, P.; Bertani, T. In Renal Pathology: with Clinical and Functional Correlations; Brenner, B. M., Ed.; JB Lippincott Company: Philadelphia, 1994; p. 1154.
2. Arya, M.; Anvari, B.; Romo, G. M.; Cruz, M. A.; Dong, J.-F.; McIntire, L. V.; Moake, J. L.; Lopez, J. A. Blood 2002, 99, 3971–3977.

3. Ono, T.; Mimuro, J.; Madoiwa, S.; Soejima, K.; Kashiwakura, Y.; Ishiwata, A.; Takano, K.; Ohmori, T.; Sakata, Y. Blood 2006, 107, 528–534.
4. Mannucci, P. M.; Parolari, A.; Canciani, M. T.; Alemanni, F.; Camera, M. J Thromb Haemostasis 2005, 3, 397–399.
5. Mannucci, P. M.; Canciani, M. T.; Forza, I.; Lussana, F.; Lattuada, A.; Rossi, E. Blood 2001, 98, 2730–2735.
6. Reiter, R. A.; Varadi, K.; Turecek, P. L.; Jilma, B.; Knoebl, P. Thromb Haemostasis 2005, 93, 554–558.
7. Studt, J. D.; Budde, U.; Schneppenheim, R.; Eisert, R.; von Depka Prondzinski, M.; Ganser, A.; Barthels, M. Am J Clin Pathol 2001, 116, 567–574.
8. Petibois, C.; Cazorla, G.; Cassaigne, A.; Deleris, G. Appl Spectrosc 2002, 56, 1259–1267.
9. Heise, H. M.; Marbach, R.; Koschinsky, T.; Gries, F. A. Appl Spectrosc 1994, 48, 85–95.
10. Berger, A. J.; Koo, T.-W.; Itzkan, I.; Horowitz, G.; Feld, M. S. Appl Optics 1999, 38, 2916–2926.
11. Rohleder, D.; Kiefer, W.; Petrich, W. Analyst (Cambridge, UK) 2004, 129, 906–911.
12. Rohleder, D.; Kocherscheidt, G.; Gerber, K.; Kiefer, W.; Kohler, W.; Mocks, J.; Petrich, W. J Biomed Optics 2005, 10, 031108/031101–031108/031110.
13. Qu, J. Y.; Wilson, B. C.; Suria, D. Appl Optics 1999, 38, 5491–5498.
14. Clarkson, J.; Smith, D. A. FEBS Lett 2001, 503, 30–34.
15. Kitagawa, T.; Hirota, S. In Handbook of Vibrational Spectroscopy: Applications in Life, Pharmaceutical and Natural Sciences; Chalmers, J. M.; Griffiths, P. R., Eds.; John Wiley & Sons: Chichester, 2002; pp. 3426–3446.
16. Asher, S. A.; Ludwig, M.; Johnson, C. R. J Am Chem Soc 1986, 108, 3186–3197.
17. Rock, G.; Berger, R.; Lange, J.; Tokessy, M.; Palmer, D. S.; Giulivi, A. Transfusion 2001, 41, 232–235.
18. Hoffman, M.; Jenner, P. Am J Clin Pathol 1990, 93, 694–697.
19. Gerritsen, H. E.; Turecek, P. L.; Schwarz, H. P.; Lammle, B.; Furlan, M. Thromb Haemostasis 1999, 82, 1386–1389.
20. Schneppenheim, R.; Budde, U.; Oyen, F.; Angerhaus, D.; Aumann, V.; Drewke, E.; Hassenpflug, W.; Haberle, J.; Kentouche, K.; Kohne, E.; Kurnik, K.; Mueller-Wiefel, D.; Obser, T.; Santer, R.; Sykora, K.-W. Blood 2003, 101, 1845–1850.

Reviewing Editor: Ronald Hester

2.9 UV-resonance Raman spectroscopic investigation of human plasma for medical diagnosis. [MH9]

M. Harz, C. L. Bockmeyer, P. Rösch, R. A. Claus, J. Popp

Medical Laser Application **2007**, 22, 87-93.

Available online at www.sciencedirect.com
ScienceDirect
Medical Laser Application 22 (2007) 87–93
Medical Laser Application
www.elsevier.de/mla

UV-Resonance Raman spectroscopic investigation of human plasma for medical diagnosis

Michaela Harz[a], Clemens L. Bockmeyer[b], Petra Rösch[a], Ralf A. Claus[b], Jürgen Popp[a,c,*]

[a]*Institute of Physical Chemistry, Friedrich-Schiller-Universität Jena, Helmholtzweg 4, D-07743 Jena, Germany*
[b]*Department for Anesthesiology and Intensive Care Medicine, Friedrich-Schiller-Universität Jena, Erlanger Allee 101, D-07747 Jena, Germany*
[c]*Institute of Photonic Technology, Albert-Einstein-Straße 9, D-07745 Jena, Germany*

Received 15 May 2007; accepted 15 June 2007

Abstract

An analysis of plasma proteins, in particular the precise determination of its concentration or activity as well as in general the molecular composition of the sample is of relevance for the diagnosis of inflammation-associated coagulopathies. Recently, the evaluation of the fine tuned balance between the multimeric acute phase protein "Von-Willebrand Factor (VWF)" and its inactivating enzyme was spotlighted by several observational studies. However, current diagnostic approaches of the multimer composition of Von-Willebrand Factor are based on electrophoretic separation and immunoblotting requiring a time schedule up to several days. In this study UV-resonance Raman (UVRR) spectroscopy was applied, as a promising approach for a more rapid methodology since this technique allows to exclusively monitor protein vibrations. Hence, we provide UV-resonance Raman spectroscopy with multivariate evaluation for a real-time diagnosis and therapeutically monitoring of inflammation-associated coagulatopathy subsequent to the presence of highly active Von-Willebrand Factor multimers in patients' plasma.

Keywords: Human plasma; UV-resonance Raman spectroscopy (UVRR); Classification; Multivariate analysis

Introduction

Microangiopathy is typified by thrombocytopenia, organ failure and hemolytic anemia [1]. Thrombotic microangiopathy (TMA) is characterized by an increased blood coagulation in small arterioles and capillaries. Dysfunction of the endothelium is induced by systemic infection or by endogenous or exogenous stress mediators (e.g. by injury of the endothelium). It results in the generation of thrombotic aggregates resulting in vascular plaque formation, impairment of blood flow and vascular occulsion. During agglutination thrombi in the microcirculation are mainly composed of aggregated platelets with small amounts of fibrin and huge amounts of Von-Willebrand Factor (VWF). VWF is an adhesive and multimeric plasma glycoprotein essential for platelet adhesion and thrombus formation during hemostasis. The protein is synthesized in endothelial cells and megakaryocytes circulating in plasma as multimers up to 20,000 kDa in size. Since

*Corresponding author. Tel.: +49 3641 948320; Fax: +49 3641 948302.
E-mail address: juergen.popp@uni-jena.de (J. Popp).

1615-1615/$ - see front matter © 2007 Elsevier GmbH. All rights reserved.
doi:10.1016/j.mla.2007.06.001

VWF mediates the adhesion of platelets among each other and to the subendothelium its agglutinative properties are a critical function of its size, since the larger the molecule, the more active it is in promoting platelet adhesion or spontaneous aggregation resulting in a thrombophilic state [2]. The proteolytic activity of the protease ADAMTS-13 (A Disintegrin-like And Metalloprotease with ThromboSpondin type 1 motif, member 13) results in the limited degradation of the VWF. However, e.g. in patients with severe infections, disseminated intravascular coagulation or the catastrophic antiphospholipid antibody syndrome a decreased activity of ADAMTS-13, severe thrombocytopenia and an elevated thrombotic microangiopathies (TMA) ratio could be observed [3–5]. Diminished ADAMTS-13 activity results in the appearance and accumulation of ultralarge VWF multimers in plasma [6]. At present, these unusually large VWF multimers in plasma are identified by electrophoresis [7]. However this diagnostic tool suffers various disadvantages such as time consuming analysis as well as insufficient reproducibility and comparability between laboratories making it unfeasible for real-time diagnosis and therapeutical monitoring. For an earlier therapy initiation and the possibility of therapeutical monitoring, faster analytical techniques are needed. As a promising approach Fourier Transform infrared spectroscopy (FT-IR) [8,9] and UV-resonance Raman (UVRR) spectroscopy [10] can be applied. UVRR spectroscopy offers a potentially useful probe of plasma analysis, via resonance enhancement of vibrational signals from macromolecules, like aromatic amino acids and proteins [11–13].

Blood contains plasma (55%) and corpuscular components (45%) such as erythrocytes, leucocytes and platelets. Plasma consists of about 90% water and 8% proteins and further components such as salts, carbohydrates and fats. Because the content of plasma proteins of immuno globulins and albumine does not change during TMA these proteins were discarded by preparing cryoprecipitates. Cryoprecipitates mainly consists of the proteins fibrinogen (factor I), factor VIII and VWF as a VWF-factor VIII-complex as well as of glucose. [14,15].

In this study UV-resonance Raman spectroscopy was applied for the characterization of human plasma samples of healthy donors and patients with thrombotic microangiopathy of different origin. Additionally plasma components of cryoprecipitates such as proteins (factor VIII, ultralarge VWF, VWF-factor VIII-complex and fibrinogen), aromatic amino acids tryptophan, tyrosine and phenylalanine, glucose, as well as endogenous dyes (hemoglobin and bilirubin) and lipoproteins were investigated to elucidate the plasma composition and differences in plasma spectra of healthy donors and patients. Due to the complexity of the spectra multivariate evaluation was applied for the classification of plasma samples of healthy donors and patients.

Material and methods

Preanalytical sample preparation

Upon approval of the local ethical committee, 200 µl citrated plasma from healthy controls as well as from patients with thrombotic microangiopathy of different origin diagnosed by a residual proteolytic activity of ADAMTS13 < 20% as determined by the method of Gerritsen [16] were cryoprecipitated by thawing on ice for 45 min after freezing at −80°C for about 6 h. Afterwards the samples were centrifugated at 15,000 x g for 30 min at 4 °C. The supernatant was discarded and the cryoprecipitated pellet resolubilized in a total volume of 200 µl phosphate buffered saline (PBS) solution. For UV-Raman analysis, the cryoprecipitated protein mixture was spotted onto fused silica plates and dried in vacuo.

The plasma components were purchased from Sigma-Aldrich (Taufkirchen, Germany). Recombinant factor VIII was purchased from Baxter (Vienna). The substances were diluted in water or PBS in appropriate concentrations and spotted onto fused silica plates and dried in vacuo. For comparison of VWF multimers differing in length and thrombophilic activity, two different VWF specimens were used: (i) ultralarge VWF was obtained from recombinant protein synthesis [17], (ii) low molecular weight VWF was obtained by limited proteolysis of *rh*VWF by ADAMTS13 at mild denaturating conditions (1.5 M urea) in the presence of Ba^{++} over 2 hrs. as described previously [14].

Spectroscopic instrumentation

UVRR spectra were collected using a micro-Raman setup (HR800, Horiba/Jobin Yvon) with a focal length of 800 mm, a 40x broadband anti-reflection coated UV objective (LMU UVB) with a numerical aperture of 0.5 and a 2400 lines/mm grating. The entrance slit was set to 300 µm. A video camera, which is sensitive in the UV and in the visible spectral range, was used for positioning of the samples under the microscope. An excitation wavelength of 244 nm is applied, provided by a frequency doubled argon ion laser (Innova 300, MotoFReD, Coherent, Dieburg, Germany). Approximately 1 mW was delivered to the sample. The wavenumber resolution of the HR800 spectrometer is 4 cm^{-1}. Raman scattered light was detected by a nitrogen-cooled CCD camera with an accumulation time set to 100–240 s for each spectrum.

To minimize possible photo degradation, plasma samples were rotated at 6 rpm on a turning knob, moving it in x,y-direction after each rotation.

Chemotaxonomic analysis

Differentiation between cryoprecipitated plasma samples of healthy controls and patients with TMA was performed with unsupervised classification methods the hierarchical cluster analysis (HCA) and the principal component analysis (PCA). HCA analysis was done with the program "Opus Ident 3.1" (Bruker Optics, Ettlingen, Germany) and PCA analysis with "The Unscrambler®" from CAMO Process AS; Version 9.2, Reutlingen, Germany).

Results and discussion

In Fig. 1, representative UV-resonance Raman spectra of plasma samples of healthy donors (A) and patients with thrombotic microangiopathy (B) are depicted, illustrating considerable variations in the absolute and relative intensities of the bands at 1551 cm^{-1}, 1615 cm^{-1} and 1650 cm^{-1} between patients with TMA and healthy donors. Differences in the absolute intensities are due to the inhomogeneous distribution and variations in thickness resulted by surface tension across the plasma spot. Most of the samples show an increased intensity at 1615 cm^{-1} compared to the signal at 1650 cm^{-1}. The signal at 1551 cm^{-1} is due to vibrations of tryptophan. The signal at 1615 cm^{-1} can be attributed to in-plane ring stretching vibrations of aromatic amino acids. The band at 1650 cm^{-1} can be assigned to the amide I vibration, the C = O stretching and N-H in plane bending vibration, as well as to the amino acid phenylalanine. The amide III mode is located at 1243 cm^{-1} and results from the N-H and C-C_α vibration.

For plasma characterization several plasma components such as high abundant proteins, aromatic amino acids, lipoproteins and endogenous dyes were investigated. In Fig. 2A UV-resonance Raman spectra of a human plasma sample of a healthy donor (a), recombinant factor VIII (b), ultralarge VWF multimers (c), proteolyzed VWF fragments (d), fibrinogen (e) and VWF-factor VIII-complex (f) are illustrated. The plasma Raman spectrum is in best agreement with the spectrum of fibrinogen (e). VWF-factor VIII-complex was investigated too since VWF is linked to the clotting factor VIII to form a complex to ensure proteolytical protection of factor VIII. The spectrum of VWF-factor VIII-complex (f) reveals the same Raman bands of the plasma sample, except of the peaks at 893 cm^{-1}, 1322 cm^{-1}, 1409 cm^{-1} and 1493 cm^{-1} that are absent in the plasma spectrum. Proteolyzed VWF fragments (d) give only one intense Raman band at 1009 cm^{-1}. The Raman spectrum of ultralarge VWF multimers (c) appears also similar to the ones of the plasma sample,

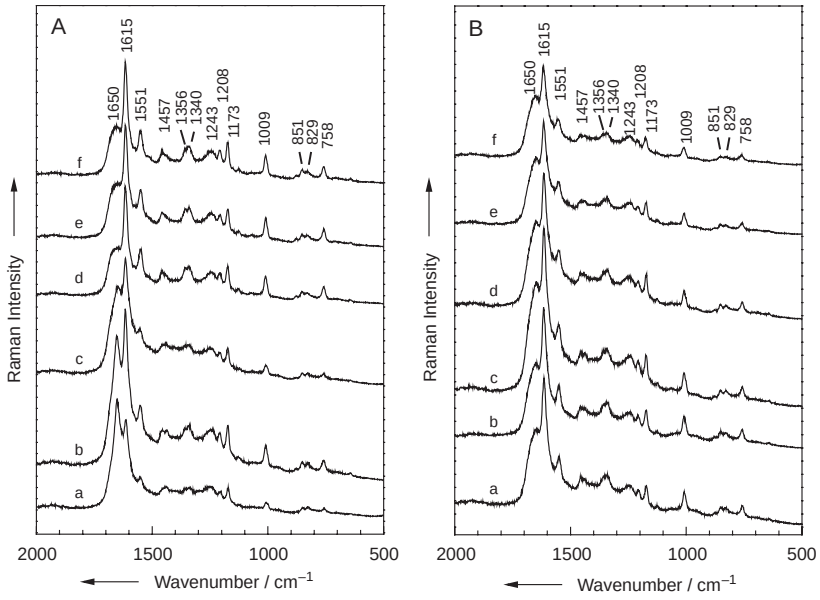

Fig. 1. UV-resonance Raman spectra of human plasma samples of healthy donors (A) and patients with thrombotic microangiopathy (B).

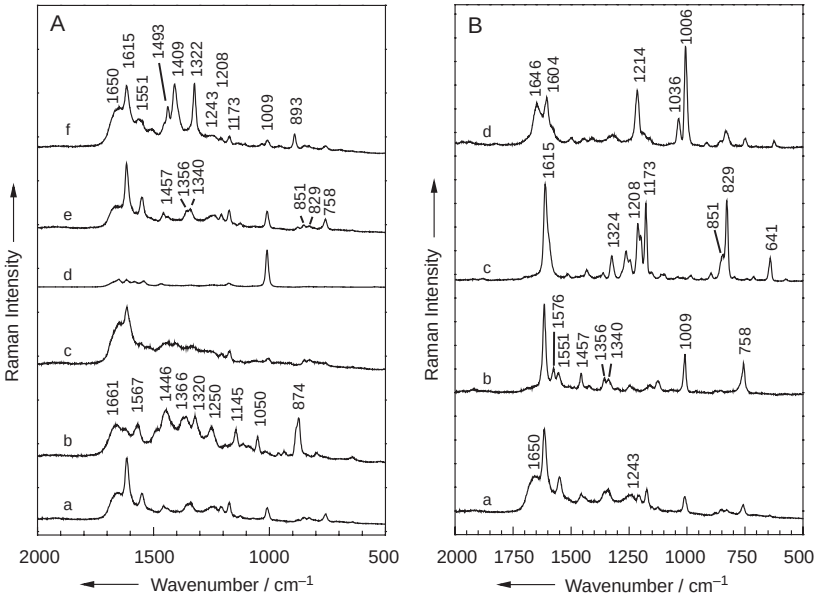

Fig. 2. A: UV-resonance Raman spectra of a human plasma sample of a healthy donor (a), recombinant factor VIII (b), ultralarge VWF multimers (c), proteolyzed VWF fragments (d), fibrinogen (e) and VWF-factor VIII-complex (f). B: UV resonance Raman spectra of blood plasma of a healthy donor (a), tryptophan (b), tyrosine (c) and phenylalanine (d).

although the bands are less intense. The Raman spectrum of the clotting factor VIII (b) shows two prominent bands at 874 cm^{-1} and 1446 cm^{-1} and various weaker peaks at 1145 cm^{-1}, 1250 cm^{-1}, 1320 cm^{-1}, 1366 cm^{-1}, 1567 cm^{-1} and 1567 cm^{-1}.

Comparing the UVRR signals of plasma components with those of cryoprecipitated human plasma reveals that the most common peaks arise from the amino acids tryptophan, tyrosine and phenylalanine due to the selective enhancement of macromolecules for deep UV Raman excitaion. Fig. 2B depicts UV-resonance Raman spectra of blood plasma from a healthy donor (a) compared to aromatic amino acids Raman spectra of tryptophan (b), tyrosine (c) and phenylalanine (d). The in-plane C = C ring stretching mode of all aromatic acids gives rise to a band at 1615 cm^{-1} (W1, Y8a) [14–16].

Tryptophan (b) exhibits characteristic bands at 758 cm^{-1} (W18) and 1009 cm^{-1} (W16) due to symmetric benzene/pyrrole in-phase and out of phase breathing modes. The 1340 cm^{-1} and 1356 cm^{-1} doublet (W7) can be attributed to the vibration resulting from the Fermi resonance between the N_1-C_8 stretching in the pyrrole ring and combination bands of the out-of-plane bending. The signal of the C-C stretching vibration of the pyrrole ring can be found at 1551 cm^{-1} (W3). The band at 1576 cm^{-1} (W2) is due to in-plane pyrrole ring vibrations. Tyrosine (c) gives rise to a band at 641 cm^{-1} that can be attributed to the ν_{6b} ring deformation. The peaks of tyrosine at 829 cm^{-1} (2Y16a) and 851 cm^{-1} (Y1) are caused by Fermi resonance between the ν_1 symmetric ring stretching fundamental and the first overtone of the out-of-plane ν_{16a} ring deformation. The in-plane C-H bending vibration involves a signal at 1173 cm^{-1} (Y9a). The signal of the ring C-C_β stretching mode of tyrosine (Y7a) and phenylalanine (d) (F7a) is located at 1208 cm^{-1}. The signal of phenylalanine at 1604 cm^{-1} derives from the in-plane ring stretching vibration (F8a). An additional band of phenylalanine is seen for the ring breathing mode at 1006 cm^{-1} (F1) as well as for in-plane C-H bending vibration at 1036 cm^{-1} (F18a).

To emphasize the differences in the relative intensities between the Raman bands at 1615 and 1650 cm^{-1} several endogenous dyes such as bilirubin and hemoglobine as well as a lead structure for human lipoproteins the high density lipoprotein from human plasma were investigated. In Fig. 3 the corresponding UV-resonance Raman spectra of blood plasma from a healthy donor showing an increased intensity at 1615 cm^{-1} compared to the signal of 1650 cm^{-1} (a), a human plasma sample of a healthy donor showing an decreased intensity at 1615 cm^{-1} relative to the signal of 1650 cm^{-1} (b), lipoprotein (c) as well as hemoglobin (d) and bilirubin (e) are represented. Only lipoproteins exhibit an increased intensity at 1650 cm^{-1} compared to the signal

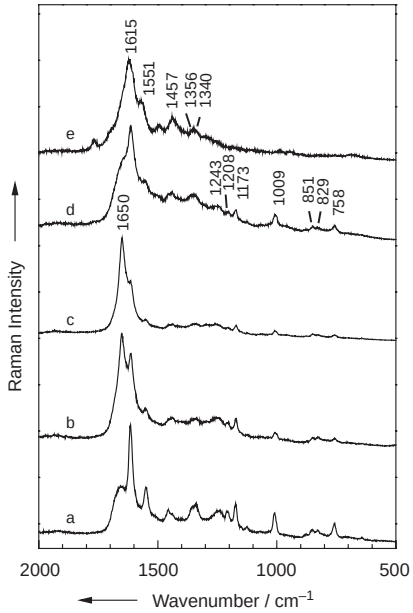

Fig. 3. UV-resonance Raman spectra of blood plasma of a healthy donor showing an increased intensity at 1615 cm^{-1} compared to the signal of 1650 cm^{-1} (a), of a human plasma samples of a healthy donor showing an decreased intensity at 1615 cm^{-1} relative to the signal of 1650 cm^{-1} (b), high density lipoprotein from human plasma (c) as well as endogenous dyes hemoglobin (d) and bilirubin (e).

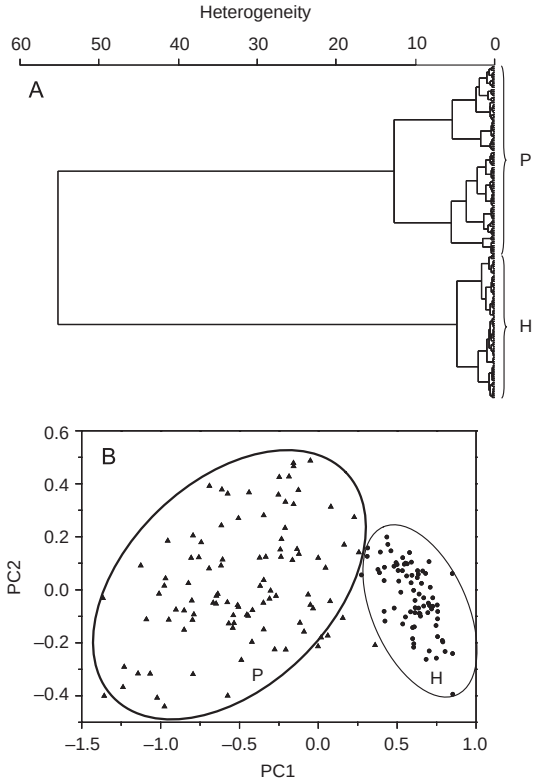

Fig. 4. A: Dendrogram resulting from hierarchical cluster analysis of the first derivative of plasma sample spectra of healthy controls (H) and patients with thrombotic microangiopathy (P) based on the spectral range of 600 – 1800 cm^{-1}. B: PCA scores plot of the first and second principal component PC1 and PC2 for the first derivative of the spectra of human plasma samples of healthy donors (H) and patients with TMA (P).

at 1615 cm^{-1}. Therefore the plasma samples with the enhanced band at 1650 cm^{-1} offer a high content of lipoproteins. Normally cryoprecipitated plasma should not contain lipids with high concentrations. So with resonance Raman spectroscopy it is possible to detect preparation failure.

In order to classify the analyzed plasma samples of healthy donors and patients with thrombotic microangiopathy HCA and PCA were performed. Only spectra showing no enhanced peak at 1650 cm^{-1} were taken for classification. Before using both chemometric analysis methods, the first derivative of the spectra (Savitzky-Golay, 9 points, polynomial order of 2) was calculated and a "Range Normalization" was carried out both with the program "The Unscrambler®" from CAMO Process AS; Version 9.2, Reutlingen, Germany). The spectral range between 600 cm^{-1} and 1800 cm^{-1} was chosen for classification.

For HCA the spectral distances between every spectrum were calculated with the Standard method. Ward's Technique was used to calculate the spectral distances between a newly created cluster and all the other spectra or identified clusters. Fig. 4A shows the results obtained by HCA for cryoprecipitated plasma samples based on 175 spectra of eight healthy controls and of ten different patients' samples. Two distinct clusters can be observed; all of the healthy controls are separated from patients' spectra as an individual cluster.

PCA is also capable of separating cryoprecipitated plasma samples of healthy volunteers and diseased persons. Fig. 4B shows the PCA scores plot of the first and second principal component PC1 and PC2 for spectra of human plasma samples of 76 healthy donors and 99 patients' samples with TMA. The plot shows that the healthy person's scores are tightly grouped and well separated from the patient's cluster, which results in a more dispersed group.

Conclusions

This study demonstrates that UV-resonance Raman spectroscopy is a suitable approach for the analysis of

human plasma samples and its components without complex and laborious pre-analytical procedures. With excitation in the UV signals from proteins are selectively enhanced. Thereby the major signals apparent in human plasma were identified as vibrations arising from the aromatic amino acids tryptophan, tyrosine and phenylalanine. Additional bands can be attributed to amide I and III vibrations. Furthermore within this study a preparation failure could be discovered for plasma samples offering an enhanced band at $1650\,cm^{-1}$ in the Raman spectrum. These samples offer a high content of lipoproteins.

The hierarchical cluster analysis as well as the principal component analysis offers the possibility for a differentiation of cryoprecipitated plasma samples of healthy controls and patients of thrombotic microangiopathy.

This study demonstrates the great potential of the UVRR spectroscopy to characterize of plasma samples. Furthermore a more effective and specific differentiation between cryoprecipitated plasma of healthy donors and patients with TMA utilizing multivariate evaluation could be achieved. Hence this method could be a prospective excellent tool for therapeutical monitoring. The aim of further investigations deals with establishing a data base for UVRR-spectroscopic data that include patients' samples with various disease states. This will be followed by classification of unknown samples and correlation with electrophoretic methods.

Acknowledgement

We gratefully acknowledge support from the Deutsche Forschungsgemeinschaft (PO 563/7-1) and IZKF Jena (TP 4.8, Thrombotic microangiopathy in sepsis'). Human recombinant VWF protein was a generous gift of Prof. Schneppenheim, UKJ Hamburg. Tutorials for electrophoretical separation of VWF multimers by Prof. U. Budde, Labor Arndt & Partner, Hamburg, are gratefully acknowledged.

Zusammenfassung

UV-Resonanz-Raman-spektroskopische Untersuchungen von Blutplasma für die medizinische Diagnose

Die Analyse von Plasmaproteinen, insbesondere die genaue Bestimmung von deren Konzentration oder Aktivität sowie allgemein die molekulare Zusammensetzung der Probe, ist für die Diagnose von entzündungs-bedingten Gerinnungsstörungen von Bedeutung. In letzter Zeit ist die Ermittlung der genau abgestimmten Balance zwischen dem multimeren Akute-Phase-Protein „Von Willebrand Faktor (VWF)" und seinem spaltenden Enzym in den Blickpunkt verschiedenster Forschungsstudien gerückt. Derzeitige Methoden zur Diagnose der Multimerzusammensetzung des Von Willebrand Faktors basieren auf elektrophoretischer Separierung und Immunoblotting, die jedoch einen Zeitplan von bis zu mehreren Tagen beanspruchen. In dieser Studie wurde die UV-Resonanz-Raman (UVRR)-Spektroskopie als ein vielversprechender Ansatz für eine schnellere Methodik angewendet, da es diese Technik erlaubt, verstärkt Proteinschwingungen zu untersuchen. Demzufolge haben wir die UV-Resonanz-Raman-Spektroskopie mit Hilfe von multivariaten Berechnungsmethoden zur Echtzeit-Diagnose und zur therapeutischen Überwachung von entzündungsbedingten Gerinnungsstörungen verwendet. Grundlage dafür ist die Anwesenheit von hoch aktiven „Von Willebrand Faktor" Multimeren ausschließlich in den Plasmaproben von Patienten.

Schlüsselwörter: Blutplasma; UV-Resonanz-Raman-Spektroskopie (UVRR); Klassifizierung; Multivariate Analyse

Resúmen

Aplicación de la Espectroscopia Raman de Resonancia UV en muestras de plasma humano para el diagnóstico médico

El análisis de las proteínas del plasma, en particular la determinación exacta de su concentración o actividad, así como la composición molecular de la muestra, es de gran importancia para la diagnóstico de las coagulopatías asociadas a inflamación. Recientemente, el análisis de la delicada regulación entre la proteína multimérica de fase aguda Factor de Von-Willebrand (VWF) y su enzima inactivante, ha sido el foco de investigación de numerosos estudios. Sin embargo, los métodos de diagnóstico actuales para la determinación de la composición multimérica del factor de Von-Willebrand requieren varios días de trabajo, ya que se basan en la separación electroforética e immunoblotting. En este trabajo introducimos la espectroscopía UVRR (*UV-Resonance Raman*) como una aproximación prometedora para una metodología más rápida, dado que permite el monitoreo exclusivo de las vibraciones de las distintas proteínas. Por consiguiente, en este estudio se utilizó la espectroscopía UVRR junto a un análisis multivariado, para el diagnóstico en tiempo real y el monitoreo terapéutico de las coagulopatías asociadas a inflamación, subsecuente a la presencia de multímeros altamente activos del Factor de Von-Willebrand en el plasma de pacientes.

Palabras clave: Plasma humano; Espectroscopía Raman de Resonancia UV (UVRR); Clasificación; Análisis multivariado

References

[1] Remuzzi G, Ruggenenti P, Bertani T. Renal pathology: with clinical and functional correlations. In: Brenner BM, Ed. Philadelphia: JB Lippincott Company; 1994. p. 1154.
[2] Arya M, Anvari B, Romo G M, Cruz MA, Dong J-F, McIntire LV, Moake JL, Lopez JA. Blood 2002;99: 3971–7.
[3] Ono T, Mimuro J, Madoiwa S, Soejima K, Kashiwakura Y, Ishiwata A, Takano K, Ohmori T, Sakata Y. Blood 2006;107:528–34.
[4] Mannucci PM, Parolari A, Canciani MT, Alemanni F, Camera M. Journal of Thrombosis and Haemostasis 2005;3:397–9.
[5] Mannucci PM, Canciani MT, Forza I, Lussana F, Lattuada A, Rossi E. Blood 2001;98:2730–5.
[6] Reiter RA, Varadi K, Turecek PL, Jilma B, Knoebl P. Thrombosis and Haemostasis 2005;93:554–8.
[7] Studt JD, Budde U, Schneppenheim R, Eisert R, von Depka Prondzinski M, Ganser A, Barthels M. American Journal of Clinical Pathology 2001;116:567–74.
[8] Petibois C, Cazorla G, Cassaigne A, Deleris G. Applied Spectroscopy 2002;56:1259–67.
[9] Heise HM, Marbach R, Koschinsky T, Gries FA. Applied Spectroscopy 1994;48:85–95.
[10] Harz M, Claus RA, Bockmeyer CL, Baum M, Roesch P, Kentouche K, Deigner HP, Popp J. Biopolymers 2006; 82:317–24.
[11] Clarkson J, Smith DA. FEBS Letters 2001;503:30–4.
[12] Kitagawa T, Hirota S. Handbook of Vibrational Spectroscopy: Applications in Life. In: Chalmers JM, Griffiths PR, editors. Pharmaceutical and Natural Sciences. Chichester: John Wiley & Sons; 2002. p. 3426–46.
[13] Asher SA, Ludwig M, Johnson CR. Journal of the American Chemical Society 1986;108:3186–97.
[14] Rock G, Berger R, Lange J, Tokessy M, Palmer DS, Giulivi A. Transfusion 2001;41:232–5.
[15] Hoffman M, Jenner P. American Journal of Clinical Pathology 1990;93:694–7.
[16] Gerritsen HE, Turecek PL, Schwarz HP, Lammle B, Furlan M. Thrombosis and Haemostasis 1999;82:1386–9.
[17] Schneppenheim R, Budde U, Oyen F, Angerhaus D, Aumann V, Drewke E, Hassenpflug W, Haberle J, Kentouche K, Kohne E, Kurnik K, Mueller-Wiefel D, Obser T, Santer R, Sykora K-W. Blood 2003;101: 1845–50.

2.10 Minimal invasive gender determination of birds by means of UV-resonance Raman spectroscopy. [MH10]

M. Harz, M. Krause, T. Bartels, K. Cramer, P. Rösch, J. Popp

Analytical Chemistry **2008**, 80, 1080-1086.

Anal. Chem. **2008,** *80,* 1080−1086

Minimal Invasive Gender Determination of Birds by Means of UV-Resonance Raman Spectroscopy

M. Harz,[†] M. Krause,[†] T. Bartels,[‡] K. Cramer,[‡] P. Rösch,[†] and J. Popp*[,†,§]

Institut für Physikalische Chemie, Friedrich-Schiller-Universität Jena, Helmholtzweg 4, 07743 Jena, Germany, Klinik für Vögel und Reptilien, Universität Leipzig, An den Tierkliniken 17, 04103 Leipzig, Germany, and Institut für Photonische Technologien, Albert-Einstein-Strasse 9, 07745 Jena, Germany

The identification of avian gender is important for prosperous breeding of birds. Since birds do not possess external genital organs, endoscopic investigations, blood analysis, and molecular biological methods are applied to determine the gender in monomorphic species. However, anesthesia and blood sampling impose stress on the examined bird and should be avoided in terms of animal protection. Here we report on the application of UV-resonance Raman spectroscopy as a minimal invasive method for gender determination of birds via an evaluation of feather pulp samples. Sample preparation for this investigation method is simple and facilitates a quick and easy analysis. The UV-resonance Raman spectra of the feather pulp sample extracts are dominated by DNA and protein signals. The different DNA content in male and female chicken allows for gender differentiation via its characteristic Raman fingerprint. The classification either to male or female chicken is ideally accomplished by support vector machines due to the fact that no unknown classes are involved. Recognition rates of about 95% were compared to less effective results of the unsupervised hierarchical cluster analysis. Within the scope of our investigations, principal component analysis was also applied to determine the important spectral regions for the classification of chicken's feather pulp samples.

The knowledge of a bird's gender is vital to bird keepers and aviculturists for the establishment of breeding pairs or breeding flocks. Furthermore, the poultry industry has an enormous interest in identifying the gender of poultry at a very early stage of body development. Since, for example, the feeding conditions are different for either gender, this has economic reasons.[1] In contrast to mammals, birds do not possess external genital organs. Thus, secondary sexual characteristics such as body size, plumage color, or other phenotypic sexual characteristics have to be used for a gender determination. If a distinct sexual dimorphism is missing, ethological parameters as mating behavior or phonation can provide further information for gender diagnosis. However, in numerous monomorphic bird species no reliable gender determination can be accomplished on the basis of external or behavioral characteristics. Furthermore one is also dependent on alternative methods for gender determination of immature or sexually inactive birds. Among endoscopic evaluations of the gonads of anesthetized birds[2−4] and investigations of the hormone status, molecular biological methods (e.g., DNA−PCR)[5−11] in particular provide reliable results in these cases. In the poultry industry, vent sexing is commonly used. Here a manual sorting of newly hatched male and female poults on the basis of differences in cloacal morphology is accomplished with a high accuracy of 95%.[12] Despite their good reliability, the described methods are time-consuming and stressful for the birds and should be avoided in terms of animal welfare. Furthermore, birds can be injured during blood sampling, and both sampling procedure and analysis presuppose trained specialists as well as special laboratory equipment. Last, anesthesia proposes an increased risk for the birds' health. Fatalities due to anesthetic accidents are extremely unacceptable, not least if the examined species is rare and expensive, such as certain parrots. Hence the use of alternative, less impacting methods would be preferable to preserve the bird's health.

A promising minimal invasive option is the application of Raman spectroscopy for the analysis of complex biological samples. Depending on the Raman laser excitation wavelength, a selective enhancement of different sample constituents can be achieved.[13−22] The application of deep UV excitation wavelengths

* Corresponding author. Phone: (+49)3641 948320. Fax: (+49)3641 948302. E-mail: juergen.popp@uni-jena.de.
† Friedrich-Schiller-Universität Jena.
‡ Universität Leipzig.
§ Institut für Photonische Technologien.

(1) Shalev, B. A.; Pasternak, H. *Poult. Sci.* **1998**, *77*, 859−863.
(2) Satterfield, W. C. *Vet. Clin. North Am.: Small Anim. Pract.* **1990**, *20*, 1353−1367.
(3) Korbel, R. *Tieraerztl. Prax.* **1993**, *21*, 41−46.
(4) Prus, S. E.; Schmutz, S. M. *Avian Dis.* **1987**, *31*, 420−424.
(5) Bermudez-Humaran, L. G.; Garcia-Garcia, A.; Leal-Garza, C. H.; Riojas-Valdes, V. M.; Jaramillo-Rangel, G.; Montes-De-Oca-Luna, R. *J. Exp. Zool.* **2002**, *292*, 677−680.
(6) Huynen, L.; Millar, C. D.; Lambert, D. M. *Mol. Ecol.* **2002**, *11*, 851−856.
(7) Clinton, M.; Haines, L.; Belloir, B.; McBride, D. *Br. Poult. Sci.* **2001**, *42*, 134−138.
(8) Griffiths, R.; Double, M. C.; Orr, K.; Dawson, R. J. G. *Mol. Ecol.* **1998**, *7*, 1071−1075.
(9) Nomura, O.; Nishimori, K.; Nakabayashi, O.; Yasue, H.; Mizuno, S. *J. Steroid Biochem. Mol. Biol.* **1998**, *67*, 143−148.
(10) Gill, D. V.; Robertson, H. A.; Betz, T. W. *Gen. Comp. Endocrinol.* **1983**, *49*, 176−186.
(11) Tell, L. A.; Lasley, B. L. *Zoo Biol.* **1991**, *10*, 361−367.
(12) Bramwell, R. K. *Avian Advice* **2003**, *5*, 4−5.
(13) Frosch, T.; Schmitt, M.; Popp, J. *J. Phys. Chem. B* **2007**, *111*, 4171−4177.
(14) Schmitt, M.; Popp, J. *J. Raman Spectrosc.* **2006**, *37*, 20−28.

10.1021/ac702043q CCC: $40.75
Published on Web 01/16/2008

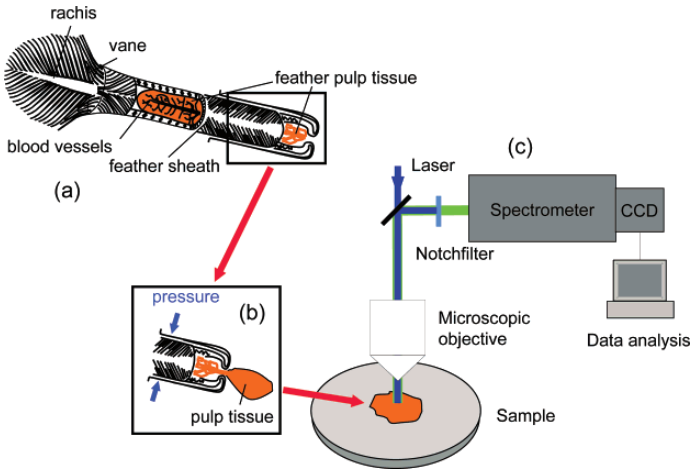

Figure 1. Principle scheme of minimal invasive gender determination of birds by using a feather (a): easy extraction of DNA-rich cell material of the feather pulp by pressing the feathers from tip to base (b) followed by direct recording of a Raman fingerprint spectrum and data analysis (c).

yields a selective enhancement of macromolecules such as aromatic amino acids in proteins as well as DNA bases. The scattering intensity increases up to 10^6 by the electronic resonance enhancement thus improving the signal-to-noise ratio significantly.[23,24] Hence, UV-resonance Raman (UVRR) spectroscopy with excitation in the deep UV region is a powerful approach to study samples with high protein and/or DNA content.

Here we report on the successful application of UVRR spectroscopy to determine the gender of birds. This approach is based on the fact that genome size is larger in male birds as compared to females. In chickens, the difference relative to the respective DNA content amounts to about 2%.[25] This difference should be detectable by means of UVRR spectroscopy since other sample components such as carbohydrates or lipids contribute negligible Raman signals in the deep UV region. After extraction of the DNA-rich cell material by pressing the thawed feathers from tip to base, no further extensive sample preparation is required.

EXPERIMENTAL SECTION

Sample Preparation. Feather samples were collected in a flock of 6-week-old layer chickens (Lohmann Brown) of both sexes. Growing contour feathers containing pulp tissue were manually picked from the skin and were separately stored in vials at −20 °C.

The extraction of cell material containing DNA was carried out by pressing the thawed feathers from tip to base and smearing the obtained liquid sample directly onto a fused-silica surface for drying.

Spectroscopic Instrumentation. UVRR spectra were recorded using a micro-Raman setup (HR800, Horiba Jobin-Yvon, Bensheim, Germany) with a focal length of 800 mm and a 2400 lines/mm grating. The wavenumber resolution of the HR800 spectrometer was 4 cm^{-1}. As excitation wavelength, a frequency-doubled argon-ion laser (Innova 300, MotoFReD, Coherent, Dieburg, Germany) at 244 nm was applied. The laser power on the sample was ca. 1 mW. The laser beam was focused onto the sample by a 40× broad-band antireflection coated UV objective (LMU UVB) with a numerical aperture of 0.5. The entrance slit was set to 300 μm. A video camera, which is sensitive in the UV and in the visible spectral range, was used for positioning the samples under the microscope. The Raman scattered light was detected by a nitrogen-cooled CCD camera with an accumulation time set to 60 s. The samples were rotated and moved in the *x*,*y* direction after each rotation to obtain an average spectrum over a large sample area in order to minimize possible photodegradation by UV radiation.

Figure 1 summarizes this quick and reliable approach for minimal invasive gender determination of birds: the procedure includes the easy extraction of DNA-rich cell material of the feather pulp (a) by pressing the feathers from tip to base (b) followed by the direct recording of a Raman fingerprint spectrum and data analysis by the application of chemometrical methods for gender classification (c).

Data Preprocessing and Classification. A total of 18 male and 16 female chicken samples were analyzed by recording about 10 Raman spectra of each sample. Overall, a number of 326 UVRR spectra were recorded.

(15) Gaus, K.; Rösch, P.; Petry, R.; Peschke, K. D.; Ronneberger, O.; Burkhardt, H.; Baumann, K.; Popp, J. *Biopolymers* **2006**, *82*, 286−290.
(16) Neugebauer, U.; Schmid, U.; Baumann, K.; Holzgrabe, U.; Ziebuhr, W.; Kozitskaya, S.; Kiefer, W.; Schmitt, M.; Popp, J. *Biopolymers* **2006**, *82*, 306−311.
(17) Harz, M.; Claus, R. A.; Bockmeyer, C. L.; Baum, M.; Rösch, P.; Kentouche, K.; Deigner, H. P.; Popp, J. *Biopolymers* **2006**, *82*, 317−324.
(18) Krause, M.; Radt, B.; Rösch, P.; Popp, J. *J. Raman Spectrosc.* **2007**, *38*, 369−372.
(19) Neugebauer, U.; Schmid, U.; Baumann, K.; Ziebuhr, W.; Kozitskaya, S.; Deckert, V.; Schmitt, M.; Popp, J. *ChemPhysChem* **2007**, *8*, 124−137.
(20) Rösch, P.; Harz, M.; Schmitt, M.; Popp, J. *J. Raman Spectrosc.* **2005**, *36*, 377−379.
(21) Rösch, P.; Harz, M.; Peschke, K.-D.; Ronneberger, O.; Burkhardt, H.; Schuele, A.; Schmauz, G.; Lankers, M.; Hofer, S.; Thiele, H.; Motzkus, H.-W.; Popp, J. *Anal. Chem.* **2006**, *78*, 2163−2170.
(22) Rösch, P.; Harz, M.; Peschke, K. D.; Ronneberger, O.; Burkhardt, H.; Popp, J. *Biopolymers* **2006**, *82*, 312−316.
(23) Carey, P. R. *J. Biol. Chem.* **1999**, *274*, 26625−26628.
(24) Turpin, P. Y.; Chinsky, L.; Laigle, A. *Stud. Phys. Theor. Chem.* **1987**, *45*, 369−385.
(25) Tiersch, T. R. *World's Poult. Sci. J.* **2003**, *59*, 24−31.

Prior to the chemometric analysis of the Raman spectra, the first derivative of the spectra (Savitzky−Golay, 13 smoothing points) was calculated to realize both a background correction and a signal-to-noise ratio enhancement. The final data preprocessing step consisted in a vector normalization of the spectra. Out of a large variety of classification methods, two methods, namely, the supervised nonlinear classification method support vector machine (SVM) and the unsupervised classification method hierarchical cluster analysis (HCA), are used to characterize the data set. These are well-established methods to classify biological and medical samples.[26,27] The preprocessed data set was employed by SVM using radial basis function kernels.[28] This algorithm allows for differentiating all background information from important signals. No restriction to a special wavenumber region was done since every small spectral difference might be of importance to achieve the best differentiation results. The results were obtained by performing leave-one-out tests and testing validation data.

The results were compared to the analysis of the HCA. Therefore, the program package "Opus Ident 3.1" (Bruker Optics, Ettlingen, Germany) was used accounting the factorization method and the Ward's algorithm for calculating the spectral distances.

Furthermore, the evaluation of essential wavenumber regions for classification could be performed by accomplishing a principal component analysis (PCA). Therefore, the software "The Unscrambler" (CAMO Process AS; version 9.2, Reutlingen, Germany) was applied. This software uses a cross validation to verify the results. Here a subsample set containing the original Raman spectra recorded from each sample was created for all 34 samples. The Raman bands of interest in the wavenumber range between 1140 and 1730 cm^{-1} were compared to the loadings receiving by PCA.

RESULTS AND DISCUSSION

The aim of the investigations presented in the following was a gender determination of chickens. The analysis of feather pulp containing mostly DNA is possible by means of UVRR spectroscopy in combination with chemometric data analysis.

Qualitative Signal Assignment. The prominent bands of the feather pulp UVRR spectra are assigned by comparing those with the UV Raman spectra of well-known constituents.

Figure 2 shows the average UVRR spectra of the extract from male (black) and female (gray) feather pulp samples of chickens. The spectra are baseline corrected and vector normalized. The two Raman spectra show slightly different intensity patterns. Therefore, the Raman difference spectrum by subtracting the female from the male UVRR spectrum was calculated identifying the most pronounced differences between female and male feather pulp UVRR spectra in the wavenumber region between 600 and 1800 cm^{-1}. The difference signals in positive direction correspond to higher band intensities in the averaged male feather pulp spectrum. The main differences appear around 1648, 1615, 1594, 1500, 1480, 1452, 1336, 1172, and 1007 cm^{-1}. Since DNA and protein components are enhanced by UV excitation, the signal assignment can be focused to these components. Figure 3 compares an averaged UVRR spectrum of a male feather pulp sample with those of pure calf thymus DNA and the hen egg white lysozyme protein being characteristic for a chicken environment. The wavenumber labeling of the Raman bands in Figure 3 is ordered as follows: the protein bands are labeled on top and marked with a dotted line, the DNA bands are in the middle and marked with a dashed line and the superposition of DNA and protein information is found at the end of the legend with a continuous line. A complete band assignment is summarized in Table 1.

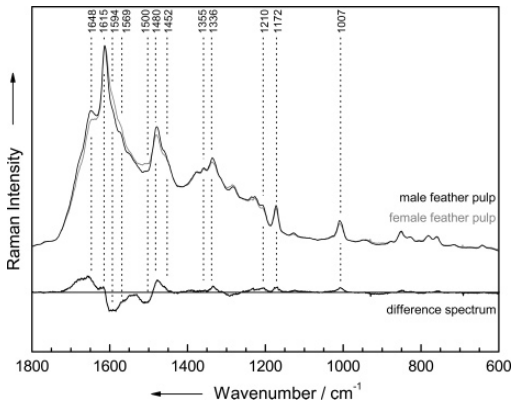

Figure 2. Averaged UVRR spectra of male and female chickens' feather pulp samples (baseline correction, vector normalization) and difference spectrum by subtracting the female from the male UVRR spectrum.

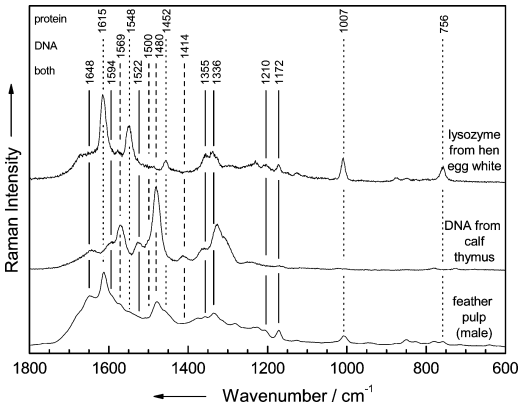

Figure 3. UVRR spectrum of a male chickens' feather pulp sample compared to a DNA spectrum of calf thymus and a protein spectrum of hen egg white lysozyme.

The Raman bands of the feather pulp at 1648, 1480, 1569, 1355, and 1172 cm^{-1} can be assigned to the DNA building blocks (nucleic acid bases, nucleosides, and nucleotides). The band at 1648 cm^{-1} can be identified as the CO and CC stretching vibration of the nucleic acid thymine. The two purine bases guanine and adenine contribute to the Raman band at 1480 cm^{-1} with its triene vibration and the CN stretching vibration, respectively. Adenine and guanine also contribute with a NH_2 deformation to the band at 1569 cm^{-1}. The two pyrimidine bases, thymine and cytosine,

(26) Harz, M.; Rösch, P.; Peschke, K. D.; Ronneberger, O.; Burkhardt, H.; Popp, J. *Analyst* (*Cambridge, U.K.*) **2005**, *130*, 1543−1550.
(27) Wood, B. R.; Caspers, P.; Puppels, G. J.; Pandiancherri, S.; McNaughton, D. *Anal. Bioanal. Chem.* **2007**, *387*, 1691−1703.
(28) Rösch, P.; Harz, M.; Schmitt, M.; Peschke, K.-D.; Ronneberger, O.; Burkhardt, H.; Motzkus, H.-W.; Lankers, M.; Hofer, S.; Thiele, H.; Popp, J. *Appl. Environ. Microbiol.* **2005**, *71*, 1626−1637.

Table 1. Raman Band Assignment of DNA and Protein in Feather Pulp Spectra

bands (cm^{-1})	protein	DNA	ref
756	tryptophan, phenylalanine: symmetric benzene/pyrrole in-phase breathing mode		31, 33
1007	phenylalanine, tryptophan: symmetric benzene/pyrrole out-of-phase breathing mode		31, 33, 38
1172	tyrosine: in-plane C−H bending	C, T: CC and CN stretching	33, 38, 39
1210	tyrosine, phenylalanine: ring C−Cβ stretching		33, 38
1336	tryptophan: Fermi resonance between N1−C8 stretching in pyrrole ring and combination bands of out-of-plane bending	A: C5N7, N7C8 stretching G	31, 38, 40
1355	tryptophan: Fermi resonance between N1−C8 stretching in pyrrole ring and combination bands of out-of-plane bending	G: N7C8, N1C6, N5N7 stretching	33, 38, 40
1369		C: C4N, N2C2 stretching T: C6H bending, ring stretching	40
1414		A, G: C4N9 stretching, C8H deformation	39, 40
1452	tryptophan: minor ring mode		
1480		G: C8H deformation, N9C8 and C8N7 stretching A: C8H deformation, N9C8 stretching	31, 32, 39, 40
1500			
1522		C: N3C4 stretching	39, 40
1548	tryptophan: C−C stretching vibration of the pyrrole ring		33, 38
1569	tryptophan: in-plane C−C stretching mode of pyrrole ring	A, G: NH2 deformation vibration	32, 33, 38
1594		G: NH2 bending, C2N stretching C: NH2 bending, C4N stretching	40
1615	tyrosine, tryptophan: in-plane C=C ring stretching		33, 38
1648	amide I: C−O stretching vibration and N−H in-plane bending	C: C2=O stretching T: C4=O−C4C5 stretching G: N2H2 scissoring	31, 32, 34, 39, 40

generate the bands at 1355 and 1172 cm^{-1}, which can be assigned to CC and CN stretching motions.[29−32]

Furthermore, protein bands are found at 1648, 1615, 1569, 1452, 1355, 1336, 1210, 1172, 1007, and 756 cm^{-1} and can be assigned to three aromatic amino acids phenylalanine, tryptophan, and tyrosine. The band at 1648 cm^{-1} contributes to the CO stretching vibration and NH in-plane bending vibration of the amide I mode. The band around 1615 cm^{-1} is due to the in-plane CC ring stretching mode of tryptophan and tyrosine. The bands at 1569, 1355, 1336, and 756 cm^{-1} also arise from tryptophan, more precisely from CC and CN pyrrole stretching and bending vibrations, whereas the band at 1452 cm^{-1} contributes to a minor ring mode of tryptophan. The band at 1172 cm^{-1} finds its origin from an in-plane CH bending vibration of tyrosine. Tryptophan and phenylalanine exhibit a characteristic band at 1007 cm^{-1} due to breathing modes of the benzene and pyrrole rings.[31,33,34]

In summary it can be said that the main differences between female and male feather pulp UVRR spectra result from different DNA contents of both genders. The Raman difference signals (see Figure 1) being not characteristic for either female or male feather pulp and therefore not useful for a gender determination arise in the range of 1450 and 1350 cm^{-1}, between 1150 and 1010 cm^{-1}, and below 1000 cm^{-1}.

Chemometric Analysis. The results presented above demonstrate that female and male feather pulp Raman spectra exhibit subtle differences. However, for a quantitative gender determination a chemometric analysis is required. Prior to this analysis the first derivative of the 326 UVRR spectra from male and female feather pulp was calculated and vector normalized afterward. Different chemometric methods were applied for the quantification of variances between male and female chicken feather pulp samples.[35,36]

Support Vector Machine. Supervised classification methods like nonlinear SVMs require additional information about the sample which can be added to the spectral information as attributes. The quantity of attributes determines the number of classes for the classification. By means of mathematical algorithms, the best separation area of the multidimensional problem is calculated. The problem for differentiating two classes (male and female) can be ideally solved by SVM since no class of unknown features has to be taken into account.

The analysis uses higher dimensional vector spaces because each Raman spectrum contains 2109 data points. The result is a classification model in terms of a multidimensional function. Beside the relevant DNA signal information, the spectra are influenced by the background, protein variations, or pyrolysis effects. These spectral artifacts are taken into account to achieve a closer reality simulation and make the model more robust. To estimate the calibration model, the validation results of both the leave-one-out validation test set and an independent data set of unknown spectra are calculated. The independent data set of

(29) Neugebauer, U. Ph.D. Thesis, Friedrich-Schiller University Jena, Jena, Germany, 2007.
(30) Neugebauer, U.; Schmid, U.; Baumann, K.; Simon, H.; Schmitt, M.; Popp, J. *J. Raman Spectrosc.* **2007**, *38*, 1246−1258.
(31) Overman, S. A.; Bondre, P.; Maiti, N. C.; Thomas, G. J., Jr. *Biochemistry* **2005**, *44*, 3091−3100.
(32) Thomas, G. J., Jr. *Annu. Rev. Biophys. Biomol. Struct.* **1999**, *28*, 1−27.
(33) Asher, S. A.; Ludwig, M.; Johnson, C. R. *J. Am. Chem. Soc.* **1986**, *108*, 3186−3197.
(34) Kitagawa, T.; Hirota, S. In *Handbook of Vibrational Spectroscopy: Applications in Life, Pharmaceutical and Natural Sciences*; Chalmers, J. M., Griffiths, P. R., Eds.; John Wiley & Sons: Chichester, U.K., 2002; pp 3426−3446.
(35) Beebe, K. R.; Pell, R. J.; Seasholtz, M. B. *Chemometrics—A Practical Guide*; John Wiley & Sons, Inc.: New York, 1998.
(36) Henrion, R.; Henrion, G. *Multivariate Datenanalyse—Methodik und Anwendung in der Chemie und verwandten Gebieten*; Springer-Verlag: Berlin, 1995.

Table 2. SVM Results by Leave-One-Out Method[a]

data set		classification result		estimation (%)	
	real no. of samples	male chicken	female chicken	correct	wrong (error type)
male chicken	171	168	3	98.3	1.7 (type I)
female chicken	155	10	145	93.6	6.4 (type II)
				95.9	4.1

[a] The recognition rate for male and female chickens' samples is demonstrated for all 326 spectra.

Table 3. SVM Results by Test Set Method[a]

data set		classification result		estimation (%)	
	real no. of samples	male chicken	female chicken	correct	wrong (error type)
male chicken	57	56	1	98.2	1.8 (type I)
female chicken	52	4	48	92.3	7.7 (type II)
				95.4	4.6

[a] The original data set of male and female chickens' samples is split into a data set for calibration (217 spectra) and a data set for validation (109 spectra).

Table 4. Number of Correctly and Wrongly Classified Spectra of Male and Female Chickens' Feather Pulp Samples of the Full Data Set (326 Spectra) Resulting by HCA

data set		classification result		estimation (%)	
	real no. of samples	male chicken	female chicken	correct	wrong (error type)
male chicken	171	123	48	71.9	28.1 (type I)
female chicken	155	30	125	80.6	19.4 (type II)
				76.3	23.7

unknown spectra was achieved by dividing randomly the data set into the calibration set of 217 spectra (two-thirds of all spectra) and the validation set of 109 spectra. Therefore, two classification results can be discussed. The classification rates of the leave-one-out validation test set are shown in Table 2. When taking all spectral and attributed information into account, 98.3% of the male and 94.8% of the female feather pulp samples can be classified correctly. The validation results of the data set of unknown spectra are summarized in Table 3. The classification is possible with a probability of 98% for male and of 92% for female feathers. These recognition rates of both the validation data set and the unknown feather pulp samples have comparable error variances as manual vent sexing with an accuracy of about 95%.

These results can be compared to those obtained for an unsupervised HCA. For such an analysis only the spectral data set is required, and no further information about class affiliation (features) of the objects (spectra) are included into the similarity calculation. Table 4 presents the HCA classification results in detail. The classification rates for female decreases to 81% and for male to 72%. These results demonstrate that the variances of the spectra are too high for an acceptable classification. Thus,

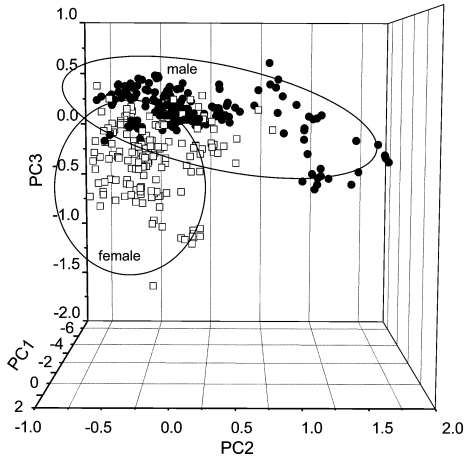

Figure 4. Three-dimensional diagram of the PCA-scores plot of male and female feather pulp samples spectra in the spectral range between 1140 and 1730 cm^{-1}.

supervised classification methods such as SVM are advantageous, also in consideration of the possibility for the identification of unknown samples.

Principal Component Analysis. The SVM showed to be a practical separation tool between female and male chicken samples with recognition rates of about 95%. In order to determine the decisive spectral regions for the classification of chicken's feather pulp samples a PCA was applied to the original normalized data set. The PCA is used to model the data and to determine the spectral variances associated with the feather pulp of male and female chickens. The variation of the data set is described via a few basis vectors or principal components (PC). More precisely, the first PC describes the greatest part of the data set variance, whereas higher PCs describe only noise. The coordinates of the data according to the new axes are called scores, and the contributions of the original variables to the PCs are called loadings. After the calculation, similar spectra group together in the scores plot. The loadings plot provides information of the variables (wavenumbers of the spectrum) that are important for group separation.

Figure 4 shows the three-dimensional diagram of a scores plot of the first three principal components of 326 male and female chicken feather pulp samples' UVRR spectra for the wavenumber range between 1140 and 1730 cm^{-1}. The scores plot reflects a clear separation of male and female feather pulp samples. It is possible to separate both genders with a few principal components, although the groups are disperse and sometimes overlap each other. The diffuse grouping originates from several reasons; for example, fluctuations in excitation power can influence the Raman intensity but are corrected by scaling methods. The spectral background resulting from variations in the sample thickness can be corrected by calculating the first-derivative spectra. Furthermore, a different sample composition, e.g., the ratio between DNA and protein content, can influence the spectrum quality. This effect is illustrated in Figure 5 A. An enlarged protein content which can be seen at the 1452 cm^{-1} band showing almost the same intensity as compared to the amount of DNA represented by the 1480 cm^{-1} mode (compare Table 1) is demonstrated in spectrum

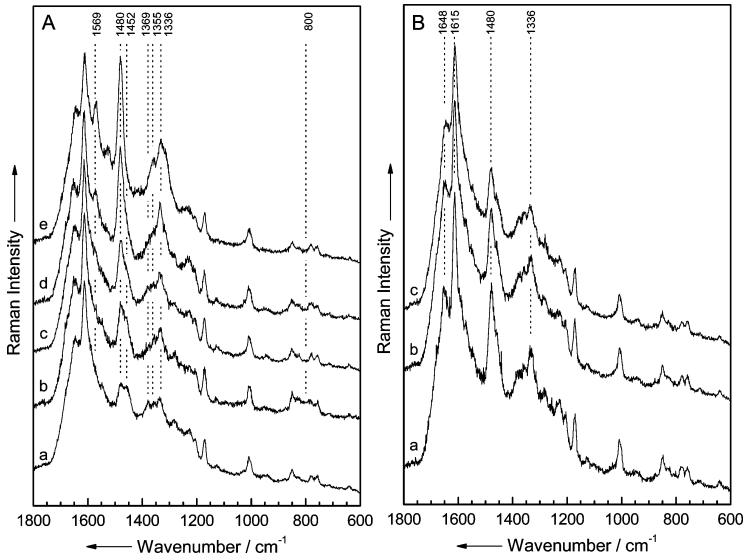

Figure 5. (A) Influence of different cell compositions on the Raman spectra: spectrum a with a heightened protein content, spectrum b with a dominant background signal of quartz, spectra c and d as mixture spectra of variations between protein and DNA composition, and spectrum e with an increased DNA content. (B) Influence of photochemical degradation during a measurement (curves a−c: increasing pyrolysis).

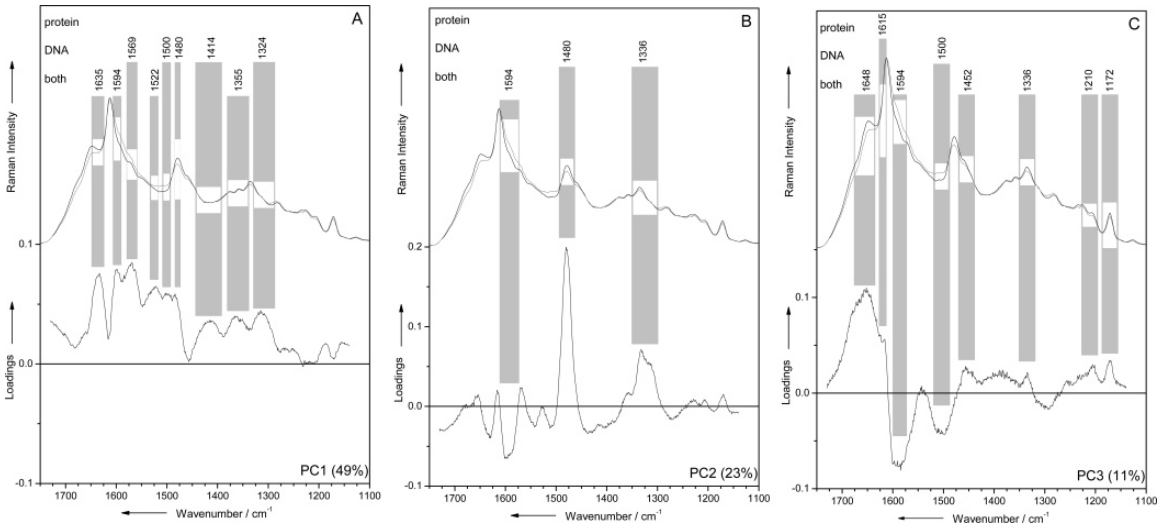

Figure 6. Loading plots of the first three principal components highlighting regions associated with large loadings compared to average spectra of the first derivative of the male and female chickens' feather pulp samples.

a. In contrast, a high DNA content discernible by the enhanced band intensities at 1569, 1480, and 1355 cm^{-1} is represented by spectrum e. During the Raman measurements, a spectral superposition between spectra, which are dominated by protein (spectrum a) or DNA (spectrum e) contents (spectra b, c, and d) occurred. The mode of sample preparation can also influence the Raman spectrum when too thin sample smears are used. In spectrum c, this effect is visualized where a broadened band at 800 cm^{-1} occurs due to the background spectrum of the quartz slide. Furthermore, small variations in signal intensities can be attributed to inhomogeneous surface tension as well as to possible photodegradation of the sample due to UV light irradiation. Figure 5B illustrates the influence of a progressive photodegradation of the samples during the measurement. In comparison to the nondegraded spectrum a, spectrum b shows a less and spectrum c a stronger degradation effect noticeable by decreased signal intensities at 1480 and 1336 cm^{-1} relative to the signal at 1615 cm^{-1}.

In order to determine the data set variances associated with feather pulp of male and female chickens, the loading plots need to be interpreted. In Figure 6A−C the average spectra of the male and female chickens' feather pulp samples (above) and the loading plots of the first three principal components PC1, PC2, and PC3 (below) are compared. Signal regions reflecting information of DNA, proteins, or both are marked with a rectangle and labeled with the respective wavenumber positions. The PC1 loading plot

(Figure 6A) shows nine different signal regions with high loadings. The spectral regions of 1569, 1500, 1522, and 1480 cm^{-1} as well as the region of 1414 and 1324 cm^{-1} show positive loadings and are correlated to DNA information. The wavenumber regions of 1635, 1594, 1522, and 1355 cm^{-1} represent both DNA and proteins bands.

The loading plot of PC2 (Figure 6B) includes three spectral regions with intensive loadings containing DNA information (1480 and 1336 cm^{-1} bands). Bands originating from both proteins and DNA are found in the wavenumber region around 1594 cm^{-1}.

The loading plot of PC3 (Figure 6C) shows eight strong loading regions. The first region around 1615 cm^{-1} represents protein information, and the second region at 1500 cm^{-1} yields DNA information. The regions at 1648, 1594, 1452, 1336, 1210, and 1172 cm^{-1} are correlated to both DNA and protein information.

These first three PCs can clarify 83% of the data set variation and focus with strong loadings on 13 different wavenumber regions in the range between 1660 and 1336 cm^{-1}. Due to the deep UV excitation wavelength leading to a selective enhancement of aromatic amino acids in proteins and DNA bases, the different wavenumber regions can be correlated to a superposition of DNA and proteins signals.

CONCLUSIONS AND OUTLOOK

Gender determination of birds is important for poultry industry as well as for bird keepers. Current invasive analysis methods imply increased risk for the bird's health. The work presented within this paper nicely demonstrates that UVRR spectroscopy of feather pulp is a capable alternative and minimal invasive method for gender determination.

The sample collection can be performed without distressing the animals in contrast to other methods like endoscopic surgery or blood analysis. The risk of anesthetic problems is excluded. The sample preparation is simple, and the sample extracts can directly be analyzed to achieve a Raman fingerprint spectrum within 1 min. For gender determination, the spectrum will be compared to a setup database by chemometrical methods. Thus, this approach presents a quick and easy method for gender determination.

In this contribution the influence of the selectively enhanced feather pulp constituents of the feather extracts to the feather pulp Raman spectrum was discussed. For that purpose the Raman spectra of the extract material were compared to those of pure DNA and proteins.

Different chemometrical methods were used to elucidate the spectral characteristics of male and female chicken samples. For classifying the recorded spectra, in this approach the supervised classification method SVM was applied. A classification model was created and applied to unknown samples for gender determination. The SVM showed to be a practical separation tool for female and male chicken samples with recognition rates of about 95%. The influence of spectra with increased photodegradation or with enhanced protein signals rates did not influence the classification results significantly.

In order to determine the important spectral regions for the classification of chicken's feather pulp samples a PCA was applied. The first three principal components can elucidate 83% of the data set variation and are necessary for a satisfactory differentiation between male and female feather pulp spectra. The loadings plots showed seven different wavenumber regions in the range between 1660 and 1336 cm^{-1} that are important for group separation. Since an excitation wavelength in the deep UV was applied a selective enhancement of aromatic amino acids in proteins and DNA bases is achieved. Therefore, the different wavenumber regions are correlated to a superposition of DNA and proteins signals.

The principle application of UVRR spectroscopy for a gender determination of birds has been demonstrated so far for chickens. In future work these investigations need to be extended to other birds like turkey. Here, a quick and simple gender determination has to be provided for optimizing the feeding conditions to reach better economic profits in poultry industry.

In the future the exploratory focus is also on better classification accuracy. The value of 98.5% which is the commercial accuracy acceptance of automated gender sorting of avian embryos[37] must be the goal. It can be reached by optimizing the sample preparation and sample handling to generate more homogeneous spectra. The minimization of photodegradation will be one of the main aspects in this respect.

ACKNOWLEDGMENT

This study was supported by the Hessen Ministry for Environment, Agriculture and Consumer Protection and the Lohmann Tierzucht GmbH (Cuxhaven). We gratefully acknowledge the Fond der Chemischen Industrie for financial support.

Received for review October 2, 2007. Accepted November 19, 2007.

AC702043Q

(37) Phelps, P. *World's Poult. Sci. J.* **2003**, *59*, 32−37.
(38) Cho, N.; Song, S.; Asher, S. A. *Biochemistry* **1994**, *33*, 5932−5941.
(39) Fodor, S. P. A.; Spiro, T. G. *J. Am. Chem. Soc.* **1986**, *108*, 3198−3205.
(40) Wen, Z. Q.; Thomas, G. J., Jr. *Biopolymers* **1998**, *45*, 247−256.

Autorschaft der Publikationen

[MH1] UV Raman spectroscopy - A technique for biological and mineralogical *in situ* planetary studies.

Spectrochimica Acta Part A **2007**, 68, 1029-1035.

N. Tarcea: Anfertigung des Manuskripts

M. Harz: Kultivierung der Mikroorganismen, Durchführung von Messungen und Auswertungen, Diskussion und Korrektur des Manuskripts

P. Rösch: Diskussion und Korrektur des Manuskripts

T. Frosch: Durchführung von Messungen und Auswertungen, Diskussion und Korrektur des Manuskripts

M. Schmitt: Diskussion und Korrektur des Manuskripts

H. Thiele: Partner im Projekt OMIB, Diskussion und Korrektur des Manuskripts

R. Hochleitner: Partner im Projekt OMIB, Diskussion und Korrektur des Manuskripts

J. Popp: Projektleitung, Konzept- und Ergebnis-Diskussion, Diskussion und Korrektur des Manuskripts

[MH2] Micro-Raman spectroscopic identification of bacterial cells of the genus Staphylococcus and dependence on their cultivation conditions.

Analyst **2005**, 130, 1543-1550.

M. Harz: Kultivierung der Mikroorganismen, Durchführung von Messungen und Auswertungen, Anfertigung des Manuskripts

P. Rösch: Diskussion und Korrektur des Manuskripts

K.-D. Peschke: Partner im Projekt OMIB, Diskussion und Korrektur des Manuskripts

O. Ronneberger: Partner im Projekt OMIB, Diskussion und Korrektur des Manuskripts

H. Burkhardt: Partner im Projekt OMIB, Diskussion und Korrektur des Manuskripts

J. Popp: Projektleitung, Konzept- und Ergebnis-Diskussion, Diskussion und Korrektur des Manuskripts

[MH3] Chemotaxonomic identification of single bacteria by micro-Raman spectroscopy: Application to clean-room-relevant biological contaminations.

Applied and Environmental Microbiology **2005**, 71, 1626-1637.

P. Rösch: Anfertigung des Manuskripts, Ergebnis-Diskussion

M. Harz: Kultivierung der Mikroorganismen, Durchführung von Messungen und Auswertungen, Beiträge zur Manuskripterstellung, Diskussion und Korrektur des Manuskripts

M. Schmitt: Diskussion und Korrektur des Manuskripts

K.-D. Peschke: Partner im Projekt OMIB, Diskussion und Korrektur des Manuskripts

O. Ronneberger: Partner im Projekt OMIB, Diskussion und Korrektur des Manuskripts

H. Burkhardt: Partner im Projekt OMIB, Diskussion und Korrektur des Manuskripts

H.-W. Motzkus: Partner im Projekt OMIB, Diskussion und Korrektur des Manuskripts

M. Lankers: Partner im Projekt OMIB, Diskussion und Korrektur des Manuskripts

S. Hofer: Partner im Projekt OMIB, Diskussion und Korrektur des Manuskripts

H. Thiele: Partner im Projekt OMIB, Diskussion und Korrektur des Manuskripts

J. Popp: Projektleitung, Konzept- und Ergebnis-Diskussion, Diskussion und Korrektur des Manuskripts

[MH4] Raman spectroscopic identification of single yeast cells.

Journal of Raman Spectroscopy **2005**, 36, 377-379.

P. Rösch: Anfertigung des Manuskripts, Ergebnis-Diskussion

M. Harz: Kultivierung der Mikroorganismen, Durchführung von Messungen und Auswertungen, Diskussion und Korrektur des Manuskripts

M. Schmitt: Diskussion und Korrektur des Manuskripts

J. Popp: Projektleitung, Konzept- und Ergebnis-Diskussion, Diskussion und Korrektur des Manuskripts

[MH5] Identification of single eukaryotic cells with Micro-Raman Spectroscopy.

Biopolymers **2006**, 82, 312-316.

P. Rösch: Anfertigung des Manuskripts, Ergebnis-Diskussion

M. Harz: Kultivierung der Mikroorganismen, Durchführung von Messungen und Auswertungen, Diskussion und Korrektur des Manuskripts

K.-D. Peschke: Partner im Projekt OMIB, Diskussion und Korrektur des Manuskripts

O. Ronneberger: Partner im Projekt OMIB, Diskussion und Korrektur des Manuskripts

H. Burkhardt: Partner im Projekt OMIB, Diskussion und Korrektur des Manuskripts

J. Popp: Projektleitung, Konzept- und Ergebnis-Diskussion, Diskussion und Korrektur des Manuskripts

[MH6] On-line monitoring and identification of bioaerosols.

Analytical Chemistry **2005**, 78, 2163-2170.

P. Rösch: Anfertigung des Manuskripts, Ergebnis-Diskussion

M. Harz: Kultivierung der Mikroorganismen, Durchführung von Messungen und Auswertungen, Beiträge zur Manuskripterstellung, Diskussion und Korrektur des Manuskripts

K.-D. Peschke: Partner im Projekt OMIB, Berechnungen zur Support-Vektor-Maschine

O. Ronneberger: Partner im Projekt OMIB, Diskussion und Korrektur des Manuskripts

H. Burkhardt: Partner im Projekt OMIB, Diskussion und Korrektur des Manuskripts

A. Schüle: Partner im Projekt OMIB, Diskussion und Korrektur des Manuskripts

G. Schmauz: Partner im Projekt OMIB, Diskussion und Korrektur des Manuskripts

M. Lankers: Partner im Projekt OMIB, Diskussion und Korrektur des Manuskripts

S. Hofer: Partner im Projekt OMIB, Diskussion und Korrektur des Manuskripts

H. Thiele: Partner im Projekt OMIB, Diskussion und Korrektur des Manuskripts

H.-W. Motzkus: Partner im Projekt OMIB, Diskussion und Korrektur des Manuskripts

J. Popp: Projektleitung, Konzept- und Ergebnis-Diskussion, Diskussion und Korrektur des Manuskripts

[MH7] Analysis of single blood cells for liquor diagnostics *via* a combination of fluorescence staining and micro-Raman spectroscopy.

Analyst **2008**, *online publiziert* (DOI:10.1039/b716132h).

M. Harz: Durchführung von Messungen und Auswertungen, Anfertigung des Manuskripts

M. Kiehntopf: Partner im DFG-Projekt PO 563/7-1, Diskussion und Korrektur des Manuskripts

S. Stöckel: Durchführung von Messungen und Auswertungen, Korrektur des Manuskripts

P. Rösch: Diskussion und Korrektur des Manuskripts

T. Deufel: Partner im DFG-Projekt PO 563/7-1, Korrektur des Manuskripts

J. Popp: Projektleitung, Konzept- und Ergebnis-Diskussion, Diskussion und Korrektur des Manuskripts

[MH8] UV-resonance Raman spectroscopic study of human plasma of healthy donors and patients with thrombotic microangiopathy.

Biopolymers **2006**, 82, 317-324.

M. Harz: Durchführung von Messungen und Auswertungen, Anfertigung des Manuskripts

R. A. Claus: Projektpartner, Diskussion und Korrektur des Manuskripts

C. L. Bockmeyer: Probenpräparation von Kryopräzipitaten

M. Baum: Durchführung von Messungen

P. Rösch: Diskussion und Korrektur des Manuskripts

K. Kentouche: Projektpartner, Diskussion und Korrektur des Manuskripts

H.-P. Deigner: Projektpartner, Diskussion und Korrektur des Manuskripts

J. Popp: Projektleitung, Konzept- und Ergebnis-Diskussion, Diskussion und Korrektur des Manuskripts

[MH9] UV-resonance Raman spectroscopic investigation of human plasma for medical diagnosis.

Medical Laser Application **2007**, 22, 87-93.

M. Harz: Durchführung von Messungen und Auswertungen, Anfertigung des Manuskripts

C. L. Bockmeyer: Probenpräparation von Kryopräzipitaten

P. Rösch: Diskussion und Korrektur des Manuskripts

R. A. Claus: Projektpartner, Diskussion und Korrektur des Manuskripts

J. Popp: Projektleitung, Konzept- und Ergebnis-Diskussion, Diskussion und Korrektur des Manuskripts

[MH10] Minimal invasive gender determination of birds by means of UV-resonance Raman spectroscopy.

Analytical Chemistry **2008**, 80, 1080-1086.

M. Harz: Durchführung von Messungen und Berechnungen zur Hauptkomponentenanalyse, Spektreninterpretation, Anfertigung des Manuskripts

M. Krause: Durchführung von Messungen und Berechnungen zur hierarchischen Clusteranalyse und Support-Vektor-Maschine, Beiträge zur Manuskripterstellung

T. Bartels: Projektpartner, Probenbereitstellung, Diskussion und Korrektur des Manuskripts

K. Cramer: Diskussion und Korrektur des Manuskripts

P. Rösch: Diskussion und Korrektur des Manuskripts

J. Popp: Projektleitung, Konzept- und Ergebnis-Diskussion, Diskussion und Korrektur des Manuskripts

Publikationen

Veröffentlichungen

1. M. Harz, M. Kiehntopf, S. Stöckel, P. Rösch, T. Deufel, J. Popp, Analysis of single blood cells for liquor diagnostics *via* a combination of fluorescence staining and micro-Raman spectroscopy, *Analyst* **2008**, *online publiziert* (DOI10.1039/b716132h).

2. M. Harz, M. Krause, T. Bartels, K. Cramer, P. Rösch, J. Popp, Minimal invasive gender determination of birds by means of UV-resonance Raman spectroscopy, *Analytical Chemistry* **2008**, 80, 1080-1086.

3. N. Tarcea, M. Harz, P. Rösch, T. Frosch, M. Schmitt, H. Thiele, R. Hochleitner, J. Popp, UV Raman spectroscopy - A technique for biological and mineralogical *in situ* planetary studies, *Spectrochimica Acta Part A* **2007**, 68, 1029-1035.

4. P. Rösch, M. Harz, M. Krause, J. Popp, Fast and reliable identification of microorganisms by means of Raman spectroscopy, *Proc. SPIE-Int. Soc. Opt. Eng.* **2007**, 6633, 66331A.

5. M. Harz, C. L. Bockmeyer, P. Rösch, R. A. Claus, J. Popp, UV-resonance Raman spectroscopic investigation of human plasma for medical diagnosis, *Medical Laser Application* **2007**, 22, 87-93.

6. M. Harz, R. A. Claus, C. L. Bockmeyer, M. Baum, P. Rösch, K. Kentouche, H.-P. Deigner, J. Popp, UV-resonance Raman spectroscopic study of human plasma of healthy donors and patients with thrombotic microangiopathy, *Biopolymers* **2006**, 82, 317-324.

7. Rösch, M. Harz, M. Krause, R. Petry, K.-D. Peschke, H. Burkhardt, O. Ronneberger, A. Schüle, G. Schmauz, R. Riesenberg, A. Wuttig, M. Lankers, S. Hofer, H. Thiele, H.-W. Motzkus, J. Popp, Online monitoring and identification of bioaerosol (OMIB), *in J. Popp and M. Strehle, eds., Biophotonics. Visions for Better Health Care, Wiley-VCH Verlag GmbH & Co. KGaA, Weinheim.* **2006**.

8. M. Harz, U. Neugebauer, P. Rösch, J. Popp, Raman spectroscopic identification of bacterial cells, *GIT Laboratory Journal, Europe*, **2006** 10, 3, 26-28.

9. P. Rösch, M. Harz, M. Schmitt, K.-D. Peschke, O. Ronneberger, H. Burkhardt, H.-W. Motzkus, M. Lankers, S. Hofer, H. Thiele, J. Popp, Rapid identification of single microbes by various Raman spectroscopic techniques, *Proc. SPIE-Int. Soc. Opt. Eng.* **2006**, 6093, 60930D/1-60930D/11.

10. J. Popp, P. Rösch, M. Harz, M. Schmitt, K.-D. Peschke, O. Ronneberger, H. Burkhardt, Raman-Spectroscopy for a rapid identification of single microorganisms, *Proc. SPIE-Int. Soc. Opt. Eng.* **2006**, 6180.

11. K.-D. Peschke, B. Haasdonk, O. Ronneberger, H. Burkhardt, P. Rösch, M. Harz, J. Popp, Using Transformation knowledge for the classification of Raman spectra of biological samples, *Proc. 24th IASTED Internat. Conf. Biomed. Eng.*, **2006**, 288.

12. P. Rösch, M. Harz, K.-D. Peschke, O. Ronneberger, H. Burkhardt, J. Popp, Identification of Single Eukaryotic Cells with Micro-Raman Spectroscopy, *Biopolymers* **2006**, 82, 312-316.

13. P. Rösch, M. Harz, M. Schmitt, J. Popp, Raman spectroscopic identification of single yeast cells, *Journal of Raman Spectroscopy* **2005**, 36, 377-379.

14. P. Rösch, M. Harz, K.-D. Peschke, O. Ronneberger, H. Burkhardt, A. Schuele, G. Schmauz, M. Lankers, S. Hofer, H. Thiele, H.-W. Motzkus, J. Popp, On-Line Monitoring and Identification of Bioaerosols, *Analytical Chemistry* **2005**, 78, 2163-2170.

15. P. Rösch, M. Harz, M. Schmitt, K.-D. Peschke, O. Ronneberger, H. Burkhardt, H.-W. Motzkus, M. Lankers, S. Hofer, H. Thiele, J. Popp, Chemotaxonomic identification of single bacteria by micro-Raman spectroscopy: application to clean-room-relevant biological contaminations, *Applied and Environmental Microbiology* **2005**, 71, 1626-1637.

16. M. Harz, P. Rösch, K.-D. Peschke, O. Ronneberger, H. Burkhardt, J. Popp, Micro-Raman spectroscopic identification of bacterial cells of the genus Staphylococcus and dependence on their cultivation conditions, *Analyst* **2005**, 130, 1543-1550.

Patente

1. R. A. Claus, C. L. Bockmeyer, H.-P. Deigner, M. Harz, P. Rösch, J. Popp, R. Riesenberg, Diagnostic tool detecting the degradation status of Von Willebrand Factor multimers, *Friedrich-Schiller-Universität Jena*, **Anmeldetag: 05.06.2007**, Aktenzeichen: US 11/713,863.

2. J. Popp, P. Rösch, T. Bartels, M. Krause, M. Harz, Verfahren zur Bestimmung des Geschlechts von Vögeln, *Friedrich-Schiller-Universität Jena*, **Anmeldetag: 15.03.2007**, Aktenzeichen: DE 10 2007 013 107.2.

Vorträge

1. *Zelluläre und biomolekulare medizinische Diagnostik mittels Raman-Spektroskopie.* 1. Doktorandenseminar des Deutschen Arbeitskreises für Spektroskopie (DASp) 2008, 09/10.07.2008, Jena.

2. *Single cell analysis of liquor cerebrospinalis by means of Raman spectroscopy.* SPIE Photonics West 2008, 20.01.2008, San Jose, USA.

3. *Raman-spektroskopische Differenzierung und Identifizierung körpereigener Zellen und Mikroorganismen im Liquor cerebrospinalis für die medizinische Diagnostik.* Forschungsseminar im Institut für Klinische Chemie und Laboratoriumsdiagnostik, Universitätsklinikum Jena, 02.11.2007, Jena.

4. *Raman spectroscopic investigations of cellular components in liquor cerebrospinalis.* European Conferences on Biomedical Optics (ECBO)- Biophotonik 2007, 20.06.2007, München.

5. *Raman-spektroskopische Charakterisierung von Mikroorganismen.* Gesellschaft deutscher Chemiker (GDCh)-Kurzvortrag, 20.12.2006, Jena.

6. *Raman spectroscopic characterization of microorganisms.* Bio-Geo-Kolloquium/DFG-Graduiertenkolleg GRK 1257/1 'Alteration und Elementmobilisierung an Mikroben-Mineral-Grenzflächen', 12.12.2006, Jena.

Posterpräsentationen

1. *Raman spectroscopic study of human blood cells.*
   International Conference on Raman Spectroscopy (ICORS) 2008, London, Großbritannien;
   A. Haase, M. Harz, S. Stöckel, P. Rösch, M. Kiehntopf, T. Deufel, J. Popp.

2. *Characterization of human plasma by means of vibrational spectroscopy.*
   European Conferences on Biomedical Optics (ECBO)- Biophotonik 2007, München;
   M. Harz, R. Claus, P. Rösch, C. Bockmeyer, K. Kentouche, H.-P. Deigner, J. Popp.

3. *Investigation of Human Plasma by means of vibrational spectroscopy.*
   International Conference on Advanced Vibrational Spectroscopy (ICAVS) 2007, Korfu, Griechenland;
   M. Harz, R. A. Claus, P. Rösch, C. L. Bockmeyer, M. Baum, K. Kentouche, H.-P. Deigner, J. Popp.

4. *Vibrational spectroscopic investigation of human plasma for medical diagnosis.*
   Deutsch-Kanadischer Workshop 2007, Göttingen;
   M. Harz, R. A. Claus, P. Rösch, C. L. Bockmeyer, J. Popp.

5. *Schwingungsspektroskopische Untersuchung von kryopräzipitierten Blutplasmaproben zur Identifizierung von thrombotischer Mikroangiopathie.*
   Anakon 2007, Jena;
   M. Harz, R. A. Claus, P. Rösch, C. L. Bockmeyer, M. Baum, K. Kentouche, H.-P. Deigner, J. Popp.

6. *Mikrobiologische Reinraumüberwachung mittels Raman-Spektroskopie.*
   Anakon 2007, Jena;
   M. Krause, M. Harz, P. Rösch, J. Popp.

7. *Micro-Raman spectroscopic characterization of liquor cerebrospinalis.*
   Congress of Clinical Chemistry and Laboratory Medicine (DGKL) 2006, Mannheim;
   M. Kiehntopf, M. Harz, P. Rösch, E. Straube, T. Deufel, J. Popp.

8. *Differentiation and identification of bacterial cells in liquor cerebrospinalis by means of micro-Raman spectroscopy.*
   International Conference on Raman Spectroscopy (ICORS) 2006, Yokohama, Japan;
   M. Harz, P. Rösch, M. Kiehntopf, E. Straube, T. Deufel, J. Popp.

9. *Automated monitoring and identification of bioaerosols by Raman spectroscopy.*
   International Conference on Raman Spectroscopy (ICORS) 2006, Yokohama, Japan;
   M. Krause, M. Harz, P. Rösch, J. Popp.

10. *Microbial identification by means of Raman spectroscopy.*
International Conference on Raman Spectroscopy (ICORS) 2006, Yokohama, Japan;
P. Rösch, M. Krause, M. Harz, J. Popp.

11. *Determination of the fatty acid composition from breast milk by means of micro-Raman spectroscopy.*
Shedding Light on Disease (SPEC) 2006, Heidelberg;
M. Harz, U. Enke, P. Möckel, P. Rösch, J. Popp.

12. *UV-resonance Raman studies of proteins for medical diagnosis.*
Shedding Light on Disease (SPEC) 2006, Heidelberg;
P. Rösch, M. Harz, R. A. Claus, C. L. Bockmeyer, M. Baum, K. Kentouche, H.-P. Deigner, J. Popp.

13. *UV-resonance Raman spectroscopical study of human plasma of healthy donors and patients with thrombotic microangiopathy.*
European Conference on the Spectroscopy of Biological Molecules (ECSBM) 2005, Aschaffenburg;
M. Harz, R. A. Claus, C. L. Bockmeyer, M. Baum, P. Rösch, K. Kentouche, H.-P. Deigner, J. Popp.

14. *Identification of single yeast cells with micro-Raman spectroscopy.*
European Conference on the Spectroscopy of Biological Molecules (ECSBM) 2005, Aschaffenburg;
P. Rösch, M. Harz, K.-D. Peschke, O. Ronneberger, H. Burkhardt, J. Popp.

15. *Bacterial identification with different Raman spectroscopic methods.*
Deutsch-Kanadischer Workshop 2005, München;
P. Rösch, M. Harz, K.-D. Peschke, O. Ronneberger, H. Burkhardt, J. Popp.

16. *Mikro-Raman spektroskopische Identifizierung von einzelnen Bakterienzellen in Abhängigkeit von den Kultivierungsbedingungen.*
Biophotonik-Symposium 2005, Jena;
M. Harz, P. Rösch, K.-D. Peschke, O. Ronneberger, H. Burkhardt, J. Popp.

17. *Identifizierung einzelner Hefe- und Bakterien-Zellen unter Verwendung der Raman-Spektroskopie und statistischen Auswertemodellen.*
Biophotonik-Symposium 2005, Jena;
P. Rösch, M. Harz, K.-D. Peschke, O. Ronneberger, H. Burkhardt, J. Popp.

18. *Klassifikation von Raman-Spektren mit Support-Vektor-Maschinen.*
Biophotonik-Symposium 2005, Jena;
K.-D. Peschke, P. Rösch, M. Harz, O. Ronneberger, J. Popp, H. Burkhardt.

19. *Micro-Raman spectroscopical identification of bacterial cells of the genus Staphylococcus in dependence on their cultivation conditions.*
FT-IR Spectroscopy in Microbiological and Medical Diagnostic, 21./22.10.2004, Berlin;
M. Harz, P. Rösch, J. Popp.

20. *Raman spectroscopic analysis of microorganisms on a single cell level.*
International Conference on Raman Spectroscopy (ICORS) 2004, Gold Coast, Queensland, Australien;
P. Rösch, M. Harz, K.-D. Peschke, O. Ronneberger, H. Burkhardt, J. Popp.

Danksagung

An erster Stelle danke ich Herrn Prof. Dr. Jürgen Popp für die freundliche Aufnahme in seine Arbeitsgruppe und für die Möglichkeit, eigene Ideen in verschiedenen Themengebieten entwickeln und diese in seinen hervorragend ausgestatteten Laboren umsetzen zu können. Ich danke ihm außerdem, dass er es mir ermöglichte, an zahlreichen Tagungen im In- und Ausland teilzunehmen. Mein besonderer Dank gilt meiner Betreuerin Frau Dr. Petra Rösch. Ihr danke ich für die fortwährende Unterstützung und zahlreiche wegweisende Diskussionen. Auch möchte ich mich bei Herrn PD Dr. Michael Schmitt für die Beratung und Unterstützung bei fachlichen und organisatorischen Dingen bedanken.
Allen Mitarbeitern der Arbeitsgruppe Popp (Katrin Ackermann, Dana Cialla, Valerian Ciobota, Claudiu Dem, Thomas Dörfer, Torsten Frosch, Antje Haase, Katharina Hering, Anna Keese, Mario Krause, Antje Kriltz, Michael Kühnert, Marion Ludwig, Anne März, Thomas Mayerhöfer, Tobias Meyer, Martin Presselt, Melanie Putsche, Petra Rösch, Michael Schmitt, Stephan Stöckel, Nicolae Tarcea, Stefanie Tschierlei, Ute Uhlemann, Angela Walter) danke ich für die gute Zusammenarbeit und das freundschaftliche Klima. Ein Dankeschön gilt meinen Büromitbewohnern Martin Presselt, Mario Krause, Angela Walter, Anne März und Anna Keese für die angenehme Gesellschaft und besonders Martin für seine unterhaltsamen Ablenkungsmanöver. Vielen Dank an Torsten Frosch für die Unterstützung im UV-Raman Labor. Ich danke Matthias Baum als studentische Hilfskraft für seine engagierte Arbeit und Ausdauervermögen im UV-Raman Labor. Ebenso sei Stephan Stöckel für seine Arbeit bei der Untersuchung von Bakterien und Blutzellen aus der Gehirn-Rückenmarks-Flüssigkeit im Rahmen seiner Diplomarbeit gedankt. Dank gilt ebenfalls den Mitarbeitern des Instituts für Physikalische Chemie für die angenehme Arbeitsatmosphäre und insbesondere der Werkstatt für ihre Hilfsbereitschaft. Herrn Dr. Fr.-Wilhelm Breitbarth und Frau Ute Backhaus danke ich für die Unterstützung im Praktikum. Weiterer Dank gilt den beiden Sekretärinnen Frau Marion Krause und Frau Gisela Zeise für ihre Unterstützung bei organisatorischen Angelegenheiten sowie Herrn Dr. Dirk Bender für seine Hilfe bei Computerproblemen und Softwarefragen.
Weiterhin danke ich Herrn Prof. H. Burkhardt, Dr. Olaf Ronneberger und Klaus-Dieter

Peschke aus dem Institut für Informatik der Universität Freiburg, Herrn Dr. Andreas Schüle und Günther Schmauz des Fraunhofer Instituts für Produktionstechnik und Automatisierung, Dr. Markus Lankers der rap.ID particle systems GmbH, Dr. Stefan Hofer und Hans Thiele der Kayser-Threde GmbH sowie Dr. Hans-Walter Motzkus der Schering AG für die Zusammenarbeit im Biophotonik-Projekt OMIB (Online-Monitoring und Identifizierung von Bioaerosolen).
Für die Kooperation im Rahmen des DFG-Projektes PO 563/7-1 'Raman-spektroskopische Differenzierung und Identifizierung körpereigener Zellen und Mikroorganismen im Liquor für die medizinische Diagnostik' danke ich Herrn Prof. Dr. Thomas Deufel und Herrn OA Dr. Dr. Michael Kiehntopf vom Institut für Klinische Chemie und Laboratoriumsdiagnostik sowie Herrn Prof. Dr. Eberhard Straube aus dem Institut für Medizinische Mikrobiologie des Universitätsklinikums Jena. Ein Dank gilt ebenfalls Kay Stötzer für die Bereitstellung von Blutzellpräparaten und CSF-Proben sowie Hannelore Kräplin für die Bereitstellung von Bakterienreinkulturen.
Bedanken möchte ich mich bei Herrn Dr. Ralf A. Claus und Clemens L. Bockmeyer von der Klinik für Anästhesiologie und Intensivtherapie, Dr. Karim Kentouche von der Klinik für Kinder- und Jugendmedizin des Universitätsklinikums Jena sowie Herrn Prof. Dr. H.-P. Deigner der Biomedicinal Chemistry, School of Chemical Sciences and Pharmacy, University of East Anglia, Norwich, Großbritannien für die Zusammenarbeit und die Probenbereitstellung bei den Untersuchungen an kryopräzipitierten Blutplasmaproben.
Für die Kooperation und Probenbereitstellung bezüglich der Untersuchungen zur Geschlechtsbestimmung bei Vögeln bedanke ich mich bei Herrn PD Dr. Thomas Bartels und Kerstin Cramer von der Klinik für Vögel und Reptilien der Universität Leipzig.
Für das Korrekturlesen und die kritische Durchsicht dieser Arbeit danke ich Dr. Petra Rösch, Dr. Dirk Michaelis und Stephanie Harz.
Ganz besonderer Dank gebührt meiner Familie. Mein spezieller Dank gilt meinem Verlobten Herrn Dr. Dirk Michaelis für zahlreiche richtungsgebende Diskussionen und Anregungen zur Verbesserung dieser Arbeit. Ein großes Dankeschön geht an meine Eltern Gisela und Volkmar Harz, die mir den Grundstein für diesen Weg gelegt haben und an meine Schwester Stephanie. Vielen Dank für die vielfältige Unterstützung.

Lebenslauf

Hochschullaufbahn

seit Mai 2004	wissenschaftlicher Mitarbeiter am Institut für Physikalische Chemie der Friedrich-Schiller-Universität Jena im Rahmen einer Promotion Lehrtätigkeit im physikalisch-chemischen Praktikum; Betreuung von Seminarfach-, Praktikums- und Diplomarbeiten
Okt. 1998 - Nov. 2003	Studium zum Dipl.-Ing. (FH) im Fachbereich Medizintechnik (Studienrichtung: Biomedizinische Technik) an der Fachhochschule Jena (Note: 1,4) *Studienschwerpunkte: Labor- und Analysenmeßtechnik, medizinelektronische Geräte- und Systemtechnik, medizinische Informatik und Signalanalyse, physikalische und technische Optik, Laser- und Optotechnologie*
Okt. 2002 - Nov. 2003	Anfertigung der Diplomarbeit am Fraunhofer Institut für Angewandte Optik und Feinmechanik Jena, Abteilung Mikrooptik Thema der Diplomarbeit: (Note: 1,0) *'Oberflächen-Plasmonen-Resonanz-Sensor zur parallelen Detektion von mehreren biochemischen Proben.'*

Auszeichnung

Okt. 2004	Auszeichnung der Diplomarbeit mit dem 'Hugo-Geiger-Preis' der Fraunhofer Gesellschaft

Berufserfahrung

Dez. 2003 - Apr. 2004	studentischer Mitarbeiter am Fraunhofer Institut für Angewandte Optik und Feinmechanik Jena, Abteilung Mikrooptik *- Entwicklung und Optimierung eines Sensors zur optischen Detektion der Zusammensetzung von Fleischgemengen.*
März 2002 - Nov. 2003	studentischer Mitarbeiter am Fraunhofer Institut für Angewandte Optik und Feinmechanik Jena, Abteilung Mikrooptik *- Messsystemopimierung, Parallelisierung und Automatisierung des Verfahrens der Oberflächen-Plasmonen-Resonanz zur*

	Detektion mehrerer biochemischer Proben.
Okt. 2001 - Feb. 2002	Praxissemester bei der Firma Carl Zeiss Jena GmbH im Geschäftsbereich Ophthalmologie, Bereich Laserentwicklung *- Berechnungen und Untersuchungen zu polarisations-optischen Effekten verschiedener optischer Bauelemente und Strahlquellen.*
Aug. 2001 - Sep. 2001	Praktikum am Klinikum der Friedrich-Schiller-Universität Jena in der Klinik für Anästhesiologie und Intensivtherapie, Abteilung Medizintechnik, medizinische Rechentechnik und Dokumentation *- Sicherheitstechnische Kontrollen, Fehlersuche und Wartung medizintechnischer Geräte, Konfiguration des Patienten-Daten-Managment-Systems COPRA.*
Juni 1998 - Sep. 1998	Vorpraktikum bei der Firma Labor- und Umwelttechnik Jena GmbH *- Erstellung eines Qualtitätsmanagmentsystems, Erarbeitung von Rationalisierungslösungen, Qualitätssicherung, Gestaltung von Schaltplänen.*

Schulausbildung

1991 - 1998	Staatliches Gymnasium 'Bergschule' Apolda Abschluss: Abitur (Note: 1,5)
1986 - 1991	Grund- und Regelschule in Herressen/Sulzbach

Jena, den 03. September 2008

Michaela Harz

Selbstständigkeitserklärung

Ich erkläre, dass ich die vorliegende Arbeit selbstständig und unter Verwendung der angegebenen Hilfsmittel, persönlichen Mitteilungen und Quellen angefertigt habe.

Jena, den 03. September 2008

Michaela Harz